Lunar SECRet mission

Final Report - July 1, 2014

AE3200 Design Synthesis Exercise

N.O. Bernving - 4140656; D. Brinkman - 4181816; B.F. Gellert - 4114310
A. Gonzalez Puerta - 4176340; R.A. Makhan - 4081102; A.M. Pronk - 4153243
M. Smeets - 1526863; M. Vergaaij - 4135490; B. Verheijen - 4167058; Y.H.J. van Weersch - 4162439

Delft University of Technology

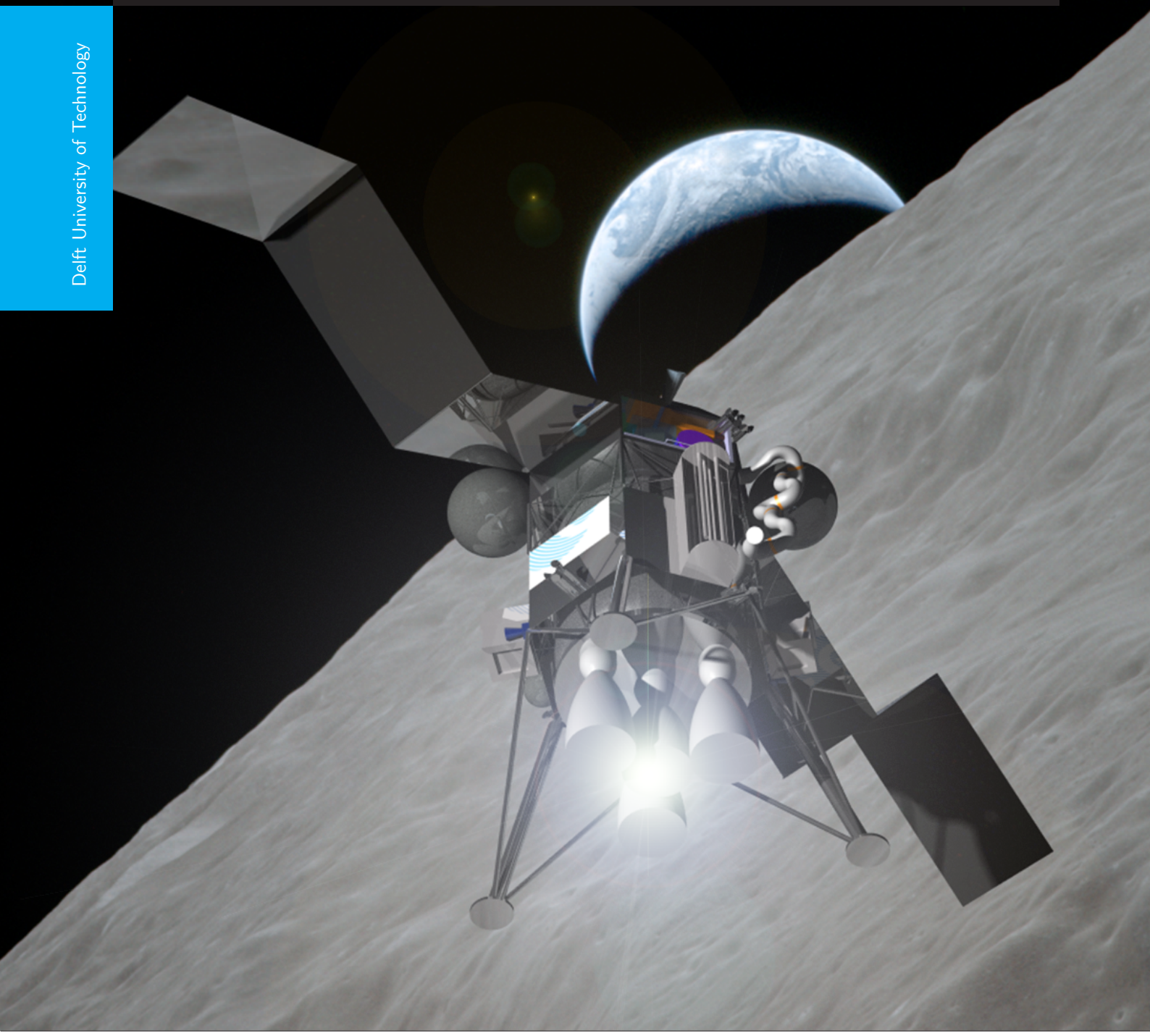

TU Delft Delft University of Technology

Challenge the future

PREFACE

This report is written by a team of ten students from the Faculty of Aerospace Engineering at Delft University of Technology. Prof. van Westrenen from the VU University of Amsterdam is the customer for this project. He has expressed his desire for a complete and thorough feasibility study for a sample return mission to the Moon. The goal of this study is to research into the development and feasibility of mission which will bring back a lunar soil sample up to two meter depth to Earth. It is required by the customer that the sample will be held at cryogenic temperatures during its return to Earth to prevent outgassing of the collected drill sample. The members of the team are Niels Orvar Bernving, Dennis Brinkman, Busso Friedrich Gellert, Alejandro Gonzalez Puerta, Rajeev Amritsingh Makhan, Anne Maria Pronk, Martijn Smeets, Merel Vergaaij, Bob Verheijen and Yorin Hubert Johannes van Weersch, who are all participating in the final project of the bachelor of Aerospace Engineering.

In the baseline report of this feasibility study a starting point was made for creating a design. In the mid-term report the project continued from that baseline and a final design was selected from five different mission concepts. In this final report, the selected final design is presented in detail. Each of the subsystems included in the spacecraft are thoroughly designed and justified. At the end of this report, the performance of the overall design is analysed and a conclusion is made regarding the feasibility of a cryogenic sample return lunar mission.

This report is written first and foremost for people involved in the project, such as the customer, tutors and coaches. In addition, the report can be used by others in a similar project who wish to gain knowledge on how a feasibility study for a sample return mission should be addressed.

We would like to thank our customer Professor W. van Westrenen for giving this team the possibility to work on this project. We would like to thank Ron Noomen, John-Alan Pascoe and Matteo Pini for their guidance during the project. We wish to acknowledge the help provided by Kenneth Salvestrini from Infrared Laboratories for giving the team valuable insight into current cryogenic cooling technology. We would like to thank Pietro Baglioni from the European Space Agency for his assistance regarding the evaluation of the ExoMars drill. We would like to acknowledge Michel van Pelt from ESA for his help during the development of the cost estimation model. We would like to thank Ingo Gerth for his support regarding landing procedures. Last but not least, we would like to acknowledge the advice provided by all the guests present during the project's baseline and midterm reviews.

SUMMARY

Previous to this report, a baseline configuration for a Lunar Sample Extraction Cryogenic Return (Lunar SECRet) mission to the Moon was made, and a list of requirements and a preliminary mission profile were constructed. In the conceptual design phase, five mission concepts were created and after a trade-off, a final design was selected. In this report the final design is examined in detail and a conclusion regarding the feasibility of the proposed mission is made.

The spacecraft will consist of several modules, namely, the orbiter, a lander, and a re-entry vehicle. The lander consists of an ascent stage and a descent stage. The spacecraft will be launched before 2025 on a Falcon Heavy rocket directly into a trans-lunar injection orbit. The orbiter will perform a mid-course correction and a braking burn to put the spacecraft into a stable low lunar orbit. The lander will then undock from the orbiter and perform a powered descent into the Wiechert J crater, at the south pole of the Moon. Shortly after touch-down, the sample extraction operation will begin. Once lunar surface operations are finished, the ascent stage will decouple from the descent stage and will initiate an ascent towards low lunar orbit where it will dock again with the orbiter. After successful transfer of the sample material to the re-entry vehicle, the ascent stage will once again undock from the orbiter and remain in low lunar orbit prior to departure of the rest of the spacecraft with the samples back to Earth. Shortly before atmospheric re-entry the re-entry vehicle will undock from the orbiter. In order for the sample to survive the re-entry phase, a cryogenic system, an ablative heat shield and parachutes will be used. After touch-down on the Earth surface, the cryogenic system will keep the sample at a temperature below 120 K while awaiting retrieval.

Several aspects of this mission are quite unusual with respect to other missions. One of the most crucial components for this mission is the cryogenic system, which is designed such that it can keep the sample below 120 K during the transfer and up to 12 hours after atmospheric re-entry, to prevent escape of trapped volatiles. This system ensures that no volatiles are lost after extraction, preserving the sample's geological history. The sample will be collected using an adapted ExoMars drill, which is mounted on the descent stage. The drill will be powered by a fuel cell, since solar panels do not supply power at the base of the crater, due to the absence of sunlight. A modified DEXARM robotic arm will be used to transport the collected sample to the cryogenic system. In a later stage of the mission, this same robotic arm is used to transport the entire cryogenic system from the ascent stage to the re-entry vehicle. This will happen in a low lunar orbit, where the re-entry vehicle is located at the nose of the orbiter. After the cryogenic system is safely stored in the re-entry vehicle, it will return back to Earth.

For each module and stage of the spacecraft, a mass and power budget has been established. As in most interplanetary space missions, the propellant has the largest mass fraction. Adding the propellant to a total dry mass of 2,292 kg results in a total wet mass of 6,527 kg. The main driver for the power budget was found to be the cryogenic system, this system requires a peak power of 480 W, which is over half of the re-entry vehicle's required power. The stage that requires most power is the ascent stage, as this houses the cryogenic system for a short amount of time as well. In addition to this system, the AOCS and thermal systems account for just over 400 W together. Including all systems, the ascent stage has to deliver a peak power of almost 1,400 W. During the mission, several different power sources are used, such as solar panels, rechargeable and non-rechargeable, batteries and fuel cells.

Using the mass budget, a cost estimation can be done. This is done using a validated NASA model, which uses the spacecraft dry mass, launch vehicle cost, and subsystem masses as input. As a result, a total life cycle cost of 476 FY2014€M is estimated. ESA's cost estimation for a similar mission results in a higher value of 670 – 720 FY2014€M. This means that both estimates are meeting the requirements. If the mission is insured for 92 %, the estimated cost equals the predicted ESA value.

A risk analysis has been performed, which identified the most critical aspects of the mission using a risk map. The cryogenics system and the drill were found to be the most critical aspects of the mission, since they both require substantial modifications to existing technology. Several aspects are qualified as *catastrophic*, but all of these are very unlikely to happen. These include the docking procedure and technology, propulsion system, and both systems used during re-entry: the heat shield and the parachute. If one of these aspects fails, the mission will not succeed, but all of these mission aspects are well within the existing state of the art, and are spaceflight-proven. The reliability of the whole system was found by applying the failure rates of each of the subsystems into an exponential reliability function. These failure rates were obtained from literature. It was

found that the system has a total reliability of 0.96, yielding a failure rate of 4 %, which is less than the 5 % established by the requirements. Like for most space systems, there is limited maintenance available after launch. In order to overcome this limitation, the system has been designed with redundancy where possible. Even though hardware repairs are impossible, potential software bugs could be solved by means of remote updates. This was taken into account when sizing the communications subsystem. The system is considered safe, though special care must be taken when loading the propellants onto the spacecraft. The ascent stage makes use of mixed oxides of nitrogen and monomethyhydrazine which are highly toxic and thus must be handled only by trained personnel. Furthermore, the spacecraft will only be launched when the weather conditions allow it, ensuring no danger to nearby conurbations.

All requirements set in the baseline report were met, which means that the verdict for the feasibility study is: feasible. As far as is known after this report, the mission should be able to succeed. Some aspects need further research, such as the drill, cryogenic system, and the launch window. When this research is completed, the mission should be able to launch successfully before 2025.

NOMENCLATURE

ACRONYMS AND ABBREVIATIONS

AG	Approach gate
AKE	Apogee kick engine
AOCS	Attitude and orbital control system
AS	Ascent stage
BER	Bit error rate
DCH	Data and command handling
DOD	Depth of discharge
DOI	Descent orbit insertion
DS	Descent stage
DSN	Deep Space Network
DSS	Deep Space Station
ECP	Electrical charge protection
EPS	Electrical power supply
ESA	European Space Agency
FBD	Functional breakdown diagram
FFD	Functional flow diagram
HG	High gate
HPBW	Half-power beam width
ISS	International Space Station
J-T	Joule-Thomson
LOI	Lunar orbit insertion
LOOS	Launch operations and orbital support
LOX	Liquid oxygen
LV	Launch vehicle
MCC	Mid-course correction
MIPS	Million instructions per second
MLI	Multi-layer insulation
MMH	Monomethylhydrazine
MON	Mixed oxides of nitrogen
NASA	National Aeronautics and Space Administration
NOAA	National Oceanic and Atmospheric Administration
PCM	Phase change material
PDI	Power descent initiation
PICA	Phenolic Impregnated Carbon Ablator

PS	Payload system
RAM	Random access memory
RCS	Reaction control system
RP1	Refined petroleum-1
RTG	Radioisotope thermoelectric generators
RV	Re-entry vehicle
SAM	Structures and mechanics
SID	Sample isolation device
SoI	Sphere of influence
T/W	Thrust-to-weight ratio
TEI	Trans-Earth injection
TG	Terminal gate
TLI	Trans-lunar injection
TPS	Thermal protection system
TS	Thermal system
UHMW PE	Ultra high molecular weight polyethylene

GREEK SYMBOLS

α	Angular section of crater angle	rad
α	Absorptivity	-
$\alpha_{1/2}$	Half-power beam width	rad
β	Angular section of crater angle	rad
β_m	Ballistic coefficient	kg/m^2
γ	Flight path angle	rad
δ	Latitude	rad
$\Delta(\cdot)$	Change in $(\cdot)$	-
ϵ	Emissivity	-
η	Efficiency	-
θ	Angular section of the visibility angle	rad
θ	Maximum deviation from z-axis to local vertical	rad
λ	Failure rate	year
μ	Standard gravitational parameter	m^3/s^2
ν	Poisson's ratio	-
ρ	Density	kg/m^3
ρ	Albedo effect	-
σ	Stress	N/m^2
σ	Boltzmann constant	$W/(m^2K^4)$
φ	Angular Section of the visibility angle	rad
χ	Heading	rad

ω_{cb}	Anglure rate of Earth	rad/s

LATIN SYMBOLS

A	Cross-sectional area	m^2
A	Area	m^2
a	Semi-major axis	m
a	Panel dimension parallel to load	m
a_E	Trajectory parameter	-
b	Panel dimension orthogonal to load	m
C	cost	€
C_D	Drag coefficient	-
c	Specific heat capacity	J/(kg·K)
c_l	Chapman's constant for Earth	$s^2\sqrt{Nm}$
c_p	Specific heat capacity	J/(m·K)
D	Diameter	m
D	Drag	N
d	Diameter	m
E	Young's modulus	GPa
E_b/N_0	Energy per bit to noise density	dB
e	Eccentricity	-
e	Antenna pointing offset	dB
F	Force	N
f	Frequency	GHz
f	Penetration per revolution	m/rev
G	Antenna gain	dB
g	Gravitational acceleration	m/s^2
H	Atmospheric density scale height	m
h	Altitude	m
h	Momentum	Nms
I	Inertia	$kg{\cdot}m^2$
I	Radiation intensity	W/m^2
I	Area moment of inertia	m^4
I_p	Impulse	N
i	Inclination	rad
K	Stiffness matrix	N/m
Kc	Specific cutting force	N/m^2
k	Thermal conductivity	W/(m·K)
k	Stiffness	N/m
L	Lift	N

L	Length of member	m
L_a	Propagation and polarisation loss	dB
L_i	Implementation loss	dB
L_l	Transmitter line loss	dB
L_p	Antenna pointing loss	dB
L_s	Space loss	dB
l	Drill penetration length	m
M	Required drill torque	Nm
M	Mass matrix	kg
m	Mass	kg
n	Rotational speed	rev/s
n	Acceleration	m/s^2
P	Power	W
P_t	Transmit power	dBW
Q	Total heat load	J/m^2
q	Heat flux	W/m^2
q	Energy flow	W
R	Data rate	bps
R	Radius	m
R	Resulting force	N
$\vec{r}$	Position vector	m
S	Propagation path length	m
S	Area	m^2
T	Temperature	K
T_s	System noise temperature	dBK
t	Time	s
t	Thickness	m
t_g	Gravity disturbance	Nm
V	Velocity	m/s
V	Penetration speed	m/s
W	Weight	N
w	Drill shaft wall thickness	m
x	Number	-
x	Distance along x-axis	m
y	Distance along y-axis	m
z	Distance along z-axis	m

SUBSCRIPTS

∞	Regarding excess velocity
a	Regarding acceleration
AKM	Regarding AKM
AOCS	Regarding AOCS system
apogee	Regarding apogee
AS	Regarding ascent stage
bat	Regarding batteries
begin	Regarding beginning of an orbital manoeuver
burn	Regarding burn
c	Regarding container
comp	Regarding compression
con	Regarding conduction
crater	Regarding crater
crit	Regarding critical load case
d	Regarding daylight
D	Regarding drag
D	Regarding downwards
dep	Regarding departure
dp	Regarding drogue parachute
drill	Regarding drill
dump	Regarding dump
e	Regarding eclipse
E	Regarding entry
Earth	Regarding Earth
eclipse	Regarding eclipse
eff	Regarding effective
end	Regarding end of an orbital manoeuver
entry	Regarding entry
EPS	Regarding EPS
ext	Regarding extended
fc	Regarding fuel cell
h	Regarding heat shield
h	Regarding washed area
Huygens	Regarding Huygens entry probe
in	Regarding incoming
inc	Regarding inclination manoeuver
inner	Regarding inner surface
int	Regarding internal

l	Regarding liquid
launch	Regarding launch
LLO	Regarding low lunar orbit
LLO-LS	Regarding difference between LLO and lunar surface
LOOS	Regarding LOOS
LV	Regarding landing vehicle
man	Regarding manoeuvre
Moon	Regarding Moon
mp	Regarding main parachute
ms	Regarding mechanism
N	Regarding nose radius
n	Regarding number
new	Regarding new value
NR	Regarding non-recurring cost
op	Regarding operations
orbit	Regarding orbit
out	Regarding outgoing
outer	Regarding outer surface
outw	Regarding outward displacement
p	Regarding parachute
perigee	Regarding perigee
pitch	Regarding pitch
PL	Regarding payload
PL-bus	Regarding payload-bus integration
prop	Regarding propellant
ps	Regarding parachute system
r	Regarding receive
R	Regarding recurring cost
rad	Regarding rejected
RCS	Regarding RCS
rel	Reliability time interval
roll	Regarding roll
RV	Regarding re-entry vehicle
s	Regarding solid
S&T	Regarding structural and thermal system
S/C	Regarding spacecraft
sc2SoI	Regarding spacecraft with respect to Moon
SECRet	Regarding Lunar SECRet mission
site	Regarding a parameter within or affecting landing site

SoI	Regarding sphere of influence
Sun	Regarding Sun
t	Regarding transmit
tar	Regarding target velocity
ten	Regarding tension
thermal	Regarding thermal subsystem
tot	Regarding total
transfer	Regarding transfer orbit
TT&C	Regarding TT&C
val	Regarding validation
x	Regarding x-component
y	Regarding y-axis
y	Regarding y-component
yield	Regarding yielding
z	Regarding z-axis
z	Regarding z-component

TABLE OF CONTENTS

1 INTRODUCTION

The surface of the Moon is a familiar sight to all. However, looking closer at its bare surface many questions arise and what goes on below the surface is an even greater secret. In this light, getting to know the chemical composition, in particular the volatiles present, of the layer beneath the lunar surface is important. This need can be explained from a purely scientific as well as from an economic point of view. On the one hand, a greater understanding of the chemical composition of the Moon will broaden our understanding of the creation of our solar system. On the other hand, the volatiles present in the lunar surface can provide a valuable resource for use on Earth or in further space exploration missions.

The main purpose of this report is to determine the feasibility of a Lunar Sample Extraction Cryogenic Return (Lunar SECRet) mission. This report presents the final design for the mission, detailing all the subsystems on-board and the methods used to size them. Furthermore, a comprehensive analysis of the selected design is given, which examines its performance and, most importantly, reviews all the established customer and technical requirements. If the final design meets all of these requirements, the mission will be rendered feasible. Should the mission result unfeasible, recommendations concerning the killer requirements will be made.

In Chapter 2 the work done in previous reports is summarised, which includes the definition of requirements and five mission concepts that were traded off for the final design. In Chapter 3 the general mission layout is given. In Chapter 4 the main methods and tools used to size the subsystems are explained, verified and validated. Chapters 5 to 8 include the layout and description of the major subsystems of each of the spacecraft modules. Chapter 9 gives a performance analysis of the final design in term of its mass, power and cost; its reliability, availability, maintainability and safety (RAMS) characteristics; its sensitivity to changes to the mission environment and to mass and power requirements; and its sustainability. Most importantly, this chapter examines whether all the requirements imposed on the system are met. In Chapter 10 an overview of the mission's future development is given together with the associated operational and logistical considerations. In Chapter 11 a conclusion is given regarding the performance of the system, the fulfilment of the established requirements and the overall feasibility of the mission. In Chapter 12 a list of official recommendations to be dealt with in future design stages is given, including aspects that were not fully covered in the current final design. Finally, in Appendices A and B, the different functions to be performed by the system are described using the Functional flow diagram (FFD) and the Functional breakdown diagram (FBD), respectively.

2 PREVIOUS WORK

In order to understand the choices that are made in the design phase described in this report, it is important to have knowledge about the decisions made in earlier phases. This chapter describes the most important results of the preceding work. First, the requirements, which were decided upon together with the customer, are discussed. Then, the conceptual design phase and its outcome are discussed.

2.1 REQUIREMENTS

During the baseline phase of the project, a set of requirements was made in consultation with the customer [1]. In order to make sure that the list of requirements is complete, a requirements discovery tree was made. It can be found in Figure 2.1. Using this tree, a list of requirements was set up. Some parts of the tree have been left out of the final list of requirements after consulting experts and the customer. Each requirement is mentioned and shortly discussed below.

LCSR-Mission-Sample-01 The project shall choose a sampling area within 370 km from the south pole of the Moon. *This requirement is important to ensure the quality of the sample. Near the poles the amount of sunlight on the surface is smaller. This means the chances of finding ice are higher, and the Helium-3 contamination originating from sunlight is smaller.*

LCSR-Mission-Sample-04 The sample shall be taken within the Shackleton, De Gerlache, Wiechert J or Amundsen crater. *These craters all have areas with permanent shade inside. In these areas, the temperatures are low enough to ensure the quality of the sample They are also large enough to land in, and have relatively flat slopes, which makes the landing easier.*

LCSR-Mission-Sample-05 The sample shall consist of a drill core down to at least 2 m depth. *This requirement ensures that the sample is useful for the scientific community. The deeper the sample, the older the soil is. A 2 m deep sample includes an interesting range of data.*

LCSR-Mission-Sample-06 The core sample shall be in powder form, fragments or intact. *This requirement ensures that the sample is useful for the scientific community. An intact sample is preferred over powder.*

LCSR-Mission-Sample-07 There shall be a core sample for at least every 25 cm of drill depth. *This requirement ensures that the sample is useful for the scientific community, and ensures a clear view of the change in sample chemistry over depth.*

LCSR-Mission-Sample-08 The sample shall be kept at temperatures lower than 120 K until retrieval on Earth. *This requirement ensures that the sample is useful for the scientific community. At higher temperatures, volatiles can escape from the sample.*

LCSR-Mission-Environment-01 The spacecraft shall withstand the expected radiation encountered during its mission time from cosmic background radiation, Van Allen belts and solar flares. *This requirement ensures that the spacecraft can survive and fulfill the mission. Note that the requirement specifies the expected radiation. If the mission duration is so short that it is highly unlikely to encounter solar flares, the expected radiation due to solar flares will be no radiation.*

LCSR-Mission-Environment-02 The spacecraft shall withstand the vacuum of deep space. *This requirement ensures that the spacecraft can survive and fulfill the mission.*

LCSR-Mission-Environment-08 Electrostatic charges shall not accumulate in the design. *This requirement ensures that the spacecraft can survive and fulfill the mission.*

LCSR-Mission-Environment-09 The spacecraft shall ensure sustainable temperatures for all subsystems. *This requirement ensures that the spacecraft can survive and fulfill the mission.*

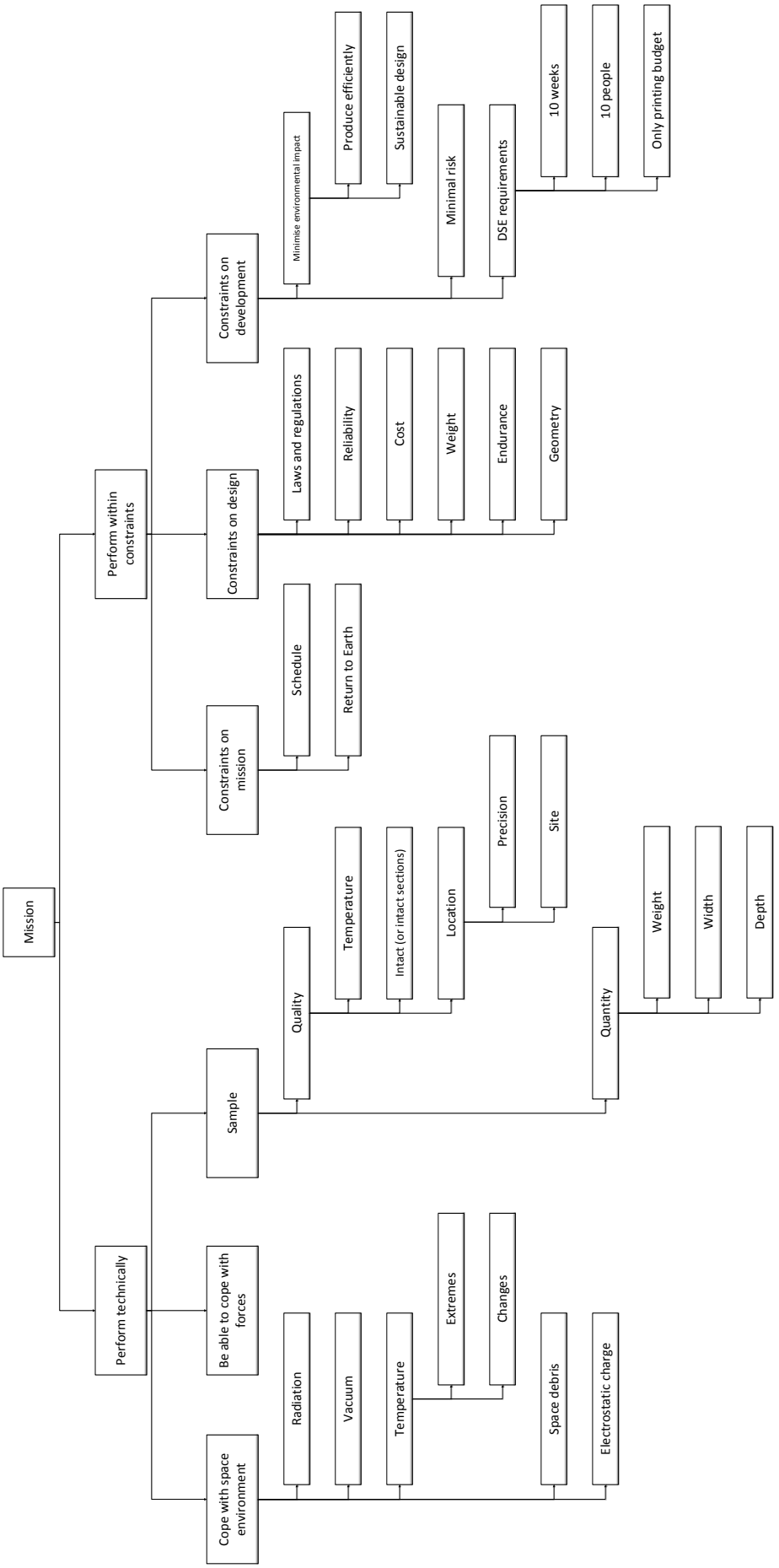

Figure 2.1: The requirements discovery tree [1].

LCSR-Mission-Forces-01 The spacecraft shall withstand axial launch forces induced by the launch vehicle (LV). *This requirement ensures that the spacecraft can survive and fulfill the mission.*

LCSR-Mission-Forces-02 The spacecraft shall withstand vibrational loads induced by the LV. *This requirement ensures that the spacecraft can survive and fulfill the mission.*

LCSR-Mission-Forces-03 The spacecraft shall withstand forces induced by its systems. *This requirement ensures that the spacecraft can survive and fulfill the mission.*

LCSR-Mission-Forces-04 The spacecraft shall withstand vibrations induced by its systems. *This requirement ensures that the spacecraft can survive and fulfill the mission.*

LCSR-Mission-Forces-05 The spacecraft shall withstand lateral launch forces induced by the LV. *This requirement ensures that the spacecraft can survive and fulfill the mission.*

LCSR-Mission-Forces-06 The spacecraft shall withstand acoustic loads induced by the LV. *This requirement ensures that the spacecraft can survive and fulfill the mission.*

LCSR-Mission-ConsMission-01 The mission shall launch no later than 2025. *This requirement ensures that the launch is not indefintely delayed. Delays can significantly increase the cost of the mission.*

LCSR-Mission-ConsMission-02 The sample shall be kept at temperatures lower than 120 K for at least 12 hours after landing on Earth. *This requirement ensures that the sample is useful for the scientific community. Linked to this requirement is the need for the retrieval crew to arrive at the landing site within 12 hours.*

LCSR-Mission-ConsDesign-01 The mission shall not be in violation with any relevant law. *This requirement is important to make sure that the mission can be performed.*

LCSR-Mission-ConsDesign-02 The mission shall have a probability of failure no higher than 5% excluding the launch phase. *This requirement is needed to make sure that the design is of sufficient quality.*

LCSR-Mission-ConsDesign-03 The life cycle cost of the mission shall not exceed €800 million including launch cost. *This requirement is needed to make sure that the mission can be financed by the space agencies involved and/or the scientific community.*

2.2 SAMPLING SITES

As was explained in the Mid-Term Report, several factors need to be taken into account for the choice of the sampling site. Firstly, the temperatures in the chosen site must never be higher than 120 K because of the requirements on the sample. The temperatures inside craters on the south pole have been measured by the DIVINER mission [2]. Secondly, the steepness of the landing site should be low such that the spacecraft can safely land. The Lunar Orbiter Laser Altimeter instrument measured the slopes found on the south pole of the Moon [3].

Based on the three factors above, four craters are selected within 370 km from the south pole as possible landing sites. Only the permanently shaded areas of the craters can be used for sampling.

Amundsen The Amundsen crater is the largest crater near the south pole of the Moon. It has been chosen as an option because inside the crater there is a part which is in permanent shade, but also a part which is in sunlight for approximately a quarter of the lunar day [4]. Note that if one desires to land in the area of the Amundsen crater which is only temporarily lit, the launch window will be influenced by this choice.

Shackleton The Shackleton crater is the crater which is closest to the south pole. It has been chosen because it has several spots near its edge which are always in sunlight [5].

De Gerlache The De Gerlache crater has, like Shackleton, been chosen because of the presence of spots in permanent sunlight near the crater edge. However, its minimum temperatures are higher than Shackleton's.

Wiechert J The Wiechert J crater is a medium-sized crater. It has been indicated in Figure 2.2, it can be found at the crossing of the 180° line with the circle, in the lower half of the picture. It has been chosen because it has high minimum temperatures and low slopes. An overview of the craters can be found in Table 2.1.

The characteristics of the craters are shown in Table 2.1.

Table 2.1: Crater characteristics.

Crater name	T_{max} [K]	T_{min} [K]	Steepness [deg]
Amundsen	260	20	5
Wiechert J	120	40	10
Shackleton	100	30	30+
De Gerlache	80	30	15

The subsequent selection was made on basis of maximal environmental temperature, to relieve the thermal and power systems, and surface flatness to facilitate landing. The choice was made to land inside the Wiechert J crater. The region of the Wiechert J, in the direction of the −60° latitude label, is characterised by a large, level area and maximum daytime temperatures of 120 K [6] [2]. Preferably, one of the regions with temperatures not exceeding 110 K would be chosen, to improve sample quality.

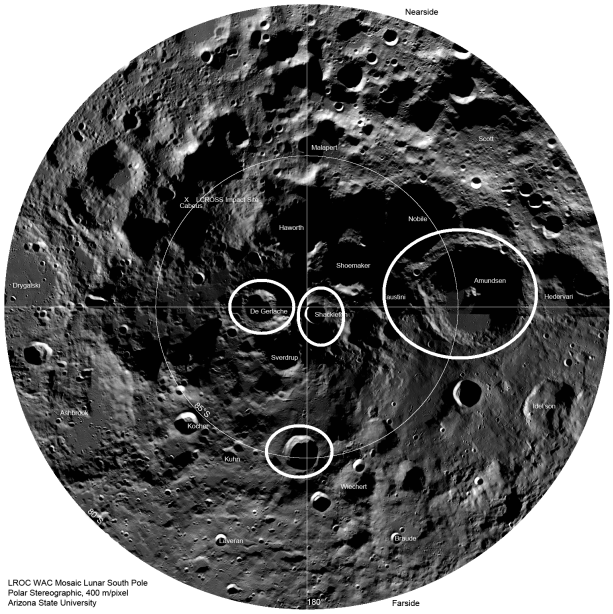

Figure 2.2: Map of the south pole of the Moon [7].

2.3 CONCEPTUAL DEVELOPMENT

After the list of requirements was made and approved by the customer, five concepts for the mission were developed and compared. All five concepts and the trade-off process will be discussed here. Note that all the given cost are in FY2014 €. From the trade-off follows the basis of the final design.

2.3.1. CONCEPT 1

The first concept is based on Luna-16, a Soviet lunar sample return mission. A spacecraft is launched to the Moon, and lands in the area of the Amundsen crater which is lit for a part of a lunar day. A small orbiter is left in low lunar orbit (LLO) to make communication between the lander and Earth possible. The lander is powered by solar panels, and during lunar operations it will be in sunlight. From the lander, a small rover powered with fuel cells drives into the permanently shaded area. The sample is retrieved using the Auto-Gopher drill system, and consists of 20 samples of 0.1 m length. The samples are then stored under multi-layer insulation (MLI) to keep them from heating up while the rover returns to the lander. The samples are moved into the cryogenic tank in the spacecraft with a robotic arm. After this, the part of the spacecraft with the samples inside ascends from the surface of the Moon and returns to Earth. The spacecraft will be brought into trans-lunar injection (TLI) by the Falcon Heavy. The mass of the spacecraft at launch is approximately 10,000 kg, and the total mission cost are €547 M. More information about this concept can be found in [8].

2.3.2. CONCEPT 2

The second concept is based on the Apollo missions. A spacecraft is launched to the Moon. There, an orbiter is left behind with the propellant and engines for the return journey. The rest of the spacecraft lands just outside of the Wiechert J crater, in a lit location. There, a hexapod robot walks into the crater. Its legs are powered by a set of actuators and the power is provided with eight radioisotope thermoelectric generators (RTGs). Upon arrival in the permanently shaded area, the sample is retrieved using a custom drill. The retrieved sample is one 2 m long cylinder. It is put in the cryogenic tank inside the hexapod robot, which then returns to the lander. The entire cryogenic tank is then moved into the part of the spacecraft which returns to the orbiter. After docking, the cryogenic tank is then moved into the orbiter, which returns to Earth. The mass at launch is about 10,600 kg, and the Falcon Heavy will bring the spacecraft into TLI. The total cost add up to €1119 M. More information about this concept can be found in [8].

2.3.3. CONCEPT 3

In the third concept, the re-entry capsule is left behind in an Earth orbit. The rest of the spacecraft launches to the Moon and lands at the edge of the Shackleton crater. It lands at a spot with nearly permanent sunlight, and powers itself with solar panels. A rover, connected to the lander with a power cable, descends into the crater. The sample is extracted with the ExoMars drill and consists of segments of 3 cm. They are stored in sets of four, in 19 cylindrical tubes within the cryogenic tank. After drilling, the rover drops the cable and drives back to the lander, powered by batteries. The drill is left behind at the sampling site. When the rover returns to the lander the cryogenic system is placed into the spacecraft. Part of the spacecraft then ascends and returns to Earth. There, it docks to the re-entry vehicle (RV), to which it transfers the cryogenic system. Finally, the RV returns to the surface of the Earth. At launch, the spacecraft mass is 23,000 kg, which will be launched into Low Earth Orbit (LEO) by the Ariane V ME. The total mission cost is €701 M. More information about this concept can be found in [8].

2.3.4. CONCEPT 4

Concept 4 uses the layout of the Apollo missions. The spacecraft is launched to the Moon and leaves an orbiter in LLO while the rest descends into the Wiechert J crater, landing in the permanently shaded area. There, the lander is powered by an RTG and batteries. The RTG is also the main heat-providing system. Drilling is performed with the ExoMars drill. Samples of 3 cm are retrieved and placed in the cryogenic tank in pairs. After this, the part of the spacecraft containing the cryogenic system ascends to the orbiter. After docking, the cryogenic system is moved into the orbiter, which returns to Earth. 17,900 kg will be launched into LEO by the Proton M, and the cost will be €475 M. More information about this concept can be found in [8].

2.3.5. CONCEPT 5

The fifth concept is very similar to concept 4. It also leaves an orbiter in LLO and lands inside the Wiechert J crater. However, it is powered by fuel cells instead of RTGs. Also, the 3 cm samples are stored in sets of four per sample cylinder. The total mass adds up to 7,000 kg, launched into TLI by the Falcon Heavy, and the total cost is €689 M. More information about this concept can be found in [8].

2.3.6. TRADE-OFF

The five concepts were compared by means of a trade-off. The details of this trade-off can be found in the Mid-Term report [8]. The conclusion of the trade-off was that the best profile for this mission is an Apollo-style concept, which lands inside the permanently shaded areas of the Wiechert J crater, like concepts 4 and 5. The choice was made to use fuel cells and not RTGs. RTGs have become very rare, and are only in the possession of some governments. These will not likely give them up for a short mission, especially not if multiple RTGs are needed to supply enough power. Therefor it was decided that it is better to use fuel cells. Thus, concept 5 becomes the basis of the detailed design phase. Its systems will be developed in more detail in the rest of this report.

3 MISSION LAYOUT

At the start of the detailed design phase the entire layout of the mission must be clear. The first part of this layout is a general overview of the mission, to be used as a base for the detailed discussion of all subsystem in later chapters. The second part is the overall configuration of the spacecraft. The last part are the astrodynamic characteristics of the used trajectories.

3.1 MISSION PROFILE

In order to understand the entire design it is important to know the timeline of the mission. As was mentioned in Chapter 2, the design will consist of an orbiter, ascent stage (AS), descent stage (DS) and RV. The mission profile is illustrated in Figures 3.1 to 3.10.

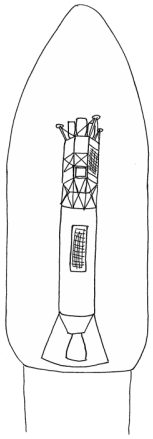

Figure 3.1: The entire spacecraft is within the fairing for launch.

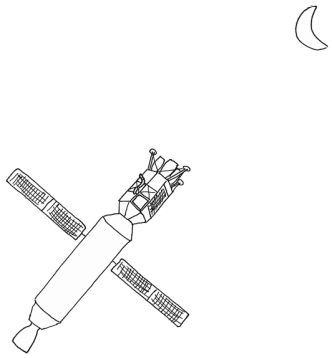

Figure 3.2: The launcher brings the spacecraft into TLI and the spacecraft performs the burns needed to arrive at the Moon.

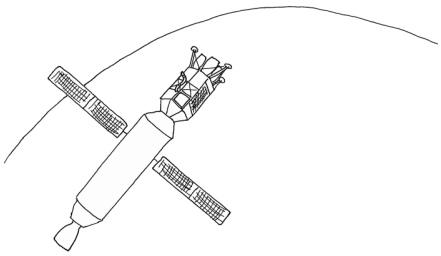

Figure 3.3: The spacecraft is in LLO around the Moon.

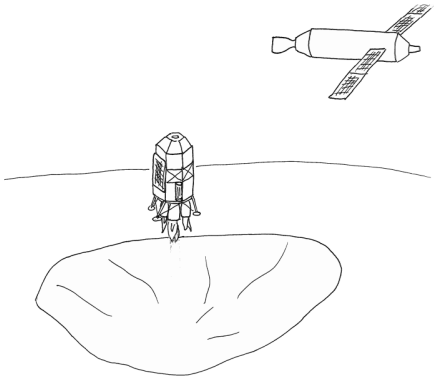

Figure 3.4: The lander descents into the Wiechert J crater.

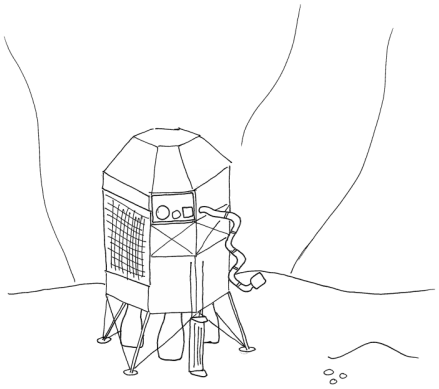

Figure 3.5: The lander stands inside the Wiechert J and retrieves the sample.

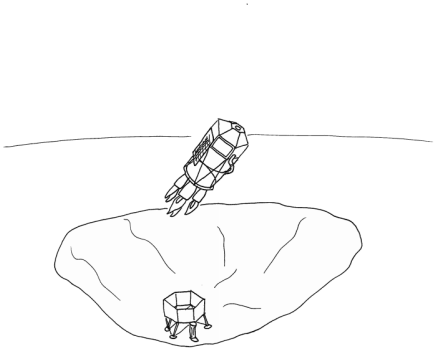

Figure 3.6: The AS ascents to the orbiter, DS stays behind.

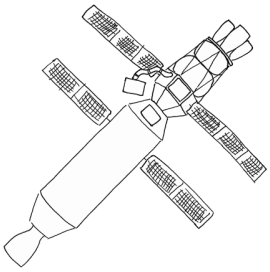

Figure 3.7: The AS and the orbiter are docked together and the samples are moved to the RV.

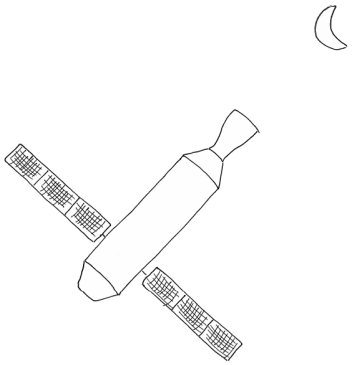

Figure 3.8: The orbiter returns to Earth.

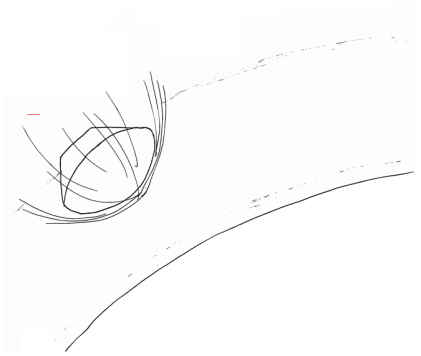

Figure 3.9: The RV re-enters into the Earth's atmosphere.

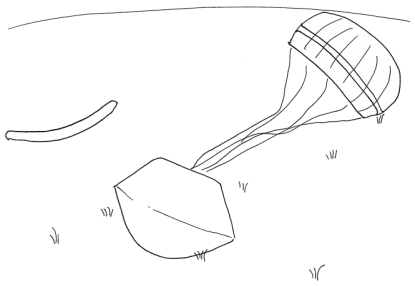

Figure 3.10: The RV has landed and waits for retrieval.

The mission starts with the launch of the entire spacecraft in the Falcon Heavy launcher, as illustrated in Figure 3.1. During the launch phase, all modules are placed within the fairing of the launcher. Most systems are shut down during the launch. The launcher will bring the spacecraft into TLI, where the spacecraft itself takes over. A high-thrust trajectory will follow. The solar panels are deployed and a system check is performed to see if all systems survived the launch. The burns necessary to arrive in the correct LLO are performed. This is illustrated in Figure 3.2.

The spacecraft arrives at LLO Moon approximately five days after launch, as illustrated in Figure 3.3. Another system check is performed to see if all systems are ready for the landing. If any potential problem is identified, the landing can be postponed up to seven days. To start the landing, the lander separates from the orbiter. It lands inside the Wiechert J crater, at 133 km from the South Pole of the Moon [9], while the orbiter remains in LLO, as illustrated in Figure 3.4. The lander is powered by a fuel cell which is placed inside the DS. After touch-down the lander performs a system check to see if any damage was sustained during the landing. Should the check identify any sources of concern, it is possible to postpone sample retrieval operations up to five days. The sample retrieval operations take approximately half a day and are illustrated in Figure 3.5. A delay of another half a day is possible here.

After sample retrieval the DS stays on the Moon's surface while the AS returns to the same orbit as the orbiter, as illustrated in Figure 3.6. It is powered by batteries and solar panels, which are deployed as soon as the AS is out of the crater. In LLO a system check is performed, and a delay of seven days is possible before the AS must be docked to the orbiter. A longer delay would result in missing the window for the return journey. When the AS and the orbiter are docked together, the samples are moved from the AS to the RV using a robotic arm, as illustrated in Figure 3.7. After this is done, the AS undocks again and performs a small burn to gain distance from the orbiter.

When the samples are in the RV the orbiter performs the burns needed to return to Earth, as illustrated in Figure 3.8. Just before the atmosphere of the Earth is reached the RV separates from the orbiter and starts re-entry, as illustrated in Figure 3.9. The RV is powered by batteries only. After touch-down on the Earth surface the RV must be able to keep the sample at temperatures below 120 K for 12 hours, as illustrated in Figure 3.10. Within this time frame the recovery team should arrive at the location of the RV to replace the power supply of the cooling system for the samples.

The entire mission profile, including all functions that need to be performed during the mission, can be found in Appendices A and B.

3.2 OVERALL CONFIGURATION

As explained in Sections 2.3 and 3.1, the spacecraft consists of several modules: an orbiter, a lander and an RV. The lander consists of an AS and a DS. In this section, the entire spacecraft is described and all the important subsystems in each module are discussed. Note that all the subsystems that are included in the spacecraft are designed to operate within the expected space environment. This means they are able to cope with the vacuum of space and the radiation expected during the mission, which does not, for example, include outbursts of solar winds. However, it will for now be assumed that these will not occur during the mission due to the time constraints given for this report. In the future collaboration with the National Oceanic and Atmospheric Administration (NOAA) might be needed, since they specialise in predicting solar flares [10]. Most of the subsystems are space qualified, however some of the used actuators and two of the receivers of the communication system are not. Space-qualified foam radome will be used to cover these components, which will make them able to withstand the space environment [11]. It can thus be concluded that the requirements LCSR-Mission-Environment-01 and LCSR-Mission-Environment-02 have been met which are stated in Section 9.6.

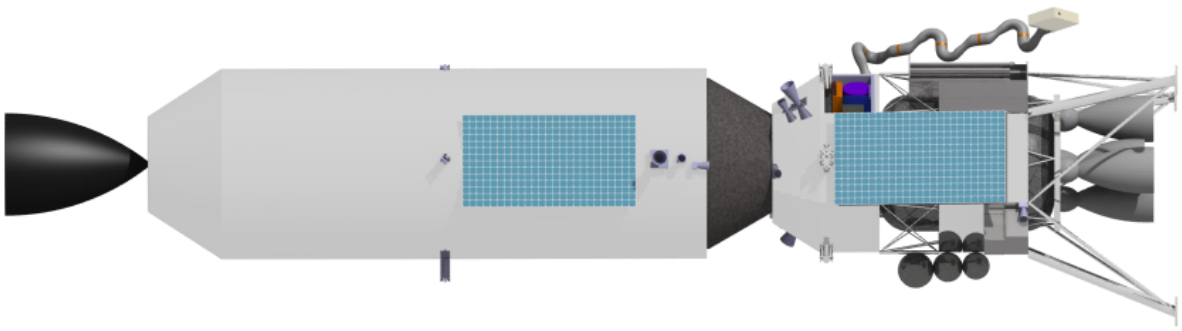

Figure 3.11: CATIA model of the complete spacecraft as it would look like upon arrival in a lunar orbit. From left to right: the orbiter, RV, AS and DS.

The entire spacecraft, as it is put in the fairing of the launcher, can be seen in Figure 3.11. The left part of the image is the orbiter. The orbiter is also illustrated in Figure 3.12. Its main function is to provide the burns

needed for transfer from the Earth to the Moon and back, and to support the other modules where needed. It consists mostly of tanks and an engine used for the burns, stored inside a cylindrical structure. An attitude and orbital control system (AOCS) is needed that is capable of delivering the required precision for the burns to enter the transfer orbits and to perform docking between the orbiter and the AS, as can be seen in Figure 3.7. Communication devices are placed on the orbiter to provide communication with Earth during the entire mission and are used as a communications relay device between the lander and the Earth during the Moon operations. A thermal control system is used to keep all systems at their operating temperatures, and solar panels and batteries are used to power the systems.

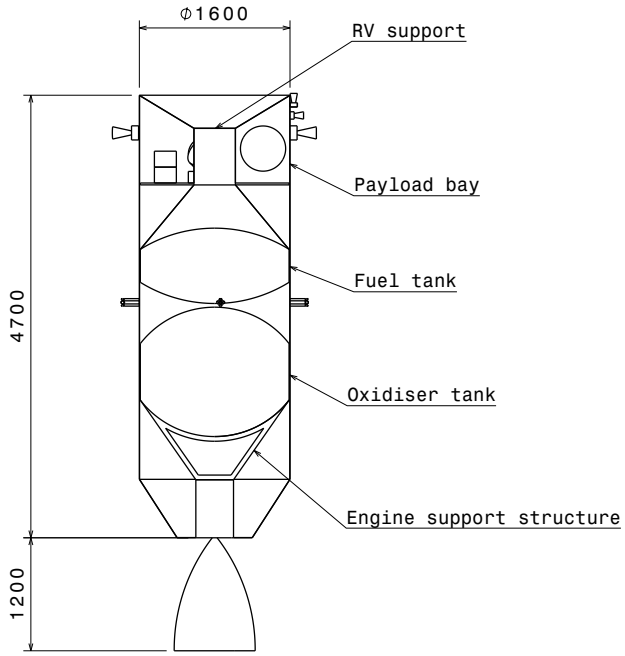

Figure 3.12: Cut-through section of the orbiter.

The RV is placed on top of the orbiter. In Figure 3.11 the RV is the darker part visible directly to the right of the orbiter. The RV can also be seen in Figure 3.13. The RV is used only in the last phase of the mission, during the re-entry phase. This phase of the mission is challenging because the loads and temperatures become far higher than in other phases of the mission. The RV contains a thermal control system capable of keeping the samples cooled during re-entry and the time after touch-down. It contains parachutes and a heat-shield to survive the re-entry as well. In addition, the RV must function for 12 hours after touch-down, to provide time for the retrieval crew to arrive. To make sure retrieval happens before the RV has run out of power, a radio beacon is placed in the RV. Lastly, the RV also contains one half of the docking system, used to dock with the AS. The RV only has batteries as an internal power source. These batteries are used during re-entry. In other phases of the mission, the power is supplied by the orbiter.

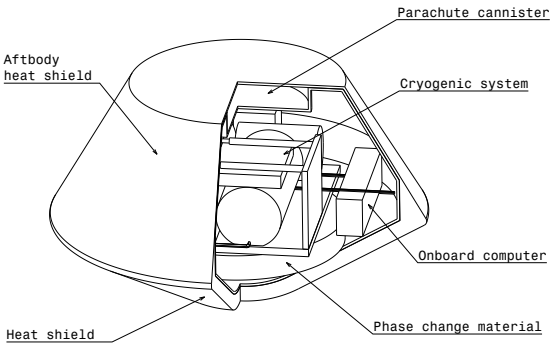

Figure 3.13: Cut-through section of the RV.

The lander is docked to the RV. In Figure 3.11 the lander is visible to the right of the RV. It contains the AS and the DS. The DS is placed around the AS and they are connected with struts. The main task of the DS is to provide the structures needed for landing. As can be seen in Figure 3.14, the landing legs are connected to the DS. The legs need sufficient length to create enough ground clearance and to keep the area around the engines within the AS clear. The ground clearance is needed to prevent pressure building up under the engines during the last phase of the landing. The cleared area to the sides of the engine is needed because the engines will heat up during the landing on the surface, which may damage other systems placed too close to them. As can be seen in Figure 3.14, the DS has three legs. This choice also influenced the shape of the DS, which has become a hexagonal shape built up from panels placed on the legs. On these panels some sensors used for the AOCS are placed. The drill used for sample extraction is placed on the DS, because it is no longer needed after drilling and can be left at the surface of the Moon. To power the subsystems within the DS, a fuel cell is used. This fuel cell is powered up while the lander is still connected to the orbiter and also provides power during the descent to the lunar surface.

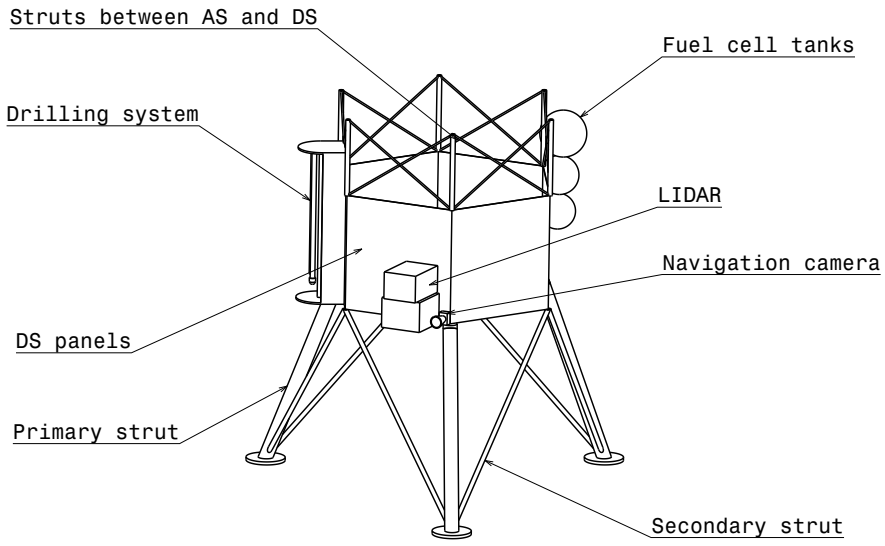

Figure 3.14: Isometric drawing of the DS.

The AS is located within the DS and can be seen in Figure 3.15. It uses the same hexagonal shape as the DS, so the lower part of the AS fits into the paneling of the DS. First, it contains the propulsion system for the descent and ascent phases at the lunar surface. Second, it contains the AOCS for these phases. Third, the cryogenic

system and robotic arm are located within the AS. The samples produced by the drill are placed within the cryogenic system by the robotic arm. The robotic arm is also used to move the entire cryogenic system from the AS into the RV while these are docked together. Fourth, the AS contains the communication systems used while the lander is on the Moon. Last, the AS holds the second part of the docking system for docking between the RV and the lander. During launch, struts are needed to keep the lander and the orbiter stable, because the docking system is not sufficient to withstand the vibrations. These struts are removed after separation from the launcher. While the AS is on the lunar surface, it is powered by the fuel cell within the DS. During ascent and docking operations it is powered by solar panels and batteries.

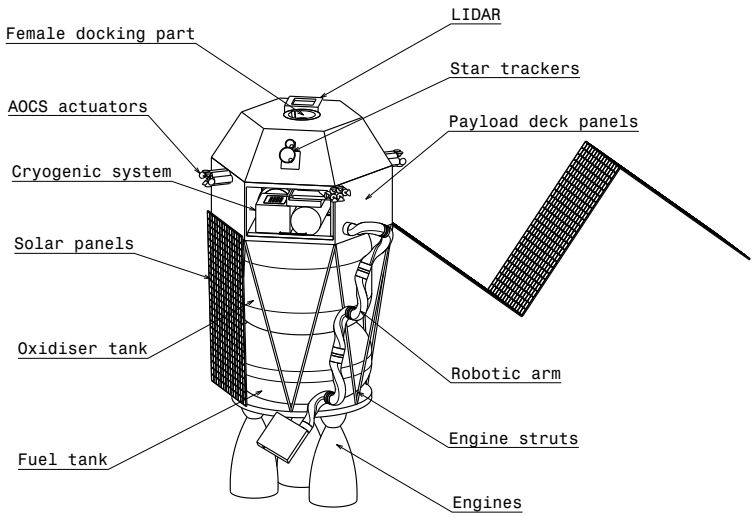

Figure 3.15: Isometric drawing of the AS.

3.3 ASTRODYNAMIC CHARACTERISTICS

This section explains the method used to compute the mission's astrodynamic characteristics, which are obtained from the trajectory's orbital elements and orbital state vectors. The trajectory is defined by propagating known initial values obtained from a ΔV-budget. The trajectory is plotted using a MATLAB simulation, which is purely used for illustration purposes. The simulation uses the spacecraft's position to determine the dominant sphere of influence (SoI), simplifying the trajectory to two separate 2-body problems. The spacecraft velocities at the boundary between Earth's and Moon's SoI are matched in direction and magnitude. This method is referred to as patched conics [12].

3.3.1. ΔV-BUDGET

As said in Section 3.1, the mission will make use of a high-thrust trajectory. Although three-body and low-thrust trajectories were also considered, a high-thrust trajectory is a good candidate for a first-order estimate, given the resources and scope of this design phase.

The trajectory consists of two phases, the first includes the flight to the Moon and the second includes the return flight. The first phase is split again in two parts. One with the spacecraft inside the SoI of the Earth and another one with the spacecraft inside the SoI of the Moon. This section will give the methods to compute the necessary ΔVs required for this trajectory. A Hohmann trajectory is used to calculate all required ΔVs.

First all initial and desired velocities are calculated using Equation 3.1. Here μ is the gravitational parameter of the Moon or the Earth and R is the initial or desired orbit radius. From this equation the geocentric velocity of the Moon (V_{Moon}), the circular velocity of the LEO (V_{LEO}) and the velocity in the desired LLO (V_{LLO}) are found.

$$V = \sqrt{\frac{\mu}{R}} \tag{3.1}$$

Next the Hohmann transfer orbit is calculated with its velocities at perigee and apogee using Equation 3.2. Now

the difference between the circular velocity at LEO and the velocity at perigee is equal to ΔV_1. The difference between the velocity in apogee and the geocentric velocity of the Moon is $V_{\infty,2}$, which is also referred to as the excess velocity. This can be seen in Equations 3.3 and 3.4. When the spacecraft enters the SoI of the Moon, its orbit is a hyperbola. The velocity in the periapsis of this orbit is calculated using Equation 3.5. The second ΔV required is the difference between this velocity and the desired orbit velocity of the circular LLO, which can be found in Equation 3.6.

$$V = \sqrt{\mu_{Earth}\left(\frac{2}{r} - \frac{1}{a_{transfer}}\right)} \tag{3.2}$$

$$\Delta V_1 = |V_{perigee} - V_{LEO}| \tag{3.3}$$

$$V_{\infty,2} = |V_{apogee} - V_{LLO}| \tag{3.4}$$

$$V_3 = \sqrt{\frac{2\mu_{Moon}}{R_{LLO}} + V_{\infty,2}^2} \tag{3.5}$$

$$\Delta V_2 = |V_3 - V_{LLO}| \tag{3.6}$$

An inclination change is required to arrive in a polar orbit around the Moon. Instead of performing an inclination change burn at the Earth or at the Moon, a midcourse correction burn is used to arrive north in the SoI. When the spacecraft enters the SoI of the Moon, it will then use the gravitational attraction of the Moon to end up in a polar orbit. Note that this burn can be done at any point during the transfer, and could be even be performed by the launcher if possible.

Here the burn is done half way from Earth to the Moon, minimising the required ΔV. The initial inclination of the LEO and thus the inclination change needed, is a direct consequence of the latitude at which the launch pad is situated. For this mission the Cape Canaveral launch pad is used, which has a latitude of 28.5 ° [13]. This latitude is close to the sum of the angle of Earth's equator w.r.t. the ecliptic plus the angle of the Moon w.r.t. Earth's equator, so the necessary inclination change is kept to a minimum for this mission. The required ΔV is computed using Figure 3.16. In Figure 3.16 first the distances A and B are calculated using the trajectory of the hyperbola inside the SoI, which are then used to calculate θ. This θ can then be used to calculate ΔV_{inc}.

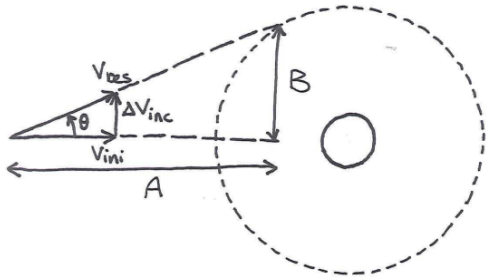

Figure 3.16: Method to calculate required ΔV for inclination change.

After the burn in the pericenter of the arrival hyperbola, the entire spacecraft will be orbiting in a polar LLO, where it has a velocity of 1.63 km/s at an altitude of 100 km. In order to land, this velocity should be nulled. Doing this requires additional ΔV, since some manoeuvring is also required, a 15 % margin is used [14]. To construct a landing scenario, an article written by I. Gerth as been used [15].

The general parameters used for all calculated ΔV budgets are given in Table 3.1. These parameters are used together with the required inputs that consist of the required LEO and LLO altitudes. This resulted in the ΔV budgets to and from the Moon, which are depicted in Tabels 3.2 and 3.3, where the only margin included is for landing and ascending on the Moon.

Table 3.1: Standard parameters and inputs.

Parameter	Value	Units
μ_{Earth}	398,600	km^3/s^2
μ_{Moon}	4,902	km^3/s^2
D_{Moon}	384,399	km
R_{Earth}	6,378	km
R_{Moon}	1,741	km
LEO	185	km
LLO	100	km

Table 3.2: ΔV budget to the Moon, where ΔV_1 is only used for a possible kick stage.

Parameter	Value [km/s]
(ΔV_1)	(3.14)
ΔV_{inc}	0.33
ΔV_2	0.81
ΔV_{Moon}	1.88

Table 3.3: ΔV budget from the Moon.

Parameter	Value [km/s]
ΔV_{Moon}	1.88
ΔV_3	0.81

Using [16] some of these values can be verified. According to [16], a transfer from LEO to TLI (ΔV_1 in Table 3.2) will need 3.1 km/s, which is equal to the value in Table 3.2. According to [16], ascending from the Moon to LLO requires a ΔV of 2.31 km/s, which is slightly above the value mentioned in Table 3.3. This is due to the fact that in this model only a 15 % margin for manoeuvring is used, and in [16] a higher margin of almost 40 % is used, but other sources claim that a 15 % margin is closer to reality [14].

Now all required ΔVs are known, Tsjolkovsky's equation, Equation 3.7 can be used to calculate the required propellant mass [12].

$$\Delta V = I_{sp} g_0 \ln\left(\frac{m_{end} + m_{propellant}}{m_{end}}\right) \tag{3.7}$$

where I_{sp} is the specific impulse of the propellant used and g_0 is the sea level gravity on Earth. m_{end} and $m_{propellant}$ are the end and propellant masses during that burn.

3.3.2. TRANS-LUNAR INJECTION

The simulation starts with the spacecraft in the SoI of the Earth and thus uses an Earth-centered inertial (ECI) frame. First, a circular 185 km orbit with 28.5° inclination is used to establish the initial conditions [13]. The inclination is determined by the location of the Kennedy Space Centre [17]. Second, an elaborated estimate is made to determine the time point when the TLI manoeuvre is initiated. This time point determines the velocity and position vector which are used to propagate the TLI orbit, which puts the spacecraft on an elliptical trajectory around Earth. Third, the mid-course correction (MCC) manoeuvre is executed at the semi-minor axis of the TLI orbit. Last, the Moon's SoI is detected by evaluating the position vector at every time-step, using Equations 3.8 and 3.9. Once the Moon's SoI is reached, the first part of the simulation is terminated.

$$\vec{r}_{sc2SoI} = \vec{r}_{Moon} - \vec{r}_{S/C} \tag{3.8}$$

$$|\vec{r}_{sc2SoI}| < r_{SoI} \tag{3.9}$$

In Equation 3.8, $\vec{r}_{sc2SoI}$ is the distance from the spacecraft to the centre of the Moon, $\vec{r}_{Moon}$ is the position of the Moon and $\vec{r}_{S/C}$ is the position of the spacecraft. All vectors are in an ECI frame, as shown in Figure 3.17. In Equation 3.9, $|\vec{r}_{sc2SoI}|$ is the distance between the spacecraft and the centre of the Moon. The radius of the Moon's SoI (r_{SoI}) is calculated in Equation 3.10 [18].

$$r_{SoI} = a_{Moon}\left(\frac{m_{Moon}}{m_{Earth}}\right)^{\frac{2}{5}} \tag{3.10}$$

In Equation 3.10 a_{Moon} is the semi-major axis of the Moon's orbit and m_{Moon} and m_{Earth} are the masses of the Moon and the Earth, respectively.

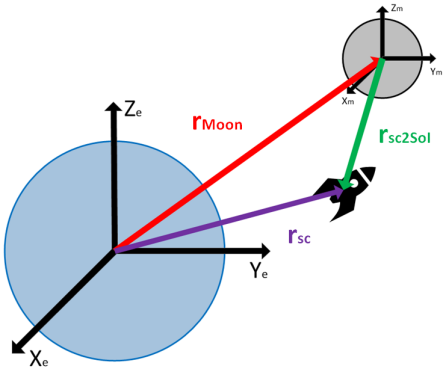

Figure 3.17: Earth, Moon and spacecraft in ECI reference frame.

The orbital elements of the three orbits in the first part of the simulation are given in Table 3.4. The followed trajectory is indicated in Figures 3.19 and 3.18.

Table 3.4: Orbital parameters outside the Moon's SoI.

Phase	a [km]	e [-]	i [deg]
LEO	185	0	28.5
TLI, before MCC	196,400	0.97	28.5
TLI, after MCC	204,583	0.94	40.5

The values in Table 3.4 show that both the TLI orbit and the orbit after the mid-course correction are elliptical orbits and allow the spacecraft to reach the Moon's SoI. This is indicated by the fact that both orbits have an eccentricity smaller than 1 and a semi-major axis larger than 159,151 km, which is half of the distance between the Earth and the start of the Moon's SoI. The mid-course correction introduces a 12° increase in the orbit's inclination and an increase of the orbit's semi-major axis. This is logical since the manoeuvre involves a velocity increase normal to the orbit plane.

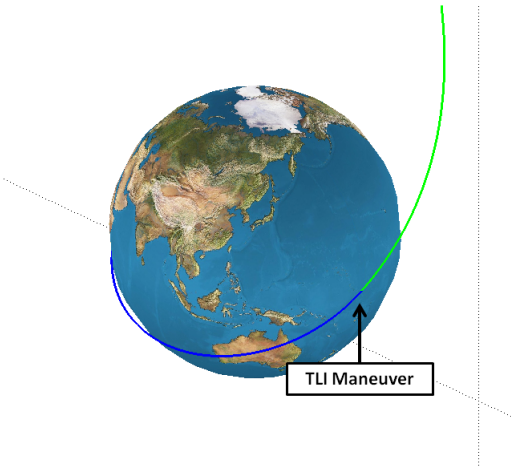

Figure 3.18: Trajectory plot from LEO to the Moon's SoI. This figure focuses on Earth in order to show the TLI manoeuvre.

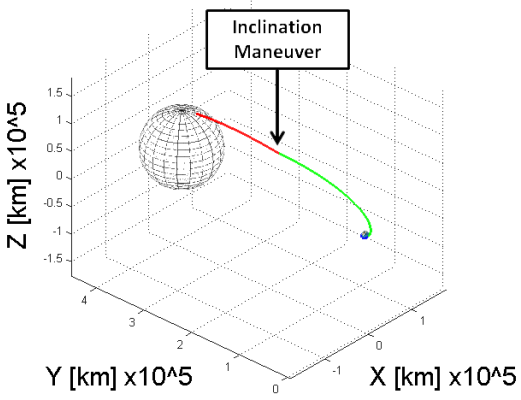

Figure 3.19: Trajectory plot from LEO to the Moon's SoI. The large sphere indicated the Moon's SoI.

The simulation indicates that the time required to reach the Moon's SoI is 3.67 days. Given that Apollo missions took about 3 days from the moment the TLI manoeuvre was started until a stable LLO was reached [19], it is concluded that the time estimated by the simulation is within reasonable bounds.

LAUNCHER SELECTION

Considering the total wet mass shown in Section 9.1, 6527 kg, only a few launchers are capable of launching the Lunar SECRet mission to the Moon. This list of launchers can be found in Table 3.5.

Table 3.5: List of launchers considered [20] [21] [22] [23] [24].

Parameter	Falcon Heavy	Falcon 9	Ariane V ES/ECA	Delta IV-H	Proton-M	Atlas V 551/HLV	Unit
$h_{fairing}$ min(/max)	13.10	13.10	12.70 (/17.00)	19.72	13.31 (/15.26)	20.79 (/26.50)	[m]
$d_{fairing}$	5.20	5.20	5.40	5.00	4.36	5.40	[m]
$m_{payload,launch}$ LEO	53,000	13,150	21,000	27,569	23,000	18,814	[kg]
$m_{payload,launch}$ TLI	13,200	?	?	?	?	?	[kg]
Cost	98.5	39.4	87.6	232.1	76.7	126.4	[M€]
a_{axial}	6.00	6.00	4.55	6.00	5.10	6.00	[g]
$a_{lateral}$	2.00	2.00	0.25	2.00	0.90	2.00	[g]

The most prominent features of Table 3.5 are all the question-marks in the '$m_{payload,launch}$ TLI'-row. This is due to the fact that for all launchers except the Falcon Heavy the launch capabilities into TLI are unknown. Having the spacecraft launched into TLI is preferred over being launched into LEO, because no kick stage is needed. A kick stage increases the cost and risk of the mission. This was the main reason that the Falcon Heavy is chosen for this mission.

Short calculations showed that when a kick stage is used the wet mass would then be around 14 tons. Using this design, the cost of the spacecraft would increase as well. However, the design would fit in the Proton M, which is a cheaper option than the Falcon Heavy. The Proton M, however, will not be in use any longer in 2025 [23]. The Ariane V is also cheaper than the Falcon Heavy, and can launch 14 tons into LEO. However, its reduction on cost is counterbalanced by the added cost and risk of adding another stage to the spacecraft itself. Thus, when looking at cost and reliability, the Falcon Heavy is the best available choice.

The midcourse correction used in Subsection 3.3.2 could also be performed by the launcher, if the launch mass is not close to the launcher capabilities. For this design, the spacecraft will perform the midcourse correction itself, so more options remain open. This means that, should the launcher be capable of performing the mid-course correction, the spacecraft will be smaller than expected and therefore more extra space is available in the launcher vehicle, which could be used for a dual launch.

3.3.3. INSIDE SPHERE OF INFLUENCE MOON

As soon as the spacecraft enters the SoI of the Moon, the primary gravitational influence on the spacecraft is from the Moon. For this reason, a Moon-centered inertial frame is used for the simulation.

As can be seen in Subsection 3.3.1, the spacecraft will end up in a hyperbolic orbit around the Moon. In order to end up at a LLO altitude of 100 km, the spacecraft has to enter the SoI at a vertical altitude of $4.36 \cdot 10^4$ km. While calculating the required ΔV for the mid-course correction burn, this arrival altitude has been taken into account. As soon as the spacecraft is close to periapsis, the circularising burn is initiated.

The orbiter will remain in this 100 km altitude LLO until the return back to Earth. At some point the lander detaches from the orbiter, in order to lower its periapsis. The landing sequence described in [15] requires a periapsis at an altitude of 15 km at an arc length of 500 km with respect to the landing site. Using this information in combination with the coordinates of the wiechert J crater, the location for the initiation of the landing sequence can be computed. In Figure 3.20a a 2D-view of the LLO and the lowering periapsis phase (clockwise from the dot close to the North pole) can be found.

The landing sequence from the 15 km periapsis will be described in Subsection 3.3.4, therefore this part of the trajectory is intentionally left blank in Figure 3.20a.

After the mission phase on the Moon has been completed, the AS has to return to the orbiter. In Figure 3.20a the dot close to the South pole represents the location of the wiechert J crater. From this point, the landing

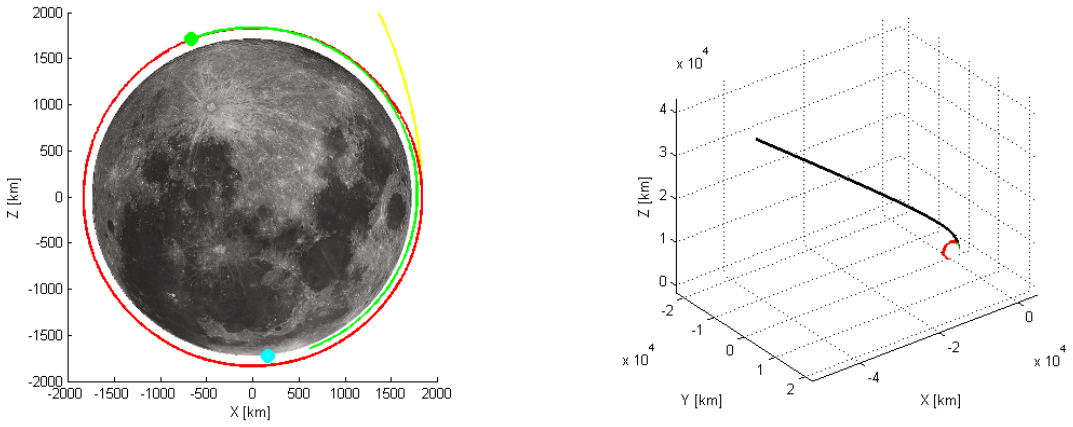

(a) Zoomed in 2D-view. **(b)** 3D-view.

Figure 3.20: Simulation inside Moon's SoI.

sequence will be used backwards to return to LLO, where the orbiter resides. In order to land and take-off, the lander and AS both require a ΔV of 1.88 km/s, which is the circular velocity of the orbiter plus a 15 % margin for manoeuvring.

The semi-major axis, a, the eccentricity, e, the inclination, i, and the elapsed time for each segment of the mission inside the SoI can be found in Table 3.6.

Table 3.6: Orbital parameters inside the Moon's SoI.

Phase	a [km]	e [-]	i [deg]	t [hrs:min]
Hyperbola	-7,515	1.24	86	17:48
LLO (1 revolution)	1,835.9	0	86	1:58
Lowering periapsis	1,793.5	0.024	86	0:56

According to Table 3.6, one orbit in LLO takes 1:58 hrs, which in combination with the dimensions of the orbit and the Moon makes an eclipse time of 28:22 min.

3.3.4. LANDING AND ASCENT SEQUENCE

In the descent phase the DS has to land inside the Wiechert J crater. A reference scenario of this phase is presented in Figure 3.21. The descent phase begins at the descent orbit insertion (DOI). At this point, the lander performs a Hohmann-transfer to an altitude of about 15 km. Afterwards the main braking phase is initiated at about 500 km downrange of the landing site. This manoeuvre is called and indicated as the power descent initiation (PDI) manoeuvre. During braking the landing site comes into the field of view and is scanned for potential hazardous risks. This point is called the high gate (HG). The main braking procedure finishes at the approach gate (AG) at which the lander was decelerated to about 70 m/s. At the AG the main landing phase starts in which the lander nulls its velocity close above the landing site and retargets to a new landing site if hazards are detected. The point above the landing site is called terminal gate (TG) and prior usually the low gate is reached which indicates the point at which the lander loses visual to the landing site. From the TG the lander descends with a constant speed until touch-down and the descent phase is executed.

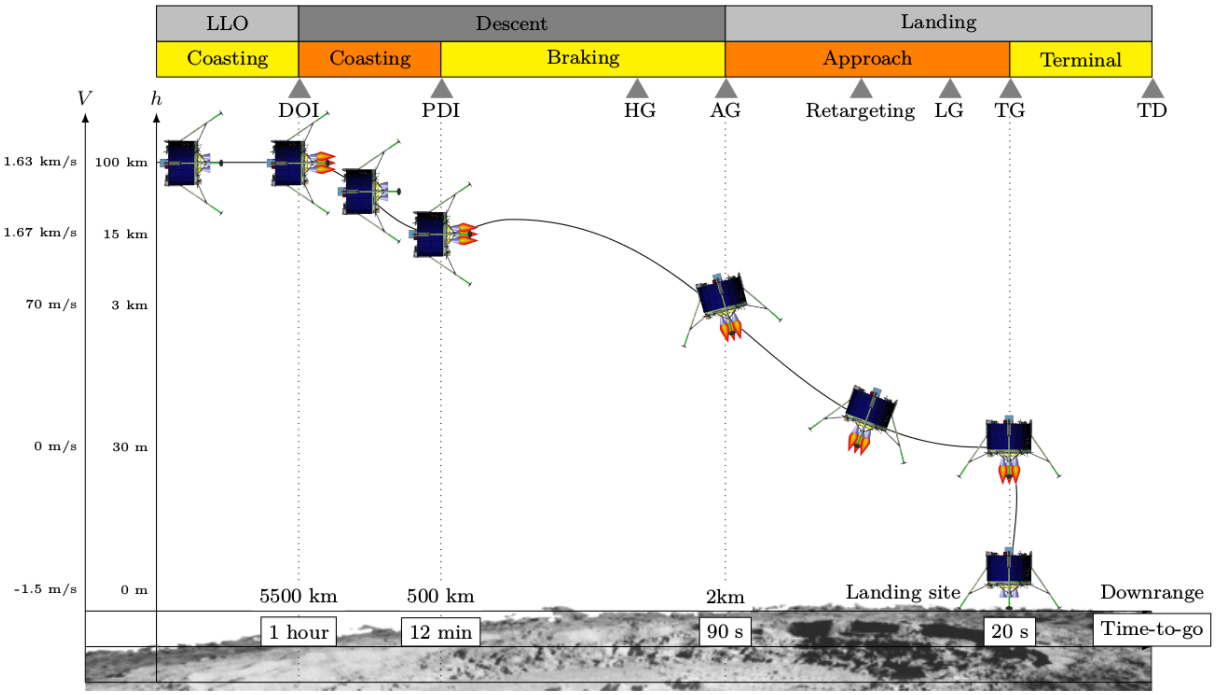

Figure 3.21: Reference landing sequence [15].

A simulation for the main landing phase of planetary landing has been performed and published by I. Gerth and E. Mooij [15]. One simulation has been performed for the ESA Lunar Lander and is chosen as reference for the landing procedure of the Lunar SECRet mission [15]. The simulation starts at the AG with −1601 m downrange, 1569 m altitude with respect to the landing site, 150 m/s horizontal speed and −40 m/s vertical speed [15]. At TG the simulation ends with nulled horizontal speed, an altitude of 15 m and a vertical speed of −1.5 m/s [15]. The duration from AG until TG is stated to be about 43 s long [15]. The last descent duration is derived from the final altitude and constant velocity to be 10 s.

In Figure 3.22 the altitude and downrange of the lander is illustrated. Furthermore, the vectors on the graph are illustrating the direction of the deceleration burns which are initiated every two seconds [15].

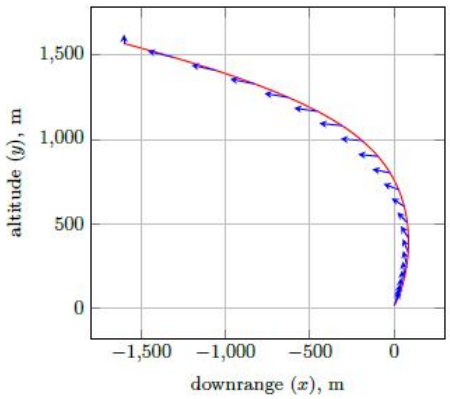

Figure 3.22: Reference landing trajectory [15].

However, the simulation does not account for obstacles during the descent phase. The lander has to land inside the Wiechert J crater which could lead the landing trajectory to interfere with the rim. This risk has been analysed by modelling the complete landing trajectory as an elliptical orbit with a semi-minor axis of 15 km and a semi-major axis of 500 km. The complete trajectory is assumed to be elliptical because in Figure 3.22 the trajectory for the main landing can be identified to be elliptically shaped and according to the scenario outline PDI is at 500 km downrange and 15 km altitude [15]. So at the downrange of −17 km which is at the edge of the

crater, the lander is at an estimated altitude of 3.9 km. Thus the lander does not interfere with the rim of the crater, as the crater is 2 km deep [25].

After drilling, the AS has to ascend to the orbiter. For ascending the same trajectory as simulated for landing is assumed. If the AS performs the descent phase backwards, meaning starting from the landing site with the acceleration vectors in opposite direction, the AS would end up at the same altitude and speed as was the case at DOI of the descent.

Due to time constraints, it was not possible to remodel the simulations. The simulation by I. Gerth and E. Mooij uses the E-Guidance algorithm [15]. It is recommended to create a simulation to analyse the landing specifically for the Lunar SECRet mission. The gravity turn algorithm is advised to be used, since it is easier to program and has been already used by the National Aeronautics and Space Administration (NASA) in the Surveyor program [26].

3.3.5. RETURN TRAJECTORY

As will be explained in Section 7.5, the re-entry phase will start at an altitude of 125 km, with a flight path angle of $-8°$. Take-off at the Moon will happen at an LLO at an altitude of 100 km. Since the simulation is made in the Earth-centered-inertial frame and the Moon-centered inertial frame, problems arise when attempting to merge all the simulations, since the Moon is orbiting around the Earth, and extra velocity components should be added. For this reason the return-trajectory is modelled as Figure 3.23, which is a simple hohmann from the Moon to the Earth. In the ideal case the RV enters the atmosphere in the same direction as the Earth rotates, to minimise the maximum heat load, this direction will be used. Section 7.4 will use this as an input for the calculations performed here.

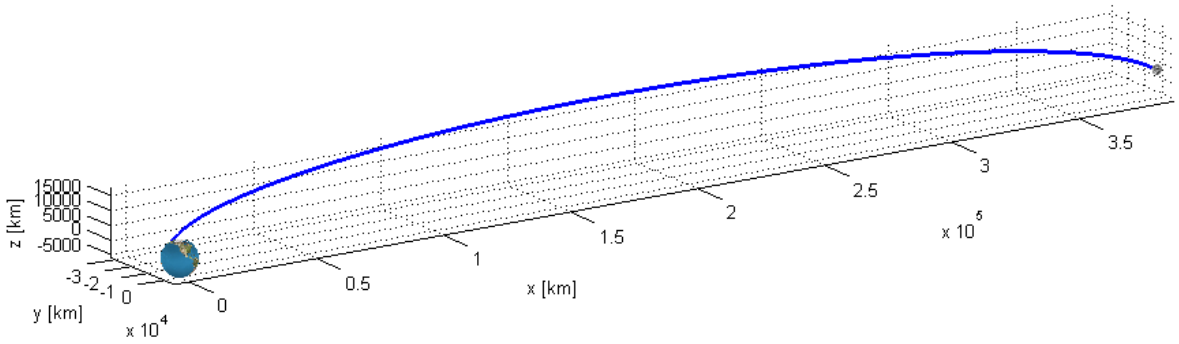

Figure 3.23: Basic return trajectory.

The take-off from LLO into trans-Earth injection (TEI) should be performed such that the final conditions at re-entry are met. The only way the RV can end up at the Earth is when the orbit is oriented in the same direction as when the spacecraft arrives (at 28.5 ° w.r.t. Earth's equator), or at the opposite side (at 18.5 ° w.r.t. Earth's equator). In any other case a burn in the polar orbit will send the spacecraft into deep space. The Moon completes one orbit around the Earth in 27.3 days (one lunar synodic month), which means that the spacecraft has two weeks after arrival until it can return back to Earth. If this window is missed, another two weeks will be added, so the orientation of the Moon w.r.t. the Earth is the same as when the spacecraft arrived (at 28.5° w.r.t Earth's equator).

The landing site on Earth will be the same as for the Soyuz missions, on the steppes of Kazakhstan. This is because an experienced recovery team, used during Soyuz missions, will be present. The cryogenic system is able to keep the sample below 120 K at an outside temperature of 20°C. This is not a problem outside the summer months in Kazakhstan [27]. The coordinates of the landing site are about 50° N latitude and 65° E longitude.

4 METHODS AND TOOLS USED

In order to design the subsystems for each module and stage a set of common methods was used. The methods used for AOCS, thermal system, power system, communication system. structures and margins are discussed, verified and validated in this chapter.

4.1 ATTITUDE AND ORBITAL CONTROL SIZING

In this section the calculation methods for the AOCS and verification and validation of these methods are elaborated.

4.1.1. CALCULATION METHOD

In order to design the AOCS systems the same computation methods were used for the different stages and mission phases. The driving factors taken into account are disturbances of the spacecraft due to gravity and the required force level due to manoeuvre requirements. Disturbances due to solar radiation, magnetic field and aerodynamics are neglected for the following reasons. First, the Moon does not have an atmosphere or a magnetic field. Therefore, there are no significant aerodynamic and magnetic forces acting on the spacecraft except during the re-entry phase. Second, the disturbance due to solar radiation depends on the centre of solar pressure and the surface area of the spacecraft. In SMAD an example for a micro satellite is given [28]and the disturbances due to Earth's gravity and solar radiation are similar. However it is assumed that for heavy satellites the moment of inertia grows more rapidly compared to the surface area of the spacecraft and the distance between the centre of gravity and centre of solar pressure remains small. Thus the disturbances due to solar radiation are neglected. The formula to compute the gravity disturbance is given in Equation 4.1 [28]:

$$t_g = \frac{3\mu}{2R^3} \left| I_z - I_y \right| sin(2\theta) \tag{4.1}$$

where μ is the standard gravitational parameter of the body that is orbited, R is the orbit's radius, I_z and I_y are the mass moments of inertia of the spacecraft and θ is the maximum deviation from the z-axis to the local vertical. The mass moments of inertia were estimated using the Catia model in which for each stage and module an equally distributed mass was assumed. However, the spacecraft is not affected by the disturbance at all times. According to SMAD the disturbance due to gravity appears over a quarter of one orbit and in a sinusoidal fashion [28]. Thus, the total momentum received over time by the spacecraft is defined as followed [28]:

$$h = t_g \frac{T_{orbit}}{4} 0.707 \tag{4.2}$$

where T_{orbit} is the orbital period and 0.707 the root mean square of a sinusoidal function. To compute the disturbance over one day, T_{orbit} can be substituted with the duration of one day, since there is a linear relationship between the orbital period and the disturbance received.

To counteract the induced momentum, the momentum has to be dumped to prevent saturation of the reaction wheels. The thruster force required to dump the momentum is obtained by dividing the to be dumped momentum (h) by the moment arm of the thruster (L) and the burn time t_{burn}. This relationship is defined in Equation 4.3 [28]. Throughout the AOCS sizing a burn time of one second for momentum dumping was decided to be reasonable and used. Additionally, the thruster arm of all thrusters is 0.8 m. The dimensions of the stages are discussed in Sections 5.1, 6.1, 7.1 and 8.1.

$$F_{dump} = \frac{h}{L \cdot t_{burn}} \tag{4.3}$$

For manoeuvres the required force level depends on the required slewing rate. The force level is given in Equation 4.4 and is defined as followed [28]:

$$F_{man} = \frac{I \cdot \ddot{\theta}}{L} \tag{4.4}$$

where I is the moment mass of inertia, L is again the moment arm of the thrusters and $\ddot{\theta}$ is the angular acceleration rate. The angular acceleration rate is further defined in Equation 4.5 [28]:

$$\ddot{\theta} = \frac{\dot{\theta}}{t_{burn}} \tag{4.5}$$

where t_{burn} is again the burn time of the thrusters and $\dot{\theta}$ is the angular velocity.

From the thruster force levels and the number of pulses, the required propellant for each stage or mission phase can be computed. For momentum dumping, one pulse over each axis is needed. For manoeuvres, two pulses over each axis are needed. One pulse initiates the slew rate and a second one stops it. The number of pulses are therefore defined in Equations 4.6 and 4.7:

$$P_{dump} = 3 \cdot t_{op} \cdot x_{dump} \tag{4.6}$$

$$P_{man} = 6 \cdot x_{man} \tag{4.7}$$

where 3 expresses the the one pulse for each axis, t_{op} is the operational time of the mission phase in days, x_{dump} is the number of dumps per day, 6 expresses the two pulses for each axis, and x_{man} is the number of manoeuvres required for the stage or mission phase.

Finally, the propellant mass can be computed by dividing the total impulse by the specific impulse multiplied by the gravitational constant. The propellant mass is defined in Equation 4.8 as followed [28]:

$$m_P = \frac{I_p}{I_{sp} \cdot g_0} = \frac{\sum F_i \cdot t_{burn_i} \cdot P_i}{I_{sp} \cdot g_0} \tag{4.8}$$

where the total impulse (I_p) is the sum of impulses needed in each spacecraft stage or mission phase.

4.1.2. VERIFICATION AND VALIDATION

To efficiently perform the calculation, a MATLAB program was created. This model was then verified by using a random input and performing the calculation with the same input by hand. The output of the hand calculation and that of the program was similar. A maximum deviation of 0.04 % was found. This can be traced back to rounding errors.

Furthermore, the method used was validated. Since no experimental data is present to validate it, the method was analysed for unit consistency and appliance to physical laws. During the analysis a mistake in the method explained in SMAD was found [28]. The disturbance received was calculated for one orbital period but was in the further calculation used as the disturbance for a complete day. The mistake was confirmed by I. Gerth [29] and has been corrected in the calculation method.

4.2 THERMAL SYSTEM SIZING

For the thermal control system the thermal equilibrium temperature is calculated, if this equilibrium temperature is within a certain range it is assumed that the thermal control system can distribute the heat within the spacecraft. The temperature range is elaborated on in Section 5.3. The method to calculate the thermal equilibrium temperature is extensively explained in the Mid-Term report [8], a small summary is provided in this section.

4.2.1. THERMAL EQUILIBRIUM TEMPERATURE MODEL

In this subsection the model created for the thermal equilibrium temperature is discussed. First the equations and parameters are explained, and lastly the assumptions for the model. The thermal equilibrium is determined by the amount of heat that enters and leaves the system. In space there is no heat flow due to conduction and convection out of the spacecraft due to the absence of a medium. The heat flow between the spacecraft and the environment therefore consists of radiation only and follows Equations 4.9 and 4.10. It should be mentioned that on the Moon there is conduction between the spacecraft and the lunar surface. Its effect however is small since the lunar surface has a very low thermal conductivity, as can be read in Section 6.6 [30].

$$Q_{in} = Q_{out} \tag{4.9}$$

$$Q_{int} + Q_{ext} = Q_{rad} \tag{4.10}$$

In this equation Q_{in} is the incoming heat, Q_{out} is the outgoing heat, Q_{int} is internal heat generated by the power dissipation, Q_{ext} is the external heat absorbed and Q_{rad} is the heat rejected by the spacecraft. The external heat can be split into three main components namely: the contribution from the Sun I_{Sun}, planetary radiation I_{IR} and the albedo effects of the nearby celestial bodies. The magnitude of these contributions depend on the exposed and total spacecraft areas, A, at which they receive their heat and the emissivity ϵ and absorptivity α of the surfaces. The external heat contribution equation is shown in equation 4.11. The heat which radiates out of the spacecraft depends on the total surface of the spacecraft and the emissivity of the area and the temperature of this area, resulting in Equations 4.12 and 4.13. The parameters which can be adapted by the engineer are the sizes of the exposed areas, and the emissivity and absorptivity.

$$Q_{ext} = A_{sun} \cdot I_{Sun} \cdot \alpha \cdot \frac{t_d}{t_{orbit}} + A_{IR} \cdot \epsilon \cdot I_{IR} \cdot F_I + \alpha \cdot I_{Sun} \cdot A_{alb} \cdot \rho_{alb} \tag{4.11}$$

$$Q_{rad} = \epsilon \cdot \sigma \cdot A_{tot} \cdot T^4 \tag{4.12}$$

$$Q_{int} + A_{sun} \cdot I_{Sun} \cdot \alpha \cdot \frac{t_{ecplise}}{t_{orbit}} + A_{IR} \cdot \epsilon \cdot I_{IR} \cdot F_{IR} + \alpha \cdot I_{Sun} \cdot A_{alb} \cdot \rho_{alb} = \epsilon \cdot \sigma A_{tot} \cdot T^4 \tag{4.13}$$

With Equation 4.13 the thermal equilibrium temperature can be calculated. The heat received from the Sun depends on orbit time, t_{orbit}, and the daylight time, t_d. If the equilibrium temperature is within the operational temperature range, 0 to 40 °C, the spacecraft thermal control system will be able to keep all systems operational. The emissivity and the absorptivity depend on the coating used [31] [32]. In the model used only two different coatings are used for the area of the spacecraft. The area of the spacecraft itself is difficult to adjust, since it is constrained by the volume of the spacecraft. However it is possible to artificially adjust the area by using radiators. This will be further elaborated in Section 5.3.

Equation 4.13 was used to create a model to calculate the equilibrium temperature of the spacecraft. The model furthermore consists of simple geometric equations to calculate the outer surface of the spacecraft. The thermal equilibrium temperature model from SMAD [33] was taken and altered for this specific use.

The main assumptions for the model are discussed below. The assumptions for the specific mission phases are stated in their respective part.

Extended surfaces First, there is no radiation from the spacecraft's extended surfaces, like the solar arrays, which re-enters the spacecraft. Normally solar cells can be mounted in such a way that it can be chosen to either let the solar arrays radiate on the spacecraft or not.

Solar array heat All heat produced by the solar cells is radiated on the backside of the solar arrays with additional radiators. The mass for these radiators is incorporated in the power system mass.

Internal heat generated All power generated is converted to heat, this is excluding the second assumption. This mass is incorporated in the power system. Further assumptions for the specific modules will be explained in their own chapters.

4.2.2. VERIFICATION

In this section a verification of the model is discussed. The model is verified by an example calculation from Spacecraft Systems Engineering [32]. The result of the example and model calculation is shown in Table 4.1. The results are 290 and 291 K for the model and verification, respectively. The model is within an acceptable range with respect to the verification, namely 1%. Validation has not been done because no comparable data has been found, however the model is within the state of the art [33].

Table 4.1: Verification of thermal equilibrium temperature.

Parameter	Value model	Value verification	Unit
A_{total}	12.57	4π	[m^2]
A_{sol}	3.14	π	[m^2]
A_{alb}	3.14	π	[m^2]
A_{IR}	3.14	π	[m^2]
α	0.15	0.15	[-]
ϵ	0.15	0.15	[-]
I_{sun}	1,371	1,371	[W/m^2]
I_{IR}	220	220	[W/m^2]
Output			
T	290	291	[K]

In this report the internal heat of the spacecraft is not calculated. First, it requires the relative position and angles of all the surfaces within the spacecraft and second, it is a highly complex model. It is recommended to perform these calculations during further development.

4.3 POWER SUPPLY SIZING

In order to size the elements of the power supply system one first needs to differentiate between the different stages and phases of the mission, as each subsystem may require a different amount of power in each phase of the mission. From this differentiation between phases and stages, a maximum power usage per stage can be found. This value for the maximum power usage will then be used to design the power supply for the specific stage.

4.3.1. METHOD DESCRIPTION

To facilitate the differentiation between mission stages and phases, an excel file was made. A part of the excel file is shown in Table 4.2. In this excel file the first column represents the different subsystems for each mission stage and the first row represent the different mission phases. The four different stages considered here are the AS, DS, orbiter and the RV and the eight different phases are the launch, transfer to the Moon, Moon descent, Moon operations, orbiter, Moon ascent, transfer to Earth and re-entry.

Table 4.2: Power supply sizing tool example.

Orbiter	...	**Orbiter [W]**	**Transfer to Earth [W]**	...
AOCS	...	152.0	152.0	...
Batteries	...	0.0	0.0	...
On-boardcomputer	...	26.3	26.3	...
Communication	...	90.0	90.0	...
Cryogenics	...	0.0	480.0	...
...	...	...	...	...
Total	...	383.2	1,068.9	...

With this summation, the total power need is determined for a stage. Of this total power need, 10 % is used

for power distribution, which includes cable losses [33]. 5 % of the total power need is made up of additional equipment not currently taken into account.

When all subsystem power requirements, including the power requirements for the power distribution system and additional equipment, are put into the excel file, the maximum power usage will be used to design the power supply of the specific stage. However, care has to be taken whether a stage uses solar panels, fuel cells or batteries (rechargeable or non-rechargeable). For all of the three options values of their specific energy/power and energy/power density are required. These values are presented in Table 4.3.

Table 4.3: Values of power supply design parameters.

	Specific power [W/kg]	**Power per unit area [W/m^2]**
Solar cells [34]	475.0	399.0
Solar cells (including array and cables)	158.3	399.0
	Specific energy [Wh/kg]	**Energy density [Wh/l]**
Battery rechargeable [35] [36]	150.0	230.0
Battery non-rechargeable [37]	500.0	470.0
	Specific power [W/kg]	**Power density [W/l]**
Fuel cells [38] [39] [40]	300.0	318.0
Fuel cells (including cable losses and housing) [38]	250.0	255.0

It should be noted that the value associated with "Solar cell (including array and cables)" was determined using [41], where it was stated that power generation was a third of the mass of the entire power supply system. It was assumed that the decrease in specific power was due to increased thickness of the solar cell and therefore the power per unit area would remain equal. Furthermore, the fuel cells as specified in [38] did not specify a power density. Therefore it was chosen to determine the power density by looking at commercially available fuel cells as found in [39] and [40]. From [39] one finds an average specific power of 250 W/kg with a power density of 326 W/L and from [40] one finds an average specific power of 250 W/kg with a power density of 204 W/L. Defining the average fuel cell density as average power density divided by the average specific power one can compute an average density of 1.08 kg/L. Thus a fuel cell with a specific power of 300 W/kg will have a power density of 318 W/L. Taking into account a margin of 20% for power density, because of cable losses and fuel cell housing, and using the lower value as specified by [38] one finds a fuel cell with a specific power of 250 W/kg with a power density of 255 W/L.

4.3.2. SOLAR PANEL SIZING

In Section 3.2 it was stated that the orbiter module and the AS will both use solar panels for their in orbit phases. The reason for the solar panel on the AS is because, as stated in Section 3.1, the AS has to survive on its own in orbit. Because the module/stage will experience a solar eclipse in the chosen orbit, the module/stage will need batteries to keep functioning during the eclipse. The batteries should have enough energy to generate the amount of power required during the eclipse period and the solar panels should be designed to generate enough power to recharge the batteries during the daylight period. Thus the amount of power the solar panels need to generate can be computed using Equation 4.14 or 4.15.

$$P_{solarpanel} = \frac{P_d t_d + P_e t_e}{t_d} \tag{4.14}$$

$$P_{solarpanel} = \frac{P_d (t_d + t_e)}{t_d} \tag{4.15}$$

where P_d and P_e are the power required during daylight and eclipse respectively and t_d and t_e are the daylight and eclipse time respectively. Equation 4.15 is derived from Equation 4.14 by assuming the power requirement for the eclipse period equals the power requirement during the daylight period. This assumption is made because some subsystems were not designed to the level of detail where their complete required power time evolution is known. However, their power requirement during the daylight period is known and therefore this assumption simplifies further analysis.

4.3.3. BATTERY SIZING

To design the batteries one needs to take into account the fact that batteries can not be completely discharged. This depth of discharge (DOD) needs to be taken into account to make sure the batteries are not destructively discharged. For the rechargeable batteries it was chosen to use a DOD of 50 % because this significantly increases the number of discharge cycles before losing a significant amount of capacity while at the same time having additional capacity in case of peak loads [32] [41]. For the non-rechargeable batteries it was chosen to use a DOD of 85 % to leave additional energy in case of higher power demands.

4.3.4. VERIFICATION AND VALIDATION

Using the methods as described above, one can design the power supply system of a module/stage equipped with either a solar panel, batteries, fuel cells or a combination thereof. However, such a method needs to be verified and validated.

Verification was done by filling in numbers in the Excel file and checking the calculation by hand. The answers computed were rounded to one digit after the decimal point. The input data and the output data are shown in Tables 4.4 and 4.5 respectively.

Table 4.4: Input for power supply verification.

Parameter	Value [W]
AOCS	100.0
Batteries	20.0
Boardcomputer	50.0
Communication	100.0
Cryogenics	600.0
Cryogenics for fuel cells	20.0
Docking operations	100.0
Drill	20.0
Hazard avoidance	20.0
Propulsion	50.0
Robotics	110.0
Structures and mechanisms	30.0
Thermal	261.4
Power distribution	174.3
Additional	87.2
Total	1,742.9

Table 4.5: Output data for power supply verification.

Parameter	Value excel file	Value by hand	Unit
Power solar panel	2,296.6	2,296.6	[W]
Mass solar panel	14.5	14.5	[kg]
Size solar panel	5.8	5.8	[m^2]
Power battery	1,742.9	1,742.9	[W]
Mass battery	11.0	11.0	[kg]
Size battery	7.17	7.2	[L]
Power fuel cell	1,742.9	1,742.9	[W]
Mass fuel cell	7.0	7.0	[kg]
Size fuel cell	6.8	6.8	[L]

From Table 4.5 it can be seen that the values as generated by the Excel file are identical to the values as calculated by hand. Thus this tool has been successfully verified.

To validate the tool one needs access to power budget of an existing spacecraft, however as no such data was available, the tool cannot be validated. It is however noted that once the validation data of the subsystem power requirements are known, the validation process is identical to the one used for the verification method.

4.4 STRUCTURAL SIZING AND MATERIALS

For the design of the mission, a range of structural methods will be used to analyse the structural integrity of the spacecraft. The structural needs of a spacecraft are mostly driven by the launch environment, in which the structure has to withstand high g-forces as well as vibrations in lateral and axial direction. The maximum values that will be designed for are shown in Table 4.6, which is derived from the characteristics of the Falcon 9. The spacecraft will be launched using a Falcon Heavy rocket, for which no publicly published specifications are currently known. The Falcon Heavy will be a heavy-lift version of the Falcon 9: to get a grasp on the loads for the Falcon Heavy, the launch envelopes of other LVs and their heavy-lift versions need to be examined. For the Atlas V, both the Atlas V 551 and its heavy-lift counterpart the Atlas V HLV have the same lateral and axial g-forces and frequencies as was shown in Table 3.5. It is thus assumed that the Falcon Heavy will have the same launch environment as the Falcon 9.

	Lateral	Axial	Unit
Vibrations	10	25	[Hz]
Accelerations	2	6	[g]

Table 4.6: Falcon 9 envelope [20].

Although the launch environment is crucial there are also other environments to consider. The orbit kick-burns also induce accelerations and the shock loads induced by landing on the Moon need to be taken into account. The structural design and the choice of materials are strongly coupled. The most important consideration when choosing materials is its capability to operate in extreme space environments. The methods used are described below as well as a verification and validation. At the begin of each method the assumptions will be given that were used in the analysis together with their impacts on the validity of the analysis. Acoustic noise causes thin panels to vibrate with large displacements which is harmful for hardware mounted to it. No detailed analysis of acoustic noise could be made due to constraints on time resources. The effect of acoustic noise will tried to be circumvented by designing some panels somewhat thicker than required and by avoiding placement of important hardware on thin panels. To provide more structural rigidity, the panels will be clamped where possible to avoid large displacements. As such requirement LCSR-Mission-Forces-06 is satisfied.

4.4.1. FAILURE MODES

For each structural component, three failure modes are examined:

Buckling failure Buckling occurs for structural components under compression when the critical buckling load is achieved. Three cases of buckling will be examined: buckling of slender members, panels, and cylinders. When a structure buckles, it deforms and loses most of its capability to carry a load. During analysis of buckling it is assumed that the material does not contain any micro-faults. In reality the material structure is not perfect, which causes the structure to buckle before its predicted buckling load. The equations used to determine the maximum allowed buckling load are given for slender members, panels, and cylindrical structures.

Pure compression When a component is loaded in compression, it can buckle if the member is slender. When the components becomes less slender, pure compression tends to become the dominant failure mode. The allowed compressive force is computed by using Equation 4.16.

$$F_{crit} = \sigma_{comp,yield} \cdot A \tag{4.16}$$

Yielding due to tension Yielding occurs when the structure starts to plastically deform due to tension. Once the yield point is passed, a part of the deformation will be permanent and non-reversible. The allowed tensile force is determined by using Equation 4.17.

$$F_{crit} = \sigma_{ten,yield} \cdot A \tag{4.17}$$

These equations will be used to assess if requirements LCSR-Mission-Forces-01 and LCSR-Mission-Forces-05 are met or not.

4.4.2. STRUT AND LEG DESIGN

A truss is an assemblage of long, slender structural elements (struts) that are connected at their ends. Trusses distribute a load throughout a range of discrete elements. The members are designed as tubular structures. They can be analysed for both the struts connecting the modules and the legs, taking the following assumptions into account:

Truss members are connected by smooth pins. This assumption states that all members are free to rotate around the pinned ends. This assumption causes resulting bending moments to be omitted at the pins. As a result no stresses due to bending will occur in the member.

Loads are applied only at the joints of the truss. Truss theory prescribes that all forces act at the pins of the members of the truss. For the truss structures in the spacecraft design the loads are not applied along the members.

Mass of the members is neglected. The truss also has to carry the forces induced by its own mass, which is a small percentage of the total mass it has to carry. The computed loads will thus be lower than they actually are. However, since the mass-ratio between struts and total structure is small, this difference is negligible.

The first two assumptions cause the members to be two-force members that are only loaded in tension and compression. The stresses by tension and compression are called primary stresses. If pin deformations result in the misalignment of struts, the forces will no longer act through the centroidal axes of the member. This will introduce bending in the structure which causes secondary stresses in the member. Secondary stresses can be neglected if the members are stiff and the joints are rigid. For the analysis of the struts between each spacecraft module, as well as the legs of the DS, the model of Figure 4.1 in coherence with Equation 4.18 is used. In this model, three forces inside the struts are computed as a function of the resultant force R. Members 1 and 3 are defined as the secondary struts. Member 2 is defined as the primary strut.

$$\begin{bmatrix} \frac{x_{outw,1}}{D_1} & 0 & -\frac{x_{outw,2}}{D_3} \\ \frac{y_h}{D_1} & \frac{y_h}{D_2} & \frac{y_h}{D_3} \\ \frac{z_{outw}+z_{ext,1}}{D_1} & -\frac{z_{outw}}{D_2} & -\frac{z_{outw}+z_{ext,2}}{D_3} \end{bmatrix} \begin{pmatrix} F_1 \\ F_2 \\ F_3 \end{pmatrix} = \begin{pmatrix} R_x \\ R_y \\ R_z \end{pmatrix} \tag{4.18}$$

where the length of each member is described by (see Figure 4.1).

$$D_1 = \sqrt{\left(z_{outw} + z_{ext,1}\right)^2 + y_h^2 + x_{outw,1}^2} \tag{4.19}$$

$$D_2 = \sqrt{z_{outw}^2 + y_h^2} \tag{4.20}$$

$$D_3 = \sqrt{\left(z_{outw} + z_{ext,2}\right)^2 + y_h^2 + x_{outw,2}^2} \tag{4.21}$$

The following distances are defined:

z_{outw} The outward distance of member 2 along the z–axis.

$z_{ext,1}$ The extended distance of member 1 along the negative z–axis.

$z_{ext,2}$ The extended distance of member 3 along the negative z–axis.

y_h The height of members 1, 2 and 3 along the y–axis.

$x_{outw,1}$ The outward distance of member 1 along the x–axis.

$x_{outw,2}$ The outward distance of member 3 along the x–axis.

For the legs, $x_{outw,1}$ and $x_{outw,2}$ are equal, just as $z_{ext,1}$ and $z_{ext,2}$. For the struts between the modules the values will be different for one another. Since the spacecraft has a hexagon shape, the forces are assumed to be evenly distributed along the starting point of the struts in one-sixths of the entire load (see Figure 4.1). This resulting force R is composed of an x, y and z-component force (R_x, R_y and R_z) as was indicated in Equation 4.18. The maximum allowed force before buckling can be determined using Equation 4.22, assuming both ends are free to rotate (as was stated in the assumptions):

$$\frac{F_{crit}}{A} = \frac{\pi^2 EI}{L^2} \tag{4.22}$$

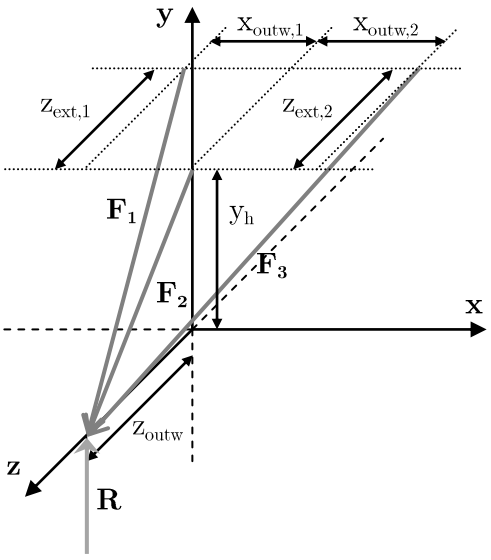

Figure 4.1: Relative positions in the strut structure.

4.4.3. PANEL DESIGN

The AS and DS both have a hexagonal platform composed of six side plates, which protects hardware and passes down the load through the structure. The following assumptions have been made:

Point forces by struts are evenly distributed along the panel edges. The forces that are introduced are assumed to be evenly distributed over the panels. In reality point forces cause high local stresses which have to be accounted for.

The plates are clamped at two sides. Due to the hexagonal shape of the structure, the ends of each panel are clamped. This causes the critical buckling load to increase (see factor k in Equation 4.23).

For buckling of the panels the following equation can be used [41]:

$$\frac{F_{crit}}{A} = \frac{k\pi^2 E}{12\left(1-\nu^2\right)}\left(\frac{t}{b}\right)^2 \tag{4.23}$$

In Equation 4.23 the factor k is dependent on the relationship between the a and b parameters (See Figure 4.2 for the meaning and orientation of a and b in respect to loading). Since both unloaded edges are clamped, it can be seen from Figure 4.3 that the k value is about 7 for almost each ratio of a and b. This is a conservative approach: taking the lower values for the ratio a and b would lead to a higher critical buckling load.

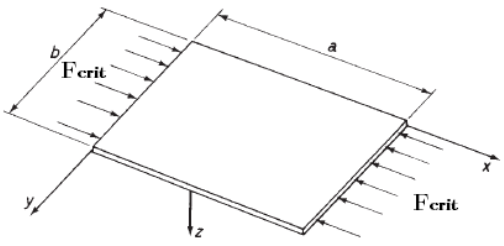

Figure 4.2: Buckling a flat skin plate [42].

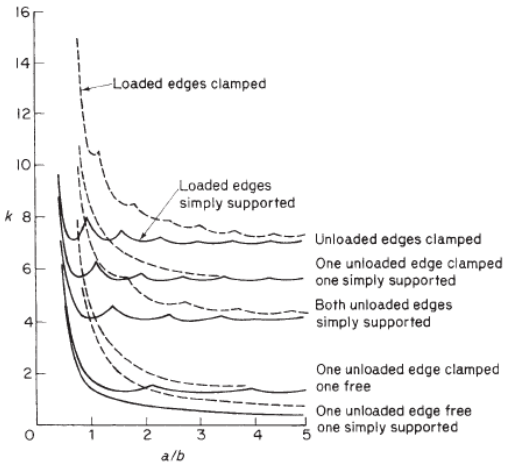

Figure 4.3: Buckling coefficients for flat plates in compression [42].

4.4.4. CYLINDRICAL STRUCTURES

The orbiter will contain a cylindrical structure that carries the compressional load of the AS and DS including its propellants during launch. Since it is loaded under compression, it should be checked for buckling and pure compression failure modes. For pure compression failure, Equation 4.16 is used. For the critical buckling force of a cylindrical structure, Equation 4.24 is used [41]:

$$F_{crit} = EA\left(9\left[\frac{t}{R}\right]^{1.6} + 0.16\left[\frac{t}{L}\right]^{1.3}\right) \tag{4.24}$$

The definition of the variables of Equation 4.24 is shown in Figure 4.4.

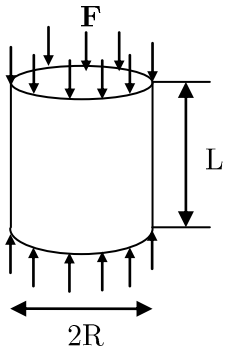

Figure 4.4: Schematic overview of cylindrical parameters.

4.4.5. VIBRATIONAL ANALYSIS

The spacecraft will have to withstand the lateral and longitudinal vibrations during launch. For this the structure should have a sufficient stiffness. The following assumptions have been made:

The struts and the adapter act as springs. Only the struts and the adapter will be assumed to act as the springs in the mass-spring model. The orbiter, AS and DS are assumed to be rigid lumped masses. In reality the structure within the modules will not be completely rigid but will be flexible.

The struts are completely horizontal. The angles between the struts are neglected and assumed to be zero. As a result of this, the stiffness of each strut will be measured along its longitudinal axis. For lateral vibrations this means the stiffness value that is calculated is lower relative to its true value. Since there is an angle between the struts, the diagonal members will have increased stiffness in lateral direction due to part of the beam vibrating in its axial direction: axial stiffness is considerably higher for a long slender member than its bending stiffness. For axial vibrations this means that the diagonal beams lose some of their axial stiffness due to its orientation. However, since axial stiffness is considerably higher than bending stiffness, this difference will be neglected. Using the diagonal struts between the DS and the AS as an example:

$$\frac{\frac{EA}{L}}{\frac{3EI}{L^3}} = \frac{AL^2}{3I} = \frac{3.8\cdot10^{-5}\cdot0.90^2}{3\cdot1.89\cdot10^{-10}} = 5,417 \tag{4.25}$$

This shows that the axial stiffness is $5,417$ as high as the bending stiffness.

The spacecraft fitted in the launch fairing will be modelled using a three degree of freedom system as is shown in Figure 4.5. It will have three masses, which are the orbiter (which includes the RV), AS and DS.

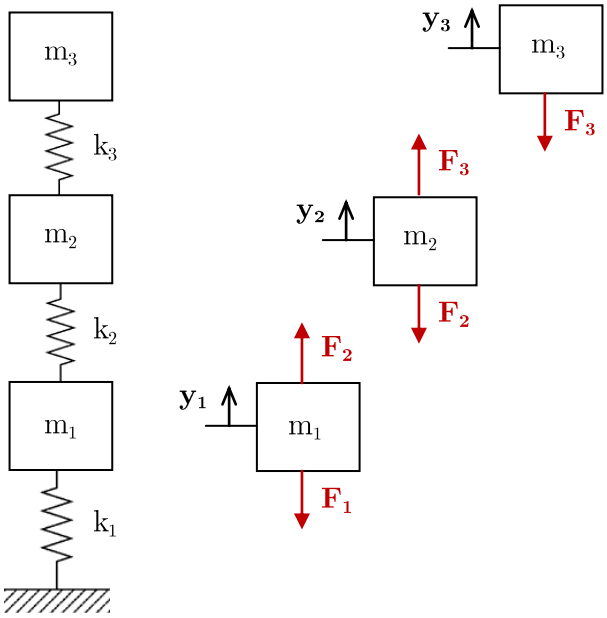

Figure 4.5: Mass-spring system with three degrees of freedom, fixed at the bottom.

The loads will have the following values:

$$\begin{aligned} F_1 &= k_1 \cdot y_1 \\ F_2 &= k_2 \cdot (y_2 - y_1) \\ F_3 &= k_3 \cdot (y_3 - y_2) \end{aligned} \tag{4.26}$$

The equations of motions for the masses are:

$$\begin{aligned} m_1 \ddot{y}_1 &= -F_1 + F_2 \\ m_2 \ddot{y}_2 &= -F_2 + F_3 \\ m_3 \ddot{y}_3 &= -F_3 \end{aligned} \tag{4.27}$$

Combining the above:

$$\begin{aligned} m_1 \ddot{y}_1 + (k_1 + k_2) y_1 - k_2 y_2 &= 0 \\ m_2 \ddot{y}_2 - k_2 y_1 + (k_2 + k_3) y_2 - k_3 y_3 &= 0 \\ m_3 \ddot{y}_3 - k_3 y_2 + k_3 y_3 &= 0 \end{aligned} \tag{4.28}$$

This equation can be written in matrix-vector format:

$$\begin{bmatrix} m_1 & 0 & 0 \\ 0 & m_2 & 0 \\ 0 & 0 & m_3 \end{bmatrix} \begin{Bmatrix} \ddot{y}_1 \\ \ddot{y}_2 \\ \ddot{y}_3 \end{Bmatrix} + \begin{bmatrix} k_1 + k_2 & -k_2 & 0 \\ -k_2 & k_2 + k_3 & -k_3 \\ 0 & -k_3 & k_3 \end{bmatrix} \begin{Bmatrix} y_1 \\ y_2 \\ y_3 \end{Bmatrix} = \begin{Bmatrix} 0 \\ 0 \\ 0 \end{Bmatrix} \tag{4.29}$$

or, in short:

$$\mathbf{M}\underline{\ddot{y}_1} + \mathbf{K}\underline{y_1} = \underline{0} \tag{4.30}$$

Since all struts are assumed to be parallel to one another, the equivalent spring stiffness of all struts between a module can be added up. To determine the natural frequencies of the entire system, the characteristic equation of Equation 4.31 has to be solved for both lateral and longitudinal vibrations.

$$\det(\mathbf{M} - \omega_{nat}^2 \mathbf{K}) = 0 \tag{4.31}$$

Solving the characteristic equation will yield three natural frequencies for each case. These values should exceed the values that are given in Table 4.6. The vibrational analysis will be discussed in Section 8.5.

4.4.6. MATERIALS

The materials used for the spacecraft structure must allow the spacecraft to successfully perform its mission while keeping mass low. For this a high specific strength is needed and a high specific stiffness. Several candidates were considered for the structural components: magnesium, aluminium, steel, titanium and carbon materials.

Aluminium 6061 was chosen: a space-graded alloy used for all components, because of its high specific strength and easy formability relative to the other space materials [32]. It is a material that is used in lander configurations and will be applied as the primary material in the Lunar SECRet mission [43]. It is cheap and widely available, unlike titanium, which is expensive to procure and hard to form [44]. Magnesium has a good specific strength but is less workable than aluminium. It is also chemically active and requires a surface coating making it more expensive to produce [44]. Steel was not used because of its low specific strength. Carbon materials are very lightweight and have excellent thermal resistance, and are used in spacecraft struts [44]. However, the wide availability and low cost of aluminium made it to be the best choice for the spacecraft. The material properties of aluminium 6061 can be found in Table 4.7.

Property	**Value**	**Unit**
Young's modulus	68.9	[GPa]
Yield strength	276	[MPa]
Compressive strength	276	[MPa]
Density	2,700	[kg/m^3]
Poisson's ratio	0.33	[-]

Table 4.7: Aluminium 6061 material properties [45].

The compressive strength is assumed to be equal to the tensile yield strength. Due to the use of the same material everywhere, thermal stresses caused by expansion of materials due to heat are avoided for a part.

4.4.7. VERIFICATION AND VALIDATION

The structural methods described in this section are bundled in a code to evaluate the design. To determine the forces in the struts the structure is assumed to operate as a truss structure. As such, bending and shear are by definition neglected. In reality these forces are present and they will thus introduce some error when validating the model. For structural components like the panels and the payload deck panel, a proper finite-element analysis has to be performed to make a first detailed evaluation. However, finite-element analysis of the design also contains errors since the design assumes that the struts pass on point forces which will introduce high local stresses in the model. The way to validate the model is to make a physical model and test it. Lunar conditions can not be properly simulated since the gravity environment is different on the Moon, which is an important aspect to consider during physical testing.

A code was written to apply all the equations mentioned in this section. The code is verified by checking the method with worked-out examples. For the strut structure design, the method was verified using a Statics exam of 2011 [46]. For Figure 4.1 the following inputs were used:

- x_{outw} = 0.3 m
- y_h = 1.2 m for the primary strut, 0.35 m for the secondary struts
- z_{outw} = 0.55 m
- R = 746 N

Running these values in the code yielded a compressive force of 1,046 N in the main strut, and a tensile force of 240 N in the secondary struts. These were the same results as for the exam and thus the code was properly verified. The panel design is verified by applying zero-valued inputs, which resulted in zero forces (as expected).

4.5 COMMUNICATIONS SYSTEM SIZING

A communication system was designed for both the lander and orbiter module, which can be seen in the communication flow diagram in Figure 4.6. The lander module gets input data (e.g. temperatures of the subsystems) which is processed by the onboard computer and sent to the orbiter module using the transmitter and antenna. The lander module can also receive commands (e.g. performing drilling operations for sample retrieval) from the orbiter module by using the receiver and antenna. Furthermore, the orbiter module also gets input data and is able to communicate with both the lander module and an Earth ground station.

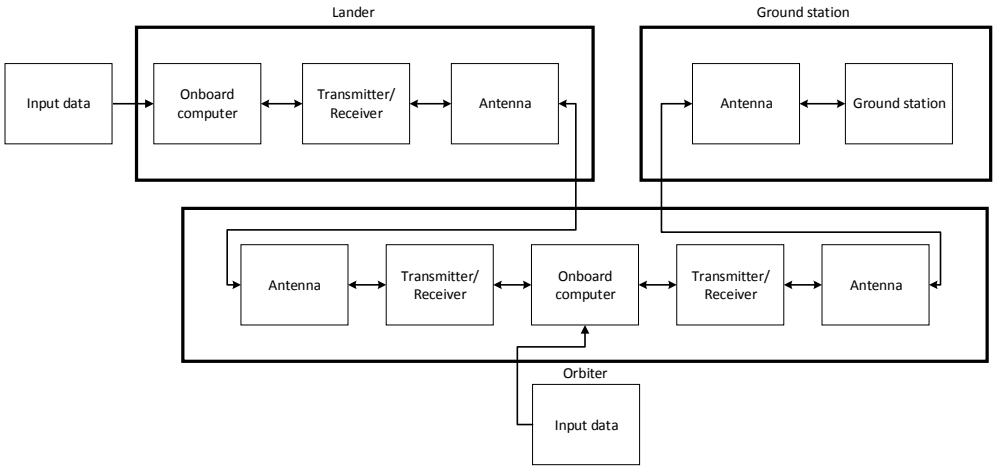

Figure 4.6: Communication flow diagram.

The designs for both modules were started by performing a link budget calculation. In order to perform the link budget calculations, the visibility time between orbiter and lander per orbital period was needed to be determined for both the orbiter and lander module. An estimation of the visibility time was made in a 2D plane, as can be seen in Figures 4.7 - 4.9.

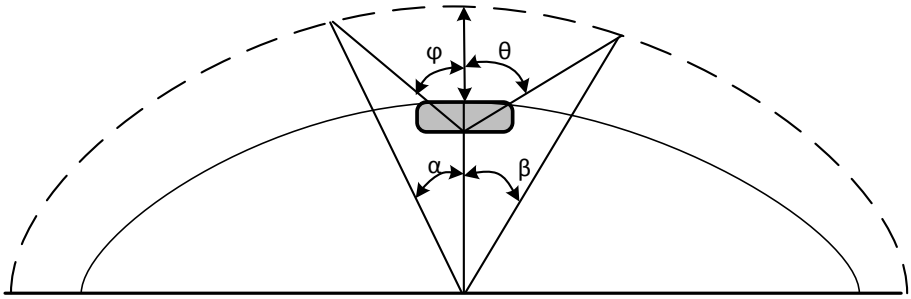

Figure 4.7: Angle definition of the visibility problem.

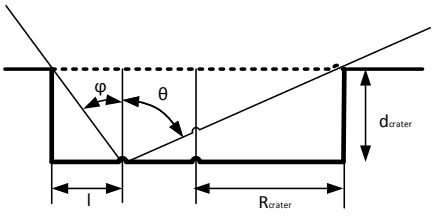

Figure 4.8: Zoom-in of the crater angles.

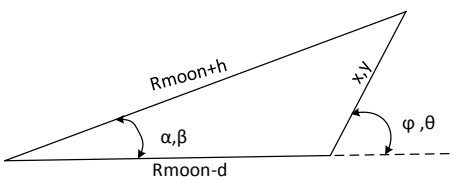

Figure 4.9: Zoom-in of all angles.

From Figure 4.8 it can be seen that φ and θ can be computed by using Equations 4.32 and 4.33 respectively:

$$\varphi = \arctan\left(\frac{l}{d_{crater}}\right) \tag{4.32}$$

$$\theta = \arctan\left(\frac{2R_{crater} - l}{d_{crater}}\right) \tag{4.33}$$

where l is the distance of the lander with respect to the left side of the crater, d_{crater} is the depth of the crater and R_{crater} is the radius of the crater.

From these angles one can calculate the angles with respect to the Moon's center, as can be seen in Figures 4.7 and 4.9, using the law of cosines twice. The final results are shown in Equations 4.34 and 4.35.

$$x^2 + \left(2\left(R_{moon} - d_{crater}\right)\cos\varphi\right)x - \left(\left(R_{moon} - d_{crater}\right)^2 - \left(R_{moon} + h\right)^2\right) = 0 \tag{4.34}$$

$$\alpha = \arccos\left(\frac{\left(R_{moon} + h\right)^2 + \left(R_{moon} - d\right)^2 - x^2}{2\left(R_{moon} + h\right)\left(R_{moon} - d\right)}\right) \tag{4.35}$$

where h is the altitude of the orbiter above the Moon and R_{moon} equals the lunar radius. One can compute β by changing $\varphi \rightarrow \theta$, $x \rightarrow y$ and $\alpha \rightarrow \beta$ in Equations 4.34 and 4.35 and θ is computed using Equation 4.33.

Using the angles φ and θ, one can compute the visibility time using Equation 4.36.

$$T_{vis} = (\varphi + \theta)\sqrt{\frac{\left(R_{moon} + h\right)^3}{\mu_{moon}}} \tag{4.36}$$

where φ and θ are in radians. The only variable left in these equations is the distance of the lander with respect to the left side of the crater, which was the input of a Matlab code made to find the minimum and maximum visibility time. The inputs of the code are shown in Table 4.8 and the results are shown in Table 4.9. The verification values have been computed by doing the calculations by hand but continuing calculations with numbers rounded to one decimal. These results are shown in Table 4.9.

Table 4.8: Inputs of Matlab code to compute visibility time of the lander to the orbiter.

Parameter	Value	Unit
R_{moon}	1,736	[km]
h	100	[km]
d_{crater} [25]	2	[km]
R_{crater}	17	[km]
μ_{moon}	4,902	[km^3/s^2]

Table 4.9: Minimum and maximum visibility time of the lander to the orbiter.

Parameter	Value code [s]	Verification value [s]
$T_{vis_{min}}$	312	311
$T_{vis_{max}}$	525	523

The minimum and maximum visibility time are obtained when one sets $l = 0$ and $l = R_{crater}$ in Equations 4.32 and 4.33 respectively. This is equivalent to a lander location at the edge and in the middle of the crater respectively.

Now that the visibility time of the lander to the orbiter is known, one needs to know the visibility time of the orbiter to Earth. The method used to estimate this visibility time is equivalent to the method used to compute the eclipse time in Section 3.3 and therefore the results will be identical.

Using the visibility time of the lander with respect to the orbiter and the visibility time of the orbiter with respect to Earth together with the amount of data estimated, one can determine the required data rate. The amount of data was determined based on the number of telemetry (TM) points, each telemetry point represents a sensor that generates data. The number of TM points is dependent on the complexity of the TM system. A simple TM system has a maximum of 200 TM points, whereas a complex TM system has 1,000 or more TM points [41]. The whole spacecraft (including all the stages) has about 4,200 TM points, which can be seen in Table 4.10. The RV module is a simple TM system, because there are not a large number of subsystems with sensors that generate data. The DS and orbiter module are complex TM systems, the AS is an even more complex TM system due the robotic arm and docking system.

Table 4.10: Data generation of stages/modules.

Data generation	TM points	Data rate [bps]
DS	1,000	13,000
AS	2,000	26,000
Orbiter module	1,000	13,000
RV module	200	2,600
Timestamps	-	64
Sensortagging	-	1,680
Total	4,200	56,344

Each TM point generates 8 bytes (equals 64 bits) of data, which is sampled at a sampling frequency of 0.2 Hz (one sample per 5 s) [33]. This results in 13 bps for one TM point. The timestamps in Table 4.10 are needed to assign the time (and date) to each TM and generate 10 bytes per 5 s per system [47], resulting in 64 bps for all systems. Also an additional 3 bytes are incorporated to tag each TM point every minute, which allows the receiver to check whether the signal corresponds to the expected subsystem. Thus, the generated data rate for the whole spacecraft is 56,344 bps. Combining this information with the time for the orbiter to complete one orbit around the Moon, the data generated was determined. The data was then multiplied with the visibility time, which resulted in the data rate R of the communication system. This was used in Equation 4.37, which is part of the link budget analysis. In Equation 4.37 the energy-per-bit to noise-density, E_b/N_o, is calculated [33]:

$$\frac{E_b}{N_o} = EIRP + L_a + L_s + L_{pr} + L_i + G_r + 228.6 - 10\log(T_s) - 10\log(R) \tag{4.37}$$

$$EIRP = P_t + L_l + G_t \tag{4.38}$$

$$L_s = 92.45 + 20\log(R) + 20\log(f) \tag{4.39}$$

$$L_{pr} = -12\left(\frac{e_r}{\alpha_{1/2}}\right)^2 \tag{4.40}$$

where EIRP is the effective isotropic radiated power, which is determined in Equation 4.38. In Equation 4.38 P_t is the transmit power, which is specific for each antenna. The transmitter line loss, L_l, has a typical value of -1 dB [33]. Further, G_t is the transmit antenna gain and G_r is the receive antenna gain, these are specific for each antenna. In Equation 4.37 the propagation and polarization loss, L_a, was determined using [33]. L_s is the space loss, which is described in Equation 4.39, where f is the frequency of the signal that is sent. The receive antenna pointing loss, L_{pr}, is described in Equation 4.40, in which e_r is the receive antenna pointing offset and $\alpha_{1/2}$ is the half-power beam width (HPBW). T_s is the system noise temperature, which was determined using [48] and L_i is the implementation loss which has a typical value of -2 dB. After the E_b/N_o was determined, it was checked whether the signal could be sent without too many errors.

In order to send an acceptable signal in terms of the bit error rate (BER), a value of 10^{-5} BER was used to determine the minimum required E_b/N_o [48]. The value of E_b/N_o corresponds to the value of the BER, depending on the type of modulation (e.g. BPSK modulation) that is used [33]. It is also common to include a margin of 3 dB [33]. This means that in order to send a signal with a certainty that there aren't too many errors, the calculated E_b/N_o has to be higher than the minimum required E_b/N_o including the 3 dB margin.

The calculations for the link budget were verified using [33], where a model is given to perform the link budget analysis. After performing the analysis, the results were validated by implementing the inputs of the link budget table in [48]. It was then concluded that the model used in this report is suitable, since the outputs were exactly the same as the one presented in [48]. Also, the model used in this report was compared with the model of [49] and the differences were negligible.

4.6 PROPELLANT TANK SIZING

The required propellant mass is computed by inserting the ΔV values indicated in Section 3.3 into Equation 4.41:

$$\Delta V = I_{sp} g_0 \ln\left(\frac{m_{begin}}{m_{dry}}\right) \tag{4.41}$$

where I_{sp} is the engine's specific impulse, g_0 is Earth's gravitational acceleration, m_{begin} is the mass at the beginning of the manoeuvre and m_{dry} is the mass at the end of the manoeuvre. The propellant mas is defined by Equation 4.42.

$$m_{prop} = m_{begin} - m_{dry} \tag{4.42}$$

The mass of the fuel and oxidiser are computed using Equations 4.43 and 4.44 together with the mixture ratios shown in Table 4.11.

$$m_{fuel} = \frac{m_{prop}}{a+b} \cdot a \tag{4.43}$$

$$m_{oxidiser} = \frac{m_{prop}}{(a+b)} \cdot b \tag{4.44}$$

where m_{prop} is the mass of the propellant and a and b are the propellant's mixture ratio parameters.

Table 4.11: Propellant mixture ratios and density.

Propellant	**a**	**b**	**Fuel density** [kg/m^3]	**Oxidiser density** [kg/m^3]	**Specific impulse** [s]
RP1/LOX	1.00	2.56	806	1140	317
MMH/MON	1.00	2.27	880	1370	325

The propellant mass of those modules/stages equipping fuel tanks is shown in Table 4.12. Once the mass of the fuel and oxidiser is known, the capacity of the corresponding tanks can be estimated using the density of the contained agent. Propellant tanks are only attached on the orbiter and the AS. The propellant type was derived from the engine requirements and the criteria behind engine selection are given in Sections 5.4 and 8.4.

Table 4.12: Propellant mass and tank volume for the orbiter and AS.

Module/stage	**Propellant**	**Fuel mass** [kg]	**Oxidiser mass** [kg]	**Fuel tank** [m^3]	**Oxidiser tank** [m^3]
Orbiter	RP1/LOX	300	1,775	0.373	1.557
AS	MMH/MON	540	1,226	0.614	0.895

Modified Astrium 700 – 1108L Ti6AlV tanks were used, thus the mass of the tank and piping was scaled linearly with the required tank capacity [50]. These are blow-down tanks thus no pumps are needed. The mass of all the propellant tanks is shown in Table 4.13.

Table 4.13: Dry propellant tank mass.

Module/stage	**Propellant**	**Fuel tank mass** [kg]	**Oxidiser tank mass** [kg]
Orbiter	RP1/LOX	45	82
AS	MMH/MON	27	41

4.7 MARGINS

During the early stages of the design, preliminary numerical values for system characteristics have to be generated. This involves giving best estimates for the mass and power required by all subsystems and predicting the ΔV needed for the mission profile. However, as the design matures, the values for these parameters tend to increase as more detail becomes known about the exact layout of the system. To prevent the surprise of values that turn out higher than anticipated and ending up with support systems that are under-designed for the eventual spacecraft, estimated values are artificially increased. This is done by taking consistent margins over

the estimated parameters, where the magnitude of each margin should reflect the level of certainty about the estimate.

Given the level of detail applied in this feasibility study, the parameters for which margins were deemed applicable were mass, power, ΔV and data transmission rate estimates. For mass, power and ΔV estimates, margins were established in line with European Space Agency (ESA) guidelines [51]. For both mass and power budgets, these margins were set up as follows:

- A margin of 5% of the initial estimate for off-the-shelf items.
- A margin of 10% of the initial estimate for off-the-shelf items requiring minor modifications.
- A margin of 20% of the initial estimate for off-the-shelf systems requiring major modifications or a mostly new design.

For every selected item or subsystem, a margin in one of these three categories has been applied, yielding the nominal estimated value. In addition, a 20% system level margin has been applied to the total power and mass estimates for the AS, DS, orbiter and RV each as a whole [51].

Cost has been estimated using mass data including this last 20% system level margin. Given this fact, the choice was made not to add another margin level here.

For the ΔV budget ESA stipulates the use of a 5% margin on the ΔV predicted for accurately calculated manoeuvres. The former applies to both trajectory and orbit maintenance manoeuvres in this report. For the ΔV determined for the AOCS, a 100% margin is required [51].

A margin of 20% has been been applied to the estimated data rate. This number has been chosen in line with the highest of the margin options encountered for the power and mass estimates, as defined by ESA [51].

5 ASCENT STAGE

Using the methods presented in Chapter 4, the detailed design for the AS was made. This chapter describes the layout of the AS and the design of the most important subsystems. It concludes with the mass and power budget of the entire AS.

5.1 ASCENT STAGE LAYOUT

The AS is the module of the spacecraft that will land and takeoff from the Moon. It will contain the cryogenics system together with the robotic arm. The robotic arm will take the sample from the drill of the DS and put it in the cryogenics system container. After the sample is taken, the AS will use the DS as a launch platform and takeoff to dock with the orbiter. There the cryogenics system will be transferred to the RV after which the AS is discarded.

The AS is composed of a payload deck at the top, two propellant tanks in the middle and an engine mounting structure at the bottom. It has a height of 3.6 m and a diameter of 1.5 m. A schematic overview of the AS (with partially deployed solar panels) is shown in Figure 5.1. A schematic view of the AS including dimensions is shown in Section 5.5.

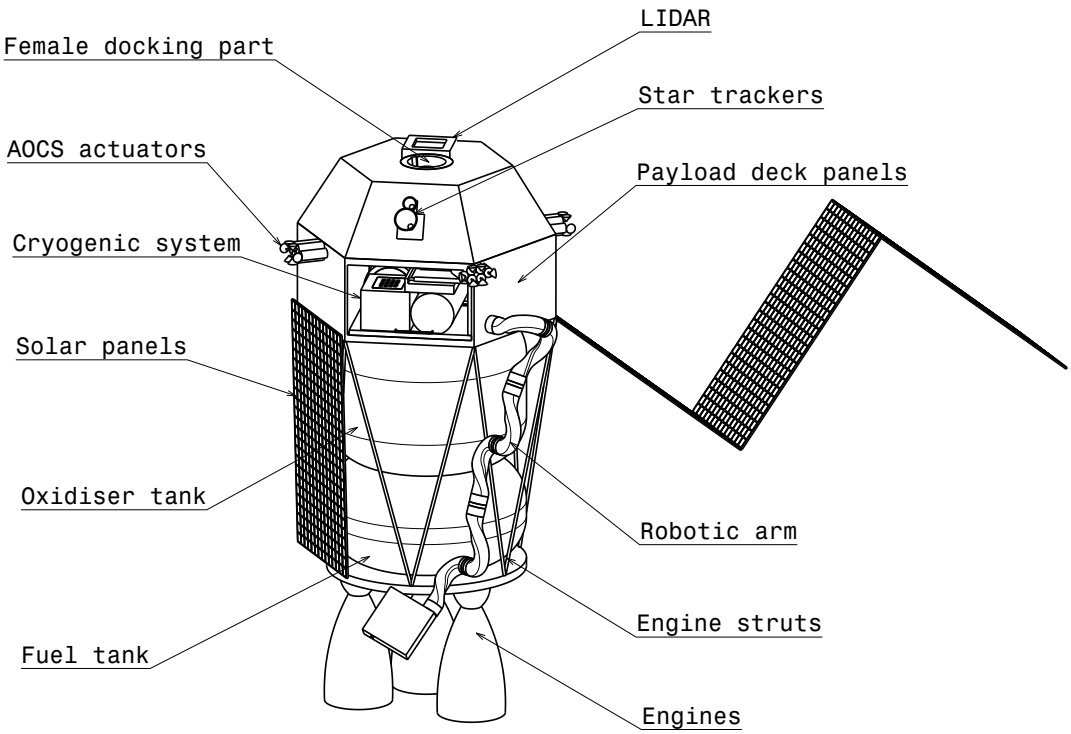

Figure 5.1: Schematic overview of the AS.

The payload deck is a hexagonal platform with a side length of 0.75 m and a panel height of 0.5 m to accommodate the cryogenic system. One panel in the AS is left open so that the cryogenics system can be ejected

to allow for sample transfer. The robotic arm can then store the samples from the drill (which is connected to the DS) in a dewar. The robotic arm will be used to carry the cryogenic system and transfer it to the RV. The payload bay contains the onboard computer and antennas as well as solar panels and batteries. During launch the male docking part of the RV is connected to the female docking part of the AS. The AS will dock at the male part again after it has lifted off from the lunar surface. The female docking port is on top of the AS with a depth of 0.4 m.

Two propellant tanks are used which contain monomethylhydrazine (MMH) as fuel, and mixed oxides of nitrogen (MON) as oxidising agent. The fuel tank has a height of 0.60 m and the oxidiser tank a height of 0.88 m. Both the tanks have a diameter of 1.11 m.

The mounting structure is connected to the AS by the means of struts which are connected to the edges of the hexagonal platform. The AS will land on the Moon and takeoff there, for which it will use the same engines. This means that no additional engines are needed on the DS to brake enough before reaching the lunar surface. Four engines are used (which is described in detail in Section 5.4) with an approximate height of 0.79 m.

5.2 ATTITUDE AND ORBITAL CONTROL SYSTEM

In this section the AOCS for the AS is described. An AOCS is needed to navigate and control the attitude of a spacecraft. First, the requirements for the design are stated. Second, the design of the AOCS is elaborated. Third, the mass and power budget of the AOCS in the AS is presented and last, it is checked if the requirements are met.

5.2.1. SUBSYSTEM REQUIREMENTS

The design of the AOCS system in the AS is driven by the required pointing accuracy, required pitch rates and location of operation. The AS has to dock with the orbiter. The chosen docking system requires a pointing accuracy of less than 3 ° as described in Section 5.10. However, the landing and ascending procedures consist of several main engine burns and a high pointing accuracy increases the efficiency of each burn. Thus, it was decided that the pointing accuracy should be less than 0.5 °. The required pitch rate is derived from a landing simulation by E. Mooij and I. Gerth [15]. The pitch profile can be found in Figure 5.2. It illustrates the pitch of the spacecraft for the main landing procedure which starts at about 1,600 m downrange [15]. From the pitch profile the pitch rate is estimated to be 300 °/min and is taken as the required pitch rate. Furthermore, the landing procedure is short, but docking at 100 km altitude could take several days if something goes wrong. Therefore, it was decided that the AS has to be able to deal with disturbances at 100 km altitude for at least 1 week.

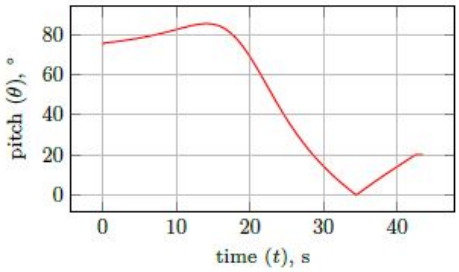

Figure 5.2: Pitch profile of main Moon landing phase [15].

5.2.2. AOCS DESIGN

The design of the AOCS is split up in actuators, sensors and controllers.

Actuators Given the method explained in Section 4.1, the required force to manoeuvre is 29 N for pitching and 9.2 N for rolling, the disturbance momentum is $6 \cdot 10^{-4}$ Nm and the disturbance over one day is 10.1 Nms. In the calculation the burn times to initiate and stop manoeuvres was set to 3 s.

To perform the manoeuvres bi-propellant thrusters produced by Astrium were chosen [52]. They provide a force of 22 N and can use the propellant of the main engine in the AS. Thus they do not require an extra propellant tank. The thrusters are grouped in sets of six which are evenly distributed around the AS. So

each set is opposite to another one and has four thrusters for pitching and two thrusters for rolling. In this fashion the thruster sets located on opposite sites of the spacecraft can be used together for pitching and have to be used together for rolling to not induce a pitching moment while rolling. However, it has to be mentioned that both pitching thrusters which are pointing in the same direction have to be used together, since they are mounted with a small offset from the middle axis of the spacecraft. This causes the thrusters to produce a pitching moment over the other pitching axis as well, if they are used individually. Thus, the maximum force available for pitching and rolling is 88 N and if one thruster fails, the available force to initiate or stop a manoeuvre would reduce to 44 N. This is still 15 N more than required for pitching and 34.8 more N than required for rolling. Thus it can be concluded that redundancy is present.

To withstand the gravitational disturbances, reaction wheels are chosen. The reaction wheel W18 by MOOG Inc. supplies a torque of 0.248 Nm [53]. The storage capacity is 18 Nms and it is the lightest reaction wheel produced by MOOG Inc. [53]. Four reaction wheels are chosen to be installed in the AS. Three are in line with the axis system of the AS and a fourth one is in line with a plane which is at an angle to the three main planes for redundancy.

The propellant mass was calculated using the method explained in Section 4.1 as well. The number of manoeuvres was estimated from the landing time of the landing procedure since the ascending procedure follows the same profile as the landing procedure except the spacecraft and the Δ V are in the opposite direction. The main landing phase in which most attitude changes are needed lasts about 45 s [15]. To account for the attitude changes in the approach phase, 90 s are used as manoeuvre time reference. So if the AOCS has to be active the complete time, 15 manoeuvres are needed which is the worst expected case. In addition to the ascent, the AS also has to dock to the orbiter. To perform this operation, the same number of manoeuvres is assumed. Thus including the 100 % margin defined by ESA, 60 manoeuvres are needed for the AS. The same margin is applied on the duration time for docking which has been defined in Section 3.1 to be 7 days and thus became 14 days. The resulting propellant mass is 11.2 kg. However, the propellant needed for the transfer from Earth to Moon and for the descent is stored in the AS as well. Therefore, the total propellant mass in the AS is 40.14 kg. Details about the descent phase and Earth to Moon transfer are given in Sections 6.2 and 8.2.

Sensors The spacecraft has to know in which position and attitude it is to change to the desired attitude. To measure the speed or angle of rotation and acceleration and velocity of the AS, two inertial measurement units (IMU) produced by Honeywell [54] are used. One of them is mounted for redundancy. However, IMUs become inaccurate over time and have to be reset to a reference frame. That is why two star trackers from JenaOptronik [55] are mounted on the AS. These star trackers have an accuracy of less than 1.5 arcsec and require one Ebox, which contains the electronics, to function [55]. The length of cabling for the star trackers was estimated to be 2 m per star tracker. Furthermore, in order to perform docking, the AS is equipped with one LIDAR system from JenaOptronik and two navigation cameras from Malin Space Science Systems [56][57]. The LIDAR system enables the possibility to dock autonomously. It identifies the position of the AS relative to the orbiter and is mounted on the top of the AS to give a clear line of sight. Nevertheless, redundancy is needed and a LIDAR system is very heavy compared to other sensors. Thus the two space cameras are mounted as backup on the top of the AS as well. In case the LIDAR system fails, manual docking from Earth is possible. However, it has to be taken into account that a time delay of 1.36 s of the signal sent from and received at Earth will be present. So at the time only small manoeuvres are allowed, since correction commands could arrive too late at the orbiter and do not have the desired effect. In addition to the sensors mentioned so far, 10 sun sensors from MOOG Inc. are mounted on the AS as well [58]. The sun sensors are spread all over the AS to identify which direction the solar arrays and thus the AS should point to. A cabling length of 2 m per sensor which was estimated does not add significant mass to the AS.

Controllers The AOCS is controlled by the onboard computer. The computer is discussed in detail in Section 5.6.

The actuators, sensors and controllers have to be connected to have a functioning AOCS. The interactions are illustrated in Figure 5.3. The process starts with the desired attitude and the estimated actual attitude. Then the onboard computer determines the required attitude changes and sends the signal to the thrusters and reaction wheels. Then the attitude of the spacecraft is changed but at the same time it is also influenced by disturbances and the properties of the spacecraft. Although the propellant is liquid, the total spacecraft is assumed to be rigid. At that point the feedback loop goes back to the start to give an updated estimation of the actual attitude which is determined with the sensors.

A total overview of the components can be found in Figure 5.4 and the input and output data of the calculation are presented in Tables 5.1 and 5.2.

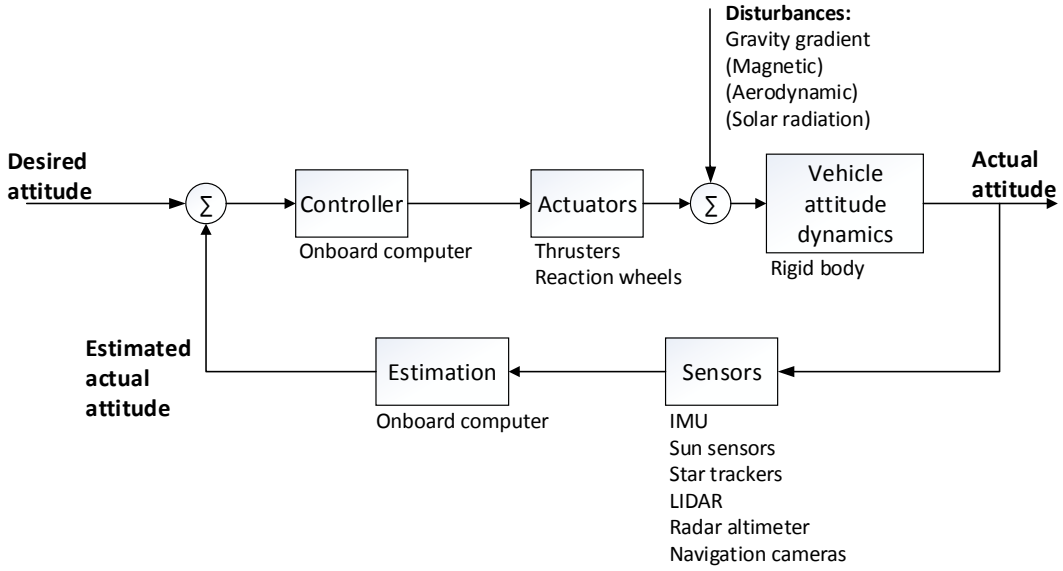

Figure 5.3: AOCS diagram.

Table 5.1: AOCS calculation input of the AS.

	$I_{x,y}$ [kgm^2]	I_z [kgm^2]	$\dot{\theta}$ [°/min]	T_{op} [days]	x_{man} [-]	$t_{burn_{man}}$ [s]	$t_{burn_{dump}}$ [s]	I_{sp} [s]	h [km]	μ km^3/s^2
Ascent	798	252	300	0.41	30	3	1	290	0	4,902.8
Docking	798	252	300	14	30	3	1	290	100	4,902.8

Table 5.2: AOCS calculation output of the AS.

	F_{pitch} [N]	F_{roll} [N]	t_g [s]	h [Nms]	m_{prop} [kg]
Ascent	29	9.2	$6.6 \cdot 10^{-4}$	0.4	5.5
Docking	29	9.2	$5.3 \cdot 10^{-4}$	10.1	5.7

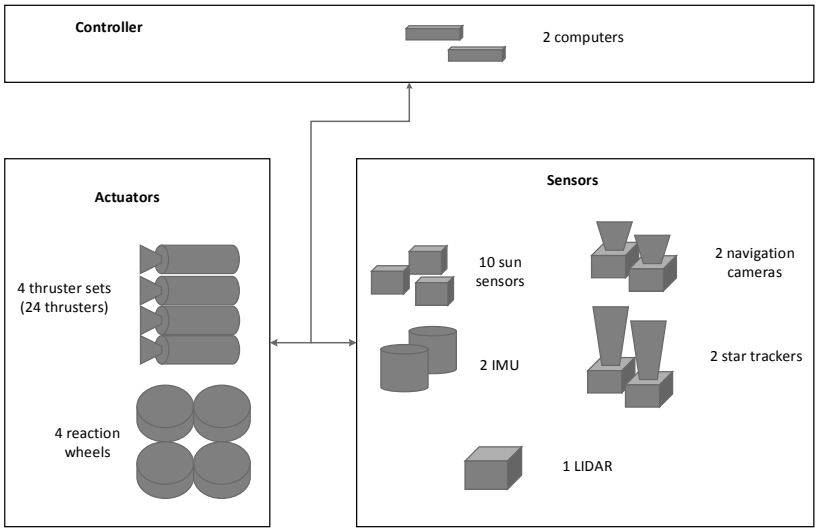

Figure 5.4: AOCS components in AS.

5.2.3. MASS AND POWER BUDGET

The mass and power budget of the AOCS can be found in Table 5.3. The total mass of the AOCS in the AS including a 5 % margin is 111 kg. The total power including a 5 % margin is 188 W. The margin of 5 % for both the mass and the power was chosen since all products are off-the-shelf.

Table 5.3: AOCS mass and power budget of the AS.

Component	**Unit mass [kg]**	**Number total (active)**	**Mass [kg]**	**Unit P_{req} [W]**	**P_{req} [W]**	**T_{ope} [°C]**
Sensors						
IMU	4.70	2 (1)	9.40	32	32.0	-30 to 65
Star tracker (ASTRO 10)	1.47	2 (1)	2.94	20.5	20.5	-40 to 40
Ebox star tracker	1.36	1	1.36	0	0	-40 to 50
Star tracker cabling	0.29	4	1.16	0	0	- -
Cosine sun sensor	0.02	10	0.24	0	0	-50 to 80
Sun sensor cabling	0.01	20	0.26	0	0	- -
Navigation camera	0.60	2(2)	1.19	2.5	5.0	-20 to 40
LIDAR	13.80	1(1)	13.80	35	35.0	-35 to 65
Actuators						
Thrusters (22N)	0.65	24	15.60			NA
Propellant			40.14			- -
Reaction wheel W18	4.95	4	19.80	29	87.0	-15 to 60
Sum			105.89		179.5	-15 to 40
Margin			0.05		0.05	
Nominal			111.19		188.48	

5.2.4. AOCS REQUIREMENTS

The requirements defined in Section 5.2.1 are met by the AOCS. It is able perform the required manoeuvres and withstand the expected disturbances while ascending and docking. Furthermore, the AOCS is redundant and is therefore not affected by single subsystem failures.

5.3 THERMAL SYSTEM

A thermal control system is present in each module of the spacecraft. Due to convection and radiation heat is spread through the subsystems of the modules. The thermal control system is to ensure that each subsystem is cooled or heated to be operational. It is assumed that if the spacecraft is within the equilibrium temperature range the thermal control system can distribute the required amount of heat to the subsystems [33]. Since the complete spacecraft is involved, it is complex to design a thermal control system. In addition, it is not possible to analyse a single module of the spacecraft, the whole spacecraft is to be analysed. In this section only the ascent phase is treated for the thermal system. The thermal system for the lander and Moon operations are treated in Section 6.3, the thermal system for re-entry is explained in Section 7.6. Finally the mission phases 'transfer to Earth', 'transfer to the Moon' and the orbiter is explained in Section 8.3.

In Section 4.2 it was explained how the thermal equilibrium was calculated. The result of this calculation, together with the most important input parameters, for the ascent phase is presented in Table 5.4. For the ascent phase it is assumed that the spacecraft is in continuous sunlight, and the that albedo effect and planetary radiation of the Moon are present. If the thermal equilibrium temperature is within 0 to 40 C°, the thermal control system will be able to handle the internal heat [33] [32].

In Table 5.4 the main input data for the thermal equilibrium temperature model, as explained in Section 4.2, is given. The absorptivity and the emissivity are calculated based on the relative area, which is shown in Equation 5.1. In this equation A_i is the ith surface where n represents the total number of surfaces.

$$\alpha_{eff} = \frac{\sum_{i=1}^{N} \alpha_i A_i + \alpha_{i+1} A_{i+1}}{A_{total}} \tag{5.1}$$

The solar intensity is 1,371 W/m^2 near Earth and Moon [33]. The planetary radiation from the Moon is 305 W/m^2, based on the black body temperature of the object [59]. However the planetary radiations variates with respect to the distance between the spacecraft and the Moon. The further away the spacecraft is from the celestial body the less radiation it receives from that body, the same principle holds for the albedo effect[32]. The calculation for the intensity of the Moon radiation Q_{in}, including the height, is shown in Equation 5.2. The albedo effect at this height is calculated using a similar method. The reflectivity of the Moon is 12%, the radius of the Moon is 1,737 km, Q_{int} is the energy generated in this particular mission phase and the other values are design parameters of the spacecraft [59].

$$Q_{IR} = \sigma T^4 \frac{R^2}{(R+h)^2} = 5.67 \cdot 10^{-8} \cdot 271^4 \frac{1737^2}{1837^2} = 305 \text{ W/m}^2 \tag{5.2}$$

Table 5.4: Thermal equilibrium of the AS - inputs.

Variable	Value	Unit
α_{eff}	0.16	[-]
ϵ_{eff}	0.31	[-]
I_{sol}	1,371	[W/m^2]
I_{IR}	305	[W/m^2]
σ [60]	5.67·10^{-8}	[m^{2}kg/s^{2}K]
t_e/t_d	0.2411	[-]
T_{Moon}	271	[K]
A_{tot}	14.5	[m^2]
A_{sun}	2.7	[m^2]
A_{moon}	2.7	[m^2]
h	100	[km]
R_{body}	1,737	[km]

Table 5.5: Thermal equilibrium of the AS - outputs.

Variable	Value	Unit
Q_{solar}	456	[W]
Q_{IR}	222	[W]
Q_{alb}	31	[W]
Q_{int}	1,700	[W]
T	312	[K]

The AS temperature, if the area is unchanged, is incompatible with the lander module. Because the internal heat generated by the ascent stage was to high while using a CuO coating. The characteristics of CuO are 0.08 and 0.25 for absorptivity and emissivity, respectively [31]. However the surface areas of the spacecraft can be increased to decrease the equilibrium temperature, the basic principle of a radiator. The additional surface calculated which is required equals 3.5 m^2 with an aluminium paint coating as used for the other modules

[31]. The aluminium paint has a absorptivity of 0.4 and a emissivity of 0.5. As can be seen in Table 5.5, the equilibrium temperature is 312 K and thus within the required temperature range. It can be concluded that requirement LCSR-Mission-Environment-09 is met for the AS [33] [32].

5.3.1. THERMAL CONTROL ELEMENTS

The internal heat regulation of the system is done with heat pipes, and radiators. The AS will need radiators since the equilibrium temperature is relatively high compared to that in the other phases. The mass and power estimations for the AS are 23 kg and 160 W, this is including the additional radiator area [33]. To be conservative in an estimation for mass and power for the thermal control system the estimations are based on concept 5 of the Mid-Term Report. The estimations of concept 5 are based on a percentage of the dry mass, the drymass of this design is lower [8].

5.4 PROPULSION SYSTEM

The AS requires a propulsion system that is capable of bringing the lander module from LLO to the lunar surface as well as propelling the AS alone back to orbit. The AS equips three 890 N Aerojet engines and a single 4.0 kN engine manufactured by Aerojet. The four engines provide a combined thrust of 6.67 kN and are fed with MON and MMH. The engines perform three main manoeuvres: a braking burn to lower the Moon periapsis down to 15 km altitude; a powered descent to bring the lander to rest and an ascent burn to reach LLO again. The spacecraft's thrust-to-weight ratio (T/W) and burn time at each manoeuvre are given in Table 5.6. A T/W between 1.3 and 1.5 prior to the powered descent is needed in order to implement an efficient landing profile [61]. The braking burn and the powered descent burn are merged together since the simulation shows that the braking burn requires negligible ΔV when compared to the powered descent. The reason behind the four-engine configuration is that there are no single off-the-shelf engines that provide a T/W in the $1.3-1.5$ range.

Table 5.6: Summary of manoeuvres where the Aerojet engines are used.

Manoeuvre	ΔV [km/s]	S/C mass prior to manoeuvre [kg]	T/W [-]	Burn time [min]
Powered descent	1.88	2,756	1.46	41.33
Ascent burn	1.88	857	4.68	5.12

Both MON and MMH are stored in modified Astrium $700-1108$L Ti6AlV blowdown tanks [50]. These tanks are shortened in order to decrease the capacity down to 0.884 m^3 for the MON tank and 0.606 m^3 for the MMH tank, as indicated in Table 4.12. The freezing and boiling temperatures of the propellant are shown in Table 5.7. In order to achieve the $273-313$ K equilibrium temperature range established in Section 4.2, a cooling system for the MON tank is required. A Peltier effect cooler with a heat lift of 1 W at 170 K could be used to ensure a tank temperature within MMH's operational range [62]. The heat lift specifies the rate at which heat can be extracted from the tanks. The Peltier effect cooler is considered an off-the-shelf component as it has flown to space in the past [62]. The MMH tank cooler has not been designed in detail and is thus also left as an official recommendation to be dealt with at later phases in the project.

Table 5.7: AS propellant operational temperatures.

Compound	Agent	Freezing temperature [K]	Boiling temperature [K]
MON	Fuel	262	295
MMH	Oxidiser	221	364

The tanks are pressurised with Helium gas at 2,930 kPa as required by the Aerojet engines [63]. The pressurant mass is estimated using Equation 5.3, as established in [33].

$$m_{pressurant} = \frac{P_{eng} \cdot V_{proptank}}{R_{He} \cdot T_{He} - \frac{P_{eng}}{\rho_{He}}} \tag{5.3}$$

where $m_{pressurant}$ is the mass of the pressurant, P_{eng} is the required engine chamber pressure, $V_{proptank}$ is the volume of the propellant tank to be pressurised, T_{He} is the temperature of the pressurant inside the tank, R_{He} is the gas constant for the pressurant and ρ_{He} is the density of the pressurant inside the tank. It was found that 7.48 kg of Helium is required to pressurise the AS tanks.

5.5 STRUCTURES AND MATERIALS

This section will describe the structural performance of the AS. A design of the struts between the AS and the orbiter is given together with a design of the panels, engine struts and the payload deck. For the AS the driving environment is the launch environment on Earth, where the DS causes a compressive force on the AS.

During launch, the DS exerts a force on the AS through the struts with its mass of 417 kg as well as the engine with its mass of 21 kg. The struts are assumed to carry all the loads: they are designed to withstand the entire compression force with no transmission through the propellant tanks. It is assumed that this force is divided equally over all six strut connections points and divided equally along the panels, as was stated in Section 4.4.3. The maximum g-force was shown in Table 4.6 to be 6 g in axial direction and 2 g in lateral direction. The dimensions in Figure 5.5 will be used in the calculations, combined with the fact that the panels of the AS have a dimension of 0.75 m.

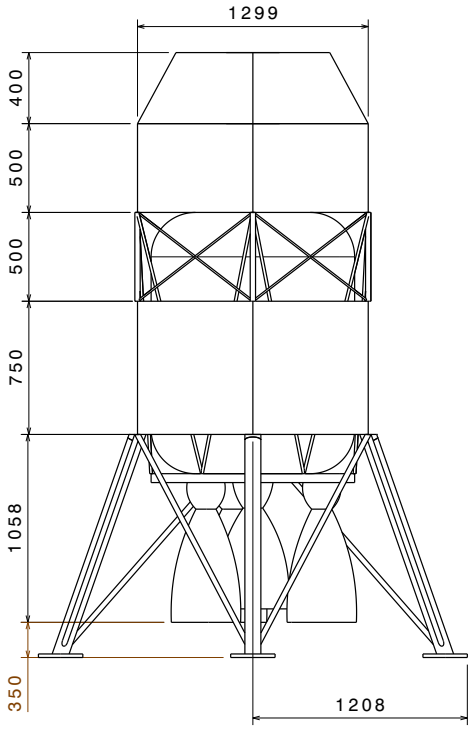

Figure 5.5: Schematic overview of the combined AS and DS (units in [mm]).

5.5.1. STRUTS BETWEEN AS AND ORBITER

Using Equation 4.18 the force in each member between the AS and orbiter is calculated. An axial force of 160.8 kN and a lateral force of 53.6 kN acts on the struts during launch due to the gravitational loads. At each strut there is an axial load of 26.8 kN and a lateral load of 8.9 kN. Since the spacecraft is connected only at the adapter, there will also be a bending moment induced by the spacecraft lateral acceleration. In Figure 5.6 Figure 5.5 is shown simplified showing just the struts connecting the AS and DS.

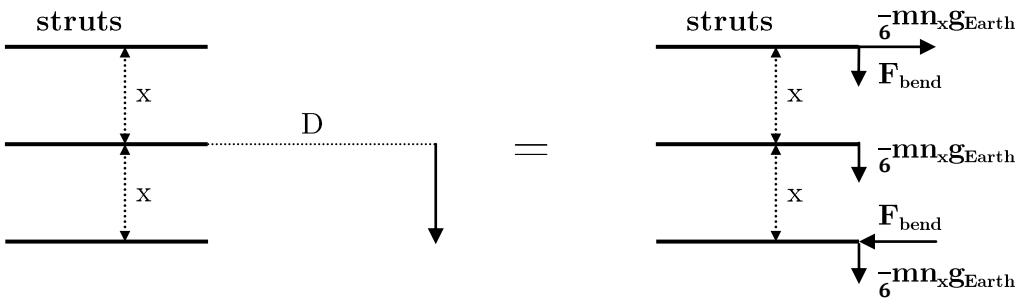

Figure 5.6: Representation of the bending forces as an axial and lateral force.

In Figure 5.6, x is the distance between two struts viewed from the side, and D the distance of the centre of mass of the combined AS and DS.

$$F_{bend} = \frac{D(m_{DS} + m_{AS} n_{lat} g_{Earth})}{4x} = 64.1 \text{ [kN]} \tag{5.4}$$

The centre of gravity is assumed to be at the centre of the combined AS and DS. This force is added to the 26.8 kN load leading to a combined axial load of 90.9 kN. Using Equation 4.18, the forces in each member can be computed. The primary strut has a resulting compressive force of 11.2 kN. The primary struts are chosen to have an outer radius of 19 mm and a thickness of 6 mm, leading to a moment of inertia of $8.0 \cdot 10^{-8}$ m^4 and an cross-sectional area of $6.0 \cdot 10^{-4}$ m^2. For determining the critical buckling load in the primary strut Equation 4.22 will be used.

$$F_{crit} = \frac{\pi^2 EI}{L^2} = 16.2 \text{ [kN]} \tag{5.5}$$

which leads to a safety factor of 1.5. Thus the structure is capable of dealing with the gravitational forces during launch.

The secondary struts have a radius of 11 mm and a thickness of 3 mm with a moment of inertia of $8.3 \cdot 10^{-9}$ m^4 and an area of $1.8 \cdot 10^{-4}$ m^2 and are in tension with $2.8 \cdot 10^4$ N. To determine if the secondary strut does not yield, Equation 4.17 is used.

$$\frac{F_{ten}}{A} = 162 \text{ [MPa]} \tag{5.6}$$

The yield strength of aluminium 6061 is 276 MPa [45]. This leads to a safety factor of 1.7. Thus, the structure is structurally sound for tension in the secondary struts. There is no compression in the secondary struts.

5.5.2. ENGINE STRUTS

The engine causes a compressive force during Moon landing and take-off due to thrust, and a tensile force while on the Moon surface by the gravitational pull of its mass. Struts that connect the engine mounting with the AS panels are used that take up these forces. The distance between the engines and the AS panels is 1.47 m and the loads are transferred via two struts (instead of three as for the AS-DS connection). These struts are also connected to the corners of the hexagon. The thrust of the engines is 6,670 N as seen in Section 5.4. This force will only occur during take-off and landing on the Moon. It is assumed that the force of the thrust is transferred through the struts only, and not through the propellant tank. The struts have a thickness of 2 mm and an outer radius of 9 mm. When the engines are activated, each strut pair will be compressed by a force of 1.1 kN, divided over two struts. The length of each strut is 1.51 m (composed of a horizontal distance of 0.38 m and vertical distance of 1.47 m). The force in each strut can be determined using Equation 4.18.

$$F_{eng,comp} = 538 \text{ [N]} \tag{5.7}$$

The struts have a moment of inertia of $3.3 \cdot 10^{-9}$ m^4 and a cross-sectional area of $1 \cdot 10^{-4}$ m^2. Aluminium 6061 is chosen as the material. The critical buckling load is determined using Equation 4.22 to be 955 N, resulting in a safety factor of 1.77. During the Moon operations, the Moon gravity will put a gravitational force on the engine. The strut design is driven by the buckling load and with the geometrical properties chosen as in Figure

5.5, the safety factor of the tensile loads is 822, which is considerably high. The tensile safety factor implies that the struts can carry significantly more tensile loads than the gravitational pull on the engine.

5.5.3. PANEL DESIGN

The compressive forces of the struts are transmitted through the panels of the AS. The panels have to be checked for buckling. Aluminium 6061 is used which has a Poisson's ratio of 0.33 and a Young's modulus of 68.9 GPa [45]. The panels have a height of 0.5 m, a length of 0.75 and a thickness of 2.5 mm. As was stated in Section 4.4.3, a k of 7 is used. Equation 4.23 is used to determine the critical buckling load for the panels.

$$F_{crit} = \frac{k\pi^2 EA}{12\left(1-\nu^2\right)}\left(\frac{t}{b}\right)^2 = 41.22 \text{ [kN]} \tag{5.8}$$

The DS as well as the engine is exerting a force on the panels of the AS. The same bending load as for the struts is acting on the AS panels. It is assumed that these forces are divided equally along the panels. The force that is acting on each panel is also 9.5 kN, slightly more than for the struts because of the engine mass. The critical load is higher than the applied load with a safety factor of 4.33. The thickness can be decreased further, however this can cause problems due to acoustic noise (which is not favourable for thin plates as was mentioned in Section 4.4).

5.5.4. PAYLOAD DECK

On top of the AS the docking mechanism is located as is seen in Figure 5.1. A structure around this is made to increase the stiffness of the spacecraft such that it can withstand the launch vibrations. This structure is modelled as a cylinder with a height of 0.4 m, outer radius of 0.65 m and a thickness of 3 mm. The payload deck also contains a panel to which all the hardware (like the cryogenic system) is attached. The thickness of this panel could not be analytically analysed, as for such a shape a finite element analysis is more suitable. The panel has an area of 1.95 m^2 and is chosen to have a thickness of 2.5 mm.

5.6 DATA AND COMMAND HANDLING

The two main components of the data and command handling (DCH) system are the onboard computer and the data storage hardware. In Figure 5.7 the overall DCH system is presented. Note that this is a general overview of the system and is presented only to visualise how the DCH system works. A number of subsystems generate data or receive commands, the amount of data generated was determined in Section 4.5 and the number of commands will be discussed later in this section.

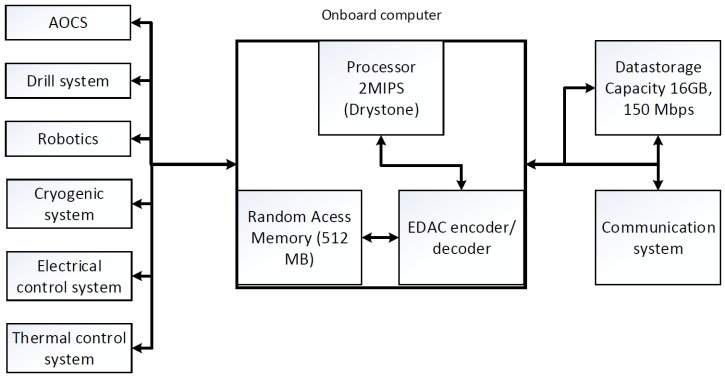

Figure 5.7: Data handling block diagram.

These subsystems send the generated data to the onboard computer and the onboard computer can then send commands to the subsystems. The OBC750 was chosen as onboard computer for its processing power of 2 million instructions per second (MIPS), random access memory (RAM) of 512 MB and data protection against a single event upset [64]. The OBC750 can either send the data directly to the communication system or to the data storage hardware in case communication is not possible at that moment in time. The HSDR was chosen as data storage device with a storage capacity of 16 GB, a data rate of 150 Mbps and can directly send data to

the communication system [64]. The HSDR was chosen for its combination of low mass (1 kg) and low power (15 W). Note that both the OBC750 and HSDR are included two times for redundancy.

The amount of data the AS onboard computer needs to process is the AS data generation plus the DS data generation, since the DS does not have a DCH system. Using Table 4.10 and additional calculations, the total amount of data that is generated per second and needs to be processed is found to be about 40,264 bps. This directly influences the amount of data that needs to be transmitted from the AS to the orbiter module, which will be explained in Section 5.7.

The data rate at which the AS can receive commands (or software updates) from the orbiter module is at maximum 1.06 Mbps, the AS receiver will be elaborated upon in Section 5.7. For now it is important to know what amount of data can be received per orbit, since this determines the number of received commands per orbit. The visibility time is 312 – 525 s, as calculated in Section 4.5. Using the minumum time of 312 s, the maximum received data is about $3.47 \cdot 10^8$ bits per orbit. Sending a command message takes 48 – 64 bits, which means $5.42 \cdot 10^6$ commands (in case of 64 bits) can be received per orbit [33]. This number of commands will probably be sufficient to perform the operations on the Moon [49]. However, more research is needed to determine the exact number of commands is that should be sent per orbit. In the improbable case more commands are needed to be received, groups of commands can be stored in the HDSR. For example, drilling and storing one sample can be implemented into a group of commands, and if the orbiter module can activate that group of commands by only sending one command, it saves data that needs to be sent.

5.7 COMMUNICATION SYSTEM

In this section the communication system of the AS will be discussed. As mentioned in Section 5.6, the communication system of the AS provides a communication link to the orbiter module for both the AS and DS. The communication system architecture of the AS was incorporated in the communication flow diagram in Figure 4.6. In this figure it can be seen that the main components of the communication system are the transmitter, receiver and antenna, and each of these components are incorporated twice in the AS for redundancy. This means if one component fails, there will be a backup component which will be activated (from a standby mode) to take over the work of the failed component. The chosen components are presented in Table 5.8 and relevant parameters are included. It can be seen that the components operate in the S-band frequency, which is between 2.0 and 2.3 GHZ [33]. The (transmitted) power, gain and HPBW will be used in the link budget. Another element of the link budget calculation is the data rate that is required for operations, which needs to be within the data rate range of the transmitter of the AS and the receiver of the orbiter module (which also uses a HISPICO receiver).

Table 5.8: AS communication system components.

Component	Frequency [GHz]	Data rate	Power [dBW]	Gain [dB]	HPBW
Transmitter (SSTL) [64]	2.20 - 2.29	9.60 kbps - 10.00 Mbps	6.02	-	-
Receiver (HISPICO) [65]	2.20 - 2.30	0 - 1.06 Mbps	-	-	-
Patch antenna (SSTL) [64]	2.00 - 2.50	-	0 - 10.00	6.98	35 deg

To determine the required data rate, the amount of data generated per orbit is needed, which is about 40,264 bps. The MATLAB code mentioned in Section 4.5 was also used to compute the orbit time, which is about 7,060 s. The visibility time of the AS with respect to the orbiter module was determined to be 312 s. Including a safety margin of 20 % for additional data that might be needed, this results in a data rate of 1,068 kbps that the AS needs to send every pass-by of the orbiter.

The data rate is included in the link budget in Table 5.9, where three main divisions are made: "AS parameters" includes information about the transmission of the signal, "Propagation path" includes information about the path the signal travels and "Orbiter parameters" includes information about the reception of the signal. Most elements in Table 5.9 have been explained before, therefore not all elements will be discussed. The pointing offset for both the transmit and receive antenna were determined by multiplying the HPBW with 0.2 [48]. The distance between the orbiter and the AS is about 102 km, since the orbiter is at an altitude of 100 km and the crater depth is about 2 km. Using the MATLAB code that was also used in Section 4.5 the maximum angle θ in Figure 4.8 was calculated to be 15.92◦. The propagation path length was then determined to be 106 km, using θ and the distance between the orbiter and the AS. The pointing losses and space loss were determined using Equations 4.40 and 4.39, respectively. The propagation and polarisation loss is negligible, since the Moon does

not has an atmosphere. The system noise temperature was determined using [48], where typical system noise temperatures are given for several frequencies. Using Fig.16-16 of [33] the required E_b/N_0 for QPSK modulation was determined to be 9.6 dB.

Table 5.9: Link budget - AS to orbiter module.

Symbol	Description	Value	Unit
AS parameters			
f	Frequency	2.29	[GHz]
P_t	Transmit power	6.02	[dBW]
L_l	Transmitter line loss	-1.00	[dB]
$\alpha_{1/2_t}$	Transmit antenna HPBW	35.00	[°]
e_t	Transmit antenna pointing offset	7.00	[°]
L_{pt}	Transmit antenna pointing loss	-0.48	[dB]
G_t	Transmit antenna gain	6.98	[dB]
EIRP	Equivalent isotropic radiated power	12.00	[dBW]
Propagation path			
S	Propagation path length	106.00	[km]
L_s	Space loss	-140.15	[dB]
L_a	Propagation and polarisation loss	0	[dB]
Orbiter parameters			
$\alpha_{1/2_r}$	Receive antenna HPBW	35.00	[m]
e_r	Receive antenna pointing offset	7.00	[°]
L_{pr}	Receive antenna pointing loss	-0.48	[dB]
G_r	Receiver antenna gain	6.98	[dB]
T_s	System noise temperature	-21.30	[dBK]
R	Data rate	1,067.61	[kbps]
E_b/N_0	Energy per bit to noise density	22.52	[dB]
BER	Bit error rate	10^{-5}	[-]
Req E_b/N_0	Required energy per bit to noise density for QPSK	9.60	[dB]
L_i	Implementation loss	-2.00	[dB]
Margin	Margin (>3 dB)	12.93	[dB]

Note that a link budget analysis was also done for sending data from the orbiter module to the AS, using the same method. The only difference was the higher data rate of 1,085.44 kbps. The margin was still higher than 3 dB though. This means that the AS receives signals from the orbiter module without too many errors as well.

5.8 CRYOGENIC SYSTEM

In this section the cryogenic system used in the AS and the RV is explained. First, a final choice for the cryogenic system that will be used for this mission is made. Second, a detailed design of this cryocooler is given, elaborating on the different elements of the system. Third, the dewar is designed. Last, the integration of the spacecraft and cryogenic system is explained, elaborating on the operations of the cryogenic system and the transfer to the RV.

5.8.1. CRYOCOOLER SYSTEM CHOICE

In the Mid-Term Report a summary was given about the research on cryogenic systems [8]. This research resulted in two different systems, which were chosen on basis of their mass, power usage and other secondary characteristics. These two systems are the reverse-Brayton cycle cryocooler and the Joule-Thomson (J-T) cryocooler [66] [67] [68]. In the next two paragraphs both systems will be discussed.

The first cryocooler system treated is the J-T-cryocooler used in concept 5. The disadvantages and advantages are listed to give an overview of this design.

Advantage/disadvantage The J-T cryocooler used in concept 5 of the Mid-Term Report is a cryocooler built around the dewar using cold-plate technique to cool down the substance. The cold plate functions as a heat sink and cools the substance from one side. The temperature in a single sample will not be equal throughout the height of the sample, because the sample is cooled from one side when using cold-plate technology. Additionally, the lunar surface is a good insulator. The advantage of using cold-plate technology is that it does not need moving parts to operate and is in general less complex.

Disadvantage The cryocooler is developed for Earth applications and thus is not space graded. The compressor is normally cooled with air, in space the design should be adapted to ensure the compressor does not overheat [67].

Disadvantage The mass is comparable to the other system, but the power usage is much higher than that of the reverse-Brayton cycle, the difference is 250 W on a total of 650 W. The J-T-cooler mass is 34 kg [69] [67] [68].

Disadvantage The system accompanied by the compressor introduces large vibrations into the spacecraft. The structure and dewar should then take this into account, resulting in additional mass [67].

Advantage The cooling capacity (heat lift), which is the amount of energy the cooler can extract from a system, of this system is 24 W. This is higher than that of the reverse-Brayton cooler, which has maximum heat lift of 21.3 W [68].

Advantage The manufacturer was willing to share information on their product [69]. The manufacturer of the reverse-Brayton was not willing to share additional information [70]

The second cryocooler system is a reverse-Brayton cryocooler used in concept 4 of the Midterm Report [8] [66].

Advantage/disadvantage The Reverse-Brayton cooler uses a cooling flow to cool down, this has as advantage that the substance is cooled evenly. The disadvantage of a cooling flow is that the gas of the flow is subject to motions of the spacecraft [32].

Disadvantage The Brayton-cryocooler is a two-stage cooler, the second stage cools the flow from 118 K to around 65 K. This second stage is unnecessary and adds to the mass. There is no off-the-shelf implementation.

Disadvantage Reverse-Brayton cryocoolers are normally highly complex systems [62] [66].

Advantage The mass is slightly lower than that of the J-T-cooler, namely 30 kg. The power usage is between 200 and 400 W, where the higher the power setting the higher the cooling capacity. However its cooling capacity is 21.3 W at maximum at 118 K and 13.6 W at 100 K for the cooling flow [66].

Advantage The information on how the cooling system works is more detailed than the J-T-cooler, including the different elements of the system and the temperature of those elements.

The disadvantages do not lead to mission failure, but should rather be accounted for in the design process when using a particular system. In the end, the reverse-Brayton cryocooler was chosen, because the temperature was spread evenly through the substance and the lower mass and power requirements. From now on the reverse-Brayton cooler will simply be referred to as cooler or cryocooler.

5.8.2. DETAILED DESIGN OF THE BRAYTON-COOLER

In this section the design of the cooler is explained in detail and adapted to the custom needs of this mission. The cooler has been chosen to be used in this mission, however this system cannot directly be implemented in the spacecraft. As mentioned in Subsection 5.8.1, the system has a second stage cooling the flow to 65 K with a heat lift of 1.8 W. This second stage is not needed for this specific mission, as the first stage can cool to 100 K with a heat lift of 13.6 W. The heat lift required for the re-entry phase is approximated to be 12 W for a temperature of 125 K [71]. Leaving the second stage out of the cooler the cooler mass becomes 27.2 kg. No power breakdown was given in the article, it is assumed that the cryocooler still has a maximum power consumption of 400 W [66].

The cycle gas for the cryocooler is neon. The elements of the cycle are explained in the schematic of the cooler shown in Figure 5.8. The numbers in the schematic represent the diameter and the length of the system in cm. In Figure 5.9 the different parts of the cryocooler are indicated with their temperature and entropy.

Starting at the compressor, the compressor compresses the neon, causing it to flow through the system. The heat of compression and other heat losses of electronics are rejected at the heat sink indicated in the schematic, though the schematic may imply that the heat sink is before the compressor, it should be noted that the heat sink is used by the recuperator and the compressor. After the compressor the flow goes through the aftercooler where the cooling flow is cooled down to cool the substance. The flow goes through recuperator and then to the turbine and heat exchanger. The recuperator cools the flow before it expands in the turbine. The heat exchanger ensures that the flow exchanges its heat with the sample. The heat gained due to cooling the sample, should be radiated into space. This is is done as it approaches the heat sink after the recuperator [66].

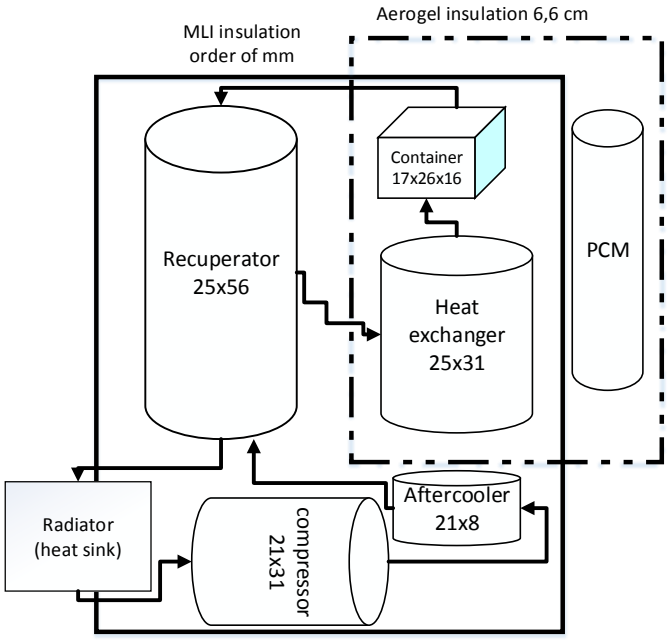

Figure 5.8: Schematic overview of the cryogenic system, numbers indicate diameter and length respectively.

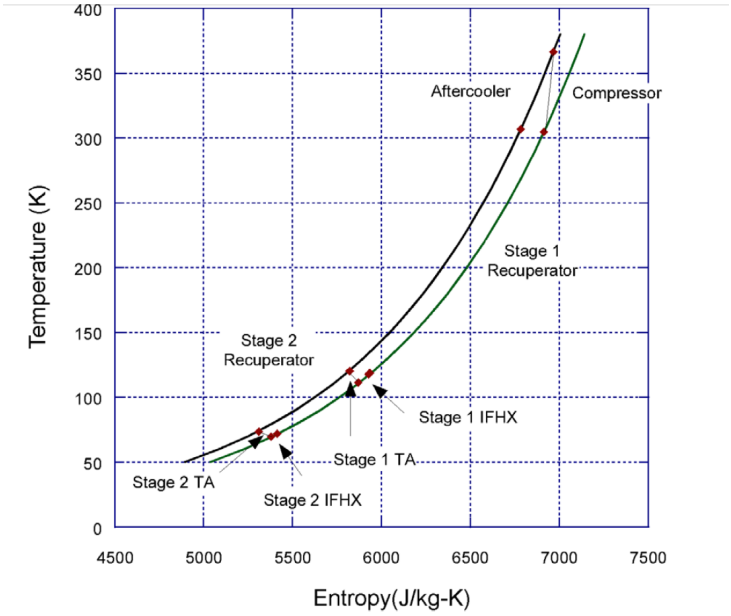

Figure 5.9: Temperature and Entropy graph of the cycle of the cryocooler [66].

5.8.3. DEWAR DESIGN

Off-the-shelf dewars for space applications are usually isolated tanks used to store flows. The dewar in this mission needs to store the solid Moon samples. First of all, it means that it is more difficult cool the substance because the flow cannot come into contact with the sample due to risk of contamination. Second, the dewar has to open in order to place the samples inside, features for which there are no commercial available dewars.

Each sample has its own tubes in the container, these tubs are fixed in a rack with the purpose that the samples will be less subjected to vibrations. In addition it allows the cooling flow, flow past the tubes. The flow is sealed off with a thin plate of titanium. The casing of the rack is to ensure that the flow will not contaminate the sample and that the container will be able to withstand vibrations and forces. Titanium has good ductility at cryogenic temperatures [72] [73]. It should be mentioned that no calculations have been made to verify if the container can withstand the forces or vibrations encountered on the mission, the design is qualitative. The mass and size have been estimated using existing dewars and the sample size.

The size of a sample is 2.2 cm in diameter and 10 cm in length as will be explained in Section 6.5. The wall thickness of the holder of a single sample is 1 mm. A spacing of 1 cm between the samples leaves a 4 mm gap for the cooling gas to flow through the system. Then an additional 2 cm was taken into account for insulation of the container and place to let the gas flow easily through the container. The size of this rack is 11.4x14.5x12 cm (lxwxh). Using the additional factor of the division between the inner radius and outer radius of commercial dewars the final size becomes 17x21x18 (lxwxh). Finally a cover with rail system is used to open and close the container when putting the samples in the container. This cover takes an additional 5 cm including additional insulation. The mass of the container is 11 kg based on the inner volume of the dewar designed and compared to commercial dewars [74].

5.8.4. INTEGRATION IN DESIGN

The cryogenic system as a whole has two main interactions with the spacecraft. First the robotic arm has to put the samples into the container, for which a cover system with actuators is designed. The entire cryogenic system is shown in Figure 5.10. Two actuators are used to push the cover over the container. The actuators' mass and length are 2.34 kg and 20 cm, respectively [75]. There is one additional problem: to get the container out of the spacecraft the entire cryogenic system has to be pushed out of the spacecraft for 40 cm, for this function two additional actuators are used, and the cryogenic system is added on a plate and rail system. The actuators' mass and length are 3 kg and 47.5 cm, respectively [76].

The second operation is that the cryogenic system is moved from the AS to the RV. A plate is added beneath the cryogenic system where the entire cryogenic system is connected, allowing an easier transfer. Furthermore the cryogenic system is wrapped in MLI to insulate the system for the heat influx from direct sunlight and the albedo effect and planetary radiation from the Moon [77]. The third operation is that the cryogenic system is connected to the phase change material (PCM), which functions as a heat sink for the cryogenic system while re-entry and retrieval.

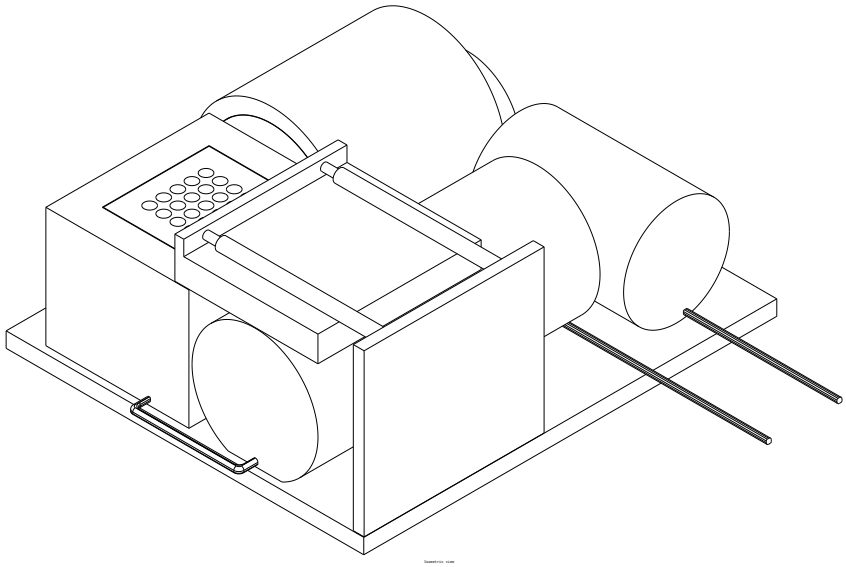

Figure 5.10: Isometric drawing of the cryogenic system.

5.8.5. RE-ENTRY AND RETRIEVAL

One of the most critical phases for the mission is the re-entry of the RV. The re-entry phase is very short, but the system will be subjected to high mechanical loads and thermal loads. It is unknown if the cryogenic system can handle these mechanical loads, because the company producing this system does not want to share additional information.

The estimated heat lift required for the re-entry to keep the sample at cryogenic temperatures is 11 W [71], however the uncertainty in their design was substantial, resulting in a design for a cryogenic system which has a much higher heat lift capacity. The heat influx at time of re-entry is unknown, however the re-entry phase is short as explained in Section 7.5 (excluding the landing phase where the parachute system is operational). The retrieval of the spacecraft is more critical, because the spacecraft cannot dump the heat outside the spacecraft and the atmosphere will warm up the spacecraft. To counter this the container, the cold parts of the cryogenic system and the PCM are insulated in aerogel beads. The thickness of the insulation needed is 6.6 cm, including a 20% safety factor. The calculation for the required insulation will be discussed in the next paragraphs.

To calculate the thickness of the insulation required Equation 5.9 is used. This equation cannot be applied directly, because the area mentioned depends on the thickness, thus an iterative process is needed. It is assumed that the temperature does not change over time and starts at 100 K, T_1, and second, that the surrounding temperature, T_2, is 293 K. This means that the average heat influx, Q_{out}/t, used is higher than 21.3 W used in the calculation. Aerogel beads with a thermal conductivity of 0.01 W/mK were used as insulator [60] [78].

$$\frac{Q_{out}}{t} = -kA(T_2 - T_1) \tag{5.9}$$

5.8.6. HEAT SINK

The system has a constant heat input of 21.3 W into the cooling flow from the sample, which needs to be expelled. It was chosen to use a PCM as heat sink for the cryogenic system as this was the most compact method of absorbing the heat flux. A PCM works by absorbing the heat through the change of phase of the material. There are many different types of PCM's available commercially, each with different applications.

The heat sink used during re-entry is connected to the compressor, which is the element of the cryogenic system with the highest temperature. This is done because then the temperature difference will be most beneficial as can be derived from Equation 5.9. The temperature of the flow in the compressor is about 340 K as can be viewed in Figure 5.9. To be conservative the temperature is taken to be 300 K. The melting temperature of the selected PCM should be below this value. When this is the case, one can compute the minimum mass of the selected PCM's with Equation 5.10 [32] [33].

$$Q_{abs} = mc_s(T_m - T_0) + mL_H + mc_l(T_{max} - T_m) \quad (5.10)$$
$$Q_{abs} = \dot{q}_{in} t \quad (5.11)$$

where Q_{abs} is the total absorbed heat, $\dot{q}_{in}$ is the input heat flux, t_{op} is the required operational time in which the heat flux needs to be absorbed, c_s and c_l are the specific heat capacity of the PCM in their solid and liquid phase respectively, L_H is the solid to liquid latent heat, T_m and T_0 are the melting and begin temperature of PCM respectively, and T_{max} is the maximum temperature of the cooling flow [33].

Equations 5.10 and 5.11 can be solved for mass to give an expression for the minimum mass, as shown in Equation 5.12.

$$m_{min} = \frac{\dot{q}_{in} t_{op}}{c_s(T_m - T_0) + L_H + c_l(T_{max} - T_m)} \quad (5.12)$$

A MATLAB script can be used to find the lowest value for the PCM mass. Table 5.10 shows the inputs of the MATLAB script and Table 5.11 shows the output of the MATLAB script. The starting temperature was chosen to be a temperature 5 K lower than the melting temperature, as higher would cause some of the PCM to liquify already therefore losing efficiency and because lower would case higher strain on the thermal system.

Table 5.10: Inputs for MATLAB script to determine lightest PCM [79].

PCM type	L_H [J/kg]	c_l [J/(kg· K)]	c_s [J/(kg·K)]	T_m [°C]
HS26N	$2.05 \cdot 10^5$	850	3,400	-25.6
HS23N	$2.00 \cdot 10^5$	850	3,400	-22
HS10N	$2.20 \cdot 10^5$	3,473	13,892	-11
HS07N	$2.30 \cdot 10^5$	900	3,600	-7
HS01P	$2.90 \cdot 10^5$	990	3,960	0

Table 5.11: Outputs of the MATLAB script to determine the lightest PCM.

PCM type	Mass [kg]
HS26N	3.8
HS23N	2.7
HS10N	3.7
HS07N	3.6
HS01P	46.5

Thus it can be seen that the HS23N is the lightest choice for the PCM material with a mass of 2.7 kg.

The mass of the cryogenic system is 64 kg including the actuators, dewar, additional piping and the connector for the robotic arm. Adding a additional 20% as margin results in a mass final mass of 77 kg. Furthermore it uses 400 W in both the AS and RV, to ensure there is in all phases of the mission the required heat lift capability. It can be concluded from this section that requirements LCSR-Mission-ConsMission-02 and LCSR-Mission-sample-08 are met.

5.9 ROBOTIC ARM

In the AS, a robotic arm is needed for two operations. First, the robotic arm is used to transfer the samples from the drill described in Section 6.5 into the cryogenic system described in Section 5.8. Second, the robotic arm is used to move the cryogenic tank out of the AS into the RV while they are docked in orbit, after the sample has been retrieved.

In order to reduce development risk and to increase reliability, an off-the-shelf robotic arm is used. In order to perform both actions mentioned above it should be at least 2 m long: This is the distance between the mounting location of the arm and the location were samples are retrieved by the arm. No such robotic arm currently exists. However, the DEXARM, developed by ESA, is a 1.2 m long robotic arm which has a design that can be adapted to become 2 meters, by extending each arm segment [80]. The original DEXARM is shown in Figure 5.11.

The original DEXARM has a mass of 25 kg. Elongating the parts between the joints will increase the mass to 35 kg [80]. The power needed for the arm is dependent on the actions that must be performed. During the mission, the robotic arm needs to be able to move a tool (described below) containing the samples from the drill to the cryogenic storage. Together, their mass is just over 10 kg, and these actions will be performed only in the gravity environment of the Moon. The original DEXARM is capable of moving 10 kg at 1g [80]. Because

the length of the robotic arm is nearly doubled, the moment arm is also nearly doubled. This means that the elongated arm should be capable of carrying slightly over 5 kg in Earth-gravity and 30 kg in Moon-gravity. This is more than sufficient to carry the 10 kg mentioned above. Also, the robotic arm must be capable of moving the cryogenic system from the AS into the RV. This is done in orbit, so the gravitational forces and therefore the mass are of no concern. Because the AS and the orbiter are powered by solar panels while they orbit the Moon, there is no time limit for the transfer of the cryogenic system. This means that the forces needed are very low. In short, it can be said that the joints as used in the original DEXARM are still sufficiently strong for the elongated design, and thus the required power remains 100 W. With this power, the elongated DEXARM is capable of delivering 20 N and 200 Nm [80].

Figure 5.11: 3D model of the original DEXARM [80].

It can be seen in Figure 5.11 that the arm consists of seven joints, of which three are elbow joints, also called folding joints. The other four, including the last joint at the end of the arm, are shoulder joints, also called rotating joints. The last joint has a connection mechanism which is used twice. First, the connection mechanism fits on the connection pad of the cryogenic system. When the arm is connected to the cryogenic system it can move the cryogenic system from the AS to the DS. Second, the connection mechanism also fits on a tool used for retrieving the sample from the drill. This tool is already attached to the robotic arm before launch. Inside the tool there is a hollow tube of 10 cm depth and with a radius of 1.1 cm. This is the same size as the sample storage cylinders in the cryogenic storage. As will be explained in Section 6.5, the drill delivers a continuous 2 m long, 1 cm radius sample, with a liner of 1 mm thickness around it. The drill will have a mechanism to lift up the top of the continuous sample into the cylinder inside the tool. Inside this tool there is a sharp disc attached to an actuator. The disc is quickly pushed through the sample, to separate the 10 cm inside the tool from the rest of the sample. This is the same working principle as is used in drills of the ExoMars and the Rosetta missions [81] [82]. After the disc is pushed through the sample, the robotic arm moves the tool towards the cryogenic system, and brings the cylinder with the sample in line with an empty storage cylinder. The disc is pulled back and a small actuator pushes the sample out of the tool into the storage. This process is repeated 20 times, for each of the samples. When the AS returns to the orbiter, the tool is left behind on the surface.

5.10 DOCKING SYSTEM

After the sample is retrieved, the AS returns to the orbiter. There, the sample and the cryogenic system must be moved into the RV. In order to keep the AS and the RV in stable relative positions, a docking system is used.

The docking mechanism is only used to keep the relative positions the same. No material needs to move through the docking mechanism, since the cryogenic system with the samples is moved from the AS into the RV using the robotic arm discussed in Section 5.9. Also, the only loads it must be able to carry are the forces and

moments introduced by the movements of the robotic arm. The AOCS system does not introduce any loads, because the AOCS of the orbiter and the AS work together. This means that there shall never be a force of more than 20 N or a moment of more than 200 Nm on the docking system, which are the maximum loads by the arm as described in Section 5.9.

Because of these relatively low loads compared to other docking mechanisms and the fact that no transfer through the docking mechanism is needed, the system can be far smaller than most of the docking systems currently used in space. Most docking systems are currently used on the International Space Station (ISS), and must be large enough to allow transfer of goods and humans through them. Also, the loads encountered on the ISS are far higher, because the ISS is far larger than the spacecraft for this mission, and because the ISS is in an orbit low enough to still encounter some influence by the atmosphere, which introduces some loads.

The docking systems which are not designed for the transfer of humans or goods all have a similar design. They consist of a male and a female part, which fit together. The female part grabs hold of the male part when they are close enough together, which is called the soft catch. Then, the male part is secured strongly in place by the female part, which is called the hard catch. An example of such a system is the docking mechanism which was used for the docking between the Gemini and Agena spacecraft [83].

In this spacecraft, the male part will be placed on the RV, and the female part on the AS. The male part is based on a hollow, truncated cone with a radius of 10 cm at the base and 5 cm at the top, and a length of 40 cm. The walls are made of titanium, and the thickness is 1 cm. At 10 and 30 cm from the top, grooves are present around the cone. These grooves are used for the hard and the soft catch. Also, on a part of the arc, the radius is 1 cm larger. This elevation is used to make sure that the RV and the ascent vehicle are placed at the correct relative rolling angle. All-together the mass of the male part is 15 kg.

The female part consists of a cylinder with an outer radius of 15 cm and a length of 40 cm. The inside of the cylinder is the negative of the male part, without the grooves. At 10 cm from the top, at the location of the first groove in the male part, 5 hinges powered by actuators are present. If the actuators extend, the hinges move into the groove. This is used for the soft catch. At 30 cm from the top, 5 blocks which can be moved into the hollow part by actuators are present. If the actuators extend, these blocks fit exactly into the second groove. The blocks are used for the hard catch. The structure of the female part, between the outer cylinder and inner cone, is mostly hollow to save on mass. The total mass of the female part, which is made of titanium, including the needed actuators, is 50 kg.

The male part of the docking system is shown in Figure 5.13, and the female part is shown in Figure 5.12, Note that in the female part, the hinges and blocks are shown in extended position.

The docking can be performed entirely autonomously. The LIDAR system described in Section 5.2 is used to make sure the AS and RV are properly aligned at the start of the docking operations. Using the sizes of the docking system it can be calculated that the AOCS needs to be capable of a pointing accuracy of 3° to make sure the slim end of the male part is directed into the wide end of the female part.

Figure 5.12: The female part of the docking system.

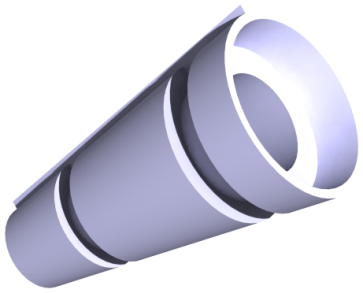

Figure 5.13: The male part of the docking system.

5.11 POWER BUDGET

In order to design the power supply one first needs to know the total amount of power required by each subsystem. Then when the required power for each subsystem for each mission phase as specified in Section 4.3 is known one can find the phase which requires the most amount of power. The results are shown in Table 5.12 where the transfer to Earth, orbiter and re-entry phases are left out, as during these phases the AS does not partake in these phases.

Table 5.12: Power budget for AS.

AS	Launch [W]	Transfer to Moon [W]	Moon descent [W]	Moon operations [W]	Moon ascent [W]
AOCS	0.0	0.0	0.0	0.0	188.5
Onboardcomputer	26.3	26.3	26.3	26.3	26.3
Communication	0.0	0.0	0.0	49.7	49.7
Cryogenics	0.0	0.0	0.0	480.0	480.0
Cryogenics for fuel cells	24.0	24.0	24.0	0.0	0.0
Docking operations	0.0	0.0	0.0	0.0	84.0
Propulsion	0.0	35.0	0.0	0.0	36.8
Robotics	0.0	0.0	0.0	110.0	110.0
Thermal	10.8	18.3	10.8	142.7	209.0
Power distribution	7.2	12.2	7.2	95.1	139.3
Additional	3.6	6.1	3.6	47.6	69.7
Total	71.9	121.9	71.9	951.4	1,393.3

Three things should be noted from Table 5.12. Firstly that all power requirements include margins using the same values for these margins for a specific subsystem as mentioned in Table 5.13. Secondly that during the ascent phase not all subsystems are active at all times during this phase. For example, docking operations will only commence when the spacecraft is already close to the orbiter, therefore the propulsion system will no longer be active as all major burns have already been done. Also docking operations, as described in Section 5.10, will require power only for a short duration instead of continuously. Furthermore, because of the percential dependence of thermal, power distribution and additional on the total amount of power, if the number of subsystems that require power simultaneously decreases, these subsystems will also require less power. Lastly the required power of certain subsystems are their maximum required power. For example, the required power for the cryogenics is the maximum amount of power this subsystem can require. It is however currently not known whether this power is required at all times and therefore the worst case was taken.

5.12 POWER SUPPLY

Using the methods as described in Section 4.3 and using the values of the specific power and power density as given in Table 4.3 one can size the power supply system. As mentioned in Section 3.2 the AS will have a solar panel and batteries as a power source.

First, the power the solar panels must generate is computed using Equation 4.15 with the results shown in Equation 5.13.

$$P_{sp} = \frac{1,393.3 \cdot (5,357 + 1,702)}{5,357} = 1,836 \text{ [W]} \tag{5.13}$$

However, as mentioned in Section 4.7 the power required should have an additional system level margin of 20 %. Therefore the design power for the solar panels will be 2,203 W. This value for the power will then be used to calculate the mass and size of the solar panels, using values from Table 4.3. The mass of the solar panels will then be 13.9 kg and the area will be 5.52 m^2.

Using the same method for the batteries one find that the design power for the batteries equals 1,672 W. The size of the batteries were computed by using Equation 4.15, with the results shown in Equations 5.14 and 5.15, where the term outside the brackets represents the DOD for the rechargeable batteries.

$$m_{bat} = \left(\frac{1,672 \cdot (1,702/3600)}{150}\right) \cdot \frac{1}{0.5} = 10.6 \text{ [kg]} \tag{5.14}$$

$$V_{bat} = \left(\frac{1,672 \cdot (1,702/3600)}{230}\right) \cdot \frac{1}{0.5} = 6.9 \text{ [L]} \tag{5.15}$$

As a last step, the power system can be summarized in an electrical block diagram (EBD), as depicted in Figure 5.14. Here it should be noted that the electrical charge protection (ECP) system is included in the voltage regulator and power distribution system. Therefore the power supply system satisfies the LCSR-Mission-Environment-08 requirement.

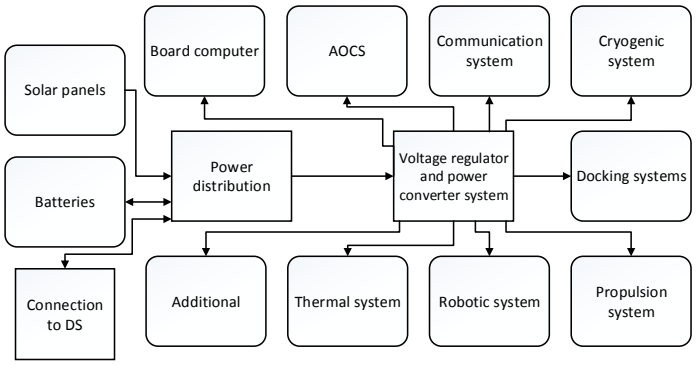

Figure 5.14: Electrical block diagram for the AS.

5.13 MASS BUDGET

Now that all systems needed aboard the AS are known and have been sized, an overview of the mass budget can be generated. This overview is given in Table 5.13. All final module or stage masses will be rounded to the nearest integer value.

This mass budget serves two purposes. In the first place, it provides a clear overview of the main components present in the AS, their respective masses and how each subsystem contributes to the grand total mass of the stage. Furthermore, it serves as a tool to identify those subsystems that drive the, in this case, mass of the design. By having this overview, the subsystems can be identified where mass reduction would be most fruitful.

Looking at Table 5.13, three main subsystems can be identified for which a reduction in mass may result in a significantly lighter total design. These system are, in descending order of mass contribution, the AOCS, the docking system and the cryogenic system. A reduction in the mass of these items would then in turn reduce the demands placed upon structural components and certain support systems. The total mass saved there, would then in turn reduce the demands placed on the propulsion system and reduce the propellant mass required. The subsequent snowball effect between reductions in structural and propulsion mass can then be exploited.

Table 5.13: AS mass budget. [a] [b] [c] [d]

AS	Estimated mass [kg]	Margin	Nominal mass [kg]
Robotic arm	35.00	0.10	38.50
Female part of docking system	50.00	0.20	60.00
Docking port	13.22	0.05	13.88
Strut interface AS and engines	4.63	0.05	4.86
Engine fixation system	1.02	0.05	1.07
Strut interface AS and orbiter[a]	9.57	0.05	10.05
AS top and bottom panels	10.63	0.05	11.16
Hardware attachment panels	13.15	0.05	13.81
Cryogenic sample storage system[b]	64.00	0.20	76.80
Communication system	9.68	0.10	10.65
Computer system	8.00	0.10	8.80
AOCS	105.89	0.05	111.19
Solar array	13.90	0.20	16.68
Battery system	10.60	0.20	12.72
Power distribution system	4.0	0.20	4.80
Thermal system	23.00	0.20	27.60
Cryogenic system for fuel cell	6.00	0.20	7.20
Additional support systems	26.00	0.20	31.20
AS Engine system	20.39	0.05	21.41
Oxidiser tank	41.00	0.05	43.05
Fuel tank	27.00	0.05	28.35
Nominal mass at launch			**554**
Total mass at launch		0.20[d]	**665**
Wet mass at launch			**2,431**
Propellant mass at launch			**1,766**
Nominal dry mass at descent			**544**
Total dry mass at descent		0.20[d]	**652**
Wet mass at descent			**2,419**
Propellant mass at descent			**1,766**
Sample[c]	1.60	-	1.60
Nominal dry mass at ascent			**546**
Total dry mass at ascent		0.20[d]	**654**
Wet mass at ascent			**1,144**
Propellant mass at ascent			**490**

[a] Only present until separation with orbiter. Remove for mass at decent.
[b] Only present until docking.
[c] Only present after drilling operations. Add for mass at at ascent.
[d] System level margin over corresponding nominal value.

Furthermore, Looking at the the design for the robotic arm, based on the DEXARM robotic arm concept, one way to reduce system mass has already been put forward by its designers. Rusconi et al. stated that a weight reduction of 0.7 kg could be achieved by replacing several aluminium components with carbon fibre reinforced plastic ones [80]. In case the length of the design would be scaled up to 2 m length, a more significant mass saving due to this change was predicted. Mass reductions for the cryogenic system might be achieved if more extensive knowledge about its exact workings would be available. However, attempts to obtain additional information from the manufacturer have thus far not yielded results [70]. Along a similar line of thought, a more detailed analysis of the docking procedure and loads involved, would allow for a better optimised and thus lighter docking system.

As can be seen in Table 5.13, the largest individual mass contribution to the AS mass budget is that of the propellant carried at launch. Using a propulsion system with a higher specific impulse, this part of the launch mass could be reduced drastically. Furthermore, a reduction in the dry mass of the AS itself would also yield a reduction in the propellant mass required, thus reducing total launch mass even further.

6 DESCENT STAGE

Using the methods as described in Chapter 4, the detailed design for the DS is made. This chapter describes the layout of the DS and the design of the most important subsystems. It concludes with the mass and power budget of the entire DS.

6.1 LAYOUT

The DS is a hexagonal platform that will make physical contact with the lunar surface. It contains the legs on which the lander stands and provides a platform on which the AS can launch from the Moon. The DS contains a drilling system which is composed of an adapted ExoMars drill design. The fuel cell is attached on the back size It has three main legs which are supported by secondary struts (see Figure 6.1). The DS contains six plates which carry the payload. The panels have a side length of 0.75 m, just as the AS. The panels have a height of 0.75 m to which most of the DS systems are attached. The drilling system and the LIDAR system are connected at the corner because the panels are clamped there. Oscillations due to acoustic noise will tried to be avoided this way. Two actuators slide the drill down so it can drill at the proper distance from the ground.

The distance of 0.5 m between the AS and DS is bridged by the use of a truss structure. In axial direction, a truss structure is made which is composed of six primary vertical members and twelve secondary sideways struts. In lateral direction, six struts are used to connect the DS with the AS.

The legs are 1.41 m high, and they have an outward distance of 0.5 m with respect to the corner of the hexagonal platform. The legs are also designed as a truss structure, with one main primary strut supported by two secondary struts (see Figure 6.1. The height allows for an engine clearance of 0.35 m. This distance is needed to prevent pressure build-up beneath the engine causing the engine to fail.

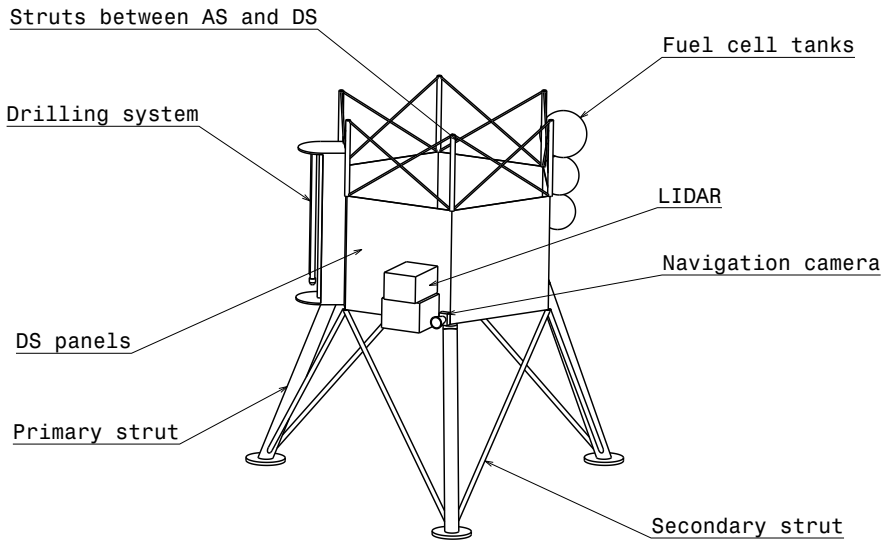

Figure 6.1: Schematic drawing of the DS.

6.2 ATTITUDE AND ORBITAL CONTROL SYSTEM

In this section the AOCS for the DS is described. First, the requirements for the design are given. Second, the design of the AOCS is elaborated. Third, the mass and power budget of the AOCS in the DS is presented and last, it is checked if the requirements are met.

6.2.1. SUBSYSTEM REQUIREMENTS

As described in Section 5.2.1 the trajectory to land on the Moon is the same as for the launch from the Moon. Thus, the pitch rate and pointing accuracy requirements are the same and the lander shall be able to pitch with a pitch rate of 300 °/min and the pointing accuracy shall be less than 0.5 °. Additionally, the lander shall be able to handle the disturbances during landing.

6.2.2. AOCS DESIGN

The design of the AOCS is split up into actuators, sensors and controllers.

Actuators The required force to pitch and roll the lander were calculated with the methods elaborated in Section 4.1 to be 45.2 and 11.8 N respectively. Since the lander consists of the AS and DS, the DS can use the AOCS components of the AS. The thrusters of the AS are able to supply 88 N for both pitching and rolling as has been described in Section 5.2.2. If one thruster fails, the available thrust force reduces to 44 N. In that case the required 45.2 N cannot be met for pitching. However, the high pitch rate is required for the main landing after the main braking in the approach phase. Thus, most propellant has been already used when the main landing procedure is performed. From this follows, that the required force reduces. The average of the required force for the lander and the stand-alone AS is 37.1 N which is below the 44 N available in the worst case. Nevertheless, it is possible to roll the lander by 90° and pitch around the other axis. Thus redundancy is present.

The same reasoning holds for the reaction wheels. The calculated expected disturbances are $1.1 \cdot 10^{-3}$ Nm and 0.7 Nms. The reaction wheels in the AS are capable of cancelling these gravitational disturbances as well and therefore it can be concluded that the DS does not have to be equipped with actuators.

The mass of the propellant was computed as explained in Section 4.1. For landing 30 s were used including the 100 % margin which is defined by ESA [51]. Propellant mass for momentum dumping is not required for the DS, since the reaction wheels are able to store all the disturbance momentum received during landing and can dump it on the surface of the Moon. The resulting propellant mass is 8.57 kg. However, the propellant is stored in the main tank of the AS. Thus the propellant mass is listed in the mass and power budget of the AS and not of the DS.

Sensors Apart from the sensors already present in the AS, the DS is equipped with two LIDAR systems, one radar altimeter and two navigation cameras. The sensors are required to provide guidance for the landing. Since the landing site is in constant shadow, sensors which function in darkness are needed. That is why the DS is equipped with two additional LIDAR systems. A LIDAR system is a laser-based technology which sends a laser beam and analyses the reflected light and therefore does not need present light to operate. The two LIDAR systems are mounted at the bottom of the DS to have a clear view on the landing site. One of the LIDAR systems is mounted for redundancy because the LIDAR system on the AS cannot be used in this phase because it does not have line of sight to the landing site. Although the cameras cannot produce pictures in darkness, they are still needed to locate the correct crater during the approach phase. Thus next to each LIDAR also one camera is mounted. The radar altimeter was chosen to be able to identify the altitude of the lander at an early stage of the landing phase. It is produced by Honeywell and can track altitudes up to 2,400 m [84]. The maximum target distance for the LIDAR system is 1,500 m [56].

Controllers The sensors are connected to the AOCS of the AS. Therefore, no additional computer is needed.

A total overview of the components can be found in Figure 6.2 and the input and output data of the calculation are presented in Tables 6.1 and 6.2. The interactions between the actuators, sensors and controllers have been explained and can be found in Section 5.2.2.

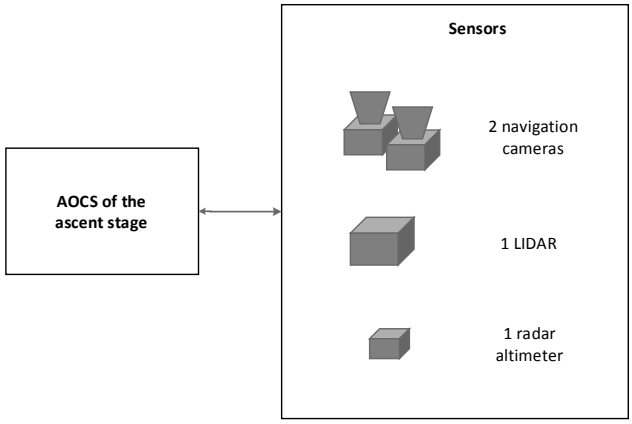

Figure 6.2: AOCS components in DS.

Table 6.1: AOCS calculation input of the DS.

	$I_{x,y}$ [kgm^2]	I_z [kgm^2]	$\dot{\theta}$ [°/min]	T_{op} [days]	x_{man} [-]	$t_{burn_{man}}$ [s]	$t_{burn_{dump}}$ [s]	I_{sp} [s]	h [km]	μ km^3/s^2
Landing	1,242	324	300	0.41	30	3	1	290	0	4,902.8

Table 6.2: AOCS calculation output of the DS.

	F_{pitch} [N]	F_{roll} [N]	t_g [s]	h [Nms]	m_{prop} [kg]
Landing	45.2	11.8	$1.1 \cdot 10^{-3}$	0.7	8.57

6.2.3. MASS AND POWER BUDGET

The mass and power budget of the AOCS in the DS can be found in Table 5.3. For both the mass and the power a margin of 5 % was chosen, since all products are off-the-shelf. The total mass of the AOCS in the DS is 32 kg and the total power is 59 W.

Table 6.3: AOCS mass and power budget of the DS.

Component	Unit mass [kg]	Number total (active)	Mass [kg]	Unit P_{req} [W]	P_{req} [W]	T_{op} [°C]
Sensors						
Navigation camera [57]	0.59	2(2)	1.19	2.5	5	-20 to 40
LIDAR [56]	13.80	1(1)	13.80	35	35	-35 to 65
Radar [84]	1.36	1(1)	1.36	16	16	-51 to 49
Sum			30.15		56	-20 to 40
Margin			0.05		0.05	
Nominal			31.66		58.80	

6.2.4. AOCS REQUIREMENTS

The requirements defined in Section 6.2.1 are met by the AOCS. It is able perform the required manoeuvres and withstand the expected disturbances while landing in the shadow of the Wiechert J crater. Furthermore, the AOCS is redundant and is therefore not affected by single subsystem failures.

6.3 THERMAL SYSTEM

In this section the thermal control system of the lander is treated during Moon operations. First the assumptions are explained, second the results of the calculations are shown in Table 6.4, last a qualitative design of the thermal control systems is given for the lander.

6.3.1. ASSUMPTIONS

The first assumption is that the Moon does not radiate any heat in the crater and thus cannot be used as source of heat. This means that apart from the conductivity of the Moon surface the choice of the Wiechert J on basis on the radiating temperature is invalid. That the Moon radiation does not have an effect can be shown by the calculation shown in Equation 6.1. In this equation T is 110 K (temperature in wiechert J), σ is the Boltzmann constant and ϵ is for simplicity taken as 1 to be conservative [59]. The Moon radiates 5.67 W/m^2, resulting in a total heat influx of 28 W, which is less than 2 % of the total heat radiated off the spacecraft [59].

$$q_{IR} = \epsilon\sigma T^4 = 1 \cdot 5.67 \cdot 10^{-8} \cdot 110^4 = 5.67\text{W/m}^2 \tag{6.1}$$

The second assumption is that the heat loss due to conduction in the leg is zero. This is assumed because regolith is a good insulator and the legs are constructed such that there is only a small cross-sectional area to exchange the heat [85]. In addition it simplifies the model since there is no need to solve the heat equation for a situation where the boundary values are unknown.

The last assumption is that the fuel cell produce heat, unlike the solar cells. The fuel cell power efficiency is 50%, the other half is transformed by the cell into heat [86] [87].

6.3.2. THERMAL MODEL RESULT

With the assumptions as stated in Section 4.2 the model is used to calculate the equilibrium temperature. The results are shown in Tables 6.4 and 6.5. As can be seen from Table 6.5, the equilibrium temperature equals 286 K, which is within the required temperature range as mentioned in Section 5.3. It can be stated that from the thermal equilibrium temperature the requirement LCSR-Mission-environment-09 is met. For the AS the coating was already chosen, influencing the design choice for the descent stage. The coating chosen for the DS is the same as used for the other modules, namely an aluminium paint. The estimates for the required mass and power for the thermal control system are 55 kg and 22 W respectively. These estimates are based on concept 5 [8] [33].

Table 6.4: Thermal equilibrium of the DS - input for the model.

Parameters	Values	Unit
α_{eff}	0.15	[-]
ϵ_{eff}	0.303	[-]
σ	$5.67 \cdot 10^{-8}$	[(m^{2}kg)/(s^{2}K)]
A_{tot}	14	[m^2]

Table 6.5: Thermal equilibrium of the DS - output of the model.

Parameters	Values	Unit
Q_{solar}	0	[W]
Q_{IR}	0	[W]
Q_{alb}	0	[W]
Q_{int}	2776	[W]
T	309	[K]

6.3.3. THERMAL CONTROL SYSTEM DESIGN

The internal heat of the spacecraft is produced mainly by the fuel cell which is placed in the DS. However most of the heat is needed in the AS since most critical systems are placed there. The heat will be transferred with a heat pipe system, which uses the heat produced by the fuel cell to create a heat flow to the AS to radiate heat in the AS. These heat pipes will go through the centre of the spacecraft, between the DS and AS to minimise the heat loss.

In addition heaters are placed to ensure that there is enough heat for the critical systems. For example, the legs can become too brittle for the ascent phase to serve as landing platform, if they are too cold. In this case additional heaters can be placed to ensure good mechanical properties for the landing platform. The masses and power required for these heaters are included in the estimation for mass and power.

Some additional considerations should be mentioned. The lander can be wrapped in Multi-Layered Insulation (MLI) keeping heat within the spacecraft and the heat pipes to the AS can be wrapped in MLI as well, minimising further heat loss out of the spacecraft.

6.4 STRUCTURES AND MATERIALS

The DS will touch the lunar surface physically and thus requires a leg structure which supports both the DS and the AS. The DS provides a platform from which the AS will takeoff before it arrives in lunar orbit. The DS stage is driven by the Moon operations phase. During launch the DS is located on top of the spacecraft in the fairing. Because it is stowed this way it receives little compression forces during launch compared to the other modules. Compressive forces during landing and take-off from the Moon will drive the design.

6.4.1. LEG DESIGN

The first choice in the design of the legs is the number of legs. The surface inside a crater may contain rocks with a variety of sizes. In the case that a four-legged lander lands with one of its legs on such a rock, one leg of the four-legged configuration will not touch the ground. When there are disturbances in the equilibrium (for example when the engine is turned on) the lander will swing around the axis that is formed by the leg that has landed on the rock and the leg opposite to it due to its bilateral symmetry. If this situation occurs for a three-legged lander, the spacecraft can not swing along an axis since there is no bilateral symmetry. Taking this into account, it is chosen to use a three-legged configuration for the DS.

The dimensions of the legs are driven by stability requirements and engine clearance requirements. For the engines to take-off successfully, there has to be clearance between the nozzle and the ground. If this is not the case, pressure builds up causing the engine to fail. An engine clearance of 35 cm was assumed for proper operations, but no proper reference was found about the required value.

Before the legs can be sized, the dynamic loads which occur during landing need to be evaluated. The speed at which the spacecraft hits the ground is 1.5 m/s as was shown in Section 3.3.4. Proper shock absorption needs to be provided to dissipate the kinetic energy of the spacecraft at landing. A hydraulic spring is used to dampen the landing. The OEMXT 3/4 X1 hydraulic shock absorber will be used. It has a maximum reaction force of 2 kN, a mass of 1.2 kg and a diameter of 90 mm [88]. Hydraulic springs can pose problems due to outgassing in space environments but are self-resetting. Because of this and its successful application during the Surveyor mission it is chosen to use hydraulic springs [89]. For an impact velocity of 4 m/s, a spacecraft centre of gravity acceleration of 8 g was found [43]. The Lunar SECRet mission hits the ground with 1.5 m/s: assuming 8 g is a conservative value to model the dynamic loads for the Moon landing.

The legs are designed such that one leg can take the entire load of the spacecraft. Due to the use of a conservative estimation for the landing loads, a safety factor is already included. If the legs would be sized for an equal distribution of the landing forces, this would mean that the legs would break while landing. The following resulting force will be applied at each leg contact point:

$$F_{dyn} = (m_{AS} + m_{DS} - m_{LLO-LS}) n_{Moon} g_{Moon} = 16.8 \text{ [kN]} \tag{6.2}$$

The mass of the AS includes the propellant that is left at touch-down, so the propellant mass for braking (m_{LLO-LS}) is omitted. Using Equation 4.18 the forces in each strut are computed. The dynamic compressive force in the primary strut acting on one leg is 66.4 kN and the secondary struts have a tensile force of 39.5 kN. It is chosen that the primary strut has an outer radius of 45 mm (to accommodate the hydraulic spring) and a thickness of 3 mm, and the two secondary struts an outer radius of 15 mm with a thickness of 3 mm. The moment of inertia and cross-sectional area of the primary strut are $7.8 \cdot 10^{-7}$ m^4 and $8.2 \cdot 10^{-4}$ m^2 respectively. For the two secondary struts it is $2.3 \cdot 10^{-8}$ m^4 and $2.5 \cdot 10^{-4}$ m^2 respectively. These parameters can be used to compute the critical buckling force using Equation 4.22.

$$F_{crit} = \frac{\pi^2 EI}{L^2} = 2.4 \cdot 10^5 \text{ [N]} \tag{6.3}$$

This results in a safety factor of 3.6, which is high because of the required radius of the springs. The tension force in the secondary strut is 39.5 kN. The stress should not exceed the yielding stress of aluminium 6061 which

is 276 MPa [45]. Equation 4.17 is used to compute the tensile stress.

$$\frac{F_{ten}}{A} = \frac{3.95 \cdot 10^4}{2.5 \cdot 10^{-4}} = 155 \text{ [MPa]} \tag{6.4}$$

The safety factor is thus 1.8 which makes the design structurally sound.

It can be concluded that the legs are properly designed for the dynamic lunar environment. Since the dynamic environment is by definition a factor on top of the static environment, the legs are properly designed for static conditions as well.

6.4.2. STRUTS BETWEEN ASCENT STAGE AND DESCENT STAGE

Using Equation 4.18 the force in each member between the AS and DS is calculated. An axial force of 25.2 kN and a lateral force of 8.4 kN are acting on the struts. At each strut there is an axial load of 4.2 kN and a lateral load of 1.4 kN. Since the spacecraft is connected only at the adapter, there will also be a bending load induced by the spacecraft lateral acceleration (see Figure 5.6).

$$F_{bend} = \frac{D m_{DS} n_{lat} g_{Earth}}{4x} = 4.5 \text{ [kN]} \tag{6.5}$$

This force is added to the 4.2 kN load leading to a combined axial load of 8.7 kN. The primary struts are chosen to have an outer radius of 15 mm and a wall thickness of 5 mm, leading to a moment of inertia of $3.2 \cdot 10^{-8}$ m^4 and a cross-sectional area of $3.9 \cdot 10^{-4}$ m^2.

Using Equation 4.18, the forces in each member can be computed. For the primary strut, a compression force of $1.12 \cdot 10^4$ N is found. For determining the critical buckling load Equation 4.22 will be used:

$$F_{crit} = \frac{\pi^2 EI}{L^2} = 2.1 \cdot 10^5 \text{ [N]} \tag{6.6}$$

which leads to a safety factor of 1.94. Thus the structure is capable of dealing with the launch gravitational forces.

For the secondary strut a tensile force of 2.2 kN is found. The secondary struts are chosen to have an outer radius of 5 mm and a wall thickness of 3 mm, leading to a moment of inertia of $4.8 \cdot 10^{-10}$ m^4 and a cross-sectional area of $6.6 \cdot 10^{-5}$ m^2. To determine if the secondary strut does not yield, Equation 4.17 is used.

$$\frac{F_{ten}}{A} = 140 \text{ [MPa]} \tag{6.7}$$

The yield strength of aluminium 6061 is 276 MPa [45]. This leads to a safety factor of 1.96. Thus, the structure is structurally sound for tension in the secondary struts. There is no compression in the secondary struts.

6.4.3. PANEL DESIGN

The panels are designed to carry the payload of the DS, including the drilling system as well as pressurant tanks and sensors. The panels of the DS take up the dynamic forces of the AS and DS including its propellants during landing, and will be designed for buckling. The plate structure is hexagonal, with each side have a length and height of 0.75 m and a wall thickness of 2 mm. Equation 4.23 will be used to assess the critical buckling force for the panels:

$$F_{crit} = \frac{k\pi^2 EA}{12\left(1-\nu^2\right)}\left(\frac{t}{b}\right)^2 = 54.2 \text{ [kN]} \tag{6.8}$$

Aluminium 6061 is used as material for the panels. The resultant force that acts on the panels is the same as for the legs. This leads to a safety factor of 2.2.

6.4.4. VIBRATION CONSIDERATIONS

Due to vibration considerations (which will be explained in Section 8.5), the structure needs to be reinforced in lateral direction in order to provide sufficient stiffness for lateral vibrations. Six struts are added that connect the AS with the DS. They have an outer radius of 5 mm and a wall thickness of 1 mm. This is done because

the equivalent stiffness of the connection between the DS and AS increases such that the lateral frequency requirement is not violated. Before applying these struts the lateral frequency would have been 3.2 Hz. After applying them it becomes 30 Hz, well above the 10 Hz requirement as stated in Table 4.6.

6.5 DRILL

As a means of extracting the core sample from the lunar surface, the choice has been made to use a drilling system [8]. In this section, the first step will be to elaborate on the drill system chosen. Subsequently a physical outline of the drill system will be presented. Finally the drill's deployment and retrieval of the sample will be detailed. Note that the main goal in this design phase is not to create a complete drill design. It is to provide a first conceptual outline of a drill system, based on that used by the ExoMars, that will be tailored to the Lunar SECRet mission.

6.5.1. SYSTEM SELECTION

In line with the design choices made in the Mid-Term Report and embodied in the concepts as presented in Section 2.3, the choice has been made to use a drilling system to obtain the lunar core sample [8]. From the drill systems selected in the preliminary design phase the Auto-Gopher drill, as used by concept 1, and the specific custom drill system envisioned by concept 2, were discarded. The main reason for rejecting the Auto-Gopher system was the lack of information that could be retrieved about the system [90]. Despite an attempt from the design team, no relations have as yet been established with Honeybee. The custom drill design created for concept 2 was rejected because of the high vertical force it required [8]. The choice was therefore made to base the drill on the ExoMars system, as used in concepts 3, 4 and 5 [8].

At the start of the detailed design phase, two issues with the standard ExoMars system were uncovered. To begin with, the standard ExoMars system has to retract from the drill hole to retrieve each individual 3 cm long sample. This adds time to the operations at the sampling site and given the extreme thermal environment and operational time limit imposed by the fuel cell system, it is desirable to minimise time required on the Moon for the mission. The other drawback is that the precise sample ejection mechanism used by the ExoMars drill is not known, which is required for an optimal integration with the other subsystems. The choice was therefore made to use a modified multi-rod ExoMars drive train system and create a custom drill shaft and recovery mechanism. The drive-train mechanism is contained in a casing, which has dimensions of approximately 1 by 0.3 by 0.3 m.

6.5.2. DRILL SYSTEM DESIGN

In this subsection the design of the drill shaft and bit, liner and its integration with the DS will be discussed in more detail.

DRILL SHAFT AND BIT DESIGN

As stated, the drill system will use the ExoMars' drive-train system to extract the sample from the lunar surface. The drill shaft itself will consist of several sections of hollow shaft that will be stacked on top of each other as the drill progresses into the lunar surface. These extension drill shafts are stored inside the modified ExoMars drill in the way for which the system is designed. At the tip of the first drill section the drill bit is located. The material selected for the hollow shafts and bit is titanium, because of the low temperature of the lunar regolith in which they need to operate [72]. The initial drill shaft and each extension shaft will contain a non-rotating liner on the inside to protect the sample, which will be discussed later in this section. Equations 6.9 to 6.12 are used for the sizing of the shafts [91].

$$V = \frac{l}{t} \tag{6.9}$$

$$f = \frac{V}{n} \tag{6.10}$$

$$F_D = 0.63 \frac{f \cdot w \cdot Kc}{2} \tag{6.11}$$

$$M = \frac{d^2 \cdot Kc \cdot f}{8000} \tag{6.12}$$

First of all, the required speed (V) is calculated. The drill system will be designed to reach 2.20 m surface penetration within 6 hours. Given this drilling time (t) and drill depth (l) a penetration speed of 6.11 mm/min is required. The number of revolutions is set by the drill used. In lunar regolith, a safe rotational speed (n) is 60 rev/min [92]. This means that penetration per revolution (f) becomes 0.102 mm/rev. For the required force and moments, the thickness of the drill shaft's wall (w) needs to be known. The sample diameter has been set at 2 cm. For the liner, made of ultra high molecular weight polyethylene (UHMW PE), a thickness of 1 mm is assumed. This thickness can be small, because the liner does not need to carry any compressive load. This means that the hollow part of the drill has a diameter of 22 mm. The drill itself is set to be at least 2 mm thick to facilitate the connecting of subsequent shaft sections. Using the equations for hollow shafts found in Section 4.4 it is found that the wall thickness required to sustain the torsional and compressive loads are both smaller than 2 mm. With the 2 mm thickness, the drill can withstand a compressive force of 26 kN, and a torque of 12 kNm. Calculations were therefore performed using an outer diameter of 26 mm. Lastly, the specific cutting force (Kc) of the lunar regolith is required, which is not a known number at this time. The specific cutting force of hardened steel was used as a very conservative substitute, which is 300 N/mm^2. This leads to a required downwards force (F_D) of 250 N, and a torque (M) of 2.58 Nm. Given a gravitational acceleration at surface level of 1.62 m/s^2 on the Moon, and the dry mass of the DS and wet mass of the AS at the lunar surface, as can be found in Table 6.8 and 5.13 respectively, the lander weight can be determined to be 2529 N [59]. This weight is sufficient to ensure the lander can exert the required amount of force on the drill.

The outer diameter of the drill bit is larger than that of the rest of the shaft to accommodate the sample isolation device (SID) that is housed there. The SID will be used to separate the bottom of the drill core from the lunar rock and prevent it from sliding out of the drill as it is being retracted. In the current design, the SID will consist of two sphere sections that, when activated, will snap inwards to seal of the end of the drill shaft. This is the same working principle as applied in the ExoMars drill, as seen in Figure 6.4. An assessment will have to made in later stages of design of this system's ability to cut through lunar regolith at conditions as expected on the sampling site. The SID is attached to the liner in order to keep the sample in place as the sample is being retrieved. The bit itself will have a material wall thickness of 2 mm, like the drill shaft. A sketch of the drill bit can be seen in Figure 6.3.

The ExoMars drill drive-train is, without modifications, already capable of delivering these amounts of torque, and vertical force and this penetration rate [93]. The standard system has a mass of 21 kg and power requirement of 80 W [82]. Taking the changes to be made to the standard system into account, a conservative mass estimate for the Lunar SECRet drill system has been set to 30 kg and required power is estimated to be 100 W.

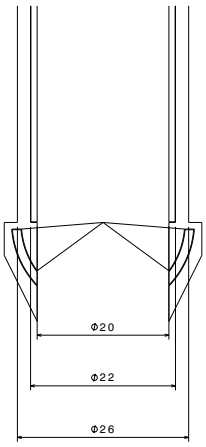

Figure 6.3: Sketch of the drill bit including SID. For illustrative purposes only.

Figure 6.4: SID as used on the ExoMars drill [93].

LINER DESIGN

The drill liner performs three major functions. In the first place it forms a barrier between the sample and the environment. In this role it prevents lubricants used on the inner surface of the drill from affecting the sample, friction between the drill and drill core, and contact between the vacuum of space and the sample during sample recovery. Besides this, the liner will provide rigidity to the sample during processing. In case sections of the core sample would consist of powder-like material, it contains that powder and prevents distortion to some degree. Finally, the liner will play an important role in the processing mechanism itself. To meet the requirements that follow from these functions, the liner material will have to be stiff, offer some degree of impermeability to gasses and remain operational at temperatures below 120 K. UHMW PE is a material that fits these requirements, with service temperatures down to 23 K and a Young's modulus upwards from 690 MPa [94] [95] [96]. At later stages of design, care should be taken that the exact design of the liner will allow the cutting tool to through the liner, as well as through the sample.

Given the fact that the liner will keep the sample together in case it turns out to be of a powder-like consistency, it can be ensured that the sample will be returned in the form of either powder, fragments or intact rock. It can therefore be stated that requirement LCSR-Mission-Sample-06 has been met.

It is known from the ExoMars drill, that drilling characteristics have been chosen such that interaction between the drill and sample should never result in the temperature of the sample increasing by more than 5 K [97]. In addition, the non-rotating liner will protect the sample from friction with the drill shaft and provide a thermal barrier. Given that the maximum and minimum daytime temperatures of the sampling site are respectively 120 K and 40 K, the requirement of the sample never exceeding a temperature of 120 K is met as long as a landing location and moment will be selected at which the surface temperature is at least below 115 K. This is realistic in the Wiechert J crater [2]. Requirement LCSR-Mission-Sample-08 is therefore met as far as drilling operations are concerned.

SYSTEM INTEGRATION WITH DS

Regarding the integration of the drill system with the rest of the spacecraft, several items need to be addressed. The drill will be attached to the side of the DS and lowered to the ground with vertical guide rails, which are attached along both sides of the drill. These rails are driven by two linear actuators located in the side the DS [98]. As a first step for this integration, attention is paid to the vibrational loads introduced into the structure by the drill system. It proved not possible to obtain the operational vibrations created by the ExoMars drill system [97]. Because of this, no structural design has yet been made for the guide rails that form the interface between the drill system and DS. No verdict could be made on whether the rails would be compatible with this load case. To protect the lander from the vibrational load, a damping system may need to be added to the actuators that support the drill rig. Besides this, as stated, the drill needs a downwards applied force of 250 N. The two guide rails will therefore have to be able to withstand a load of 125 N without buckling. As a final point, the drill system will have to be connected to the power supply of the lander and the central computers for data and command processing. This interface will be provided by a cable assembly that is stored inside the supportive guide rails.

It can be stated that the forces exerted by the drill system on the rest of the lander will not endanger the lander's structural integrity. The guide rails with which the drill is lowered from its stored to its operational position can later be sized not to buckle under the compressive load of 125 N per rail required for operating the drill. Furthermore, since the supportive structure of the DS has been designed to withstand launch loads, it is assumed this 250 N of load integration can be dealt with adequately. Regarding the drill, it can therefore be stated requirement LCSR-Mission-Forces-03 can be met.

6.5.3. OPERATIONAL PROCEDURE

In this subsection the procedure of drill deployment and sample recovery will be detailed.

Upon landing, the drill will be deployed from its stored, upright position on the side of the DS of the lander. Using the actuators from the deployment mechanism, the drill system is then lowered to ground level where operations can commence.

When at the ground, the drill system will start by driving a first 70 cm long hollow drill shaft, tipped with the drill bit, into the ground. When the first section of drill shaft has penetrated the lunar surface to an extent dictated by the ExoMars drill system, an extension shaft will be placed on top of it. This exact penetration

extent is not available yet, but should be such that enough of the initial shaft is inside the drill drive train mechanism to secure it to the following shaft. The liner of each new shaft will be connected to the previous one using a mechanical joint. The connection in the drill drive shafts itself is made using existing ExoMars drill technology.

A total of three hollow extension drill shafts, each with a length of 60 cm, will subsequently be added to the initial 70 cm shaft. The full length of the drill shaft, including the bit, will therefore be 2.50 m. Each shaft is added as soon as its predecessor has penetrated the soil to a predefined extent. This process yields a final drill depth of 2.20 m, which means the last 30 cm of liner contains no sample. This allows the drill system to meet the requirement of retrieving a sample down to 2.00 m depth. The final 20 cm of the final extension rod will exist of exposed liner material, not encased in titanium. This which will be used in retrieving the sample from the drill.

Located in the top of the drill housing are sets of guide wheels. As soon as the SID has been activated, the drill drive-train will engage reverse gear and retract the drill until a 20 cm section of exposed liner is clamped by the guide wheels. These wheels will then turn, pulling the liner with the sample within upwards. The exact workings and sizing of this recovery system should be subject to further, more detailed research.

As soon as the top of the liner has reached the top of the drill housing, a hatch in the top of the drill housing will slide open. The guide wheels will then proceed to guide the sample and liner up, until the top 10 cm of the liner are outside the drill casing. A sample cutting tool attached to the end of the robotic arm will then proceed to remove the top 10 cm of liner, which does not yet contain any sample, and discard it. At this point the guide wheels lower the liner and sample until below the slide and the slide closes, thus protecting the sample inside the liner somewhat from the lunar environment. This step is repeated twice more, so all liner without sample is removed. After the empty top 30 cm of liner has been removed a cycle is followed that consists of waiting for the cutting tool to arrive at the top of the drill, opening the slide, filling the sample cutting tool with a 10 cm piece of liner encased sample, retreating the sample after cutting and closing the hatch. The robotic arm places each of the recovered samples in the cryogenic system after obtaining it from the drill. This cycle is continued until 20 samples of 10 cm have been recovered.

By retrieving 20 samples of 10 cm, a complete 2 m long core sample is obtained and by storing the samples per 10 cm it is ensured that, even if the samples would get disturbed inside the canister, at least a 10 cm resolution remains. This means requirement LCSR-Mission-Sample-05 and LCSR-Mission-Sample-07 have been met.

6.6 LANDING SITE CONTAMINATION

In the Mid-Rerm Report the possibility was put forward that landing on the sampling site might cause the lunar surface to heat up, causing a loss of sample quality [8]. First-order calculations were performed to investigate the increase in temperature which can be expected in the lunar soil during landing.

Thermal conditions in the regolith for the top 5 cm have been analysed using Fourier's Law of conductive heat transfer is applied, as expressed in Equation 6.13. To this end, a 1 by 1 cm reference area (S) placed directly underneath the main lander engine has been considered. This area was then discretised into 1 cm^3 cubes, ending at depths of 1, 2, 3, 4 and 5 cm (parameter s).

$$q = \frac{k \cdot S \cdot \Delta T_{con}}{s} \tag{6.13}$$

where q is the energy flow in into each cube measured in W, k is the thermal conductivity of lunar regolith in W/(m·K) and ΔT_{con} is the temperature difference between the exhaust plume and the lunar subsurface driving the conduction expressed in K. The chemical rocket plume is estimated to have a temperature of 4100 K [99]. The lunar surface will be at most 120 K. A typical value for k at the lunar surface encountered in literature is $1.5 \cdot 10^{-3}$ W/(m·K), which increases with depth [30] [100] [101]. However, Sakatani et al. states that even near surface, values near $1 \cdot 10^{-2}$ W/(m·K) may be encountered [101]. This value will therefore be used for computations. As stated in Section 3.3.4 the final vertical descent of the lander to the landing site will last for about 10 s. Let the time during which the engine influences the landing site surface (t_{site}) be these full 10 seconds, the hottest part of the plume maintain contact with and conduction be the heat transfer mechanism. In this way the total energy absorbed directly under the main engine may be determined for each depth. In this model, the temperature differences between each of the 1 cm^3 cubes are assumed to be small compared to

those between each cube and the exhaust plume. Heat flow due to temperature differences of adjacent cubes is therefore neglected.

The increase in temperature resulting from the inflow of energy may be determined by Equation 6.14, where c is the specific heat of lunar regolith in J/(kg · K) and m the mass of the cube under investigation. The lowest value for c presented by Hemingway, for temperatures in the range of 120 K, is 322.6 J/(kg · K) [100]. In addition, a low regolith density of 1300 kg/m^3 is given here. These lower estimates will be used for conservatism. Assuming all parameters remain constant during t_{site} and applying Equation 6.13 and 6.14 yields temperatures directly beneath the main descent engine as found in Table 6.6.

$$\Delta T_{site} = \frac{q \cdot t_{site}}{c \cdot m} \tag{6.14}$$

Table 6.6: Heat transfer to and temperature in lunar soil directly below descent engine.

Depth [cm]	Heat transfer [W]	ΔT_{site} after 10 s of exposure [K]
1	0.40	9.5
2	0.20	4.7
3	0.13	3.2
4	0.10	2.4
5	0.080	1.9

These are temperature increases as encountered in the lunar regolith, immediately under the descent engine and using worst-case parameter values in all calculations. Since the drill will be deployed from the side of the spacecraft, heating at the location where the drill will take the sample will already be less than indicated in Table 6.6. Since in Subsection 6.3.1 it has been stated that heating of the spacecraft due to thermal radiation from the Moon can be neglected, the easiest way to ensure landing does not increase the regolith temperature to above 120 K would be to plan the landing for a time and exact site at which surface temperatures are expected to be lower than 110 K. In this way, the requirement to keep the sample under 120 K at all times is not compromised by landing on the sampling site. Since the Wiechert J crater has a maximal and minimal daytime temperature of 120 K and 40 K respectively, this is a possibility at the chosen site [2].

6.6.1. VERIFICATION AND VALIDATION

Verification of this tool has been carried out by setting the plume temperature equal to the temperature of the lunar surface. This should yield a ΔT_{con} of 0, and therefore a ΔT_{site} of zero. The value for ΔT_{con} has also been halved with respect tot that used for the calculations earlier in this section, which yielded a decrease in temperature change of 50%, as was expected. In addition, the thermal conductivity k has been set to both 0 and half the value used in the calculations. As expected, this resulted in no heat flow and therefore a ΔT_{site} of 0 K, and half the values for ΔT_{site} found in Table 6.6 respectively.

A first-order validation of the model has been performed, testing the model's ability to perform basic conduction problems. The calculation belonging to example 1.1 from [102] has been performed using this model, and outcome data matched.

Proper validation of the model is not possible since no experimental test can be performed within the scope of this project. Ideally, this model would be tested using a smaller scale MON/MMH engine, having similar thermal characteristics as the engines used in the mission. Taking a large body of lunar stimulant that has been cooled to 110 K and exposing it to the engine plume for 10 s would then give an indication of the thermal behaviour of the system. The data from this test, could then be used to validate the preliminary estimation tool.

6.7 POWER BUDGET

In order to design the power supply one first needs to know the total amount of power required by each subsystem. Then when the required power for each subsystem for each mission phase as specified in Section 4.3 is known one can find the phase which requires the most amount of power. The results are shown in Table 6.7

where only the Moon descent and Moon operations are included, because the DS has either no active subsystems or the DS has been discarded in the other phases.

Table 6.7: Power budget of the DS.

DS	Moon descent [W]	Moon operations [W]
AOCS	58.8	0.0
Cryogenics for fuel cells	0.0	24.0
Drill	0.0	110.0
Robotics	0.0	10.0
Thermal	12.6	30.9
Power distribution	8.4	20.6
Additional	4.2	10.3
Total	84.0	205.7

6.8 POWER SUPPLY

Using the methods as described in Section 4.3 and using the values of the specific power and power density as given in Table 4.3 one can size the power supply system. As mentioned in Section 3.2 the DS will be powered by a fuel cell. However, as stated in Section 3.1, the entire lander is powered by the fuel cell located in the DS during lunar operations. Therefore the fuel cell must generate enough power to power the equipment on both the DS and the AS during lunar operations.

From Tables 5.12 and 6.7 one can find that a total power of 1,157 W needs to be generated by the fuel cells. However, as mentioned in Section 4.7 the power required should have an additional system level margin of 20 %. Therefore the design power for the fuel cells is 1,388.4 W. Using the values of the specific power and power density as given in Table 4.3, the mass and size of the fuel cell were computed. The mass of the fuel cell will then be 5.6 kg and the volume of the fuel cell will be 5.4 L.

To compute the fuel consumption one needs the thermal efficiency, which was found to be 50 % for the chosen fuel cell [86] [87]. Using the specific energy of hydrogen and the maximum operational time as mentioned in 3.1, the required hydrogen mass was computed. The results are shown in Equation 6.15.

$$m_{LH_{2_{fc}}} = \frac{P_{fc_{design}} t_{op}}{E_{\rho_{H_2}} \eta_{fc}} = \frac{1388.4 \cdot (6 \cdot 24 \cdot 3600)}{142 \cdot 10^6 \cdot 0.5} = 10.2 \text{ [kg]} \tag{6.15}$$

where t_{op} is the operational time, $E_{\rho_{H_2}}$ is the specific energy of liquid hydrogen and η_{fc} the thermal efficiency of the fuel cell [103]. One can then compute the mass of the required liquid oxygen (LOX) by using the mass ratio between LOX and LH_2, which is 1 to 8 , as shown in Equation 6.16 [41].

$$m_{LOX_{fc}} = m_{LH2_{fc}} \cdot 8 = 81.6 \text{ [kg]} \tag{6.16}$$

For the sizing of the mass of the fuel cell reactant tanks statistical relationships from the University of Maryland have been used [104]. The mass of the fuel tank is related to the mass of the fuel, the relation can be found in Equation 6.17. The relationship for the LOX tank is given by Equation 6.18. The mass of the insulation needed is related to the fuel mass by Equation 6.19 for hydrogen and Equation 6.20 relates oxidiser mass to insulation mass for tanks filled with oxygen [104].

$$m_{LH_{2\,tank}} = 0.128 m_{LH_{2\,fc}} \tag{6.17}$$

$$m_{LOX\,tank} = 0.0107 m_{LOX_{fc}} \tag{6.18}$$

$$m_{LH_{2\,insulation}} = 11.52\pi \left(\frac{3 m_{LH_{2\,fc}}}{4\pi \rho_{LH_2}} \right)^{\frac{2}{3}} \tag{6.19}$$

$$m_{LOX\,insulation} = 4.492\pi \left(\frac{3 m_{LOX_{fc}}}{4\pi \rho_{LOX}} \right)^{\frac{2}{3}} \tag{6.20}$$

where ρ_{LH_2} is the density of LH_2 and ρ_{LOX} is the density of LOX. From these equation the total mass of the fuel and oxidiser tanks for the fuel cell reactants were computed.

$$m_{LH_{2\,tank}} = 0.128 \cdot 10.2 = 1.3 \text{ [kg]} \tag{6.21}$$

$$m_{LOX\,tank} = 0.0107 \cdot 81.6 = 0.9 \text{ [kg]} \tag{6.22}$$

$$m_{LH_{2\,insulation}} = 11.52\pi \left(\frac{3 \cdot 10.2}{4\pi \cdot 71}\right)^{\frac{2}{3}} = 3.8 \text{ [kg]} \tag{6.23}$$

$$m_{LOX\,insulation} = 4.492\pi \left(\frac{3 \cdot 81.6}{4\pi \cdot 1140}\right)^{\frac{2}{3}} = 0.94 \text{ [kg]} \tag{6.24}$$

Thus the total mass of the LH_2 and LOX tanks including fuel/oxidiser are 15.3 kg for the liquid hydrogen tank and 83 kg for the liquid oxygen tank.

As a last step, the power system can be summarised in an EBD, as depicted in Figure 6.5. Here it should be noted that the ECP system is included in the voltage regulator and power distribution system. Therefore the power supply system satisfies the LCSR-Mission-Environment-08 requirement.

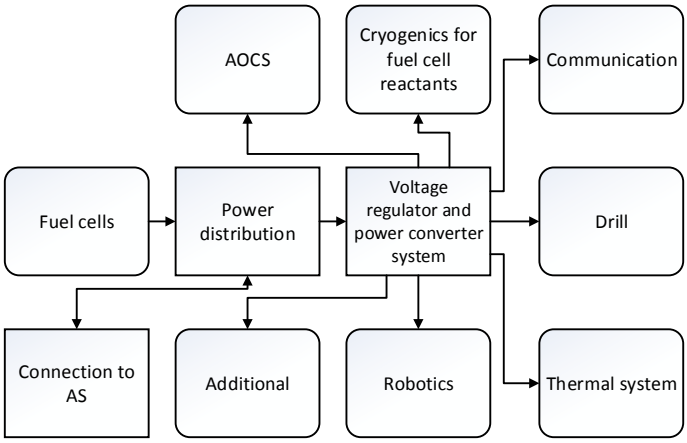

Figure 6.5: Electrical block diagram for the DS.

6.9 MASS BUDGET

As done for the AS in Section 5.13, the mass budget for the DS has been detailed in Table 6.8. Note that since the DS does not contain any propellant, the wet mass is omitted, since it is equal to the dry mass.

Table 6.8: DS mass budget. [a]

DS	Estimated mass [kg]	Margin [-]	Nominal mass [kg]
Legs	16.47	0.05	17.29
Struts connecting AS and DS	2.41	0.05	2.53
Panels of payload deck	15.19	0.05	15.95
Landing shock absorption system	3.60	0.05	3.78
Stiffening system (to handle vibrations)	2.49	0.05	2.62
Battery system	1.00	0.05	1.05
Thermal system	55.00	0.20	66.00
Cryogenics system for fuel cell	6.00	0.20	7.20
Power distribution system	4.00	0.20	4.80
Additional support systems	30.00	0.20	36.00
Drilling system	30.00	0.10	33.00
Fuel cell system	5.60	0.05	5.88
Fuel cell oxidiser, including tank	83.00	0.05	87.15
Fuel cell fuel, including tank	15.3	0.05	16.07
Water deposit tank	4.40	0.05	4.62
Sample cutting tool	10.00	0.20	12.00
AOCS	30.15	0.05	31.66
Nominal dry mass			**348**
Nominal dry mass		0.2[a]	**417**
Wet mass			**417**
Propellant mass			**0**

[a]System level margin over corresponding nominal value.

In line with what has been stated in Section 6.8, several of the subsystems in the DS could be the starting point of a mass reduction campaign. Two items for which large mass savings would considerably reduce the total mass would be the thermal subsystem and the fuel cell system, including its reactants.

A first option to be explored in this respect, would be to use more efficient space grade fuel cell systems. A higher thermal efficiency would mean less reactant needs to be taken along to the lunar surface. An optimal thermal efficiency could then be found, trading off waste heat used to heat the lander against electrical energy that could be used for this.

Regarding the thermal subsystem, in Table 6.8 this can be seen to form a major contribution to the final DS mass. Designing a more efficient thermal system or using an internal spacecraft layout that would optimise recycling of waste heat, might lead to a reduction of this value.

Reducing the mass of systems in the DS will not only reduce their demands on the DS structure (and therefore its mass), but will also affect the structure of the AS and the demand placed on the AS engines.

7 RE-ENTRY VEHICLE

This chapter describes the design of the RV for the Lunar SECRet mission. The layout is presented followed the design of different subsystems. Then the trajectory is simulated followed by the design of the RV. Afther this the thermal system is designend and the power and mass budgets concludes this chapter.

7.1 RE-ENTRY VEHICLE LAYOUT

The mission of the RV is to deliver the sample to the Earth surface. After the AS is detached from the RV and orbiter, the sample is stored in the RV and is kept at the desired temperature throughout the rest of the mission which consists of the transfer to Earth and the re-entry into the atmosphere of the Earth. This last phase induces high mechanical and heat loads and is why a separate RV is needed.

After the AS is docked to the orbiter, the RV will open a hatch that allows the placing of the cryogenic system with the sample. Then the AS is detached along with the docking mechanism and the TEI is initiated to return to Earth. When nearing Earth, the orbiter will spin up to deliver a stable rotational speed to the RV. Then the RV is detached and will be captured by the atmosphere of the Earth at a height of around 125 km. It will then enter with a velocity of 10.93 km/s and begin a ballistic entry. The RV will sustain the heat using an ablative heat shield and its structure is designed for the maximum deceleration encountered. When the deceleration drops below 3 g, a drogue chute will be deployed to provide stability in the transonic flow regime. When slowed down enough, the main parachute will be deployed ensuring a safe landing. Ground radar will track the RV to predict the landing spot and when landed, radio beacons will make sure the RV is retrieved within 12 hours. Meanwhile the cryogenic system will keep the sample at the desired temperatures, sustained by batteries included in the RV.

The layout is presented in Figure 7.1. The sizing is driven by the cryogenic system, that is transported into the RV by opening the aft body. Underneath the cryogenic system, the PCM is situated taking heat from the cryogenic system and acting as a buffer may any heath from the heat shield get through. Furthermore a parachute and batteries are included along with the onboard computer.

7.2 DOCKING SYSTEM

When the AS returns to the orbiter after the sample retrieval, it docks with the RV. The RV houses the male half of the docking system, which is described in Section 5.10. Before the orbiter and the RV return to Earth, the entire docking system is released from the RV with the use of explosive bolts.

7.3 PARACHUTE SYSTEM

In order to safely land, the RV should decelerate upon entering the Earth's atmosphere. The last part of this deceleration is done using a parachute system, which will be elaborated upon in this section. The main reason why parachutes are used instead of other systems, such as retro-rockets, is because of its long heritage.

The parachute system described here is based on that of the Huygens entry probe parachute system, which entered the atmosphere of Titan at an initial velocity of 22,000 km/s [105]. This mission is used instead of a system designed for Earth, since it is in the right mass-range when compared to the Apollo system, and other systems do not make complete mass breakdowns public. This system consists of a drogue parachute, a main parachute, a mortar, container and several mechanisms. The mortar will be used to fire the drogue parachute, which will then pull out the main parachute. The drogue parachute will also slow the RV down. The parachute system used for the Lunar SECRet mission is scaled with respect to Huygens' system using the required surface

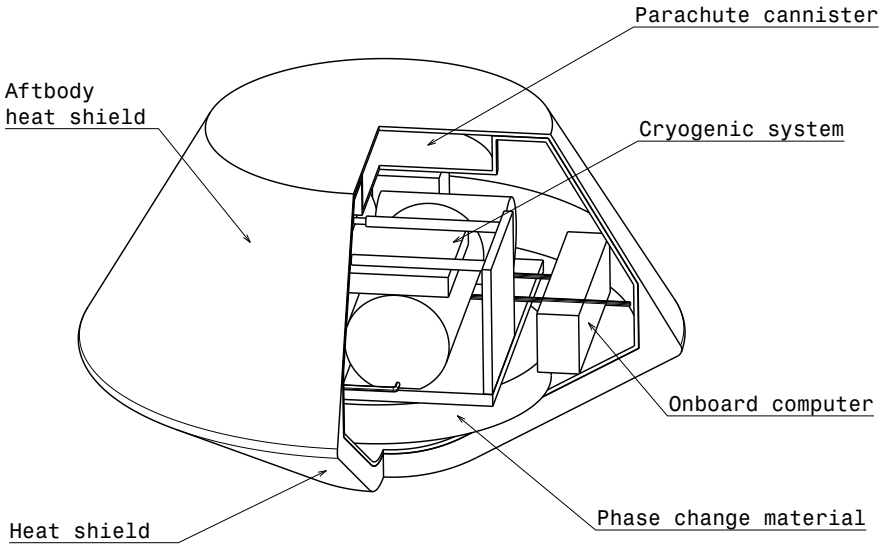

Figure 7.1: Overall lay out of the RV.

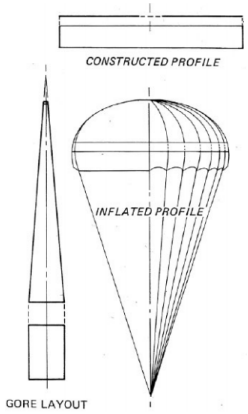

Figure 7.2: Disk-gap-band parachute [108].

area for the main parachute. This surface area, S_p, is calculated using Equation 7.1.

$$S_p = \frac{1}{C_{D_p}} \left(\frac{2 \cdot m \cdot g_0}{\rho_0 V_{final}^2} \right) \tag{7.1}$$

where C_{D_p} is the drag coefficient of the chosen type of parachute, g_0 and ρ_0 are the gravitational coefficient and density at sea level (on Earth in this case), respectively, and V_{final} is the desired final velocity.

As can be seen, the desired final velocity has a large influence on the required surface area, so this should be as high as structurally possible. A value of 10 m/s is used [106], which means that the structure has to withstand an impulse at 10 m/s when it touches the ground. Using a collapsible structure around the payload part, the systems can be expected to survive this [107].

Different types of parachutes are available for planetary re-entry. Two types of frequently used parachutes are the disk-gap-band (DGB) parachutes and conical ribbon parachutes. For this mission a DGB parachute has been chosen, since it has a verified inflation and drag performance over a range of Mach numbers from 0.05 to 2.7. In addition it has a good stability, with less than $\pm 5^\circ$. The DGB parachute has been chosen over the conical ribbon parachutes for its value of C_{D_p}, which is from 0.5 to 0.7 for the DGB parachute and is 0.5 for the conical

ribbon [109]. In addition the mass for the DGB parachutes is lower for the same surface area than that of a conical ribbon parachute, and it has a longer heritage. In Figure 7.2 an example for the DGB parachute can be found[110].

Using a value of 10.0 m/s for V_{final}, a conservative value of 550 kg for m and a value of 0.6 for C_{D_p}, S_p for the main parachute is calculated to be 146.8 m^2. Huygens' main parachute had a surface area of 54.1 m^2 [109]. Equation 7.2 is then used to calculate the final mass for the parachute system.

$$m_{ps} = \frac{S_{p_{SECRet}}}{S_{p_{Huygens}}} \left(m_{mp_{Huygens}} + m_{dp_{Huygens}} + m_{c_{Huygens}} \right) + m_{ms} \tag{7.2}$$

An explanation of the symbols used and the values can be found in Table 7.1.

Table 7.1: Huygens vs Lunar SECRet mission masses [109].

Aspect	Huygens [kg]	Lunar SECRet [kg]	Symbol
Main parachute	4.53	12.3	m_{mp}
Drogue parachute	0.64	1.73	m_{dp}
Container	1.69	4.57	m_c
Mechanism	5.16	5.16	m_{ms}
Total	12.0	23.7	m_{ps}

As can be seen in Table 7.1, the mass for the mechanism has been set to remain the same. This is because the mortar used to fire the drogue chute does not have to be larger. Other mechanisms work equally well with larger parachutes, so they do not have to be scaled either [106].

7.4 TRAJECTORY SIMULATION OF THE RE-ENTRY VEHICLE

In this section a simulation is developed, verified and validated to simulate the trajectory of the RV. The ultimate goal is to calculate design loads induced by the trajectory, shape and mass of the RV. Therefore first a simulation of the entry trajectory is developed and is then extended to aid in the mechanical design of the RV. In the end this tool is used to optimise the design of the RV and its trajectory for this mission.

A major design choice is the type of trajectory that the RV will perform. Three types of re-entry are distinguishable, a ballistic entry, a gliding entry and a skipping entry. In the last one, the vehicle repeatedly enters and exits the atmosphere, reducing speed each time until the final drop to the surface. While reducing speed is beneficial, this type induces a long flight time and high heat load compared to the other types. Therefore this type was discarded immediately. The main difference between ballistic and gliding entry is the presence of lift. No lift is present in the case of a ballistic entry and this type of entry has been used for former sample return missions Genesis, Stardust and Hayabusa. A gliding entry is used for all manned vehicles like for example the Space Shuttle, because the main advantage of a gliding entry is the reduced g-load. As the vehicles in this case transport humans, there is indeed a constraint on the maximum g-load. Another advantage is the option of controlling the trajectory, so more landing options become available. However a control system is then needed adding complexity and mass. Also a gliding flight has a longer duration compared to a ballistic re-entry, and for that duration the heat loads have to be sustained. Because of the longer duration, the total heat load is higher compared to a ballistic entry, requiring a more demanding cooling system.

For the Lunar SECRet mission, the sample and its cryogenic cooling system have an unknown limit in terms of g-loads for this time being. The main issue would be the total heat load, as the cryogenic cooler can only cool for a limited heat load. Although peak heat flux and peak deceleration are much higher for ballistic entry, because of the short duration the total heat load is much lower. Taking into account the reduced complexity, the ballistic entry is chosen as the best option for the Lunar SECRet mission. For the rest of the design, it is therefore assumed the RV does not generate any lift and has an angle of attack of zero during the entry. This is a valid assumption as the shape of a ballistic RV will have a very low L/D ratio, even if the RV would have an angle of attack.

To simulate the re-entry trajectory a simulation based on the equations of motion is developed. The equations of motions are given in Equations 7.3, 7.4 and 7.5 for a spherical Earth with an atmosphere at rest, so no wind

is included. The airspeed is set equal to the ground speed and no traverse forces are acting on the RV. Furthermore the mass is constant, no thrust is present and the gravitational acceleration is assumed constant. These equations are derived in [111] and are used for this simulation. The assumptions made are acceptable because for this mission also a ballistic re-entry is considered. In order to accurately predict the flight path angle, it is important to include the sphericity of the Earth and its rotation with the angular rate ω_{cb}. The equation for the change in the flight path angle γ then becomes as stated in Equation 7.6 when lift is neglected. Here δ is the latitude set at 50°, the latitude of the landing site, and χ the heading set at 90° as the RV will be heading east when entering the atmosphere.

$$m\frac{dV}{dt} = -D - mg\sin\gamma \tag{7.3}$$

$$mV\frac{d\gamma}{dt} = L - mgcos\gamma\left(1-\frac{V^2}{V_c^2}\right) \tag{7.4}$$

$$\frac{dR}{dt} = \frac{dh}{dt} = V\sin\gamma \tag{7.5}$$

$$V\dot{\gamma} = -gcos\gamma + 2\omega_{cb}V\cos\delta\sin\chi + \frac{V^2}{R}cos\gamma + \omega_{cb}^2 R\cos\delta\left(\cos\delta\cos\gamma + \sin\gamma\sin\delta\cos\chi\right) \tag{7.6}$$

The expression for the drag D is given in equation 7.7. The main parameters to be determined are the density of the air ρ and the drag coefficient C_D. To accurately describe the density of the atmosphere very complex models exist that are out of the scope of this study. For a first estimation an exponential atmosphere model is used described by Equation 7.8 [111]. Where h is the attitude and H the atmospheric density scale height. A common value is $H = 7.020$ km. ρ_0 is the density at sea level and for Earth is 1.225 kg/m^3. This model of the atmospheric density is accurate enough for the scope of this simulation. However it must be noted that this model is not accurate for altitudes far above 100 km. Beyond this altitude the atmosphere consists of rarefied gas and this is out of the scope of this study. This is also why the value of C_D is assumed to be constant. During a re-entry the RV will encounter multiple flow regimes. First the free molecular flow is encountered followed by the hypersonic regime below 66 km. Below Mach 7 the supersonic flow regime will take over followed by transonic and subsonic flows. The maximum heat and mechanical loads will be encountered during the hypersonic regime and therefore the C_D during this phase is used and assumed to be constant over the whole trajectory. This is a valid assumption since a major purpose of the simulation is to determine the maximum heat and mechanical loads.

$$D = C_D\frac{1}{2}\rho V^2 S \tag{7.7}$$

$$\frac{\rho}{\rho_0} = e^{\frac{-h}{H}} \tag{7.8}$$

Now that the Coriolis and centripetal accelerations are included in the simulation using Equation 7.6 and the drag is sufficiently modelled, the simulation can be set up using an ordinary differential equation (ODE) solver in MATLAB. As input the values of the final RV design are used, these are already summarised for convenience in Table 7.2. This simulation will have the velocity V, time t, flight path angle γ and the height h as outputs for further calculations. The typical trajectory for the Lunar SECRet RV is plotted in Figure 7.3. It can be seen that γ is going to $-5°$, although the initial angle is $-8°$. Apparently the atmosphere deflects the RV a bit, changing the flight path angle. Note that the simulation is stopped when the deceleration becomes lower than 3 g. A drogue chute is then deployed and this is not incorporated in the simulation. From now on all simulations are stopped at this limit.

7.4.1. VERIFICATION OF THE TRAJECTORY SIMULATION

The simulation developed is verified by giving inputs that should have a predefined output. The drag coefficient is set to zero and this should result in no deceleration of the RV. The result was indeed only a change in velocity due to the rotation of the Earth, which is a linear line as the density has no influence on the speed if the RV does not experience any drag. Also the sea level density was set to zero and this should imply the same velocity profile as the RV again, does not experience drag. Furthermore the density should remain zero and both results were indeed in compliance with expectations. The last two checks consist of reducing the velocity down to zero in steps and comparing the results with the analytical solution. Starting at 11 km/s, with each reduction

Table 7.2: Inputs for the trajectory simulation for the Lunar SECRet RV.

Input	Symbol	Value	Unit
Atmospheric density scale height	H	7050	[m]
Sea level density	ρ_0	1.225	[kg/m^3]
Gravitational acceleration	g	9.81	[m/s^2]
Radius of Earth	R_e	6378137	[m]
Angular rate of Earth	ω_{cb}	$7.29{\cdot}10^{-5}$	[rad/s]
Initial entry velocity	V_E	10930	[m/s]
Initial entry altitude	h_E	125	[km]
Initial flight path angle	γ_E	-8	[°]
Mass	m	412	[kg]
Drag coefficient	C_D	1.44	[-]
Projected surface area of heat shield	S	1.6	[m^3]

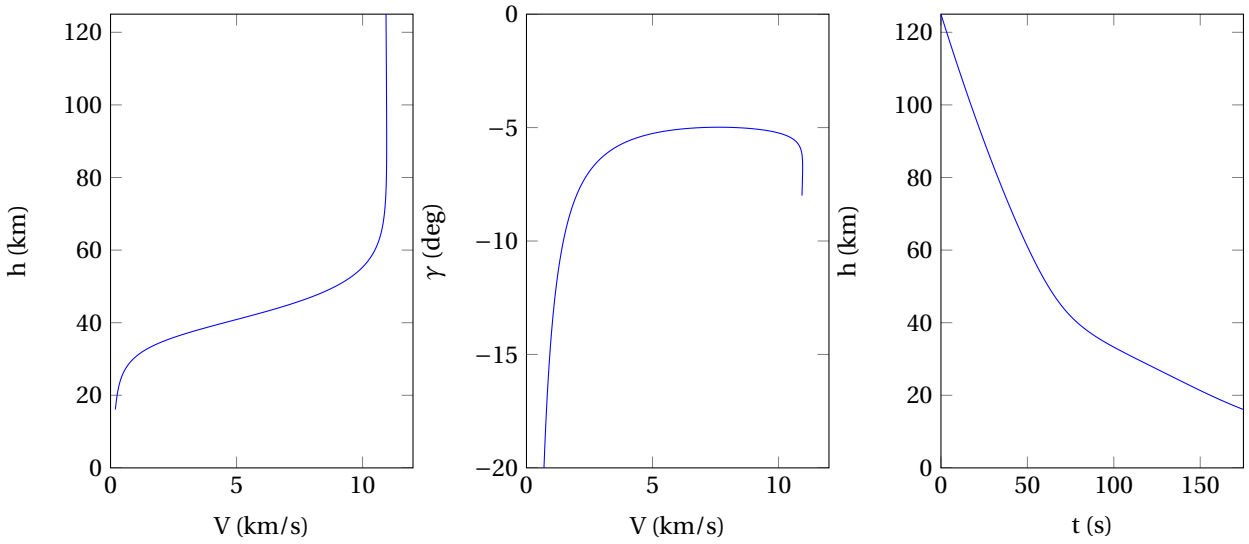

Figure 7.3: Trajectory of the Lunar SECRet RV for $\gamma_E = -8°$.

in speed it was observed that the time until the flight path angle drops below the initial γ, is reduced each time. Below an entry speed of 7 km/s, γ immediately drops because the speed is too low to sustain the initial γ. This is expected and verifies the simulation.

The last check is to compare the results with an analytical solution. This analytical solution assumes a constant flight path angle and neglects all forces and accelerations, except the drag force as this outweighs all others. So no Coriolis, centripetal and gravitational acceleration is present. The comparison for a standard trajectory for the Lunar SECRet mission is illustrated in Figure 7.4. The discrepancies can be explained by the assumptions of the analytical solutions but the shape of the graphs is the same. Taking into account all verification procedures it can be concluded that this model works as expected and can be used for further design.

7.4.2. SIMULATION OF LOADS FOR THE RV

The simulation is extended to aid in the mechanical design of the RV. Using the output of the simulation, the acceleration and heat flux can be calculated. The acceleration is important for the structural design of the RV, and based on the heat flux a thermal protection system (TPS) is designed. From the difference in velocity between each point in time, the acceleration is derived. The heat flux for the stagnation point is calculated using Equation 7.9 [111].

$$q_{stag} = c_1 \frac{1}{\sqrt{R_N}} \sqrt{\rho} V^3 \tag{7.9}$$

where the Chapman constant $c_1 = 2.0294 \cdot 10^{-4} \frac{s^2}{\sqrt{Nm}}$ and a laminar boundary layer is assumed [111]. R_N is the

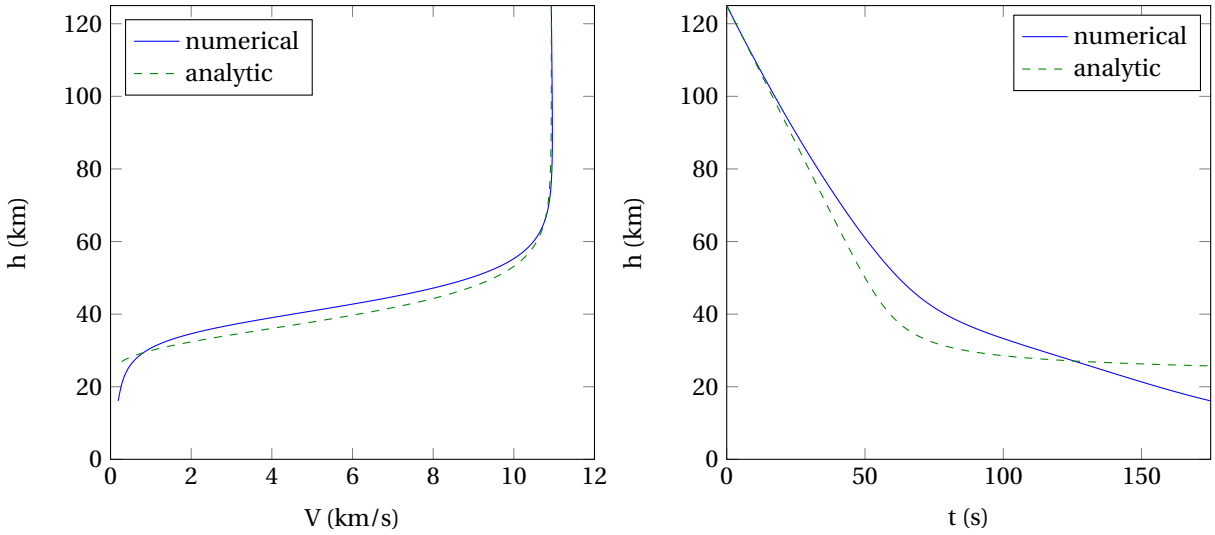

Figure 7.4: Verification of the simulation using an analytic solution.

radius of the nose of the RV and it can thus be seen that a larger nose radius will induce a lower heat flux. It has to be noted that this heat flux only incorporates heat flux due to convection. Two other forms of heat flux are radiation and catalyst heat fluxes. However in a study by A. Viviani and G. Pezzella [112] it can be clearly seen that until a speed of around 11 km/s the convective heat flux by far outweighs the other types. Only above this speed the radiation heat flux becomes important. As the RV will travel just under 11 km/s when entering the atmosphere Equation 7.9 is sufficient for this study.

Another design parameter for the heat shield material is the stagnation pressure. This pressure gives a verdict on how severe the conditions are induced on the material the heat shield consists of. Some materials are not capable of withstanding the stresses caused by the stagnation pressure. This can be calculated using simplified Newtonian flow for hypersonic velocity. Equation 7.10 gives the pressure coefficient based on the deflection angle θ. Using this equation the stagnation pressure can be determined and the maximum value will determine the heat shield materials available.

$$C_p = 2\sin^2\theta \tag{7.10}$$

The TPS is sized according to the total heat load endured during entry. This heat load is simply the heat flux of every point integrated over the whole surface area of the RV. Then this is integrated over time for the duration of the entry and this results in the total heat load during entry. However computational fluid dynamics analysis is needed to develop an accurate model for the heat flux of every point of the surface. One could chose to design the entire heat shield based on the stagnation heat flux but this option will result in an over-designed heat shield. Another method involves determining the frictional coefficient of the heat shield, a parameter that cannot be determined in the scope of this study. However it can be shown that the heat flux for a sphere varies according to Equation 7.11 for angles up to 70° [113]. Although the RV heat shield shape is not a sphere, it does resemble a sphere if the largest radius of the heat shield R_h is taken as the radius of the sphere. It then follows from Equation 7.12 and some derivation that the total heat load is the projected area multiplied by the stagnation point heat flux. These values are actually known and thus this method is included in the simulation to provide the necessary outputs. When tested, this method produced a lower heat load for the RV than when only $q_{stag}$is used for the entire surface, while the value was not that low that it should be discarded. When the result is integrated over the time and divided by the washed area S_w, being the total surface area of the heat shield, the result is the heat load in J/cm^2.

$$\frac{q}{q_{stag}} \approx cos\theta \tag{7.11}$$

$$\int q\,dA = q_{stag}\int cos\theta\,dA = \pi R_h^2 q_{stag} \tag{7.12}$$

The simulation is now used to determine the heat flux, deceleration, stagnation pressure and total heat load during the entry. In Table 7.3 the added inputs required to determine these values are summarised for the Lunar

SECRet RV. The inputs then lead to the output presented in Figure 7.5 and Figure 7.6 where also the height is included for convenience. This output is expected and will be verified and validated in the next section. Later on these outputs are used to design the RV.

Table 7.3: Added inputs for the trajectory simulation for the Lunar SECRet RV.

Input	Symbol	Value	Unit
Nose radius	R_N	0.48	[m]
Radius heat shield	R_h	0.71	[m]
Washed area	S_w	1.88	[m^2]

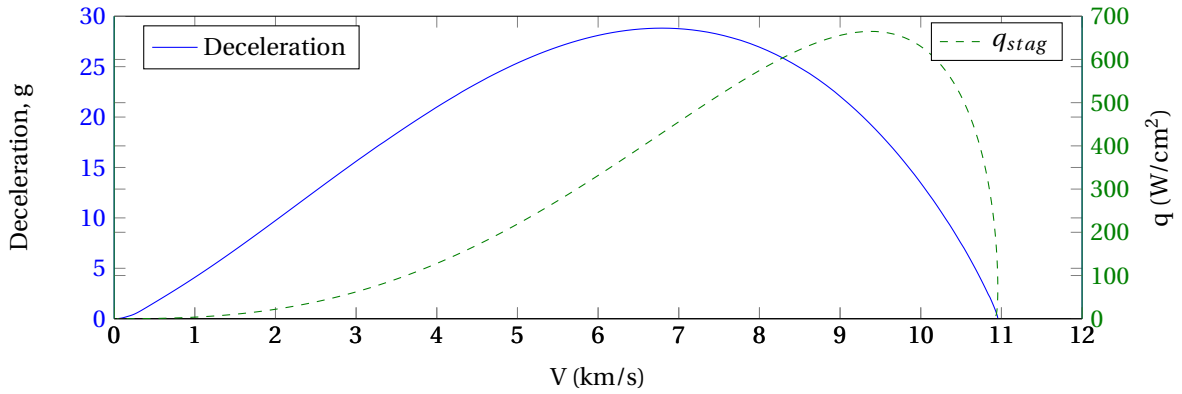

Figure 7.5: Deceleration and stagnation heat flux during entry.

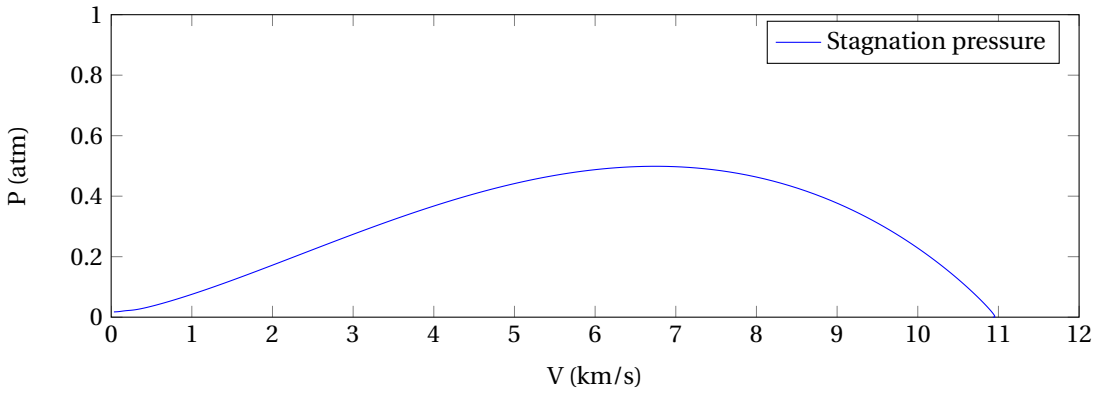

Figure 7.6: Stagnation pressure during entry.

7.4.3. VERIFICATION AND VALIDATION OF THE ENTRY SIMULATION

The total simulation is verified again by setting the same inputs to zero again. In this way it was verified that indeed the simulation is still producing expected results. The validation is done by comparing the simulation to actual data of the sample return missions Genesis and Stardust. As inputs the actual entry conditions and the shape and size are used. The outputs compared are the maximum stagnation heat flux and maximum deceleration as these values are readily available.

Validation using the Stardust mission is done using two studies [114] [115]. A large difference in maximum stagnation heat flux is discovered for this mission. This is due to the high entry velocity of Stardust, as stated previously, only heat flux due to convection is taken into account and this is valid until a speed up to 11 km/s. However Stardust entered at 12.8 km/s and thus the heat flux is far higher due to the significant radiation component. However the result is around 900 W/cm^2 which is not far below the stated value of 1100 W/cm^2 [115]. A difference of 200 W/cm^2 due to radiation is a realistic result. For the maximum deceleration a discrepancy is expected caused by the fact that re-entry starts at 200 km for the Stardust mission. So until it reaches an

altitude of 125 km where the simulation begins, it will be slowed down already while in the simulation all deceleration is performed after 125 km. This will cause the simulation to predict higher deceleration and this is indeed confirmed by the numbers. The simulation predicts a maximum deceleration of 40 g, while actually 33 g was encountered. Another factor is the constant drag coefficient that is assumed in the simulation. In reality according to a study on the aerodynamics of the Stardust sample return capsule the drag coefficient is larger for higher altitudes, causing the RV to slow down more [116]. In the simulation this is not taken into account resulting again in the fact that all deceleration is performed after 125 km of altitude.

Validation using the Genesis mission is done using a study on the aerothermodynamic environment for the Genesis sample return capsule [117]. The maximum stagnation heat flux is determined to be around 500 W/cm^2 for a smooth heat shield similar to the Lunar SECRet RV. The simulation predicts a peak stagnation heat flux of 480 W/cm^2, which is only a difference of 4%. This difference can be explained by the atmospheric density model and the assumptions of a constant drag coefficient. The maximum deceleration predicted by the simulation is 31 g, a difference of 15% compared to the actual deceleration of Genesis. This is again mainly explained by the simplified model for the atmospheric density and the drag coefficient.

These results indicate that the simulation is indeed more capable of predicting useful values for a mission with a speed and shape similar to Genesis, which is the case for the Lunar SECRet mission. It is thus concluded that this simulation is sufficient for the conceptual design of a RV with certain limitations. A more precise atmospheric model that can predict the atmosphere up to 200 km is a major recommendation for future development. Also a variable drag coefficient would aid the accuracy of the simulation.

7.4.4. STABILITY OF THE RV DURING ENTRY

In a study by Desai et al [114] the problem of stability during re-entry for the Stardust mission is addressed. The main concern is that the angle of attack would rise to a significant number, altering the flow and heating up parts of the heat shield that are not designed for this heat load. Also the trajectory would become unpredictable as lift is produced. This study is applicable to the design of the Lunar SECRet RV because the same shape of the RV is used and the trajectory is comparable. The main problem for instability lies in the hypersonic regime where an angle of attack would produce an undesired heat load and deceleration. Also the instability becomes a problem in the transonic regime, where unstable flows around the RV induce instability. For both problems the best solution is presented and this will also be used in the design for the Lunar SECRet mission. The instability in the hypersonic flow regime is mitigated by spinning the RV before atmospheric entry. This is done by the orbiter because the RV has no means to spin up. After the orbiter and RV spin rate is 15 rpm, the RV is released [118]. This solution is commonly used for other ballistic projectiles used on Earth and is a reliable solution also used for Stardust and Genesis sample return missions [118]. To provide stability in the transonic regime a drogue chute is deployed when the deceleration is below 3 g. The speed is then around Mach 2, just before the transonic regime starts. The drogue chute will provide stability and serves as the pilot chute for the deployment of the main parachute. It has to be noted that another solution is to move the centre of gravity more to the front of the nose. For this reason the batteries are placed as much to the front of the nose as possible, however due to the current shape of the cryogenic system it is not possible to store the cryogenic system in the nose.

7.5 STRUCTURES AND MATERIALS

In this section the design of the RV is treated. First the requirements and constraints are determined from where the baseline shape of the RV is designed. Then three trajectories are reviewed and a thermal protection system is designed accordingly. The section is concluded with an assessment on the internal structure of the RV.

7.5.1. REQUIREMENTS AND CONSTRAINTS

The design of the RV is mostly influenced by the trajectory and the size and mass of the RV. These three are interdependent and cause the design to boil down to a mechanical design that balances the different heat and mechanical loads caused by the trajectory. For example the flight path angle can be changed such that a larger heat shield is required. This heat shield then causes the mass to grow, which then changes the trajectory of the RV again. However some numbers are fixed or have a limit and a first step is to determine the requirements and constraints.

The list of requirements set in the baseline review can be found in Section 2.1. The most important requirements for the RV are that the subsystems including the sample must be kept at required temperatures. Also the loads induced by the entry must mainly be sustained by the structure. To aid the cryogenic cooling system the total heat load should be kept as low as possible. This can be achieved by increasing the flight path angle and reducing the duration, and thus the heat load. This also results in a reduced heat shield mass which is favourable for the mass budget. However this induces higher g-loads and at this moment no information is present what the maximum loads on the cryogenic system would be. How this interdependent problem is dealt with is described in the subsection about under and overshoot trajectories later on. The cooler should also stay intact and thus parachutes are included to ensure that the cyrogenic system can cool 12 hours from touch-down on Earth.

Constraints are a fixed entry velocity and altitude. The velocity is set by the orbit trajectory and is determined to be 10,93 km/s. The altitude is constrained by the capabilities of the simulation model and set at 125 km. As no limit load is known for the cryogenic system, a reference value of 100 g from [112] is taken for now.

As a baseline to start the design of the RV, the Genesis and Stardust sample return capsules are taken along with a flight path angle of −8° and their dimensions. This is done because a good amount of data is known for these missions, providing for example drag coefficients for the hypersonic flow regime. Also these missions resemble the Lunar SECRet mission closely. The trajectory and loads are determined by the simulation described in Section 7.4.

7.5.2. SHAPE OF THE RV

As a baseline the shape of the Stardust sample return capsule is taken as seen in Figure 7.7. The main parameter is the angle of the heat shield with respect to the horizontal which is 30.5°. A study into this angle was performed by Dave Olynick [119] at the NASA Ames research centre. An angle of 20° and 40° was considered. Although an angle of 20° increases the drag coefficient, inducing lower loads to the heat shield, the heating of the aft body heat shield is increased. The net heat load for the total vehicle is higher than for the 30° angle. For the 40° angle it is the other way around, the heat for the fore body heat shield is increased and for the aft body it is reduced, but the net heat load is again higher. So for this particular shape and angle of 30.5° is the most suitable compromise.

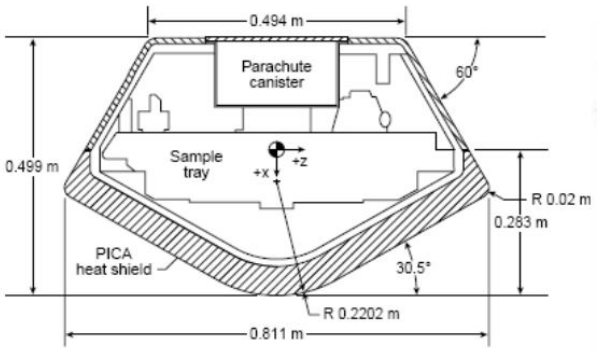

Figure 7.7: Layout of the Stardust return capsule used as a baseline.

Another factor concerning heat load is the nose radius. In Equation 7.9 it is clearly stated that an increased radius reduces the peak stagnation heat flux which is desirable. Therefore the larger nose radius of the Genesis return capsule of 0.43 m is chosen [112].

Now based on the volumes needed for the subsystems the capsule is scaled up. The driving parameter is the size of the cryogenic cooling system. This has to be transported into the RV. A hatch is designed but it was considered desirable to leave the fore body heat shield intact. Therefore the aft body must be large enough to fit this system. The PCM is placed under the cooler and the batteries are accommodated under the PCM to bring the centre of gravity more to the nose, improving stability. The RV with its dimensions is presented in Figure 7.8.

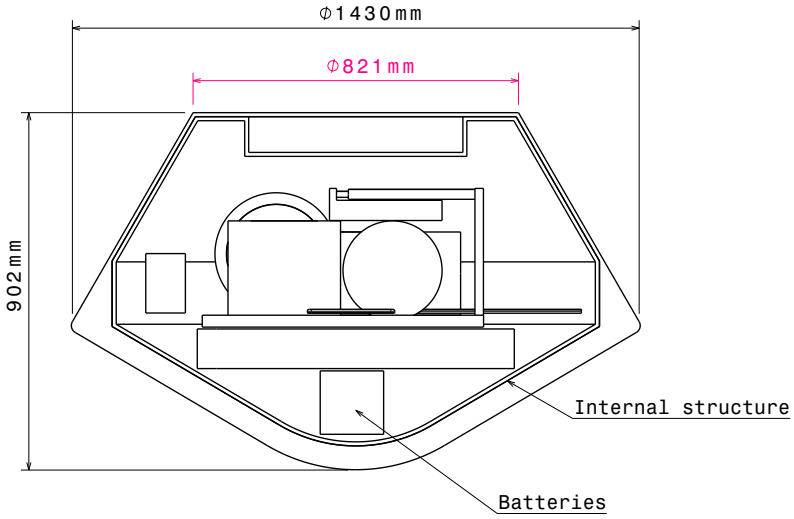

Figure 7.8: Overall layout of the RV.

7.5.3. BASELINE TRAJECTORY

Now that the RV is sized and the masses are known, the simulation can be used to determine all required values to design a trajectory and TPS. Using the flight path angle of −8 degrees, a C_D of 1.44 and a mass of 412 kg the entry is simulated. This mass includes all masses present during the re-entry trajectory including the cryogenic system and sample, but excluding the docking system as this is already detached. The resulting maximum deceleration is 28.8 g, the maximum stagnation heat flux is 665 W/cm^2 (Figure 7.5). Furthermore the maximum stagnation pressure is 0.5 atm ((Figure 7.6) and the total heat load is 18.9 kJ/cm^2. The total time of the entry until the drogue chute is opened is 174 seconds. At this time the simulation is stopped.

7.5.4. UNDER AND OVERSHOOT TRAJECTORIES

The under and overshoot trajectories determine the maximum and minimum flight path angles possible for this design. The simulation is used to determine the minimum angle which is the limit overshoot trajectory. For an angle lower than this angle, the RV will skip off the atmosphere which is highly undesirable. The minimum flight path angle is determined to be −6 degrees using the simulation. The undershoot trajectory is the trajectory determined by the maximum initial flight path angle γ_E. This is limited by the maximum deceleration the RV can sustain and is thus limited by the design limit of 100 g. The undershoot limit is bound by the maximum deceleration of 100 g. This happens at an angle of −19 degrees. The input values for the TPS design are the maximum values for the parameters summarised in Table 7.4 and are derived from the undershoot, overshoot and baseline trajectories treated before.

Table 7.4: Inputs for the thermal protection system.

Parameter	Undershoot	Baseline	Overshoot	Unit
γ_E	-19	-8	-6	[°]
Maximum deceleration	98	28.8	7.9	[g]
Maximum heat flux	1200	665	408	[W/cm^2]
Maximum stagnation pressure	1.7	0.5	0.13	[atm]
Total heat load	10.7	18.9	29.1	[kJ/cm^2]

From Table 7.4 it can be clearly seen what the effect is of γ_E. The undershoot trajectory has a very short duration, so although the peak heat flux is higher, the total heat load is not. Also the maximum deceleration and peak stagnation pressure are increased because the RV has to decelerate in a much shorter trajectory. When γ_E is less steep, the deceleration is reduced, as are the maximum heat flux and stagnation pressure. This can

be seen looking at the overshoot trajectory values. Although all values are lower, the total heat load is larger because of the increased duration. This effect of the trajectory duration was already predicted and is why a gliding trajectory was discarded early on.

7.5.5. DESIGN OF THE THERMAL PROTECTION SYSTEM

Now that all thermal loads are known, a TPS can be designed consisting of a heat shield at the front and an aft body heat shield. The cryogenic system can only cool for limited amount of heat load so the heat transported into the RV should be kept as low as possible during this design phase. Typically different materials are used as the front heat shield is required to sustain much higher thermal loads. This study will be limited to the design of the front heat shield. In order to design an aft body heat shield, CFD is needed for the calculation of thermal loads as the aft body is in the wake of the front heat shield. This is valid because the aft body heat shield requires only a small fraction of mass compared to the front heat shield. Two things are determined in this section: the type of heat shield material driven by the peak heat flux and stagnation pressure, and the heat shield mass fraction driven by the total heat load.

The TPS is designed to sustain the thermal loads of the RV during entry. Three main types of TPS are possible for re-entry mission. An active reusable heat shield that may be actively cooled or uses plumbing systems for active transpiration is seldom considered because of its very complex systems and very low technology readiness. Another reusable heat shield is the passive heat shield used in for example the Space Shuttle missions. This type relies on radiation of the heat and a low thermal conductivity. The last type is an ablative heat shield that combines re-radiation with ablation and pyrolysis for heat rejection. Ablation is the process of absorbing energy by the removal of material by melting, vaporisation, sublimation or a chemical reaction. This type is not reusable but ideal for high heat fluxes. Ablation is the first choice when the entry velocity rises above 8 km/s because of the high heat fluxes experienced. Therefore an ablative heat shield was chosen for the Lunar SECRet RV.

Figure 7.9 presents an overview of other re-entry missions using an ablative heat shield and shows at what peak heat load and peak stagnation pressures they operated. It also distinguishes TPS materials on their densities. Density is a major parameter that influences the thermal conductivity of an ablative heat shield material. Generally speaking, the lower the density, the lower the conductivity which is a highly desirable property. Using the values of Table 7.4 low density TPS material is immediately discarded as the peak heat flux for the overshoot limit is already above the limit for low density TPS material. The baseline trajectory is well within the mid-density range while the undershoot trajectory is in the high density range because of its stagnation pressure. A high stagnation pressure causes spallation of the material which is highly undesirable and is considered a failure of the heat shield.

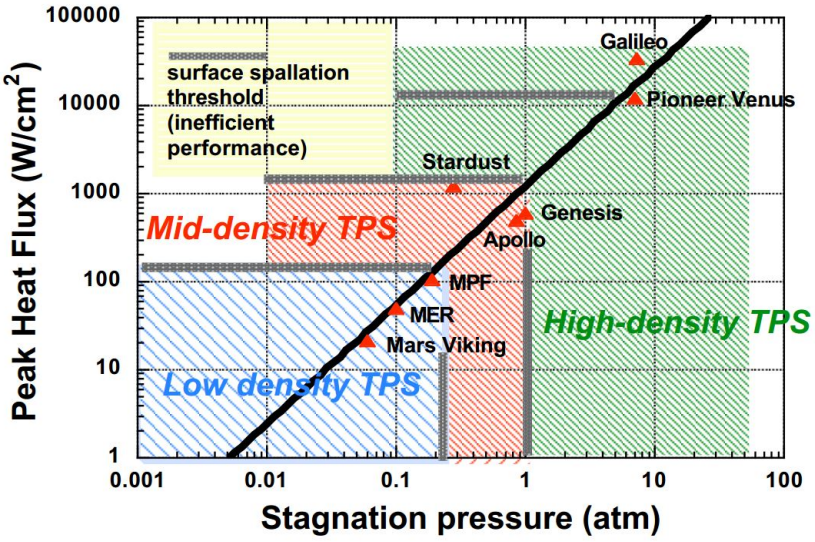

Figure 7.9: Overview of peak heat flux and stagnation pressures [112].

A relatively newly developed TPS material is Phenolic Impregnated Carbon Ablator (PICA) [120]. This is considered a mid-density TPS which has the advantage that it is possible to manufacture a wide range of densities for this type of material. It can go up to a peak heat flux of 1500 W/cm^2 and a peak stagnation pressure of 1.5 atm

[121]. This is enough for the baseline trajectory but is not viable for the undershoot trajectory. For the undershoot trajectory one would have to switch to a very heavy material, increasing thermal conductivity. Therefore it was decided to abandon the undershoot trajectory and calculate a new one, based on the capabilities of the PICA material an γ_E of 16° was found using the simulation. From a study into PICA materials a suitable type was chosen [120], named PICA-M3-13D. This is a densified type of PICA and should be capable to withstand the higher stagnation pressures. In the study, the material is tested and the temperature at a distance of 4.24 cm is measured [120]. For this type, the temperature at this distance is the lowest found in the study, which indicates this material has the best insulative properties from all materials tested in the study [120]. This is very favourable for the design of the thermal system as the loads for this system will be lower and is why this type is chosen. It was only tested at a peak heat flux of 956 W/cm^2, but similar types were tested for higher peak heat fluxes so also this material should withstand the maximum peak heat flux of the undershoot trajectory. The material has a density of 338 kg/m^3[120].

Now the mass fraction of the TPS can be estimated using a linear regression model presented in Figure 7.10. It is assumed for now that the mass fraction does not depend on the type of material used for the TPS. This is valid for now because it can be seen that a lower density TPS material requires a thicker heat shield, while a higher density TPS material requires a thinner heat shield. Using the total heat load of the overshoot trajectory a mass fraction of 18.6% is estimated. This fraction is then added to the total nominal mass of the RV including the cryogenic system. So the initial mass including a first margin, resulting in a heat shield mass of 76.6 kg or 84 kg including a 10% margin. Now that the mass is known, together with the density of the heat shield material and the shape of the heat shield, the thickness required is determined. This thickness is 12 cm and this is twice the value of the heat shield used for Genesis [112]. However the material used for the Genesis mission is more dense so this thickness is accepted.

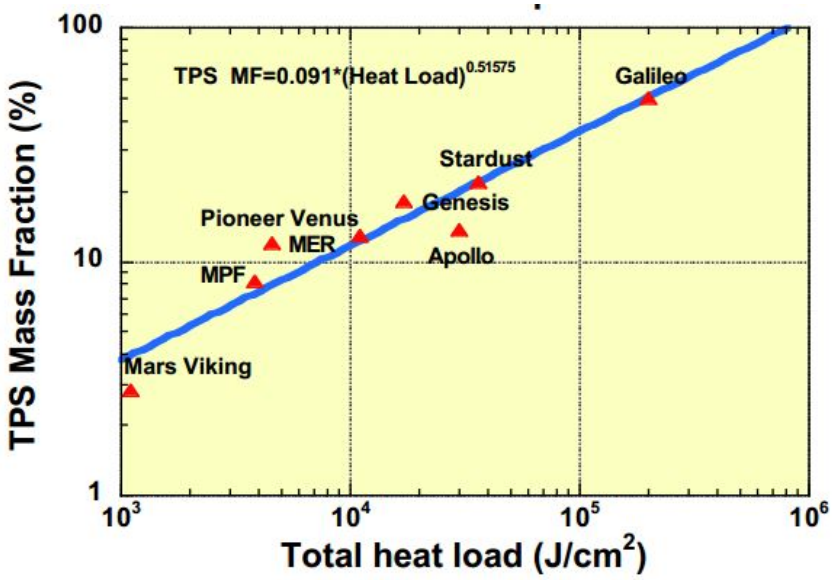

Figure 7.10: TPS mass fraction as function of the total heat load [112].

After the drogue chute is deployed, the heating of the RV has become insignificant. However the heat shield is heated up and this heat is conducted into the RV while the RV is slowed down by the drogue and main parachutes. This transfer of heat is commonly known as thermal soak and poses a potential problem for the cryogenic system. This thermal soak can become very large as the heat shield is at a high temperature and the time until touch-down is very long due to the low velocity caused by the parachutes. In order to mitigate the thermal soak the heat shield is jettisoned when the main parachute is deployed. This was also done during the re-entry of the Hayabusa and is thus a viable option [122].

With this TPS design, it is ensured that the RV is capable of meeting the requirements mentioned in the beginning of this section. It can handle both the under and overshoot trajectories as presented in Table 7.5. To aid understanding how the mass fraction is influenced, the mass fractions for all three trajectories are presented. The mass fraction for the overshoot trajectory was chosen as stated earlier. The mass fraction for the undershoot trajectory could be chosen but as the limit load of the cryogenic system is not known this is not possible for the time being. Although not presented in great depth here, ablation is a very complex phenomena and a material requires a specific heat flux for this to work efficiently. For now one TPS material is assumed but in fur-

ther studies it will become apparent that when the trajectory does not reach the peak heat flux, the material is not ablating efficiently. So in practice a TPS material is specifically suited for a specific entry trajectory.

Table 7.5: Final design of the TPS mass fraction.

Parameter	Undershoot	Baseline	Overshoot	Unit
γ_E	-16	-8	-6	[°]
Maximum deceleration	81 g	28.8	7.9	[g]
Maximum heat flux	1100	665	408	[W/cm^2]
Maximum stagnation pressure	1.4	0.5	0.13	[atm]
Total heat load	11.7	18.9	29.1	[kJ/cm^2]
Mass fraction heat shield	11.4	14.6	18.6	[-]

7.5.6. STRUCTURAL PERFORMANCE

The structure of the RV is modelled as a single cylinder and checked for compression and buckling as presented in Section 4.4. To be conservative, the maximum height and minimum diameter of the RV are used for this. A safety factor will indicate what the performance of the structure is. The material of choice for the structure is aluminium 6061 for its high specific mass. The thickness of the structure was set in such a way that it meets the mass fraction of around 20%, this thickness is determined to be 1 cm resulting in a mass of 110 kg. For the undershoot flight path angle of −16 degrees, which is inducing the highest loads, safety factors of 137 for buckling and 37 for compression are present. Although the safety factors are high, the mass is not changed because it is believed a mass close to reference mass fractions is more accurate than this first-order calculation. Due to the difficult shape of the RV, a FEM analysis is recommended and it is expected that this analysis will show a much lower safety factor. Also this ensures that this design meets the requirements for the structural integrity of the Lunar SECRet RV.

For the transfer of the cryogenic system into the RV, a hatch is required. The RV is already designed such that the cryogenic system can be transferred through the side of the aft body heat shield. This ensures that the fore body heat shield is not damaged.

7.6 THERMAL SYSTEM

The thermal system in the RV should be able to cope with the incoming heat in order to ensure that the temperature of the sample does not exceed 120 K. In this section an estimation is made of the heat conducted into the interior of the RV. Then it is calculated what the consequences are, followed by the design of a thermal system that is capable of mitigating these consequences.

From the design of the heat shield and the study into PICA materials, it can be calculated what the conductivity is of the heat shield [120]. For this Equation 7.13 is used, resulting in a heat load. Here A is the surface area, k the thermal conductivity constant for the material, ΔT the difference in temperature between two surfaces and Δt is the distance between the two surfaces. So this equation gives the heat load in Watt conducted through a material given the temperature difference and will be used to estimate the heat load conducted through the heat shield. The aft body heat shield is left out for now as no values are known. Also the heat load originating from the aft body heat shield is significantly lower compared to the fore body heat shield.

$$Q = -kA\frac{\Delta T}{\Delta t} \tag{7.13}$$

In the study on PICA materials the temperature at 4.24 cm from the hot surface of the heat shield, inside the material, is taken as the reference temperature for this calculation [120]. It is out of the scope of this feasability study to model the ablative processes and therefore this calculation is based on the value from the test [120]. This temperature is 438 K for the peak heat flux of 965 W/cm^2. In Section 8.3, a temperature of 301 K is given as the equilibrium temperature for the orbiter and RV in space. It is assumed the RV is at this temperature when entering the atmosphere. Given these two temperatures ΔT is the difference of the two.

The total thickness of the heat shield was determined to be 12 cm in Section 7.5. The temperature of the PICA material is known at 4.24 cm and Δt is taken as the difference between these two values. The thermal conductivity of PICA-M3-13D is 0.216 W/(mK) [120] and the area of the fore body heat shield is 1.88 m^2. Now that

all values are known the calculation can be done where it is assumed the entire fore body heat shield is at the temperature of 438 K at 4.24 cm from the surface. The values are summarised in Table 7.6 together with the resulting thermal conduction.

Table 7.6: Inputs and result of the heat load Q.

Parameter	Value	Unit
k	0.216	[W/(mK)]
A	1.88	[m^2]
ΔT	137	[K]
Δt	0.0876	[m]
Q	640	[W]

Now that the heat load is known, it is possible to estimate the total heat in Joules entering the interior of the RV. For this the total entry time of 174 seconds is taken as calculated in the simulation. This is a conservative value as the heat shield it not at high temperature from the very beginning. It is assumed the heat shield is jettisoned when the main parachute is opened as stated in Section 7.5. So the time between the opening of the drogue and main chutes has to be added. This value is taken from the Genesis entry and is 254 seconds [118]. This leads to a total time t_{entry} of 428 seconds that the interior is subjected to the heat load. It is assumed that the heat shield is attached to the internal structure in such a way that the entire structure is subjected to the heat load. This can be seen in Figure 7.8. Now Equation 7.14 can be used to determine the rise in temperature ΔT of the internal structure during the time that the heat load is present.

$$\Delta T = \frac{Q t_{entry}}{c_p m} \tag{7.14}$$

Here m is the mass of the structure and c_p is the specific heat capacity of the structural material aluminium 6061. The values used and its results are summarised in Table 7.7.

Table 7.7: Rise in temperature for the RV internal structure.

Parameter	Value	Unit
Q	640	[J/s]
t_{entry}	428	[s]
c_p	896	[J/kgK]
m	110	[kg]
ΔT	2.77	[K]

With a rise in temperature of 2.77 K of the structure, the final interior temperature of the RV becomes 304 K. This is within the operational limits of the cryogenic cooler as stated in Section 5.3. Therefore it can be concluded that requirement LCSR-Mission-Environment-09 is met. No additional insulation is thus required. However 18 kg of mass based on concept 5 from the mid-term report and SMAD is required for the thermal system to distribute the heat in the RV and a PCM is added to cope with the heat from the cryogenic system.

7.7 COMMUNICATION SYSTEM

The RV does not have an antenna, a receiver and a transmitter to provide any communication with an Earth ground station. Such a system is not needed due to the fact that the re-entry trajectory is quite short and during the trajectory communication blackout will happen, because ionised air is created by generated heat and pressure during re-entry [123]. This ionised air causes interference with radio signals [123]. After landing, it is of importance to locate the RV and retrieve the sample. This is done by including an acquisition-aid beacon, which has successfully been used in the past to find spacecraft which re-entered Earth's atmosphere. These beacons are usually quite small and use very low power, Gemini 7 for example only needed 0.25 W of power [124].

7.8 DATA AND COMMAND HANDLING

The RV has a DCH system to process (and store) data, which is the same as the one that the AS uses. The reason why this system is included in RV is because during the re-entry and sample retrieval all the systems in the RV need to work properly. For example, when the RV lands on the ground the electrical system is changed in terms of its power distribution, which is regulated by the onboard computer (the OBC750). The commands that might be needed during the re-entry phase are stored in the data storage hardware (HSDR), because there is no communication system in the RV which can receive commands as mentioned in Section 7.7. Since the OBC750 and HSDR are capable to process the generated data of the AS, the hardware is capable to process the generated data of the RV as well.

7.9 POWER BUDGET

This section will focus on the power budget for the RV. Only during the re-entry phase will the subsystems in the RV require power. This phase has been split up in two parts: the phase during the actual re-entry and the phase awaiting recovery.

In order to design the power supply one first needs to know the total amount of power required by each subsystem. Then when the required power for each subsystem for each mission phase as specified in Section 4.3 is known one can find the phase which requires the most amount of power. The results are shown in Table 7.8 where both the re-entry and the retrieval phase are shown.

As described in Section 4.3, of the total power need, 10 % is used for power distribution, which includes cable losses and 5 % of the total power need is made up of additional equipment not currently taken into account. This does not hold for the retrieval phase, where it was chosen to use 12 % and 6 % for the power distribution system and additional equipment respectively as this would allow for a design in which most of the additional equipment remains active during the retrieval phase while allowing for greater losses in the power distribution system.

Table 7.8: Power budget RV.

Re-entry	**Re-entry [W]**	**Retrieval [W]**
On-boardcomputer	26.3	26.3
Communication	10.0	0
Cryogenics	480.0	480.0
Robotics	10.0	0
Structures and mechanisms	10.0	0
Thermal	127.7	0
Power distribution	78.1	72.3
Additional	39.0	36.2
Total	781.1	614.8

As can be seen in Table 7.8, the most critical aspect is the cryogenic system. Due to the very strict requirements, this subsystem has to keep the sample below 120 K at all times, which requires a significant amount of power. This can also be seen from the required power for the thermal subsystem, as this is the second most driving power requirement. The next thing that stands out in Table 7.8 is the fact that during the retrieval phase, multiple systems are not active. Only systems critical for sample preservation and recovery are active.

It should be noted that the required power stated for the subsystems in Table 7.8 is the maximum amount of power needed. But it can always be the case that at the peak point, all subsystems require this power simultaneously, so the worst case scenario is used when designing and sizing the power system.

7.10 POWER SUPPLY

Using the methods as described in Section 4.3, and using the values as given in Table 7.8, one can design the power supply system. As mentioned in Section 3.2 the RV will be powered by a non-rechargeable battery. Using

the values for the specific energy and energy density, as given in Table 4.3, the required mass and size of the batteries of the RV were computed.

As mentioned in Section 3.1, the retrieval phase, during which the RV has to keep the sample at cryogenic temperatures, last for 12 hours. For the re-entry phase it was assumed that the RV would be separated 4 hours before touch-down on Earth. Thus the batteries need to be designed for 16 hours of operation.

From Table 7.8 one can find that the RV has to operate at two different power requirements. However as mentioned in Section 4.7 the power required should have an additional system level margin of 20 %. Thus the design power for both phases needs to be increased by 20 % which results in a design power of 937.3 W for the re-entry phase and 737.8 W for the retrieval phase. Using these values for the required power one can compute the mass and size of the batteries by using the values for the specific energy and energy density from Table 4.3.

$$m_{bat} = \frac{937.3 \cdot T_{re-entry} + 737.8 \cdot T_{retrieval}}{500} \frac{1}{DOD} = 29.95 \text{ [kg]} \tag{7.15}$$

$$V_{bat} = \frac{937.3 \cdot T_{re-entry} + 737.8 \cdot T_{retrieval}}{470} \frac{1}{DOD} = 31.6 \text{ [L]} \tag{7.16}$$

As a last step, the power system can be summarized in an EBD, as depicted in Figure 7.11. Here it should be noted that the ECP system is included in the voltage regulator and power distribution system. Therefore the power supply system satisfies the LCSR-Mission-Environment-08 requirement.

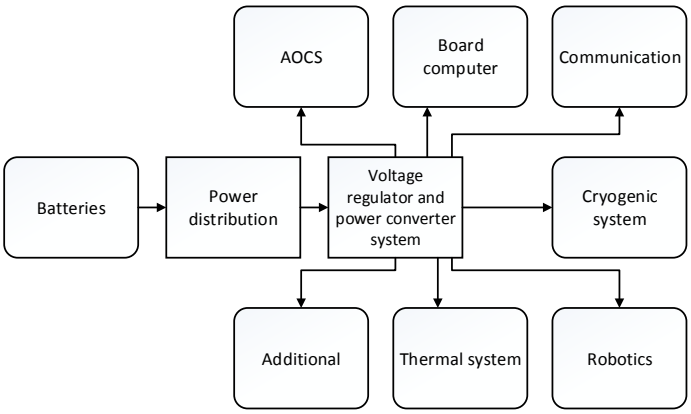

Figure 7.11: Electrical block diagram for the RV.

7.11 MASS BUDGET

In Table 7.9 the mass breakdown, as well as the total mass of the RV can be found. It may be noted that the mass of the RV changes over the course of the mission life. After the AS has docked with the RV, the container with the cryogenics and sample will be transferred from the AS to the RV. To clarify these different scenarios, two sets of total dry masses are presented.

Table 7.9: RV mass budget. [a] [b]

RV	Estimated mass [kg]	Margin	Nominal mass [kg]
Male part of docking system	15.00	0.20	18.00
Structural support system	110.00	0.10	121.00
Heat shield	76.63	0.10	84.30
Hatch system	20.00	0.10	22.00
Parachute system	23.70	0.20	28.44
Heat sink system	2.66	0.20	3.19
Computer system	2.50	0.05	2.63
Battery system	29.95	0.20	35.94
Power distribution system	4.0	0.20	4.80
Thermal system	18.00	0.20	21.60
Radio beacon system	2.00	0.20	2.40
Additional support systems	14.00	0.20	16.80
Nominal dry mass before container transfer			**361**
Total dry mass before container transfer		0.20[a]	**433**
Wet mass before container transfer			**433**
Propellant mass before container transfer			**0**
Sample[b]	1.60	-	1.60
Cryogenic sample storage system[b]	64.00	0.20	76.80
Nominal dry mass after container transfer			**439**
Total dry mass after container transfer	439	0.20[a]	**525**
Wet mass after container transfer			**525**
Propellant mass before container transfer			**0**

[a] System level margin over corresponding nominal value.
[b] Only after docking and cryogenics transfer. Add for mass after container transfer.

In the case of the RV, it can clearly be seen that the mass of the entire vehicle is driven by the cryogenic storage system. To begin with, there is the system's own mass, which forms a large part of the RV's content. Looking further, the cryogenic system's power requirement drives the sizing of the batteries, which are also a sizable contributor to the mass. Being able to reduce either or both the cryogenics' mass or power requirements, would allow for a structural support system that can be both smaller and lighter. A smaller system would in turn require a smaller heat shield and the vehicle's reduced surface area would reduce the heat influx, thus requiring a smaller thermal system. The mass of the two other main contributors to the mass budget, namely the heat shield and the structure, will decrease as the mass and size of the internal systems of the RV reduce. As a final step, the parachute system could be downsized to accommodate the new RV mass.

8 ORBITER

This chapter describes the design of the orbiter for the Lunar SECRet mission. The layout is presented followed by the design of the AOCS, thermal and propulsion systems. The structure and materials used are explained followed by the DCH for the orbiter. As the orbiter also serves as a communication relay the communication system is presented, after which a power budget is given. The mass budget concludes this chapter.

8.1 ORBITER LAYOUT

The main function of the orbiter is to transport the AS, DS and RV to and from the Earth. It is mainly designed to accommodate the engines and propellant for this purpose. It also supports the RV for most of the mission and provides the connection to the LV via an adapter. During Moon operations it acts as the relay station for communications with Earth. The layout is shown in Figure 8.1

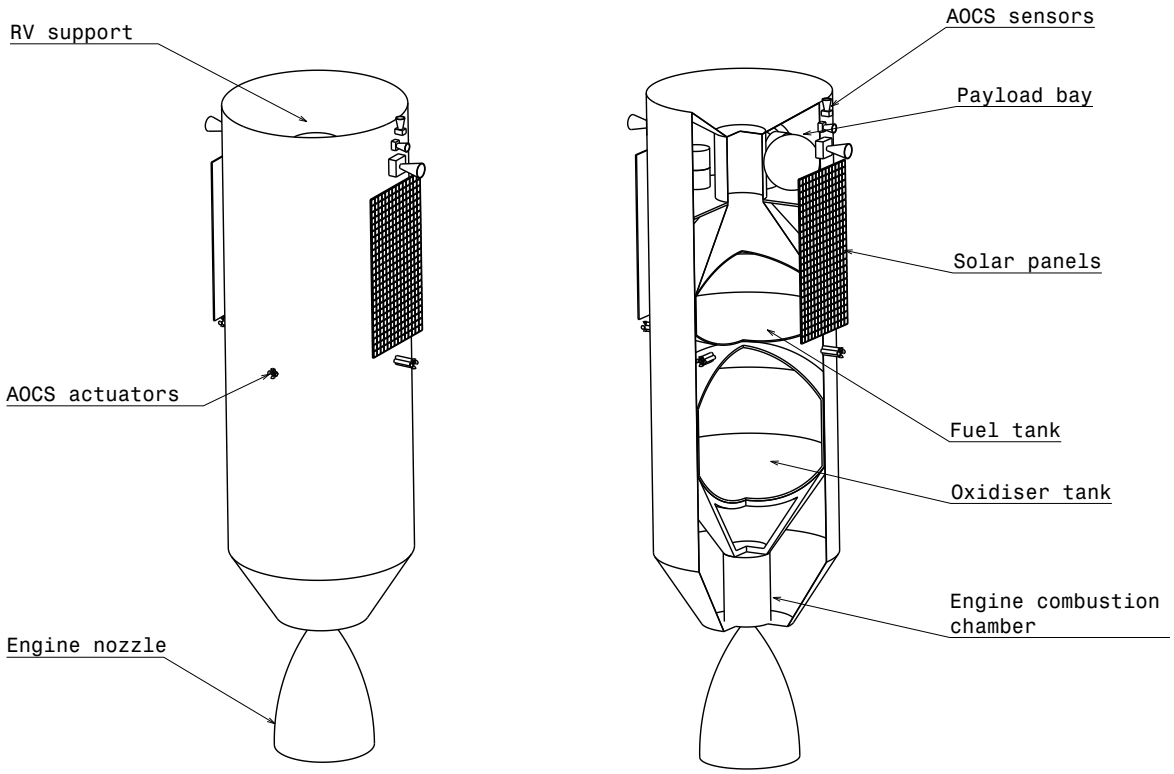

Figure 8.1: Overall layout of the orbiter.

The total length including the engine nozzle is 5.9 m and the cylindrical shaped orbiter has an outer diameter of 1.6 m. The internal layout is the same as for a bi-propellant rocket. Starting at the bottom an engine and its support structure is situated followed by the propellant tanks. This ensures most mass is situated at a low point, enhancing resistance to vibrations induced by the launcher. Above the tanks a payload bay is placed accommodating all payloads needed for the AOCS, power supply and communications. Also the solar panels are situated here and are folded into launch configuration in Figure 8.1. Navigation systems are situated outside above the solar panels and the RV fits into the top of the orbiter for optimal load distribution and to protect the

heat shield. Struts encircle the RV and these struts connect to the AS to add increased stiffness to the entire spacecraft in launch configuration.

8.2 ATTITUDE AND ORBITAL CONTROL SYSTEM

In this section the AOCS of the orbiter is described. First, the requirements of the AOCS are described. Second, the design of the AOCS is elaborated. Third, the mass and power budget of the AOCS in the orbiter is presented and last, a check whether the combined AOCS of all stages is sufficient for the transfer from Earth to Moon and whether the requirements are fulfilled is included.

8.2.1. SUBSYSTEM REQUIREMENTS

Similar to the AS, the orbiter has to be able to handle the disturbances at 100 km altitude at the Moon but also the disturbances at the Earth to Moon and Moon to Earth transfer. The pointing accuracy is the same as for the AS and DS for the same reasoning. It shall be less than 0.5°. A pitch rate requirement is not present but it was decided that the orbiter is constrained by having a slew rate of 30 °/min. According to SMAD this is a nominal slew rate [28] and enables the possibility to use the orbiter actively while docking. Furthermore, the orbiter has to be able to spin with a speed of 15 rpm to induce a spin prior to atmospheric entry to the RV. The spin stabilises the RV during re-entry and makes an AOCS system in it superfluous [114].

8.2.2. AOCS DESIGN

The design of the AOCS was again split up into actuators, sensors and controllers. It is designed to fulfil the requirements in LLO and for the Moon-to-Earth transfer. Whether the combined AOCS of all stages is able to fulfil the requirements for the Earth-to-Moon transfer is elaborated in Section 8.2.4.

Actuators Given the method explained in Section 4.1, the required force to manoeuvre is 17.1 N for pitching and 3.7 N for rolling. The burn time to initiate and stop a manoeuvre was set to 3 s. The disturbance momentum in LLO is $3.8 \cdot 10^{-3}$ Nm and the disturbance over one day in LLO is 58 Nms. For the transfer from Moon to Earth the disturbance momentum increases to $6.8 \cdot 10^{-3}$ Nm and the gravitational disturbance over one day to 102.8 Nms. The high momentum is due to the fact that the data for a 200 km altitude LEO was taken. Thus, it represents the worst case in which the spacecraft is closest to Earth.

To perform the manoeuvres thrusters are needed. For the orbiter the bi-propellant thrusters cannot be used because the orbiter main engine uses different propellant than the AS engine. That is why 20 N monopropellant thrusters from Astrium are chosen [125]. The propellant used by the thrusters is N_2H_4 [125]. The thrusters are mounted the same way as on the AS, so all thruster sets are in line when all stages are connected. The thruster sets for the orbiter consist of one thruster in each direction. This means that there are four thrusters per set which adds up to 16 thrusters in total. The available pitch force is therefore 40 N and for rolling 80 N. If one thruster fails, the available force to pitch reduces to 20 N and to spin to 40 N. Thus, redundancy is present.

To withstand the disturbances, the same reaction wheels as chosen for the AS can be used. However, the orbiter would have to dump momentum four times per day. This is not a problem as long as the computer is able to manage the momentum dumping autonomously. If the orbiter is not able to dump it autonomously, the dumping has to be initiated with a command from Earth. If dumping can be minimised to two times per day or less, operators do not have to check the status of the orbiter throughout the entire night. That is why the W54ES wheel is chosen. It has the highest momentum storage of the wheels produced by MOOG Inc.[53]. The wheel can store up to 70 Nms [53]. Again four wheels are chosen to have one spare wheel for redundancy.

The mass of the propellant was computed as explained in Section 5.2.2. It was calculated that 15 manoeuvres are needed to initiate the spin with a velocity of 15 rpm. Another 10 manoeuvres were added to adjust the attitude to the required attitude for TEI and for a midcourse correction. So including the 100 % margin the total number of manoeuvres is 50. The durations accounted for the stay in LLO and transit to Earth are derived from the operating times defined Section 3.1. It is 28 days for the stay the LLO and 10 days for the transit to Earth. Both durations include the 100 % margin defined by ESA. This results in a propellant mass for the orbiter of 11.38 kg which has a volume of 11.16 l. Besides the propellant mass, an

extra tank is needed to store it. To have minimum mass, the smallest tank offered by Astrium was chosen [126]. It has a capacity of 39 l and a mass of 8.5 kg [126].

Sensors To achieve the required pointing accuracy, two star trackers and two IMUs were chosen. The same line of reasoning holds as mentioned in Section 5.2.2. Furthermore, the orbiter is equipped with solar cells. To identify the location of the Sun, the orbiter is equipped with 10 sun sensors. Last but not least, two navigation cameras are mounted on the orbiter to support manual docking if autonomous docking fails. The sun sensors, star trackers, IMUs and navigation cameras are the same as chosen for the AS which has been described in Section 5.2.2. The cabling lengths for the sun sensors and star trackers were estimated to be 2 m per sun sensor or star tracker.

Controllers The AOCS is controlled by an onboard computer. The computer is elaborated in detail in Section 5.6.

A total overview of the components can be found in Figure 8.2 and the input and output data of the calculation are presented in Tables 8.1 and 8.2. The interactions between the actuators, sensors and controllers has been already explained and can be found in Section 5.2.2.

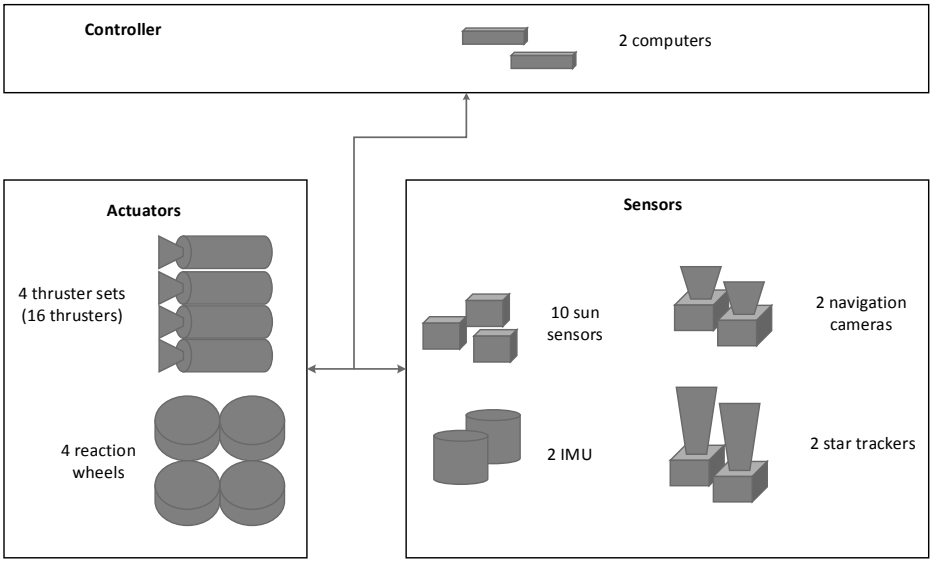

Figure 8.2: AOCS components in the orbiter.

Table 8.1: AOCS calculation input of the orbiter.

	$I_{x,y}$ [kgm^2]	I_z [kgm^2]	$\dot{\theta}$ [°/min]	T_{op} [days]	x_{man} [-]	$t_{burn_{man}}$ [s]	$t_{burn_{dump}}$ [s]	I_{sp} [s]	h [km]	μ km^3/s^2
Orbiting	4,708	1,009	30	28	0	3	1	227	100	4,902.8
TEI	4,708	1,009	30	10	50	3	1	227	200	398,600.4

Table 8.2: AOCS calculation output of the orbiter.

	F_{pitch} [N]	F_{roll} [N]	t_g [s]	h [Nms]	m_{prop} [kg]
Orbiting	17.1	3.7	$3.8 \cdot 10^{-3}$	58	2.73
TEI	17.1	3.7	$6.7 \cdot 10^{-4}$	102.8	8.65

8.2.3. MASS AND POWER BUDGET

The mass and power budget of the AOCS in the orbiter can be found in Table 8.3. For both the mass and the power a margin of 5 % was chosen, since all products are off-the-shelf. The total mass of the AOCS in the orbiter is 74 kg and the total power is 152 W.

Table 8.3: AOCS mass and power budget of the orbiter.

Component	**Unit mass [kg]**	**Number total (active)**	**Mass [kg]**	**Unit P_{req} [W]**	**P_{req} [W]**	**T_{op} [°C]**
Sensors						
IMU [54]	4.7	2(1)	9.4	32	32	-30 to 65
Star tracker (ASTRO 10) [55]	1.47	2(1)	2.94	20.5	20.5	-40 to 40
Ebox star tracker [55]	1.36	1	1.36	0	0	-40 to 50
Star tracker cabling [55]	0.29 /m	4 m	1.16	0	0	- -
Cosine sun sensor [58]	0.024	10	0.24	0	0	-50 to 80
Sun sensor cabling [58]	0.013 /m	20 m	0.26	0	0	- -
Navigation camera [57]	0.596	2(2)	1.192	2.5	5	-20 to 40
Actuators						
Thrusters (20N) [125]	0.395	16	6.32	0	0	N/A
Propellant (N_2H_4)			11.38	0	0	N/A
Propellant tank (39l) [126]	8.5	1	8.5	0	0	N/A
Reaction wheels (W45ES) [53]	6.86	4(3)	27.44	29	87	-15 to 60
Total			70.19		144.5	-15 to 40
Margin			0.05		0.05	
Nominal			73.70		151.73	

8.2.4. EARTH-TO-MOON TRANSFER

Until arrival at LLO all stages are connected and make up the complete spacecraft. Thus during Earth-to-Moon transfer, the AOCS of all stages can function together and build up the total spacecraft AOCS. Although during the Earth-to-Moon transfer only one midcourse correction and one braking burn at LLO is needed, the same pointing accuracy and pitch rate requirement as applied for the orbiter was taken to allow precise main engine burns. The computed required force to pitch is 127 N and to roll 5 N. All pitching thrusters can produce a combined pitch force of 128 N. Thus the pitching requirement is met. Furthermore, if one thruster fails, rolling to the other pitching axis is possible or the additional use of two rolling thrusters, which are located at opposite sites of the spacecraft and point in the same direction to induce a pitching moment. The requirement of 5 N is already met by only using the AOCS of the orbiter or AS.

For the calculation of the gravitational disturbances, a LEO at 200 km altitude was used. This is the worst expected case for the total spacecraft. Over one day 932.2 Nms disturbance would be received by the spacecraft. Using the reaction wheels in both the DS and the orbiter, momentum dumping has to be done 11 times per day. This is very frequently and requires continuous checking if the autonomous dumping performs as expected. However, adding more reaction wheels is not feasible, since it would increase the propellant mass of the total spacecraft.

To compute the propellant mass needed for the Earth-to-Moon transfer a transfer time of 10 days was taken to include the 100 % margin by ESA. Furthermore, it was assumed that only the thrusters of the DS are used. This assumption is valid, since slew rates of 5 °/min are not a problem and the rolling thrusters could be used in addition to achieve the required pitching moment. In that way, less propellant is needed, since the bi-propellant has a higher specific impulse. The number of manoeuvres was set to 10, including the 100 % margin. The same reasoning as mentioned in the propellant calculation for the Moon-to-Earth transfer holds. The resulting propellant mass is 20.36 kg which is stored in the main propellant tank of the AS.

The input and output data of the calculations are presented in Tables 8.4 and 8.5.

Table 8.4: AOCS calculation input of the total spacecraft at TLI.

	I_{xy} [kgm^2]	I_z [kgm^2]	$\dot{\theta}$ [°/min]	T_{op} [days]	x_{man} [-]	$t_{burn_{man}}$ [s]	$t_{burn_{dump}}$ [s]	I_{sp} [s]	h [km]	μ [km^3/s^2]
TLI	35,106	1,552	30	10	30	3	1	290	200	398,600.4

Table 8.5: AOCS calculation output of the total spacecraft at TLI.

	F_{pitch} [N]	F_{roll} [N]	t_g [s]	h [Nms]	m_{prop} [kg]
TLI	127	5	$6 \cdot 10^{-2}$	932.2	20.36

8.2.5. AOCS REQUIREMENTS

The requirements defined in Section 8.2.1 are met by the AOCS of the orbiter and total spacecraft. It is able perform the required manoeuvres and withstand the expected disturbances while orbiting and transferring to Earth. Additionally, the AOCS is redundant and is therefore not affected by single subsystem failures.

8.3 THERMAL SYSTEM

In this section the thermal control system of the orbiter and transfer to Moon and Earth are treated. First the assumptions are explained, second the results of the calculations are shown in Table 8.7. Last a qualitative design of the thermal control systems is given for the orbiter module and complete spacecraft.

8.3.1. ASSUMPTIONS

In this subsection the specific assumptions for the phases elaborated on are discussed.

Altitude effect The albedo effect and planetary radiation of the Moon near Earth is negligible and vice versa. This can be proven by calculations similar to Equation 5.2. When the altitude increases with respect to the surface of the celestial body the energy received by the spacecraft from the Moon or Earth is negligible.

Hot case and cold case The height of the spacecraft near Earth is 200 km, estimating the hot case of the transfer back to Earth before re-entry, similar scenario is calculated for arriving at the Moon. The hot case is the case when the spacecraft will receive the most energy within the mission profile, whereas the cold case is its counterpart. In the cold case the spacecraft will not receive any heat from the albedo effect of the celestial body and the planetary radiation, this assumption was not used for the orbiter orbiting around the Moon, as was used for the deep space environment.

Spacecraft viewed as one entity The spacecraft is taken as a whole instead of each of the modules apart, meaning that there is a heat transfer between the modules.

Eclipse time The orbiter is in eclipse for a quarter of the time when orbiting around the Moon as calculated in Subsection 3.3.3.

8.3.2. THERMAL MODEL RESULT

With the additional assumptions mentioned in Section 8.3.1 the model can be used to calculate each equilibrium temperature. The inputs and outputs for the hot case are shown in Table 8.6 and 8.7, where all temperatures are within the required temperature range. The coatings were already determined by the other mission phases, meaning that the orbiter uses the aluminium paint mentioned in Section 6.3. For the cold case the values of the albedo and planetary radiation where set to zero, still leaving the thermal equilibrium within the required range. The equilibrium temperatures are 279 and 284 K for transfer to Moon and transfer to Earth respectively. All equilibrium temperatures mentioned in Table 8.6 and the equilibrium temperatures for the cold case are within the required range, thus it can be concluded that the requirement LCSR-Mission-Environment-09 is met. Another input for the model, for the thermal equilibrium temperature, is the planetary radiation constant of Earth. Its value is 236 W/m^2 [59].

Table 8.6: Thermal equilibrium model - input.

Parameters	Transfer to Moon	Near Moon	Orbiter	Transfer to Earth	Unit
α_{eff}	0.34	0.34	0.32	0,32	[-]
ϵ_{eff}	0.45	0.45	0.44	0,44	[-]
I_{sol}	1,371	1,371	1,371	1,371	[W/m^2]
ρ	0.37	0.12	0.12	0.37	[-]
I_{IR}	236	305	305	236	[W/m^2]
σ	$5,67 \cdot 10^{-8}$	$5,67 \cdot 10^{-8}$	$5,67 \cdot 10^{-8}$	$5,67 \cdot 10^{-8}$	[m$^2 kg/s^2 K$]
t_e/t_d	0.2411	0.2411	0.2411	0.2411	[-]
A_{tot}	57	57	42.7	42.7	[m^2]
A_{sun}	18	19	15.7	15.7	[m^2]
A_{IR}	18	19	15.7	15.7	[m^2]
h	200	100	100	200	[km]
r_{body}	6,371	1,737	1,737	6,375	[km]

Table 8.7: Thermal equilibrium model - output.

Parameters	Transfer to Moon	Near Moon	Orbiter	Transfer to Earth	Unit
Q_{solar}	8,312	8,775	5,187	5,187	[W]
Q_{IR}	1,264	1,269	989	1,040	[W]
Q_{albedo}	2,717	885	689	725	[W]
Q_{int}	490	490	1,421	1,700	[W]
T	306	298	297	301	[K]

8.3.3. THERMAL CONTROL SYSTEM DESIGN

The mass of the thermal system and power reserved for the orbiter, is mainly used to distribute heat in the module. The surplus of electrical power can be shut down so the maximum amount of electrical power does not have to be taken into account for the equilibrium. For the mass and power the same reasoning is applied as in Subsection 5.3.1. The mass and power estimates are taken from concept 5, which are respectively 90 kg and 143 W.[8] [33]. The thermal control elements used in the orbiter are mainly heaters, heat pipes and radiators to ensure that the heat is well distributed through the spacecraft.

8.4 PROPULSION SYSTEM

The orbiter equips a 31.5 kN SpaceX Kestrel engine, fed with refined petroleum-1 (RP1) and LOX. There is a limited number of off-the-shelf engines in this thrust range, rendering the Kestrel engine the only viable candidate. Most available engines are an order of magnitude more powerful which would require a heavy structure to cope with the compression loads. The smaller engines used in geostationary satellite apogee motors do not provide sufficient thrust and the larger engines used in upper stages are too powerful and heavy, thus imposing critical structural design challenges. The Kestrel engine performs three main manoeuvres: a midcourse correction, a lunar orbit insertion (LOI) and a TEI. The spacecraft's T/W and burn time at each manoeuvre is given in Table 8.8. A high T/W ratio well above 1 ensures short burn times, boosting manoeuvre efficiency [29].

Table 8.8: Summary of manoeuvres where the Kestrel engine is used.

Manoeuvre	ΔV [km/s]	S/C mass prior manoeuvre [kg]	T/W [-]	Burn time [min]
Mid-course correction	0.28	6,527	2.88	1.76
LOI	0.81	5,839	3.22	3.66
TEI	0.81	1,389	13.54	0.65

The values shown in Table 8.8 indicate that the three main burns are relatively short when compared to previous flights [127]. The highest T/W ratio is experienced by the orbiter when performing the TEI burn, which yields

an acceleration of 2.12 g. As explained in Section 4.4, the whole structure was designed to survive up to 6 g, thus all manoeuvres are safe.

Both RP1 and LOX are stored in custom made tanks, since no off-the-shelf tanks with the right capacity were found. The volume of the LOX tank is 395 L and the volume of the RP1 tank is 1629 L, as stated in Table 4.12. The freezing and boiling temperatures of the propellant are shown in Table 8.9. The thermal equilibrium temperature of the tanks is 313 K, as established by the thermal sizing method, in Section 4.2. Cryogenic cooling is required for the LOX tank since its operational temperature range is far below the tank equilibrium temperature. As detailed in [128], a Stirling-cycle cryocooler with a heat lift of 5 W at 80 K would suffice. This cooling technology has flown in the past, at a mass of 5 kg [62] and is thus considered an off-the-shelf component. However, the cooling system for the LOX tank was not designed in detail due to time constraints and is thus left as an official recommendation to be dealt with in the future.

Table 8.9: Orbiter propellant operational temperatures.

Compound	Agent	Freezing temperature [K]	Boiling temperature [K]	Equilibrium temperature [K]
RP1	Fuel	200	420	313
LOX	Oxidiser	51	90	313

The tanks are pressurised with Helium gas at 930 kPa as required by the Kestrel engine [129]. The pressurant mass is again estimated using Equation 5.3, as explained in Section 5.4. It was found that 2.51 kg Helium is required to pressurise the orbiter tanks.

8.5 STRUCTURES AND MATERIALS

The function of the orbiter structure is to provide a backbone structure that facilitates optimal operations of all subsystems during its mission lifetime. Therefore the requirements and constraints are first determined. Afterwards the required functions and the design solution are presented together with an analysis on its performance.

The structural design of the orbiter is driven by two conditions, launch conditions and operational conditions. The launch conditions enforce vibrational, acoustic and acceleration loads. Operational conditions enforce acceleration loads caused by engine-burns, but include also protection from radiation. Loads and vibrations caused by the subsystems are the last factors for the operational conditions and are to be taken into account. For all expected loads, the requirements as stated in Section 2.1 dictate that the orbiter will provide structural integrity. It was identified that the largest axial acceleration during launch will be 6 g, while the maximum acceleration in operational conditions is around 2 g, as found in Section 4.4. So the launch acceleration is the driving requirement and will be taken into account in the design. The largest vibrational load is identified to arise during launch and thus is a requirement for the entire spacecraft in launch configuration. The orbiter is constrained by the launch fairing dimensions. As stated in the launcher manual [20] the maximum dimensions are a diameter of 4.6 m and a height of 11.4 m [20].

The main function of the structure of the orbiter is to accommodate an engine and its associated propellant tanks and provide a payload accommodation for the required payloads. Also the orbiter connects the entire spacecraft to the LV and supports the RV and the lander. In terms of mass and volume, the orbiter design is driven by the engine and propellant tanks, which is the same for a rocket. Based on this and the requirements and constraints, as a first design, the design of a simple rocket is considered. The basic layout of such a bi-propellant rocket is from bottom to top, an engine followed by the two main propellant tanks. Rockets are then connected to the next stage or their payload. Another option is to split up the propellant tanks in multiple tanks and placing them around a central structural cylinder, increasing the required diameter significantly.

Both options and their consequences were considered. The basic rocket layout would increase the height of the orbiter significantly, increasing sensitivity to vibrations, but the propellant tanks are connected to the inside of the skin of the rocket. So no additional structural mass is needed to support the propellant tanks, while the other design will need a support structure. It became apparent that the height of the orbiter would not be an issue to fit in the launcher fairing, and because of the more efficient structural design, the option of the standard rocket was selected. To mitigate the sensitivity to vibrations, the heaviest components are situated as low as possible. The basic layout of the structure and its components is given in Figure 8.3.

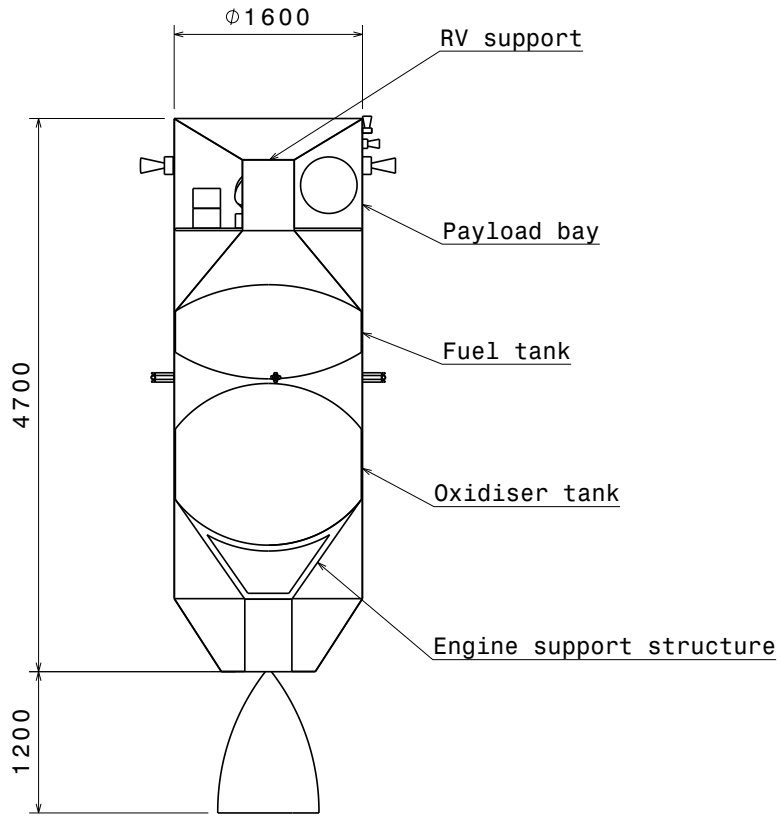

Figure 8.3: Structural design of the orbiter.

The last step is to accommodate payload and make a sufficient connection to the rest of the spacecraft. The payload is accommodated in a separate payload bay that is supported by a cone leading to a cylinder, see Figure 8.3. The cylinder with its skin would be the primary load bearing structure for the orbiter, but this cylinder supports the nosecone of the RV and provides a second load path to the rest of the spacecraft. In this way the loads can be distributed more efficiently leading to a desirable lighter, stronger and stiffer design. The top of the orbiter accommodates the shape of the RV to further enhance this concept and also protects the important heat shield of the RV. This ensures a heat shield in optimal conditions when the RV is released for re-entry. For this reason, the diameter of the RV drives the diameter of the orbiter.

The same concept as used for the payload bay structure is used for the engine support structure. A cone shaped structure distributes forces of the engine to the rest of the cylindrical structure. As can be seen in Figure 8.3, all payload is situated in the payload bay. Also the different sensors used during the mission are situated at this height to ensure easy installation and reducing the need for long cables. The solar panels are also situated at this height for the same reason. In Figure 8.3 a large empty space is left around the engine, between the propellant tanks and above the fuel tank. This is done to accommodate piping for the engine and AOCS thrusters.

STRUCTURAL PERFORMANCE

The structure consists of a cylinder with a diameter that has to accommodate the RV. It also accommodates struts placed around the RV to ensure higher stiffness to withstand launch vibrations. Therefore the required diameter was determined to be 1.6 m. To accommodate the required subsystems, the length of the orbiter was determined to be 4.7 m. With these dimensions, the cylinder can be checked for buckling and compression. Using Equation 4.24 and a thickness of 2.3 mm the critical buckling load was determined. A safety factor for buckling of 1.6 was found and for pure compression a safety factor of 9.4.

As the main structural material aluminium 6061 was selected for its high specific strength. With a 6 g launch load the required thickness using the method in Section 4.4 was determined to be 2.3 mm. This results in a structural mass of 134 kg. Another 15 kg is added for the payload bay, as an extra plate is mounted with fixations needed for the different payloads. With these safety factors present, the requirements set in Section

2.1 are met.

VIBRATIONAL ANALYSIS

All the modules of the mission have been discussed and their final masses are known. The vibrational analysis will be performed with the model shown in Section 4.4.5. The design driving environment is the launch. During launch the lateral and axial natural frequency can not exceed 10 Hz and 25 Hz respectively as was shown in Table 4.6. The mass of the DS is 417 kg, the mass of the AS including propellant is 2,431 kg and the mass of the orbiter including propellant (and RV) is 3,679 kg. Thus, the mass matrix **M** becomes as follows:

$$\mathbf{M} = \begin{bmatrix} 3,679 & 0 & 0 \\ 0 & 2,431 & 0 \\ 0 & 0 & 417 \end{bmatrix} \text{ [kg]} \tag{8.1}$$

The mass matrix will be the same for both the lateral and axial vibrational analysis. To model the spacecraft in the launch fairing, a custom-designed adapter is acting as the first spring. The struts between the modules will be used to model the springs underneath the AS and DS. The struts will be assumed to be pointed in the axial direction, such that the skewed struts are pointed in the axial direction.

Since the struts are all in series, the stiffness of all the struts can be added up to a final equivalent stiffness. The adapter is chosen to have a radius of 0.95 m, a thickness of 5 mm and a height of 0.45 m. Its area moment of inertia is $1.34 \cdot 10^{-3}$ m^4, its cross-sectional area is $2.98 \cdot 10^{-3}$ m^2 and it is made from aluminium 6061, having a Young's modulus of 68.9 GPa [45]. For lateral direction, its stiffness is as follows:

$$k_{eq1,lat} = \frac{3EI}{L} = 3.03 \cdot 10^{10} \text{ N/m} \tag{8.2}$$

And its axial stiffness:

$$k_{eq1,lon} = \frac{EA}{L} = 4.56 \cdot 10^{9} \text{ [N/m]} \tag{8.3}$$

For the AS-orbiter struts, the equivalent stiffness in lateral direction is as follows:

$$k_{eq2,lat} = 6k_{prim2,lat} + 12k_{sec,lat} + k_{dockingport,lat} = 2.12 \cdot 10^{9} \text{ [N/m]} \tag{8.4}$$

And for its axial direction:

$$k_{eq2,lon} = 6k_{prim2,lon} + 12k_{sec,lon} + k_{dockingport,lon} = 8.72 \cdot 10^{8} \text{ [N/m]} \tag{8.5}$$

For the struts between the AS and the DS, additional struts are added to provide added stiffness in lateral direction. Six extra struts are placed, each with a radius of 5 mm, a thickness of 1 mm and a length of 25 cm. Only two lateral struts are in a plane of vibration:

$$k_{eq3,lat} = 6k_{prim3,lat} + 12k_{sec,lat} + k_{struts,lat} = 1.56 \cdot 10^{7} \text{ [N/m]} \tag{8.6}$$

And for its axial direction:

$$k_{eq3,lon} = 6k_{prim3,lon} + 12k_{sec,lon} = 1.67 \cdot 10^{8} \text{ [N/m]} \tag{8.7}$$

These results are substituted in the stiffness matrix **K** for lateral and longitudinal direction. Solving the characteristic equation (Equation 4.31), the natural frequencies are found for both axial and lateral directions. Natural frequencies of 30, 178 and 459 Hz are found for the lateral direction. For the axial direction natural frequencies of 73, 116 and 192 Hz. These values exceed the vibrational envelope (10 Hz for lateral direction, 25 Hz for axial direction) of the Falcon Heavy and thus the spacecraft will not resonate and requirement LCSR-Mission-Forces-03 is complied with.

8.6 DATA AND COMMAND HANDLING

The DCH system of the orbiter module is the same as the one of the AS, which was described in Section 5.6. Again the OBC750 [64] is chosen as onboard computer, the HSDR [64] is chosen as data storage and both were included twice for redundancy. A general overview of the DCH system can be seen in Figure 5.7. Since this is

a general overview, it is not specific for the orbiter module and its subsystems. It can be seen for example that the drill system is presented in Figure 5.7, but this system is not included in the orbiter module.

The amount of data the orbiter module onboard computer needs to process is the data generated per second of all stages/modules. This was determined to be 56,344 bps and can be seen in Table 4.10. This directly influences the amount of data that needs to be sent to an Earth ground station, which will be explained in Section 8.7.

The data rate at which the orbiter module can receive commands (or software updates) from an Earth ground station is maximum 19.2 kbps, the receiver of the orbiter module will be elaborated upon in Section 8.7. The visibility time with an Earth ground station is 5357 s, which is the same as the eclipse time as stated in Section 4.5. This means that the amount of data that can be received per orbit is about $1.05 \cdot 10^8$ bits and the number of commands $1.65 \cdot 10^6$. This number of commands will be sufficient to perform the operations on the Moon, according to [49]. However, more research is needed to determine the exact number of commands to be sent per orbit. In the unlikely case that more commands are needed to be received, again groups of commands can be stored in the HSDR.

8.7 COMMUNICATION SYSTEM

The communication system architecture of the orbiter module was incorporated in the communication flow diagram in Figure 4.6. It can be seen that the communication system can be divided into two parts: one part that communicates with the AS and the other part that communicates with a ground station at Earth. The first part consists of an SSTL transmitter, HISPICO receiver and an SSTL patch antenna, which are presented in Table 8.10 including some relevant parameters. The second part consists of an SSTL transmitter, SSTL receiver and an SSTL patch antenna. These components were chosen due to their specifics (e.g. 6.98 dB gain to transmit the signal), which caused the margin to be acceptable in the link budget presented in Table 8.11. It should be noted that the chosen SSTL receiver, which receives data from an Earth ground station has a low data rate compared to the chosen HISPICO receiver, which obtains data from the AS. This is because the visibility time with an Earth ground station (5357 s) is much higher than the visibility time with the AS (312 to 525 s). Note that the communication system of the orbiter module operates in S-band frequencies, like the communication system of the AS. There is also a backup SSTL patch antenna included for redundancy, which takes over if the operating antenna fails. This holds for the transmitters and receivers as well.

Table 8.10: Orbiter module communication system components.

Component	Frequency [GHz]	Data rate	Power [dBW]	Gain [dB]	HPBW
SSTL transmitter [64]	2.20 - 2.29	9.6 kpbs - 10.0 Mbps	6.02	-	-
HISPICO receiver [65]	2.20 - 2.30	max 1.06 Mbps	-	-	-
SSTL receiver [64]	2.025 - 2.110	9.6 kbps or 19.2 kbps	-	-	-
SSTL patch antenna [64]	2.0 - 2.5	-	10	6.98	35 deg

As done before in Section 5.7 the required data rate was determined using the data generation per orbit (56,344 bps), the visibility time (5,357 s), orbit time (7,059 s) and the 20 % safety margin. This resulted in a required data rate of 89,093 bps that needs to be sent to an Earth ground station, as presented in the link budget in Table 8.11.

Table 8.11: Link budget - Orbiter module to Earth ground station.

Symbol	Description	Value	Unit
Orbiter parameters			
f	Frequency	2.29	[GHz]
P_t	Transmit power	6.02	[dBW]
L_l	Transmitter line loss	-1.00	[dB]
$\alpha_{1/2_t}$	Transmit antenna HPBW	35.00	[°]
e_t	Transmit antenna pointing offset	7.00	[°]
L_{pt}	Transmit antenna pointing loss	-0.48	[dB]
G_t	Transmit antenna gain	6.98	[dB]
EIRP	Equivalent isotropic radiated power	12.00	[dBW]
Propagation path			
S	Propagation path length	407,236	[km]
L_s	Space loss	-211.84	[dB]
L_a	Propagation and polarization loss	-0.50	[dB]
Ground station parameters			
D_r	Receive antenna diameter	34.00	[m]
η [48]	Efficiency (antenna)	0.55	[-]
$\alpha_{1/2_r}$	Receive antenna HPBW	0.31	[°]
L_{pr}	Receive antenna pointing loss	-0.32	[dB]
G_r	Receiver antenna gain	55.63	[dB]
T_s	System noise temperature	-21.30	[dBK]
R	Data rate	89,093	[bps]
E_b/N_0	Energy per bit to noise density	10.19	[dB]
BER	Bit error rate	10^{-5}	[-]
Req E_b/N_0	Required energy per bit to noise density for BPSK	4.50	[dB]
L_i	Implementation loss	-2.00	[dB]
Margin	Margin (>3 dB)	5.69	[dB]

The link budget in Table 8.11 is similar to the one presented in Section 5.7. The propagation path length is much larger, since the signal is sent from the Moon to Earth. Note that since the orbit of the Moon around Earth is slightly eccentric, the distance varies. The distance of 407,236 km constitutes the maximum distance between the Moon and Earth, which results in a space loss of −211.84 dB using Equation 4.39. Due to the Earth's atmosphere a propagation and polarisation loss of −0.5 dB was included as well [33]. Also, the required E_b/N_0 is lower, because a BPSK modulation was used instead of QPSK [64]. The receiver antenna gain (G_r) and HPBW ($\alpha_{1/2_r}$) of the (parabolic) ground station antenna were calculated using Equations 8.8 and 8.9 [33] (these apply only to parabolic antenna).

$$G_r = 20.4 + 20\log(f) + 20\log(D) + 20\log(\eta) \tag{8.8}$$

$$\alpha_{1/2_r} = \frac{21}{f \cdot D} \tag{8.9}$$

where it can be seen that both the gain and HPBW are dependent on the diameter of the ground station antenna. This means that the ground station's antenna size influences the link budget calculation. It was then calculated that the antenna needs to have a minimum diameter of 25 m, because a lower value would cause the margin in the link budget to be lower than 3 dB. After acquiring this constraint, multiple ground stations were selected with an antenna that was larger than 25 m. The reason why multiple ground stations were chosen was because there should always be one ground station with the Moon in its field of vision, which maximises the visibility time of the orbiter. During the selection process it was also determined if the ground station could operate in S-band frequencies, since the orbiter module communicates in this frequency band. This resulted in the selection of NASA's Deep Space Network (DSN), which operates antennas located at three ground station complexes that are separated by 120 deg of longitude. This separation enables to always have a spacecraft in the field of vision of at least one ground station, but only beyond 30,000 km [33]. One ground station operates in the United States (California), the Deep Space Station (DSS) 24. The second ground station, the DSS 34, is

in Australia (Canberra). The DSS 54, which is the third ground station is located in Spain (Madrid). All these ground stations are able to operate in S-band frequencies and have an antenna diameter of 34 m [130].

Note that a link budget analysis was also done for sending data from an Earth ground station to the orbiter module. The difference for this link budget was the lower data rate of 19.2 kbps, because the receiver of the orbiter can at maximum process data at a rate of 19.2 kbps. The margin for that link budget was higher than 3 dB as well, which means that the orbiter module can receive signals from an Earth ground station without too many errors.

8.8 POWER BUDGET

The power budget for the orbiter is the most versatile of the power budgets, as the orbiter is used during most of the mission phases. These mission phases include the launch, the transfer to the Moon, the orbiting phase and the transfer back to Earth. Power requirements are different for these phases, as different subsystems will be active during different phases. All phases and their respective power budgets can be found in Table 8.12.

Table 8.12: Power budget orbiter.

Orbiter	**Launch [W]**	**Transfer to Moon [W]**	**Orbiter [W]**	**Transfer to Earth [W]**
AOCS	0.0	152.0	152.0	152.0
Boardcomputer	6.3	26.3	26.3	26.3
Communication	0.0	90.0	90.0	90.0
Cryogenics	0.0	0.0	0.0	480.0
Thermal	1.4	57.5	57.5	160.3
Power distribution	0.9	38.3	38.3	106.9
Additional	0.5	19.2	19.2	53.4
Total	9.1	383.3	383.3	1,068.9

In Table 8.12 several aspects stand out. When looking at the total power requirements for each phase, the launch phase comes out with the lowest power requirement. This is because most systems do not need to be active during this phase. Again taking a look at the total power requirements, the transfer back to Earth comes out with the highest power requirement. This is due to the fact that the sample has to be kept below 120 K, which drives the power requirements for both the cryogenic system and the thermal system, which are both the systems that require most of the power during this phase. The second highest power requirement is the AOCS, which requires 152 W during each phase except for launch. This is however only a peak value, but all worst case scenarios are taken into account as it might happen that all systems peak at the same moment.

8.9 POWER SUPPLY

Using the methods as described in Section 4.3 one can design the power supply system. As mentioned in Section 3.2 the orbiter will have a solar panel and batteries as a power source. Using the values for the specific power and the power per unit area, as given in Table 4.3, the required mass and size of the power sources of the orbiter were computed.

First, the power the solar panels must generate will need to be computed using Equation 4.15 with the results shown in Equation 8.10.

$$P_{sp} = \frac{1,068.9 \cdot (t_d + t_e)}{5,357} = 1,408.5 \text{ [W]} \tag{8.10}$$

where t_d and t_e are the daylight time and eclipse time respectively and are given in Section 3.3.3.

However, as mentioned in Section 4.7 the power required should have an additional system level margin of 20 %. Therefore the design power for the solar panels is 1,690.2 W. This value for the power was then used to calculate the mass and size of the solar panels, using values from Table 4.3 for the specific power and the power per unit area. Then the mass of the solar panel will be 10.7 kg and the area of the solar panel will be 4.24 m^2.

Using the same method for the batteries a design power of 1,282.7 W was found. The mass and size of the batteries were then computed by using Equation 4.15, with the results shown in Equations 8.11 and 8.12, where the last term represents the DOD for the rechargeable batteries.

$$m_{bat} = \left(\frac{1,282.7 \cdot (t_e/3600)}{150}\right) \cdot \frac{1}{0.5} = 8.1 \text{ [kg]} \tag{8.11}$$

$$V_{bat} = \left(\frac{1,282.7 \cdot (t_e/3600)}{230}\right) \cdot \frac{1}{0.5} = 5.3 \text{ [L]} \tag{8.12}$$

As a last step, the power system can be summarised in an EBD, as depicted in Figure 8.4. Here it should be noted that the ECP system is included in the voltage regulator and power distribution system. Therefore the power supply system satisfies the LCSR-Mission-Environment-08 requirement.

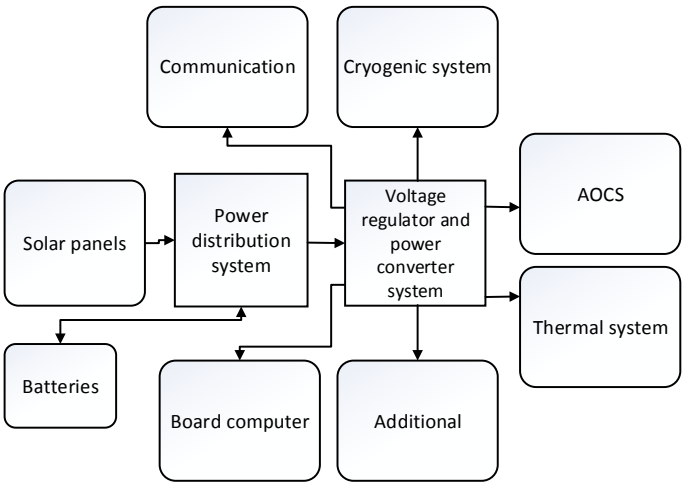

Figure 8.4: Electrical block diagram for the orbiter.

8.10 MASS BUDGET

Table 8.13 presents the mass budget as it has been established for the orbiter module.

Table 8.13: Orbiter mass budget. [a]

Orbiter	Estimated mass [kg]	Margin [-]	Nominal mass [kg]
Orbiter engine system	52.00	0.05	54.60
Oxidiser tank	82.00	0.05	86.10
Fuel tank	45.00	0.05	47.25
Engine fixation system	2.60	0.05	2.73
AOCS	70.19	0.05	73.70
Helium pressurant tanks	24.00	0.05	25.20
Communication system	9.76	0.10	10.74
Computer system	8.00	0.10	8.80
Battery system	8.10	0.05	8.51
Solar panel system	10.70	0.10	11.77
Thermal system	90.00	0.20	108.00
Power distribution system	16.00	0.10	17.60
Additional support systems	30.00	0.20	36.00
Central body cylinder	133.78	0.05	140.47
Payload bay structure	15.00	0.05	15.75
Nominal dry mass			**647**
Total dry mass		0.20[a]	**777**
Wet mass			**3,246**
Propellant mass			**2,469**

[a] System level margin over corresponding nominal value.

From the mass budget in Table 8.13, it can be observed that the orbiter has a relatively even mass distribution over the different subsystems, as compared to the RV, AS or DS. It therefore is more difficult to identify the main driving subsystems. The reason for this is the fact that the orbiter's mass is not so much driven by its own subsystems, but by the other modules it needs to support. Actions that reduce the overall mass of the AS, DS or RV, will therefore also cause an overall reduction in the mass of the orbiter.

9 DESIGN ANALYSIS

The previous chapters have given a full description of all the parts the design. In this chapter, an analysis of this design is given, which is needed to see whether or not the mission is feasible. This will lead to a complete mass and power budget, and also to a cost estimation. Then, the requirements will be analysed. After this, a risk assessment will be made and the RAMS characteristics are analysed. Also, a sensitivity analysis is performed. Lastly, the sustainability of the design is discussed.

9.1 MASS AND POWER BUDGETS

This section presents a summary of all the mass and power budgets presented so far to provide a clear overview of the design parameters for the entire mission.

In Table 9.1 the nominal and design required power can be found for each stage and module, where the design required power is obtained by adding the ESA system level margin as explained in Section 4.7. It should be noted that for the RV the first number represents the power required before landing on Earth while the second number represents the power required after landing on Earth.

Table 9.1: Power budget overview.

	Nominal power required [W]	**Design power required [W]**
AS	1,393	1,672
DS	206	247
RV	781/615	937/738
Orbiter	1,069	1,283

In Table 9.2 the dry masses of all the stages and modules are presented, as well as the wet masses at the moment of launch. Note that for the RV and DS, the dry mass is equal to the wet mass. This is because neither of these vehicles carries any propellant by itself. Since the Falcon Heavy LV has been selected for this mission, it is important the total wet mass of the spacecraft does not exceed the launchers launch capability. The Falcon Heavy can launch up to 13,200 kg into an orbit towards Mars and since the Lunar SECRet mission's launch mass lies below this capability, as can be seen in Table 9.2, it can be launched as planned using this LV [131]. The masses as presented in Table 9.2 correspond to those found in Tables 5.13, 6.8, 7.9 and 8.13.

Table 9.2: Launch mass budget overview.

	Total dry mass [kg]	**Total wet mass [kg]**
AS	665	2,431
DS	417	417
RV	433	433
Orbiter	777	3,246
Total launch mass	2,292	6,527

9.2 LIFE-CYCLE COST

In this section a cost model is presented which is used to evaluate the total life-cycle cost (LCC) of the Lunar SECRet mission. The model is validated using four missions: two missions to the Moon and two sample return

missions. In the Mid-Term Report a cost model was introduced that had the spacecraft dry mass and LV cost as input. In this section, the cost model is refined using the subsystem masses and the LV as input.

9.2.1. COST BREAKDOWN

For making a cost estimate of the Lunar SECRet mission, the USCM8 model will be used [33]. The USCM8 model uses 44 Earth-orbiting satellites (composed of 23 military, 12 NASA and 9 commercial missions) to make a parametric cost estimation based on system parameters [33]. The USCM8 cost model contains a cost estimating relationship (CER) of the spacecraft bus costs based on the entire spacecraft dry mass, as was presented in the Mid-Term Report. In the detailed design the subsystem masses are determined which are used to compute a more precise cost estimation. The inputs of the model are as shown in Table 9.3.

Table 9.3: Inputs for the USCM8 cost model.

Parameter	Symbol	Unit
Structural and thermal system mass	$m_{S\&T}$	[kg]
AOCS mass	m_{AOCS}	[kg]
Electrical power supply (EPS)	m_{EPS}	[kg]
Average non-recurring TT&C cost	$C_{TT\&C,NR}$	[FY2010$]
Payload masses	m_{PL}	[kg]
Reaction control system (RCS) volume	V_{RCS}	[cm^3]
Apogee kick engine (AKE) mass	m_{AKE}	[kg]
Engine burn-time	t_{burn}	[s]
TT&C mass	$m_{TT\&C}$	[kg]
Average launch operations & orbital support (LOOS) cost	C_{LOOS}	[FY2010$]
LV cost	C_{LV}	[FY2010$]

These inputs will be used in the cost breakdown.

Spacecraft bus The spacecraft bus cost is composed of recurring and non-recurring cost and can be determined for each subsystem. Non-recurring cost is shown on the left hand side and the recurring cost on the right hand side of the CERs of Equations 9.1 to 9.4. Equation 9.5 only contains non-recurring cost. For structural and thermal mass Equation 9.1 is used:

$$C_{S\&T} = 646 m_{S\&T}^{0.684} + 22.6 m_{S\&T} \tag{9.1}$$

For AOCS cost:

$$C_{AOCS} = 324 m_{AOCS} + 795 m_{AOCS}^{0.593} \tag{9.2}$$

For EPS:

$$C_{EPS} = 64.3 m_{EPS} + 32.4 m_{EPS} \tag{9.3}$$

For propulsion:

$$C_{Propulsion} = 20 V_{RCS}^{0.485} + (29 m_{AKM} + 0.024 t_{burn}) \tag{9.4}$$

Finally, for TT&C:

$$C_{TT\&C} = C_{TT\&C,NR} + \left(883.7 m_{TT\&C}^{0.491}\right) \tag{9.5}$$

Payload The costs related to the payload are assumed to be a weighted fraction of the bus costs. This weighted fraction is defined as the ratio between the effective payload mass and the dry mass. The payload is composed of the cryogenics system, the robotic arm and the drill. The complexity factors will be added as percentages of the payload masses, resulting in 'heavier' payload masses. These complexity factors were previously shown in the Mid-Term Report and will thus not be shown here. For the cryogenics system, a complexity factor of 1.0 is used due to the adjusted dewar system. The robotic arm is given a complexity factor of 0.2, mainly because only the segments of the existing arm have become larger. The ExoMars drill is adapted to fit the lunar environment, which gives the drill a complexity factor of 0.4.

Payload-bus integration These costs are related to planning and executing the interface, including engineering and testing. For this, Equation 9.6 is used:

$$C_{PL-bus} = 0.195 C_{NR} \tag{9.6}$$

Launch vehicle The LV will carry the spacecraft to the desired orbit. This cost is dependent on the type of LV that is used and in which orbit the spacecraft needs to be injected.

Program level These costs are composed of prime contractor and subcontractor costs for systems engineering, systems integration and test and program management. They are split up into recurring and non-recurring costs. The recurring cost is 32% of the recurring spacecraft (bus including payload) cost, and the non-recurring cost is 41.4% of the spacecraft non-recurring cost.

Ground Command & Control (GC&C) The GC&C costs are composed of the necessary hardware and software that is needed for the mission. For the mission outline, no new facilities have to be built and existing hardware and software will be used. This cost will be small compared to the other costs and is thus neglected in the total LCC.

Flight Support Operations (FSO) These are contractor costs associated with pre-launch planning and activities like launch site support and LV integration. The USCM8 model provides an average cost of 5.85 FY2010$M for FSO.

Insurance There are two types of insurance which will be considered. The first is the launch insurance, that covers the spacecraft manufacturing cost (spacecraft recurring cost), the launch (LV cost) and the on-ground support (FSO cost). The launch insurance premiums are time-dependent: after multiple LV failures the premiums tend to rise. Generally values range between 13-17% of the launch, production and ground operations cost [132]. The second type of insurance is in-orbit insurance, which accounts for all failures after launch. This type of failures is less common than launch failures and thus has a lower premium rate. Rates tend to vary between 1.2-3.7% for in-orbit failures [132].

Aerospace Ground Equipment (AGE) These are costs concerning the test and support equipment for integration, assembly and acceptance before launch. For the AGE cost the USCM8 method provides the following relationship:

$$C_{AGE} = 0.421 C_{bus,NR}^{0.907} \tag{9.7}$$

Operations The operations costs are the costs to support the space mission which includes the ground personnel and the facilities used. The operations percentage of a short-duration mission is used, taking 8% of the entire mission costs as operations cost [133].

All values are given in the monetary value of fiscal year 2010 (FY2010$K), so an inflation rate of 9.1% has to be added to update to 2014 economic conditions [134]. The budget is not escalated up to 2025, as the inflation rates are very unpredictable over such a long time.

9.2.2. VALIDATION

To validate the cost model two lunar missions and two sample return missions were used: the Lunar Reconnaissance Orbiter (LRO), Clementine, Genesis, and Stardust respectively. It is assumed that the total cost of each mission is measured in the monetary value of the year in which the mission was launched and that insurance is not included in the total cost. The USCM8 model is measured in FY2010$, so the missions are updated to 2010 economic conditions [134].

The LVs of all the considered missions are updated to 2010 economic conditions using their respective inflation rates [134]. The LRO mission was launched using an Atlas V, which has a launch cost of 159 FY2010$M [24]. The Clementine mission was launched using a Titan II missile, which has a cost of 22.5 FY2010$M [135]. Stardust and Genesis were launched using the Delta II rocket, which has a launch cost of 98 FY2010$M [136]. The values for the subsystem mass and the launch cost are shown in Table 9.4.

Table 9.4: Input for the cost model validation.

	Clementine (1993) [33]	LRO (2009) [33]	Stardust (1999) [33]	Genesis (2001) [137]	Unit
m_{dry}	259	1018	299	494	[kg]
m_{PL}	14	96	71	225	[kg]
$m_{structural}$	62	316	60	116	[kg]
$m_{thermal}$	23	81	9	16	[kg]
m_{EPS}	36	244	99	37	[kg]
$m_{TT\&C}$	13	71	18	10	[kg]
m_{AOCS}	16	61	9	10	[kg]
$m_{propulsion}$	54	122	18	37	[kg]
C_{launch}	22.5	159	98	98	[FY2010$M]

After applying theses inputs in the model this yielded the outputs shown in Table 9.5.

Table 9.5: Output for the cost model validation (real mission cost is also shown).

	Clementine (1993) [33]	LRO (2009) [33]	Stardust (1999) [33]	Genesis (2001) [137]	Unit
C_{real}	131	557	284	280	[FY2014$M]
C_{est}	127	395	218	239	[FY2014$M]
Δ C	3.5	41.0	30.1	17.0	[%]

From Table 9.4 it is derived that the average deviation of the mission cost is 22.9%. The model is based on a statistical regression of Earth-orbiting satellites. It is not designed for planetary missions like the missions shown above. The largest difference is for the LRO mission: the difference of 41% can be explained due to the long duration of the mission, which requires a higher percentage for operation as opposed to the 8% that was assumed in the cost breakdown. The average deviation will be added on top of the cost that the model predicts for the Lunar SECRet mission.

9.2.3. EVALUATION

The Lunar SECRet mission inputs are shown in Table 9.6. The payload is composed of the robotic arm (50.5 kg), cryogenics system (33 kg) and the drill system (76.8 kg). They are given a complexity factor of 1, 0.2 and 0.4 respectively as was mentioned in Section 9.2.1. A factor of 0.739 (as of June 6^{th} 2014) is taken for the conversion to FY2014€M.

Table 9.6: Input for the cost model validation.

	Lunar SECRet (2014)	Unit
m_{dry}	2,260	[kg]
m_{PL}	160	[kg]
$m_{S\&T}$	853	[kg]
m_{EPS}	113	[kg]
$m_{TT\&C}$	24	[kg]
m_{AOCS}	217	[kg]
$m_{propulsion}$	21	[kg]
t_{burn}	400	[s]
C_{launch}	135	[FY2010$M]
C_{est}	388	[FY2014€M]
C_{val}	477	[FY2014€M]

Filling in the inputs of Table 9.6 into the cost model yields a cost of 388 FY2014€M. Including the 22.9% offset of the validation, this leads to a validated total LCC of 477 FY2014€M. This number is however quite low for the Lunar SECRet mission because of the novelty of the cryogenics, the return of the sample and landing in a crater (even after applying complexity factors for the payload). Contacts with ESA provided us with the information for one of their sample return missions from the Moon [138]. They provided a total conceptual mission cost of about 750 FY2014€M composed of the following:

- Lander DS: 100 FY2014€M
- Lander AS: 100 FY2014€M
- Orbiter: 100 FY2014€M
- Earth re-entry capsule: 50 FY2014€M
- Mission prime contractor: 50 FY2014€M
- Launch (single Ariane V): 150 FY2014€M
- Ground segment and operations: 50 FY2014€M

Margins are already included in this breakdown. With this the total budget is about 650 FY2014€M. With added ESA internal costs (if it is an ESA mission) and mission level contingencies the total would be 700 to 750 FY2014€M. The Ariane V will not be used, but instead of that the Falcon Heavy with a launch cost of 100 FY2014€M (converted from 135 FY2014$M). Adding the costs of the validated model for the payload, which is about 20 FY2014€M, the total nominal mission cost would be 670 to 720 FY2014€M. If the launcher, all the stages and the ground segment are insured for a premium of 17%, the cost would increase with 85 FY2014€M to a number of 755 to 805 FY2014€M. Up to 92% of the value can be insured to reach to requirement of 800 FY2014€M.

The validated model gives a value of 477 FY2014€M for the Lunar SECRet mission, while correspondence with ESA provides a higher number. The USCM8 model has standard deviations for each of its CERs. If this deviation was also taken into account the model would yield a higher number for the cost. The truth is somewhere in-between: the cost will most likely tend to go to the ESA value. Assuming the ESA value, up to 92% can be insured before the requirement is no longer feasible. However, insuring 100% will yield a total cost of 805 FY2014€M, which is a small deviation from the requirement. Assuming the cost model value that was explained above, it can be concluded that the LCSR-Mission-ConsDesign-03 requirement is met.

9.3 MARKET ANALYSIS

With the entire mission designed and the cost known, it is useful to look into the market available for such a mission. An analysis is done for the current market. No conclusion can be drawn about the market available later in time.

Considering the current state of the space exploration market it can be seen that quite some comparable missions do exist. For example, China's Chang'e 3 project has landed on the Moon recently and China is now preparing for Chang'e 5, which will also carry drilling equipment. Also, both NASA and ESA have been looking into cryogenic sample return missions to comets, which can definitely use similar technologies as the moon mission.

Russia also plans to launch several missions to the Moon in the foreseeable future. This Moon-exploration program is called Luna-Glob, and consists of multiple missions. Both Luna-Glob 2 and Luna-Grunt will examine the Moon's crust. Luna-Glob 2 will examine a crater on the south pole, and Luna-Grunt will return up to 1 kg of surface and rock samples. From this it can be deduced that the scientific community is in need of more data and samples from the Moon's crust [139][140].

Also, NASA is currently working with private companies to take the first steps towards mining the Moon for valuable resources, such as Helium-3 and rare Earth-metals. One or more private companies will win a contract to build robots for Moon mining [141]. For such a commercial operation it is definitely useful to have detailed information about the composition of the Moon.

In short, it can be concluded that both the scientific community and commercial companies are interested in information about the composition of the Moon. The Lunar SECRet mission perfectly satisfies this need. Therefore, it is expected that the market for the mission is very good.

9.4 RISK ASSESSMENT

In order to create a clear overview of the risks associated with the final design, a technical risk map is established. This tool allows for efficient identification of those subsystems that constitute a combination of high

chance of failure and severe failure consequences. The subsystems that fall into this category can then be adequately addressed in the later stage of design by, for example, spending extra funds and effort on their detailed development, testing or the search for possible alternatives. The likelihood and severity criteria used in setting up the risk map as found in Subsection 9.4.3 are presented in respectively Subsections 9.4.1 and 9.4.2.

9.4.1. LIKELIHOOD CRITERIA

The likelihood criteria used to establish the risk map are defined as follows [133] [142]:

Very unlikely Well within existing state of the art/ proven functional space technology/ off-the-shelf with excellent track record

Unlikely Slightly advancing state of the art/minor amounts of new technology/minor modifications to existing technology/off-the-shelf with good track record/extrapolated from existing flight model

Neutral Nominal aerospace equipment using some new technology/ substantial modification to existing technology/ off-the-shelf without track record/ Based on non-flight existing engineering

Likely Significant amount of unproven technology/ significant amount of new technology needs to be developed and qualified/ working laboratory model

Very likely Major new technology/ required breakthroughs in the state of the art/ feasible in theory

9.4.2. SEVERITY CRITERIA

The severity criteria used to establish the risk map are defined as follows:

Negligible Primary mission objectives will be achieved without notable quality loss.

Marginal Primary objective will be achieved with minor quality loss.

Substantial Primary objective will at least be partially achieved.

Critical Primary objective will at most be partially achieved.

Catastrophic Primary objectives will not be able to be achieved.

9.4.3. RISK MAP

SYS Full name of the subsystem. *Likelihood of failure*; reason for likelyhood of failure as explained in Section 9.4.1. *Severity of consequence*; reason for severity of failure as explained in Section 9.4.2.

Table 9.7: Risk map for the Lunar SECRet spacecraft.

	Negligible	Marginal	Substantial	Critical	Catastrophic
Very likely					
Likely					
Neutral			SCC, SCT	SDS, CCS	
Unlikely	AOCSD/A			TSD/A, HDS, PSD, PSA	RA
Very unlikely	CLO/L, AOCSO, CSL/O			PSO, TSO	DP, DT, PA/O, HS, PS RVH

AOCSD/A Attitude and Orbit Control System DS/AS. *Unlikely*; slightly advancing state of the art due to crater environment. *Negligible*; loss of single element, redundancy in sensors and actuators.

AOCSO Attitude and Orbit Control System Orbiter. *Very unlikely*; well within existing state of the art. *Negligible*; loss of single element, redundancy in sensors and actuators.

CCS Cryogenic Cooling System. *Neutral*; substantial modifications to existing technology. *Critical*; rupture of vessel with cooling liquid, lunar sample may still be returned at higher than cryogenic temperatures, historical data may still be retrieved from the sample.

CL/O Computer Lander/Orbiter. *Very unlikely*; well within existing state of the art. *Negligible*; computer short-circuits, second redundant computer system.

CSL/O Communication System Lander/Orbiter. *Very unlikely*; well within existing state of the art. *Negligible*; main antenna fails, use of secondary back-up antenna with possibly lower data rate or signal quality.

DP Docking Procedure. *Very unlikely*; well within existing state of the art. Docking technology is flight proven as shown for the ASTRO and NextSat sattelites [143]. *Catastrophic*; crash with orbiter, samples cannot be returned to Earth.

DT Docking Technology. *Very unlikely*; well within existing state of the art. *Catastrophic*; failure to dock with orbiter, samples cannot be returned to Earth.

HDS Hazard Detection System. *Unlikely*; slightly advancing state of the art. *Critical*; potential loss of lander, in case of dangerous terrain, redundancy in sensors.

HS Heat Shield. *Very unlikely*; well within existing state of the art. *Catastrophic*; heat shield breakup, loss of RV.

PA/O Propulsion AS/Orbiter. *Very unlikely*; well within existing state of the art. *Catastrophic*; engine failure, loss of spacecraft.

PS Parachute System. *Very unlikely*; well within existing state of the art. *Catastrophic*; RV crash.

PSA Power System AS. *Unlikely*; off-the-shelf with good track record. *Critical*; launch from lunar surface, one solar array becomes inoperative, AS may still be able to perform docking, cryogenics may be compromised.

PSD Power System DS. *unlikely*; Slightly advancing state of the art. *Critical*; fuel cell stops functioning, AS may still be able to return with already secured sample.

PSO Power System Orbiter. *Very unlikely*; system is purchased off-the-shelf. *Critical*; one solar array becomes inoperative, orbiter may still be able to return with sample, cryogenics may be compromised.

RA Robotic Arm. *Unlikely*; Slightly advancing state of the art. *Catastrophic*; failure joint, no more samples may be obtained, AS returns with already secured samples or sample canister transfer becomes impossible.

RVH RV Hatch. *Very unlikely*; well within existing state of the art. *Catastrophic*; burn up in the atmosphere.

SCT Sample Cutting Tool. *Neutral*; substantial modification to existing technology. *Substantial*; Breakage of structure, no more samples can be separated with tool, redundant system, AS returns with already secured samples.

SDS Sample Drill System. *Neutral*; substantial modification to existing technology. *Critical*; failure motor, sample is retrieved from depth of less than 2 m.

SSC Sample Storage Container. *Neutral*; based on non-flight engineering. *Substantial*; loss of single storage cell, lunar sample stored in other cells will still be returned at cryogenic temperatures.

TSD/A Thermal System DS/AS. *Unlikely*; slightly advancing state of the art. *Critical*; heat pipe bursts, critical systems may remain functioning or AS may still be able to return with already secured sample on battery power.

TSO Thermal System Orbiter. *Very unlikely*; well within existing state of the art. *Critical*; heat pipe bursts, critical systems may remain functioning.

From this risk map, the conclusion may be drawn that the cryogenic cooling system, the robotic arm and the drill system are the most critical subsystems in the design. Following from this, the recommendation is made

that during later stages of the design, these systems receive additional testing, larger redundancies and other risk mitigation steps aimed mainly at the prevention of system failure.

9.5 RAMS

In this section the reliability, availability, maintainability and safety (RAMS) characteristics of the mission will be discussed. First, the maintainability of the design will be addressed, where attention will be paid to mission time slots that have been reserved for software updating and extensive checkups. Second, the reliability of spacecraft and its modules and stages will be discussed. Following these discussions, the availability of the spacecraft will be covered. Finally, a discussion on the safety considerations for this mission is presented.

9.5.1. MAINTAINABILITY

As with spacecraft in general, and planetary spacecraft in particular, the maintainability of the Lunar SECRet spacecraft is subject to several challenges.

Physical repairs after launch are very unlikely if not impossible. Given the predicted cost for the mission, as presented in Section 9.2, the mission's monetary budget will not allow for a dedicated repair mission. Furthermore, since the spacecraft will be launched directly into TLI , the option of using facilities that are already in orbit, such as the ISS, as starting point for a repair mission is also eliminated. As a final resort, the robotic arm attached to the AS may be able to perform certain basic adjustments, but it is not equipped for this purpose, nor is it intended to do so. Enabling it to perform this function properly would require additional tools, research and money.

A maintenance tool that is available, however, is to provide dedicated data packages to the spacecraft via the communication systems. Examples of these data packages are software updates, or commands to reboot a subsystem or initiate a burn to alter orbit or inclination. To allow for such data up-links, dedicated time slots have been identified in which the spacecraft can be given the command to delay the next phase of operations. These slots are one week long and placed between the arrival at the Moon by the spacecraft and the descent of the lander to the lunar surface, and the ascent of the AS from the lunar surface and docking.

These moments have been chosen respectively to allow for a full system check before the lander is sent into the crater, where it will only have reactant to provide power for one week, and to allow for a software update in case complications are encountered during the docking procedure.

Since there is no feasible way to physically maintain the system whilst in service, redundancy has to be applied to prevent a failing instrument from endangering the entire mission. Thrusters, communication systems and computers are, where possible, installed in greater numbers than strictly required. Systems for which this is not possible, due to size or mass, are the drill, robotic arm and cryogenics. These will have to be given extra attention during more detailed design phases, have internal redundancies and/or undergo more rigorous testing, to reduce the chance maintenance is needed.

9.5.2. RELIABILITY

In this subsection, an assessment of the spacecraft reliability, excluding the launch phase, is made. For the purpose of predicting this reliability, statistical spacecraft data are used.

As a first step spacecraft subsystem failure is assumed to exhibit an exponential failure rate [41]. Defining reliability (R) as the probability a system functions adequately for at least a certain time (t), a system's reliability can be modeled using Equation 9.8. Here λ is the statistical failure rate in failures/spacecraft/year and t_{rel} is the period over which the reliability is determined.

$$R = e^{-\lambda \cdot t} \tag{9.8}$$

Zandbergen [41] provides estimated failure rates for individual satellite subsystems as well as individual apogee kick engines and the spacecraft payload, which are presented in Table 9.8. The subsystems for which failure rates have been defined are the RCS, AOCS, AKE, EPS, structures and mechanisms system (SAM), TT&C system, thermal system (TS) and payload system (PS). Even though these numbers are based on satellite statistics, they can still be used to give preliminary estimations for all individual spacecraft modules and stages. The reliability

for one module or stage is generated by taking the product of all its subsystem reliabilities. The reliability of the whole spacecraft is then determined by taking the product of the reliabilities of the orbiter, AS, DS and RV. A safety factor of 50% will be added to the failure rate in cases where this mission characteristics were deemed to be more demanding, than for standard satellite missions. Second, a constant failure rate is assumed for each subsystem, irrespective of whether that subsystem is active or hibernating. Ideally, one would want to apply different statistical failure rates to those phases in which the spacecraft is either active or not, but the statistical data for such a model are not yet available at this stage of the design. Third, the time for which the reliability has to be guaranteed for each vehicle is set to start on the moment of launch. Again, a more accurate model would be to split this analysis up into a dedicated active time span, and a hibernation period.

In the period for which the reliability requirement has to be met, four phases can be identified. Phase 1 is the transfer to the Moon, lasting five days, as stated in Section 3.1. Phase 2 consists of lunar operations. This includes the seven day software maintenance window before descent and docking, seven days of descent and lunar operations, docking and the time spent waiting in orbit until the next return window [144]. Phase 3 consists of the return to Earth which lasts five days, and phase 4 constitutes the recovery on Earth, which will last 12 hours. Over all times spent in phase 1, 3 and 4 a 20% margin is taken. This has not been done for time spent in phase 2, since this phase constitutes several hard deadlines (e.g. one return window every 14 days, as stated in Section 3.3.5).

Since four engines are used in the AS, and failure rates are given per engine the reliability of each engine has to be assessed individually. No engines are included in the DS, as the entire lander operates using the AS engines. In Table 9.9 a – is used to indicate that a particular subsystem is not present in this module or stage.

The periods for which reliability has to be determined are then defined in Equations 9.9 through 9.12.

$$t_{Orbiter} = (5+5)\cdot 1.2 + 28 = 40 \text{ days} = 0.1096 \text{ years} \tag{9.9}$$

$$t_{DS} = (5)\cdot 1.2 + 7 + 7 = 20 \text{ days} = 0.05479 \text{ years} \tag{9.10}$$

$$t_{AS} = (5)\cdot 1.2 + 7 + 7 + 7 = 27 \text{ days} = 0.07397 \text{ years} \tag{9.11}$$

$$t_{RV} = (5+5+0.5)\cdot 1.2 + 28 = 40.6 \text{ days} = 0.1112 \text{ years} \tag{9.12}$$

Table 9.8: Subsystems with their respective identifiers as used in Table 9.9 and failure rates.

Subsystem identifier	Failure rate [failures/spacecraft/year]
RCS	0.012
AOCS	0.0248
AKE	0.0014
EPS	0.0092
SAM	0.0078
TT&C	0.0085
TS	0.0064
PS	0.04752

Using the estimated periods as found in Equations 9.9 to 9.12 and the statistical data from Table 9.8, the spacecraft reliability characteristics can be determined, as presented in Table 9.9.

As stated, safety factors have been applied where the Lunar SECRet mission contains aspects that increase the probability of failure. For the orbiter, this has been deemed not to be the case for any of the subsystems. In essence, it is a satellite, for which satellite statistics will be used as approximation. For the DS the thermal system and payload system have been given an additional safety factor because of the challenging thermal environment in which they operate. The structures and mechanics system has been given a safety factor because of the risks associated with damaging structures during landing and the AOCS because of the challenges of a landing in the dark. For the AS, the apogee kick engines and power system have been given a safety factor because of the challenge of having to be operated after a landing on the Moon. The loads and shocks involved in this landing may impair proper further functioning by damage or degradation due to thermal and mechanical

loading. The structures and mechanics and thermal system have received a similar treatment as for the DS. For the RV, the payload system has received a safety factor because it has to remain operational under the g-loads associated with ballistic re-entry.

Table 9.9: Statistical failure rates, operational lifetimes and reliabilities for individual subsystems, orbiter, AS, DS and RV and the total spacecraft.

Subsystem	**RCS**	**AOCS**	**AKE**	**EPS**	**SAM**	**TT&C**	**TS**	**PS**	**Total**
Orbiter									
Safety factor [-]	0	0	0	0	0	0	0	0	
Lifetime [years]									0.1096
Reliability [-]	0.9987	0.9973	0.9998	0.9990	0.9991	0.9991	0.9993	0.9948	0.9872
DS									
Safety factor [-]	0	0.5	0	0	0.5	0	0.5	0.5	0
Lifetime [years]									0.05479
Reliability [-]	-	0.9980	-	0.9995	0.9994	0.9995	0.9995	0.9961	0.9920
AS									
Safety factor [-]	0	0	0.5	0.5	0.5	0	0.5	0	-
Lifetime [years]									0.07397
Reliability [-]	0.9991	0.9982	0.9994	0.9990	0.9994	0.9994	0.9993	0.9965	0.9900
RV									
Safety factor [-]	-	-	-	0	0	-	0	0.5	
Lifetime [years]									0.1112
Reliability [-]	-	-	-	0.9990	0.9991	-	0.9993	0.9921	0.9895
Total mission reliability									0.9593

Since the probability of failure is equal to $1 - R$, and R is equal to 0.9593 in this model, the predicted chance of failure for this spacecraft, excluding launch, is 0.0407, or 4.07%. Thus satisfying requirement LCSR-Mission-ConsDesign-02.

In order to verify this model, two steps were taken. First, all failure rates were set to 0 and 0.01 respectively. From basic mathematics it is expected the former yields reliabilities of 1, which corresponds to the result from the model. In case of the latter, all safety factors were set to 0 as well, which combined yielded equal reliability estimates for the subsystems of each individual module or stage, as expected. Second, if the failure rate of each subsystem is halved, the reliability becomes the square root of the original reliability value. Performing the reliability calculations with halved failure rates indeed displays this expected characteristic. This model itself is a commonly applied way to create first-order estimates for space system reliabilities. The statistical input data are taken from approved lecture material [41]. Since no reliability data could be obtained for modern (post 1980) landers, this estimate is accepted as first approximation [145] .

9.5.3. AVAILABILITY

The availability of a product is defined as the amount of time a product is operational, divided by its amount of time in service. It is therefore a measure of how much use the operator has of the acquired system. For missions in this specific planetary sciences class, such as the Lunar SECRet, it does not serve to define a numerical value for this parameter. The entire time the spacecraft is operational, by design, is time it is in the process of securing and retrieving the sample. Thus the availability, if a numerical value would have to be given, would be 1.

9.5.4. SAFETY

In this case, safety is defined as the danger the spacecraft poses to human life or health. Using this definition, three phases in the mission can be identified during which safety is a concern: production, launch and re-entry. During all these phases, a large part of the safety concern comes from the materials used. Both the oxidiser and fuel, MON and MMH respectively, used in the lander are hazardous materials [146] [147]. The batteries used in the various spacecraft modules and stages contain hazardous chemicals as well [148] [149].

During the production phase, these hazards will be addressed by using only qualified personnel, equipment and methods during the production phase. Regarding the launch and re-entry phases the casings for these items should be designed such that dispersion will be minimised in case of disintegration of the vehicle. Besides this, these factors will affect the insurance premium to be paid. Finally, the conditions at the launch and landing site on Earth are taken into account. The launch will most likely not be allowed to proceed in case the wind profile indicates populated areas down wind. The landing will take place in the Soyuz return area in Kazakhstan, which is remote and staffed by trained personnel, thus minimising risk upon re-entry.

Furthermore, re-entry always carries some inherent dangers, induced by the fact an object is entering the Earth's atmosphere at high speed. In part, this risk is mitigated by selecting a specialised landing site in a sparsely populated area. However, part of this risk is also simply accepted, as illustrated by the regular return of Soyuz returns to Earth.

9.6 REQUIREMENTS ANALYSIS

After the baseline review, in correspondence with the customer, Prof. Van Westrenen, a list of requirements was set for the mission under design. These requirements were restated in Section 2.1. In Table 9.10, for each of the requirements, a verdict is given on whether this requirement can be met by the design or not. Following these verdicts are the chapters or sections of this report where this compliance with the requirement is further elaborated upon.

Table 9.10: Compliance matrix.

Identifier	Description	Met	Location of explanation
LCSR-Mission-Sample-01	The project shall choose a sampling area within 370 km from the south pole of the Moon.	Yes	Subsection 2.3.6
LCSR-Mission-Sample-04	The sample shall be taken within the Shackleton, De Gerlache, Wiechert J or Amundsen crater.	Yes	Subsection 2.3.6 and Section 5.2
LCSR-Mission-Sample-05	The sample shall consist of a drill core down to at least 2 m depth.	Yes	Section 6.5
LCSR-Mission-Sample-06	The core sample shall be in powder form, fragments or intact.	Yes	Section 6.5
LCSR-Mission-Sample-07	There shall be a core sample for at least every 25 cm of drill depth.	Yes	Section 6.5
LCSR-Mission-Sample-08	The sample shall be kept at temperatures lower than 120 K until retrieval on Earth.	Yes	Section 6.5, 5.8, 7.10 and Subsection 3.3.5
LCSR-Mission-Environment-01	The spacecraft shall withstand the expected radiation encountered during its mission time from cosmic background radiation, van Allen belts and solar flares.	Yes	Section 3.2 and 4.4
LCSR-Mission-Environment-02	The spacecraft shall withstand the vacuum of deep space.	Yes	Section 3.2 and 4.4
LCSR-Mission-Environment-08	Electrostatic charges shall not accumulate in the design.	Yes	Section 5.12, 6.8, 7.10 and 8.9
LCSR-Mission-Environment-09	The spacecraft shall ensure sustainable temperatures for all subsystems.	Yes	Sections 5.3, 6.3, 7.6 and 8.3
LCSR-Mission-Forces-01	The spacecraft shall withstand axial launch forces induced by the LV.	Yes	Section 5.5, 6.4, 7.5 and 8.5

LCSR-Mission-Forces-02	The spacecraft shall withstand vibrational loads induced by the LV.	Yes	Section 8.5
LCSR-Mission-Forces-03	The spacecraft shall withstand forces induced by its systems.	Yes	Section 5.5, 6.4, 6.5, 7.5 and 8.5
LCSR-Mission-Forces-04	The spacecraft shall withstand vibrations induced by its systems.	No	
LCSR-Mission-Forces-05	The spacecraft shall withstand lateral launch forces induced by the LV.	Yes	Section 5.5, 6.4, 7.5 and 8.5
LCSR-Mission-Forces-06	The spacecraft shall withstand acoustic loads induced by the LV.	Yes	Section 4.4
LCSR-Mission-ConsMission-01	The mission shall launch no later than 2025.	Yes	Section 10.2
LCSR-Mission-ConsMission-02	The sample shall be kept at temperatures lower than 120 K for at least 12 hours after landing on Earth.	Yes	Section 5.8, 7.10 and Subsection 3.3.5
LCSR-Mission-ConsDesign-01	The mission shall not be in violation with any relevant law.	Yes	Appendix C
LCSR-Mission-ConsDesign-02	The mission shall have a probability of failure no higher than 5% excluding the launch phase.	Yes	Subsection 9.5.2
LCSR-Mission-ConsDesign-03	The life cycle cost of the mission shall not exceed €800 million including launch cost.	Yes	Section 9.2

LCSR-Mission-Forces-04 can at this point in time not be stated to be met. Due to time constraints and a lack of available information at subsystem level no detailed analysis has been made of the vibrational characteristics of all subsystems. This does not mean the design cannot withstand the vibrations caused by its subsystems, but it cannot be stated yet this requirement is met. A more detailed design, including the subsystem integrations, will be needed for this.

9.7 SENSITIVITY ANALYSIS

In order to investigate the sensitivity of the design one can perform a sensitivity analysis. From the sensitivity analysis it can be shown what subsystems of the design is the most sensitive component of the design. For the sensitivity analysis the most critical parameters are changed by 20%.

9.7.1. STRUCTURAL SENSITIVITY

To perform a sensitivity analysis of the structural design, it is assumed that the masses of the module increase by 20%. Parameters like gravitational loads and vibrational loads are kept constant since they are constant for the launcher. In case a different launcher is used this will be more of a risk consideration. If the total masses of the modules increase by 20%, this means that the safety factor will go down. The same structural methods will be used to evaluate the sensitivity as for the structural design.

AS The safety factor of the struts between the orbiter and the AS will go down from 2.8 to 1.2 for buckling and from 1.7 to 1.3 for tension. The safety factor of the panels will go down from 4.3 to 3.3. The thrust does not change but the engine mass does. The safety factor due to gravitational pull on the engine struts goes down to 685 N from 822 N.

DS The safety factor of the struts between the DS and the AS will go down from 1.94 to 1.3 for buckling and from 1.8 to 1.3 for tension. The safety factor of the panels will go down from 4.3 to 3.3. The safety factor of the panels will go down from 2.2 to 1.8. For the legs of the DS, the FS will go down to 3.6 from 2.6 for buckling, from 1.8 to 1.3 for tension and from 3.4 to 2.5 for pure compression.

Orbiter For the cylindrical structure, the safety factor will go down to 1.8 from 2.0 for buckling.

The lowest lateral frequency decreases to 27 from 30 Hz, and the lowest axial frequency decreases from 73 to 64 Hz. It can be concluded that for a mass increase of 20%, the structural system is able to perform its task, however with decrease of safety factor.

9.7.2. MASS AND COST BUDGET

The sensitivity of the mass and cost will be analysed by determining the effect of increasing the dry mass of the modules by 20%. The sensitivity is analysed by increasing the dry mass of a single module, the other modules are left untouched. Then the wet mass is recalculated as described in Section 4.6. The cost model, as explained in Section 9.2 used for this report does not depend on the dry mass of single stages but rather specific subsystem masses. These specific masses were increased to account for the additional costs, the results of the sensitivity analysis are shown in Table 9.11. The baseline of the total wet mass is 6527 kg. None of the masses exceed the launcher capability and none of the costs exceed the requirement on the cost. Thus it can be concluded that the design is not sensitive for mass and cost increases.

Table 9.11: Result of the sensitivity analysis of the total cost and wet mass if a single module increases in mass.

Module	Module dry mass[kg]	Wet mass total spacecraft [kg]	Cost [FY2014 €M]
AS	686	7,116	495
DS	500	6,757	501
Orbiter	932	6,828	496
RV	520	6,695	489

9.7.3. POWER SUPPLY

The sensitivity of the power supply system will be analysed by determining the effect of increasing the power required of each module by 20 %. The sensitivity is analysed by increasing the power required of a single module, the other modules are left untouched, then the required power is recalculated as described in Section 4.3. The results are shown in Table 9.12.

Table 9.12: Sensitivity analysis of the power supply system.

Moon ascent	**Power Original**[W]	**Power new** [W]	**Mass original** [kg]	**Mass new** [kg]	**Size original** [m^2 or L]	**Size new** [m^2] or [L]
Solar panels system	2,203.1	2,643.7	13.9	16.7	5.5	6.6
Batteries	1,671.9	2,006.3	10.5	12.6	6.9	8.2
Moon descent	**Power Original**[W]	**Power new** [W]	**Mass original** [kg]	**Mass new** [kg]	**Size original** [L]	**Size new** [L]
Fuel cells	1,388.6	1,666.3	5.6	6.7	5.4	6.5
Orbiter	**Power Original**[W]	**Power new** [W]	**Mass original** [kg]	**Mass new** [kg]	**Size original** [m^2 or L]	**Size new** [m^2 or L]
Solar panels system	1,690.2	2,028.3	10.7	12.8	4.2	5.1
Batteries	1,282.7	1,539.3	8.1	9.7	5.3	6.3
Re-entry	**Power Original**[W]	**Power new** [W]	**Mass original** [kg]	**Mass new** [kg]	**Size original** [L]	**Size new** [L]
Batteries	937.4/614.8	1,124.8/737.8	33.6	40.3	35.8	42.9

From Table 9.12 it can been seen that when the power required increases by 20 %, the masses and sizes also increase by 20 %.

9.7.4. AOCS

A sensitivity analysis was carried out for the AOCS system. The effect of a 20 % mass moment of inertia increase was investigated. The results are illustrated in Table 9.13. The inertia increase leads to increase of required forces and thus required propellant. The new required forces and moments are still in the design limit for the AS and the orbiter. The designs of the DS and the total spacecraft at Earth to Moon transfer are affected by the higher required forces. The DS does not have double redundancy anymore. If one thruster fails, it has to use the other pitch axis to pitch which is still acceptable. For the total spacecraft during Earth-to-Moon transfer the pitch rate constraint cannot be met with the pitching thrusters. The pitch rate would reduce to 25 °/min. This is still acceptable, since no fast manoeuvres are needed during the Earth-to-Moon transfer.

Due to the increased propellant mass, the mass of the AOCS increases. The mass of the AOCS in the AS increases by 13.5 % to 118.9 kg. The mass of the AOCS in the orbiter increases by 4.2 % to 75.1 kg.

Thus it can be concluded that the AOCS is not very sensitive to an increases of mass moments of inertia.

Table 9.13: Sensitivity analysis of the AOCS.

	F_{pitch} [N]	$F_{pitch_{new}}$ [N]	F_{roll} [N]	$F_{roll_{new}}$ [N]	t_g [Nm]	$t_{g_{new}}$ [Nm]	h [Nms]	h_{new} [Nms]	m_{prop} [kg]	$m_{prop_{new}}$ [kg]
AS	29	34.8	9.2	11	$5.3 \cdot 10^{-4}$	$8 \cdot 10^{-4}$	10.1	12.1	40.14	48.2
DS	45.2	54.2	11.8	14.1	$1.1 \cdot 10^{-3}$	$1.3 \cdot 10^{-3}$	0.7	0.8	0	0
Orbiter	17.1	20.5	3.7	4.4	$3.8 \cdot 10^{-3}$	$4.6 \cdot 10^{-3}$	58	70	11.38	13.66
TLI	127	153	5	6.8	$6 \cdot 10^{-2}$	$7.3 \cdot 10^{-2}$	932.2	1,119	0	0

9.7.5. THERMAL

The sensitivity of the thermal system will be analysed by determining the effect of increasing the amount of heat influx. The heat generated by the spacecraft is not increased since the heat generated can be adjusted by the spacecraft, as explained in Section 8.3. The heat influx is increased with 20% for the hot case and 20% decreased for the cold case. For the cold case additional heat loss from the dissipated heat is taken into account. The result is shown in Tables 9.14 and 9.15. The range required for the thermal control system is 273 to 313 K. The transfer to the Moon for the hot case does not meet this requirement. The transfer to the Moon and Moon operations and transfer to Earth for the cold case do also not meet the required temperature range for the thermal control system. The consequence for the design is that a different coating or additional thermal control elements are to be placed in the spacecraft. For the cold case the heat generated was not adjusted, with the power unused provided by the solar arrays. This would significantly increase the equilibrium temperature.

Table 9.14: Sensitivity analysis result of the thermal equilibrium temperature - hot case.

Parameter	Transfer to Moon	Near Moon	Moon operations	AS	Orbiter	Transfer to Earth	Unit
Q_{in}	15,243	13,605	1,606	2,625	9,660	10,042	[W]
T	320	311	286	313	309	312	[K]

Table 9.15: Sensitivity analysis result of the thermal equilibrium temperature - cold case.

Parameter	Transfer to Moon	Near Moon	Moon operations	AS	Orbiter	Transfer to Earth	Unit
Q_{in}	7,042	9,136	1,284	1,976	6,629	6,922	[W]
T	264	282	270	292	282	268	[K]

9.7.6. COMMUNICATION

The sensitivity of the communication system's link budget will be analysed by determining the effect of increasing the amount of data that needs to be sent, while keeping the transmission time the same. The effect of increase in losses during communication will be analysed as well. Note that only the infeasible link budgets will be discussed here.

The 20% increase of the data was applied to all the communication links. Increasing the data and keeping the transmission time the same means that the data rate will increase, which is constrained by the maximum data rate that the transmitter can send and the receiver can process. The data rate also influences the margin calculated in the link budgets as the one presented in Table 8.11, which needs to be higher than 3 dB.

The increase that was applied to the data transmission from an Earth ground station to the orbiter module was infeasible due to the fact that the receiver of the orbiter was not able to process at a data rate of 23.04 kbps, which is higher than the maximum data rate of 19.20 kbps. Note that there is an uncertainty about the infeasibility, because the used data rate was dependent on the number of received commands. As mentioned in Section 8.6, more research is needed to determine the actual number of received commands and in reality this number might be much lower.

The data rate increase of the communication link from the orbiter module to the AS resulted in 1.27 Mbps. This was concluded to be infeasible as well, because the receiver of the AS is not able to process data higher than 1.06 Mbps. Again, the infeasibility is uncertain due to the uncertainty of the number of commands needed.

The increase that was applied to the data transmission from the AS to the orbiter module resulted in a data rate from 1.04 to 1.25 Mbps. This was concluded to be infeasible, since the maximum data rate at which the receiver of the orbiter can process signals is 1.06 Mbps.

The effect of increasing all the losses with 20% will be discussed for all the communication links as well. This increase influences the margin calculated in the link budgets, which needs to be higher than 3 dB. The only link that was concluded to be infeasible was the one from the orbiter module to an Earth ground station, since the margin decreased from 5.69 to 0.94 dB, which is lower than the 3 dB margin.

It can be concluded that most of the link budgets are sensitive to an increase in data rate, although there are some uncertainties here. It can also be concluded that the link budget between the orbiter module and the Earth ground station, are sensitive to an increase in losses during communication.

9.7.7. PROPULSION

The propulsion system is sensitive to three main variables: spacecraft dry mass, ΔV required and engine thrust. These variables are altered and their influence on the vehicle launch mass and the T/W before each manoeuvre is examined. The dry mass of each module/stage was increased by 20%, the ΔV for each manoeuvre was increased by 20% and the thrust of the engines was reduced by 20%. Results are shown in Table 9.16.

Table 9.16: Sensitivity analysis for the propulsion subsystem.

	Original	**Larger dry mass**	**Larger Δ V**	**Lower thrust**	**Unit**
Launch mass	6,527	7,383	8,266	6,527	[kg]
Thrust, orbiter	31.25	31.25	31.25	25.00	[kN]
Thrust, AS	6.67	6.67	6.67	5.34	[kN]
T/W inc	2.88	2.57	2.12	2.30	[-]
T/W LLO	3.22	2.87	2.60	2.58	[-]
T/W TEI	13.54	11.28	12.72	10.83	[-]
T/W descent	1.46	1.21	1.17	1.16	[-]
T/W ascent	4.68	3.90	4.24	3.75	[-]

The results show that the T/W before the powered descent is critically affected by the variables stated above, being lower than 1.3 in all variants. It was required that the T/W would range between 1.3 and 1.5 in order to effectively implement the method stated in [61]. All other T/W values remain within acceptable bounds and the vehicle launch mass is below the maximum allowable launch mass of the TBD launcher.

9.7.8. RE-ENTRY VEHICLE

The sensitivity will be checked for a change in entry speed, sea level density, atmospheric scale height and mass. The initial flight path angle is already covered in the under and overshoot trajectories and is thus left out.

The entry speed will be check for sensitivity using the baseline γ_E of -8 degrees as this is the most realistic entry. When the entry velocity is increased, the duration of the entry will reduce the heat load but the heat flux is increasing, yielding a higher net total heat load of $29,8$ kJ/cm^2 accompanied by a increased mass fraction of 18.48 for the heat shield. At the same time, the peak heat flux and peak g-loads will increase to 1034 W/cm^2 and 31.7 g respectively. Both remain below the maximum values for the materials and structures used. Lower g-loads are not a problem and a reduced heat load is also not a problem for the current design, so a lower initial velocity is not a problem for the current RV design. Therefore the REV is considered not very sensitive for a major change in entry velocity. However a difference of 20% is not deemed realistic for a real life entry and would also diminish the concept of the set over and undershoot trajectories in Section 7.5.

Next the atmospheric conditions in the form of the sea level density ρ_0 and the atmospheric density scale height are considered. It is almost guaranteed that the atmosphere is different from the standard conditions used in the simulation. The simulation is not very sensitive to a change in atmospheric scale height, a change of 20% will only induce a difference of lower then 5% for the peak heat flux and heat load, staying within the design limits. Changing the sea level density by 20%, induces a difference below 1% and thus the design and simulation are not sensitive for a change in the atmosphere density model.

For changing the mass, again the baseline trajectory is used. For a decrease in mass of 20%, all values are lowered except for the maximum deceleration which is increased by 0.5 g. For an increase in mass for the RV the peak heat flux and stagnation pressure is raised, as is the total heat load. However this remains will within the limits set by the under and overshoot trajectories.

9.7.9. CRYOGENIC

The sensitivity of the cryogenic system will be analysed by determining the effect of increasing the amount of heat influx. The maximum expected heat influx during the mission is 10 to 12 W [71]. If this is increased by 20%, the heat influx becomes 12 to 14.4 W, which is still well within the capability of the cryogenic system which has a heat lift of 21.3 W.

9.7.10. ROBOTIC ARM

The robotic arm is influenced by two things: the length required and the mass it must be able to move. Should 20% be added to the length, thus changing the length to 2.2 m, nothing significant changes. According to the reasoning given in Section 5.9 this would not be a problem for the joints. The mass would increase with about the same factor as the length. If the mass that the robotic arm must carry increases from 10 to 12 kg, the robotic arm can still carry it while on the Moon. Section 5.9 explained that the arm is capable of carrying approximately 30 kg in the gravity of the Moon.

9.7.11. DOCKING

The docking mechanism is influenced only by the moments that it will encounter. Should these grow by 20%, this can be counteracted by adding 20% depth to the docking mechanism. No other adaptions to the design are needed.

9.7.12. DRILL

The drill is influenced by the composition of the ground. If the specific cutting force needed for the ground is 20% higher than expected, then either the drilling time will increase, or the compressive force on the drill must increase. Changing the compressive force to 250 N does not mean a design change is needed: the current design of the drill is capable of withstanding over 10 kN compressive force and the ExoMars drive-train can provide a compressive force of 450 N [82].

9.7.13. PARACHUTES

In Equation 7.1 it can be seen that the only variable that scales the surface area is the mass of the RV. In the case that the mass of the RV increases by 20%, the required surface area would also increase by 20%. Using Equation 7.2 it can be seen that the final mass for the parachute system would then equal 27.5 kg. The mechanisms will remain the same, scaling is not needed here. This means that the design is sensitive to changes in the design, but since the parachute system only comprises about 5 % of the total mass of the RV, the final mass will not be changed by much.

9.8 SUSTAINABILITY

At the end of the design phase, it is possible to see how sustainable the final design has become. It must be noted that during the design phase, sustainability was never a driving factor, as has been explained in the Mid-Term Report [8]. In space missions, it is not easy to incorporate sustainability. By their nature, space missions are unsustainable, because of the amount of propellant used to launch a spacecraft into space. In this section, the parts of the design which are not sustainable and those which are sustainable will be treated.

The design is not sustainable on a few factors. First of all, as is true for most space missions, a large amount of propellant is used. The propellant used is detrimental to the environment, and thus also detrimental to the sustainability. The propellant used is also quite dangerous to those handling it during the assembly of the spacecraft. Care is needed to make all proceedings safe. Space debris is left in an orbit around the Moon; the AS. Debris is also left on the surface of the Moon: the DS. Both the AS and DS will become uncontrollable after

a unspecified amount of time, because they run out of power. Although this will not influence the environment of the Earth, it will influence the environment of the Moon.

Some parts of these designs are, however, quite sustainable, especially when compared to other space missions. First, no rare materials are used. For example, no RTGs are used in the design. Second, apart from the propellant, no parts of the design are dangerous to the people working on assembling the spacecraft. Third, no debris is left in an orbit around Earth, so the space debris problem around Earth does not get any worse due to this mission. Fourth, the launch vehicle used is the Falcon Heavy, which has reusable booster rockets. Last, there is some space left within the launcher fairing. This means that it may be possible to launch the spacecraft together with another mission, which greatly increases the sustainability of the mission.

A way to increase the sustainability of the mission is by mission expansion. If multiple scientific goals can be achieved by one mission, the sustainability per goal is far better. Within this mission, several options for mission expansion exist. First, it may be possible to have a shared launch. Because the diameter of the complete spacecraft is small compared to the diameter of the fairing of the Falcon Heavy, another spacecraft might be placed besides the spacecraft during launch. Second, the AS is left in orbit when the orbiter and RV return to Earth. Scientific apparatus could be placed aboard the AS to fulfil more scientific goals during its remaining lifetime.

10 FUTURE DEVELOPMENT

In this chapter, the future development needed for the mission is discussed. First the operations and logistics needed are discussed. Then, a Gantt chart is presented and discussed, which includes the main parts of the further development of the mission.

10.1 OPERATIONS AND LOGISTICS

In order for the mission to be a success, the operations and logistics have to be planned properly. At this point in time, a general overview can be given of the various stages of the operations and logistics.

Before launch, the various manufactured parts of the mission must be brought together, assembled, and cleaned. The complete and cleaned spacecraft must then be put into the LV. As it was described in Section 3.1 to use a Falcon Heavy and launch at Cape Canaveral, the pre-launch procedures will follow Cape Canaveral's procedures.

During launch, the ground crew of SpaceX will monitor the launcher and take action whenever needed. The ground segment of the mission itself is not or hardly involved.

During the transfer from Earth to the Moon, the spacecraft must be powered up, system checks have to be performed and mid-course corrections are required. For this, a ground segment is needed which is capable of communicating with the orbiter. However, to have at least one ground station pointed to the orbiter at all times one needs several ground stations, which all communicate with the ground base where personnel is present. It was chosen to use ESA's ESTRACK ground stations when the orbiter is less than 30,000 km away from the Earth as it is primarily used for Earth-orbital missions, including orbits with an apogee of 110,000 km [150]. It is noted that with ESA's new 35 m antennas it can also achieve global coverage however they cannot transmit and/or receive in the required S-band frequency range [33] [151] [152] [153]. Therefore it was chosen, as described in Section 8.7, to use NASA's DSN, since it allows for a permanent view of the orbiter when it is at least 30,000 km away from the Earth. The complex which has a view of the orbiter will then relay the received data to the ground base.

During the lunar phase, detailed monitoring of all the lander's systems are required. The entire system needs to be capable of functioning autonomously because contact with the lander is only possible when the orbiter is visible from the Earth (approximately 75 % of the orbital period) and the lander is visible to the orbiter (dependent on exact landing location, range is between 4.5 % and 7.5 % of the orbital period). When communications are possible, ground control can keep track of all proceedings. This makes it possible to make last-minute changes when required. During the time period when the lander has contact with the orbiter, the lander will also send its monitoring data from the period where no contact was possible with the orbiter to the orbiter. The orbiter will then send this monitoring data to Earth when contact between the orbiter and the Earth is possible. This allows ground personnel to check the lander's health. At all times the DSN will be used to allow communication with the orbiter.

During the return to Earth, some system checks are needed, but no new systems are turned on. Mid-course corrections will be needed and the systems need to be prepared for re-entry. In this phase the orbiter will again make use of the DSN and ESTRACK ground stations.

During re-entry, the ground crew can do very little. The major task of the ground segment is to locate the RV after touch-down and make sure that the recovery happens within 12 hours. This task is simplified by the presence of a radio beacon on-board the RV which activates after landing on Earth.

10.2 PROJECT GANTT CHART

At the closing of this project, it is important to look at how the design of the Lunar SECRet mission could be continued in the future. For this purpose, a Gantt chart has been made describing future activities in the design. The Project Gantt chart in Figure 10.1 presents the activities after the end of the DSE. It is set up using ESA standards [33] and follows the same phases and deadlines. In the Gantt chart, the most important deadlines are the reviews. First of all, a mission concept review is held. This review can be done nearly immediately after the end of this project, because this feasibility study has set a clear mission concept. This can be used as a starting point for the complete mission design. After the mission concept review, the system requirements review follows. Here, a detailed list of requirements for the entire spacecraft, as is presented in Chapter 2, is included, but also a detailed list of subsystem requirements is added. After this, a preliminary design review is held, in which the basis of the design is treated. Again, this can largely be based on the research which has been performed during this feasibility study.

After the preliminary design review, the project enters the design phase. This phase consists of the detailed design of all subsystems, leading to a complete design of the entire spacecraft. This phase ends with a critical design review, in which the entire design is discussed and frozen. Although this phase can be based on the current research, much improvement is possible and needed. More about this can be found in Chapter 12.

After the design phase, the spacecraft can be built and tested. In this phase, two deadlines are important. First of all, the test readiness review. This review must be held to establish the readiness of the design for testing. At this point, all systems are finished and built, and can be put to the test to see if they meet all requirements. After testing, a flight readiness review is held, to check if all requirement are met and if the launch can proceed. After this review, the launch should happen.

Because it is possible to encounter a delay at every review and intermediate points, a margin of two years has been taken into account. If all goes according to plan, the spacecraft will launch in 2023, which is two years before the deadline. The time estimates are based on [33].

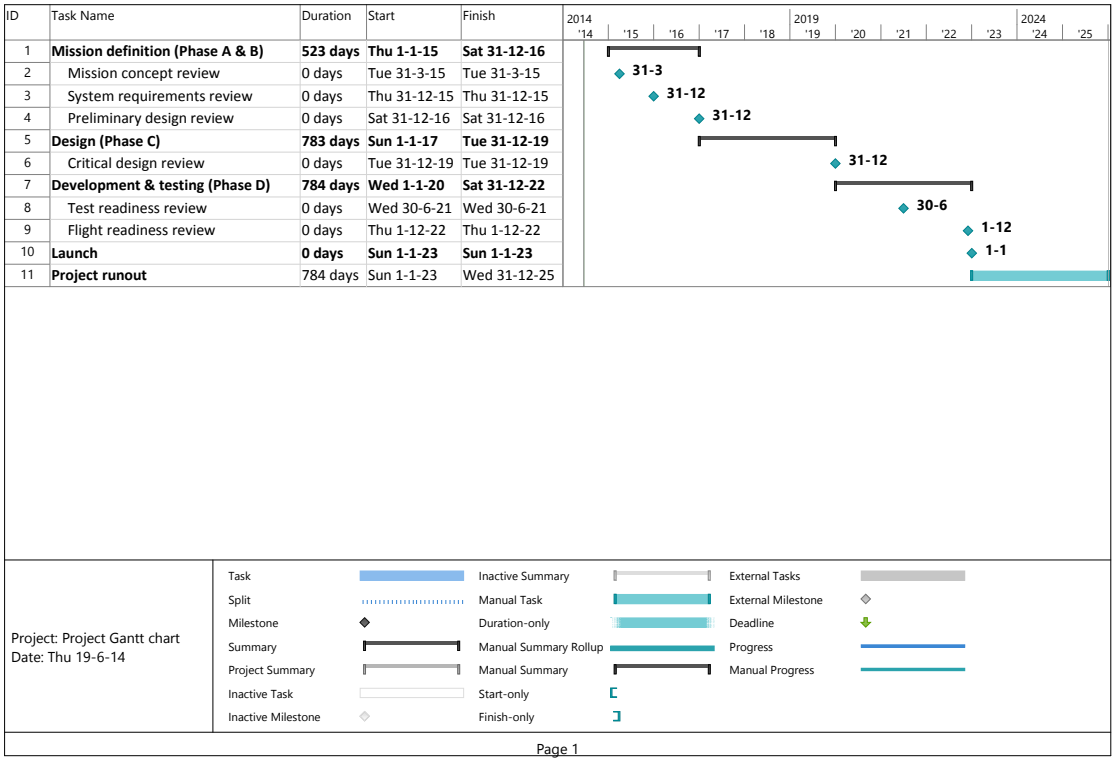

Figure 10.1: Future development Gantt chart.

11 Conclusion

The purpose of this report was to report on the detailed design phase of the project, and to come to a conclusion about the feasibility of a lunar cryogenic sample return mission. The final design consists of an orbiter, AS, DS and RV. The spacecraft is placed in the Falcon Heavy and launched into TLI. Upon arrival on the Moon the AS and DS descend to the lunar surface, where 20 drill samples of 10 cm each are retrieved. The AS returns to the orbiter with the samples in the cryogenic system. The AS docks to the orbiter with a docking port placed on the RV, and the cryogenic tank is moved into the RV. After this operation, the AS is left in an orbit around the Moon, and the orbiter and RV return to Earth. The orbiter will be left to burn up in the atmosphere while the RV descends and lands on the surface of the Earth. The wet masses of the orbiter, AS, DS and RV are, respectively, 3,246 , 2,431 , 417 and 433 kg. Altogether, this adds up to a total wet mass of 6,527 kg. The cost of the entire mission is highly dependent on the amount of insurance booked. With 92% of the mission insured the cost is €800 M.

It must be noted that in this design, not all aspects have been researched in enough detail for a complete space mission. Recommendations for future mission development can be found in Chapter 12. However, increases in cost and mass due to mistakes or underestimations of some subsystems have been taken into account by adding margins to all parts of the design. Also, during the entire study, effort was put into research in those systems which are likely to be the most critical in terms of feasibility. This includes, for example, the cryogenic system and the AOCS for landing in a dark crater. Therefore, it can be said that this mission is feasible. A mission design has been made which is capable of performing the mission, which is within the allotted cost, and meets all the set requirements.

12 RECOMMENDATIONS

In this chapter, the official recommendations for further development of the design are listed. These are mainly aspects that were not covered in the final design due to the limited available resources.

Acoustic noise for structural panels Due to time constraints the acoustic noise environment in the launch fairing has not been analysed. Acoustic noise is caused by the engine and cause high amplitude vibrations for lightweight panels. For further analysis, the acoustic noise analysis should be considered in the structural envelope.

AOCS The slender but high design of the stages is design driving for the AOCS. A design with equal width and height would decrease the maximal moment of inertia. This follows that smaller and lighter thruster can be chosen and a smaller propellant mass.

AOCS The disturbances due to magnetic fields and solar pressure were neglected because they were assumed to be small. It is recommended to compute the disturbances in the future to ensure this assumption is valid

Cryogenic system The main recommendation for the cryogenic cooler is to analyse the capability to withstand the launch and re-entry forces. The same goes for the container and the insulation material.

Drill system The drill system needs to be further detailed by a team of experts in drilling systems. Important location where more research is needed are the SID and the connection between the drilling rods.

Finite element analysis for structural components The structural analysis was performed analytically in the design and could not be properly done for panels of the payload deck or for the shape of the RV. If more accuracy needs to be achieved, a finite element analysis should be performed for the entire configuration.

Heat shield design In order to further investigate the ablative heat shield, a thorough study into ablative phenomena should be conducted. This could predict the thickness required and a more precise heat load.

Power supply subsystem During the design of the power supply system several subsystems power requirement were taken as continuous power requirement while they are only peak power requirement, or subsystems were taken to be active all the time while in fact they are only active during a part of the specific phase. This leads to an over designed power supply system. When further analysis is performed when certain subsystems are active or when they have a peak power, the power supply system will be designed lighter and smaller than it currently is.

Propulsion subsystem No cooling system is used for the LOX and MMH tanks. It is recommended that an off-the-shelf system is implemented in the future to guarantee operational temperature of the propellants.

Robot arm The robot arm is mostly a developed system. More research is needed in the design of the tool used to move samples from the drill to the cryogenic tank.

RV design The aft body of the RV is now in line with the shape of the Genesis sample return capsule and can accommodate the cryogenic system. However to further decrease heat loads, one should investigate if a increase in area of the front heat shield inducing a higher drag coefficient can be beneficial. The simulation already predicts a lower peak heat flux for larger drag coëfficient. However this would require CFD and is thus a recommendation for further study.

Thermal control The internal thermal system has not been calculated due to lack of information in this phase of the design. However at the end of this report a first-order design is made including a configuration of the spacecraft, which means the internal heat of the subsystems can be calculated and the thermal system can be sized such that all subsystems have their appropriate operating temperature. The same calculations have to be made the RV during re-entry.

Trajectory simulation The simulation currently does not compute the launch window to and from the Moon. It is recommended that this is addressed in the future in order to avoid manual computation of the launch epoch.

Trajectory simulation The simulation does not implement the orbital motion of the Moon with respect to Earth. It is recommended that this issue is addressed in the future.

Trajectory simulation The simulation does not implement the powered descent manoeuvre to the Moon in detail. It is recommended that a simulation of this powered descent is included in the future.

Trajectory simulation The landing and ascent procedure is based on a reference simulation. It is recommended to develop a simulation specificially for the Lunar SECRet mission.

Trajectory simulation for the RV In order to improve accuracy a more sophisticated atmospheric model can be implemented. Also a variable drag coefficient would aid in the performance of the simulation. To further aid the mechanical design, the radiation component for the peak heat flux can be incorporated.

BIBLIOGRAPHY

[1] DSE spring '14 group 10, "Baseline report," Tech. rep., TU Delft, May 2014.

[2] NASA, "DIVINER maps and data," Internet: http://diviner.ucla.edu/map_gallery.shtml, Retrieved: 19/05/2014.

[3] NASA, "Slopes on the south pole," Internet: http://lunar.gsfc.nasa.gov/lola/feature-20110705.html, Retrieved: 19/05/2014.

[4] Runyon, K. D. et al., "Volatiles at the Lunar South Pole: A case study for a mission to amundsen crater." *43rd Lunar and Planetary Science Conference*, 2012.

[5] Rosa, D. D. et al., "Characterisation of potential landing sites for the European Space Agency's Lunar Lander project," *Elsevier Planetary and Space Science*, Vol. 74, 2012, pp. 224–246.

[6] "Lunar Orbiter Laser Altimeter: Slopes on the south pole," Internet: http://lunar.gsfc.nasa.gov/lola/feature-20110705.html, Retrieved: 20/05/2014.

[7] Arizona State University, "LROC WAC Mosaic Lunar South Pole," Internet: http://lroc.sese.asu.edu/posts/237, Retrieved: 19/05/2014.

[8] DSE spring '14 group 10, "Midterm report," Tech. rep., TU Delft, June 2014.

[9] McDowell, J., "Lunar crater information," Internet: http://planet4589.org/astro/lunar/Craters.AW82, March 2004, Retrieved: 24/06/2014.

[10] Oceanic, N. and Administration, A., "Solar flare predictions," Internet: http://www.noaa.gov/organizations.html, Retrieved: 23/06/2014.

[11] AntDevCo, "Antenna Development Corporation - Medium Gain Patch Antennas," Retrieved: 04/06/2014.

[12] Bate, R. R., Mueller, D. D., and White, J. E., *Fundamentals of Astrodynamics*, Dover Publications Inc., 1971.

[13] Zuccarelli, V., *Earth-Moon Transfer Orbits*, Master's thesis, TU Delft, 2009.

[14] Ronald R. Sostaric, R. S. M., "Lunar Ascent and Rendezvous Trajectory Design," *31th annual AAS guidance and control conference*, NASA Johnson Space Center, 2008.

[15] Gerth, I. and Mooij, E., "Guidance for Autonomous Precision Landing on Atmosphereless Bodies," 2014.

[16] Zandbergen, B., "Delta-v (velocity increment) budget," Internet: http://www.lr.tudelft.nl/en/organisation/departments/space-engineering/space-systems-engineering/expertise-areas/spacecraft-engineering/blind-documents/delta-v/, Retrieved: 21/05/2014.

[17] NASA, "Launch sites," Internet: http://spaceflight.nasa.gov/shuttle/reference/shutref/sts/launch.html, Retrieved: 30/06/2014.

[18] Roy, A. E., *Orbital Motion*, IOP Publishing, 2005.

[19] NASA, "July 20, 1969: One Giant Leap For Mankind," Internet: http://www.nasa.gov/mission_pages/apollo/apollo11_40th.html, 2013, Retrieved: 23/06/2014.

[20] Wertz, J. R., Everett, D. F., and Puschell, J. J., *Falcon 9 launch guide: Payload user's guide*, Space Exploration Technologies Corporation, 2009.

[21] Ariane Space, *Ariane 5 user's manual Issue 5*, issue 5, revision 1 ed., July 2011.

[22] United Launch Alliance, *Delta IV Launch Services User's Guide*, June 2013.

[23] ILS Launch Services, *Proton Launch System Mission Planner's Guide*, September 2009.

[24] United Launch Services, *Atlas V Launch Services Services*, March 2010.

[25] Tangient LLC, "Lunar crater depths," Internet: http://the-moon.wikispaces.com/Catalogs+of+Lunar+Craters, Retrieved: 04/06/2014.

[26] Cheng, R., "Surveyor terminal guidance," Tech. rep., NASA, 1966.

[27] ClimaTemps, "Climate of Turgay, Kazakhstan," Internet: http://www.turgay.climatemps.com/, Retrieved: 22/06/2014.

[28] Wertz, J. R., Everett, D. F., and Puschell, J. J., *Space Mission Analysis and Design: Third Edition*, Microcosm Press, 2010.

[29] Ingo Gerth, MSc Student in Aerospace Engineering,Delft University of Technology, Private Correspondence.

[30] Sakatani, N. et al., "Experimental study for thermal conductivity structure of lunar surface regolith: Effect of compressional stress," *Icarus*, 2012, pp. 1180–1182.

[31] Ringuette, M., "Absorptivity & Emissivity," Internet http://www.solarmirror.com/fom/fom-serve/cache/43.html, Retrieved: 20/06/2014.

[32] Fortescue, P., Swinerd, G., and Stark, J., *Spacecraft Systems Engineering Fourth Edition*, Wiley, 2011.

[33] Wertz, J. R. and Larson, W. J., *Space Mission Engineering: The New SMAD*, Microcosm Press, 2011.

[34] Emcore Photovoltaics, "ZTJ Photovoltaic Cell Datasheet," Tech. rep., EMCORE Corporation, September 2012.

[35] Clyde Space, "Spacecraft Batteries," Internet: http://www.clyde-space.com/products/spacecraft_batteries, Retrieved: 13/06/2014.

[36] AA portable power corp, "High power Li-Po packs," Internet: http://www.batteryspace.com/hi-powerli-popacks.aspx, Retrieved: 13/06/2014.

[37] Maxell, "ER (Lithium Thionyl Chloride Battery)," Internet: http://biz.maxell.com/en/product_primary/?pci=9&pn=pb0004, Retrieved: 13/06/2014.

[38] NASA, "Summary: Space applications of hydrogen and fuel cells," Internet: http://www.nasa.gov/topics/technology/hydrogen/hydrogen_2009.html, Retrieved: 13/06/2014.

[39] Nedstack, "Product specifications of HP stacks," Tech. rep., Nedstack, 2014.

[40] Horizon Fuel Cell Technologies, "AEROSTACKS 200W-1000W World's lightest, highest power density stacks," Internet: http://www.horizonfuelcell.com/#!aerostacks-200w-1kw/c10tm, Retrieved: 13/06/2014.

[41] Zandbergen, B., *Spacecraft (bus) Design and Sizing*, TU Delft, October 2011, Reader.

[42] Megson, T., *Aircraft Structures for Engineering Students Fourth Edition*, Elsevier, 2007.

[43] Ponnusamy, D. and Maahs, G., "The Surveyor Shock Absorber," Tech. rep., Johns Hopkins University Applied Physics Laboratory.

[44] Centre for Astrophysics and Planetary Science, "PH508: Spacecraft structures and materials," PowerPoint presentation.

[45] Aerospace Specification Metals Inc., "Aluminum 6061-T6; 6061-T651," Internet: http://asm.matweb.com/search/SpecificMaterial.asp?bassnum=MA6061t6, Retrieved: 18/06/2014.

[46] Saunders, G., "Worked-out Statics Exam 2011," Tech. rep., TU Delft.

[47] Sundaramoorthy, P. P., Private Correspondence, 13/06/2014.

[48] Zandbergen, B., *AE2-101 - Communications I+II*, TU Delft, Reader.

[49] Dr. Angelo Cervone, Senior Lecturer at Delft University of Technology, Private Correspondence.

[50] ASTRIUM, "1207 Litre Bipropellant Tank: Model OST 24/0," Internet: http://cs.astrium.eads.net/sp/spacecraft-propulsion/propellant-tanks/1207-litre-bipropellant-tank.html, Retrieved: 16/05/2014.

[51] SRE-PA & D-TEC staff of the European Space Research and Technology Centre, "Margin philosophy for science assessment studies," 2011.

[52] Astrium, "22 N Bipropellant Thruster data sheet," Internet: http://cs.astrium.eads.net/sp/spacecraft-propulsion/bipropellant-thrusters/22n-thruster.html, Retrieved: 20/06/2014.

[53] ESA, "Reaction wheels at Bradford Engineering," Internet: http://bradford-space.com/userfiles/Paper%20EHE.pdf, Retrieved: 20/06/2014.

[54] Honeywell International Inc., "IMU data sheet," Tech. rep., Aerospace Electronic Systems, september 2013.

[55] JenaOptronik, "ASTRO 10 data sheet," Internet: http://www.jena-optronik.de/en/aocs/astro10.html, Retrieved: 20/06/2014.

[56] JenaOptronik, "RVS data sheet," Internet: http://www.jena-optronik.de/en/aocs/rvs.html, Retrieved: 20/06/2014.

[57] Malin Space Science Systems, "Space camera data sheet," Tech. rep., Malin Space Science Systems, 2013.

[58] MOOG Inc., "Cosine sun sensor data sheet," Internet: http://bradford-space.com/productline/sun_sensors/cosine_sun_sensor, Retrieved: 20/06/2014.

[59] NASA, "Moon Fact Sheet," Internet: http://nssdc.gsfc.nasa.gov/planetary/factsheet/moonfact.html, Retrieved: 16/06/2014.

[60] Fesmire, J. et al., "Aerogel beads as cryogenic thermal insulation system," Tech. rep., NASA, Dynacs Inc., Cabot Corperation.

[61] Gerth, I. and Mooij, E., "Guidance for Autonomous Precision Landing on Atmosphereless Bodies," *American Institue of Aeronautics and Astronautics*.

[62] University of Oxford, "Cryocoolers for space applications," Internet http://www.eng.ox.ac.uk/cryogenics/research/cryocoolers-for-space-applications, Retrieved: 21/05/2014.

[63] Aerojet, "Aerojet bipropellant engines," May 2006.

[64] Surrey Satellite Technology Ltd, "Communication system," Internet: www.sstl.co.uk, Retrieved: 05/06/2014.

[65] ISIS - Innovative Solutions In Space, "Communication system," Internet: http://www.cubesatshop.com/, Retrieved: 05/06/2014.

[66] Zagarola, M. et al., "Demonstration of a Two-Stage Turbo-Brayton Cryocooler for Space Applications," *International Cryocooler Conference*, 2009.

[67] Infrared Laboratories, "JT Refrigerator," Internet: http://www.infraredlaboratories.com/JT_Refrigerator.shtml, Retrieved: 13/05/2014.

[68] Polycold Systems Inc., "Cryotiger cooling system," Brochure, Retrieved: 14/05/2014.

[69] Salvestrini, K., Engineer at Infrared Laboratories, private Correspondence.

[70] Dale Copps, Library Manager at Creare Inc., Private Correspondence.

[71] Veverka, J., "Cryogenic Comet Nucleus Sample Return Mission Technology Study," Tech. Rep. SDO-12367, NASA, 2013.

[72] Mukugi, K. et al., "Low temperature mechanical properties of titanium and weld joints (Ti/Ti, Ti/Nb) for helium vessels," *The 10th Workshop on RF Superconductivity*, 2001.

[73] The Engineering Toolbox, "Young Modulus of Elasticity for Metals and Alloys," Internet: http://www.engineeringtoolbox.com/young-modulus-d_773.html, Retrieved: 19/05/2014.

[74] Infrared laboratories, "Cryogenic solutions," Tech. rep., Infrared laboratories, 2010.

[75] Actuatorzone, "8 inch actuator," Internet: http://www.actuatorzone.com/actuators/8-inch-stroke/pa-02-8-200, Retrieved: 16/05/2014.

[76] Actuatorzone, "GNC Sensors & Actuators: ASTRIX® 120," Internet: http://www.astrium.eads.net/en/equipment/astrix-120.html, Retrieved: 16/05/2014.

[77] Neumann, H., "Thermal insulation," presentation, Institue for Technical Physics.

[78] Fesmire, J. and Augustynowicz, S., "Cryogenic Thermal Insulatio Systems," presentation, NASA Kennedy Space center, Cryogenic Test Laboratory.

[79] Energy Efficiency Systems, "Phase Change Material (PCM) products," Internet: http://www.rgees.com/products.php, Retrieved: 18/06/2014.

[80] Rusconi, A., Magnani, P., et al., "Dexarm engineering model development and testing," Tech. rep., -.

[81] ESA, "CNSR SAS-1M (90-95)," Internet: http://www.esa.int/Our_Activities/Space_Engineering/Mechanisms/CNSR_SAS-1m_90-95/(print), Retrieved: 17/06/2014.

[82] Selex ES S.p.A, "ExoMars drill system," 2014, Retrieved: 20/05/2014.

[83] NASA, "Gemini project description," Internet: http://history.nasa.gov/SP-4002/p3a.htm, Retrieved: 12/06/2014.

[84] Honeywell International Inc., "Honeywell HG8500 Series Radar Altimeter," 2003.

[85] Martel, L., "Lunar Rock Densities," *PSRD*, 2012.

[86] A.M. Fernandez, PhD candidate 3ME, Private Correspondence.

[87] Barbir, F., "PEM Fuel Cells," 2010, Booklet.

[88] Enidine, "Adjustable Series Hydraulic Shock Absorbers," 2007.

[89] Sperling, F., "The Surveyor Shock Absorber," Tech. rep., Jet Propulsion Laboratory.

[90] Honeybee Robotics, Internet: http://www.honeybeerobotics.com/portfolio/auto-gopher-drill/, Retrieved: 19/05/2014.

[91] Engineering Supply Company, "Drilling calculation formulea," .

[92] Zacny, K., Glaser, D., Bartlett, P., Davis, K., and Wilson, J., "Drilling results in ice-bound simulated lunar regolith (FJS-1) as part of the construction and resource utilization explorer project (CRUX)," *Lunar and Planetary Science XXXVII*, 2006.

[93] Fusco, F., "Robotics for subsurface exploration of planetary bodies," PowerPoint presentation.

[94] Zeus, "Low Temperature Properties of Polymers," Tech. rep., Zeus, 2005.

[95] Dotmar Engineering Plastic Products Ltd., "POLYSTONE polyolefins," Brochure, Retrieved: 17/06/2014.

[96] Callister, W. and D.G.Rethwisch, *Materials Science and Engineering*, John Wiley & Sons, eighth ed., 2011.

[97] Baglioni, P., EXM Rover Manager at European Space Agency, Private Correspondence.

[98] PBC linear, "MTE Linear Actuator," Internet: http://www.pbclinear.com/MTE-Linear-Actuator?tab=ProductOverview, Retrieved: 17/06/2014.

[99] G.P. Sutton, O. B., *Rocket Propulsion Elements*, John Wiley & Sons, 2001.

[100] Hemingway, B. et al., "Specific heats of lunar soils, basalt, and breccias from the Apollo 14, 15, and 16 landing sites, between 90 and 350K," *Proceedings of the Fourth Lunar Science Conference*, Vol. 3, Silver Spring, Md. 20910, 1973, pp. 2481–2487.

[101] Sakatani, N. et al., "Thermal conductivity measurements of glass beads and regolith simulant under vacuum conditions," *EPSC Abstracts*, Vol. 8, Silver Spring, Md. 20910, 2013.

[102] IV, J. H. L. and V, J. H. L., *A Heat Transfer Textbook*, John H. Lienhard V, 2000.

[103] "Module 1: Hydrogen Properties," 2001, Booklet.

[104] University of Maryland, "Mass Estimating Relationships," Presentation, 2009.

[105] Doody, D., *Deep Space Craft: An Overview of Interplanetary Flight*, Springer, 2009.

[106] Mooij, E., PhD at Delft University of Technology, Private correspondence.

[107] Fisher, L. J., "Landing Energy Dissipation for Manned Reentry Vehicles," Tech. rep., NASA Langley Research Center, 1960.

[108] Knacke, T. W., *Parachute Recovery Systems Design Manual*, US Navy, 1978.

[109] Mooij, E., "Planetary Entry and Descent," TU Delft, 10 2013, AE4870-B Lecture slides.

[110] Lingard, S., "Parachutes for space use," 2005, 3rd International Planetary Probe Workshop.

[111] Mooij, E., *Re-entry Systems*, TU Delft, September 2013, Reader.

[112] A. Viviani, G. P., "Overview of design approach for a sample return capsule," *18th AIAA/3AF International space planes and hypersonic systems and technologies conference*, 2012.

[113] NASA, "Aerothermodynamics course by NASA," Internet: `https://tfaws.nasa.gov/TFAWS12/Proceedings/Aerothermodynamics%20Course.pdf`, Retrieved: 20/06/2014.

[114] Desai, P. N., Mitcheltree, R. A., and Cheatwood, F. M., "Entry trajectory issues for the Stardust sample return capsule." *International Symposium on Atmospheric Reentry Vehicles and Systems*, 1999.

[115] Gupta, R. N., "Aerothermodynamic Analysis of Stardust Sample Return Capsule with Coupled Radiation and Ablation," *Journal of spacecraft and rockets*, Vol. 37, No. 4, 2000.

[116] R.A. Mitcheltree, R.G. Wilmoth, F. C. G. B. F. G., "Aerodynamics of Stardust Sample Return Capsule," *NASA Langley Research Center*, 1997.

[117] Cheatwoord, F. M. et al., "Aerothermodynamic environment definition for the Genesis sample return capsule," *NASA Langley Research Center*, 2001.

[118] Desai, P. N. et al., "Trajectory reconstructin for the Genesis entry," *3rd INTERNATION PLANETARY PROBE WORKSHOP*, 2005.

[119] Olynick, D., "Aerothermodynamics of the Stardust Sample Return Capsule," *American Institute of Aeronautics and Astronautics*, 1997.

[120] Tran, H. K. et al., *NASA Technical Memorandum 110440*, 1997.

[121] Venkatapathy, E. et al., "Selection and Certification of TPS: Constraints and Considerations for Venus Missions," *NASA Ames Research Center*, 2009.

[122] Agency, J. A. E., "Asteroid explorer Hayabusa completes its return mission using ion engines," *JAXA Today*, , No. 2, 2010, pp. 15.

[123] Riley, C. and Dolling, P., *Apollo 11*, Haynes Publishing, 2009.

[124] NASA, "NASA's Gemini 7," Internet: `http://nssdc.gsfc.nasa.gov/nmc/spacecraftDisplay.do?id=1965-100A`, Retrieved: 03/06/2014.

[125] Astrium, "20 N Hydrazine Thruster data sheet," Internet: `http://cs.astrium.eads.net/sp/spacecraft-propulsion/bipropellant-thrusters/22n-thruster.html`, Retrieved: 20/06/2014.

[126] Astrium, "EPDM - Bladder Tank BT 01/0 data sheet," Tech. rep., Astrium, 2001.

[127] NASA, "Apollo 11: Day 1 part 2: Earth Orbit and Translunar Injection," Internet: `http://history.nasa.gov/ap11fj/02earth-orbit-tli.htm`, Retrieved: 30/06/2014.

[128] Pettyjohn, E., "Cryocoolers for Microsatellite Military Applications," Retrieved: 14/05/2014.

[129] Astronautica, E., "Kestrel engine," Internet: http://www.astronautix.com/engines/kestrel.htm#SAquence_1, Retrieved: 24/06/2014.

[130] NASA, "NASA's Deep Space Network," Internet: http://www2.jpl.nasa.gov/basics/bsf18-2.php, Retrieved: 20/05/2014.

[131] SpaceX, "Falcon Heavy," Internet: http://www.spacex.com/falcon-heavy, Retrieved 19/05/2014.

[132] Green, D., "The 'Total Cost of Ownership'," *Satellite Manufacturing Special - LCMSS*, , No. 2, 2013, pp. 12.

[133] Guerra, L., "NASA Cost Estimating Module," .

[134] CoinNews Media Group LCC, "US Inflation Calculator," Internet: http://www.usinflationcalculator.com/, Retrieved: 18/06/2014.

[135] Encyclopedia Astronautica, "Titan II," Internet: http://www.astronautix.com/lvs/titan2.htm, Retrieved: 18/06/2014.

[136] Spaceflight 101, "Delta II 7920H-10," Internet: http://www.spaceflight101.com/delta-ii-7920h-10.html, Retrieved: 18/06/2014.

[137] NASA, "Genesis," Internet: http://nssdc.gsfc.nasa.gov/nmc/spacecraftDisplay.do?id=2001-034A, Retrieved: 20/05/2014.

[138] van Pelt, M., Cost Engineer at ESA, Private Correspondence.

[139] Zak, A., "Luna-Grunt (Lunar Sample Return/Luna-28)," Internet: http://www.russianspaceweb.com/luna_grunt.html, Retrieved: 20/05/2014.

[140] Zak, A., "Luna-glob," Internet: http://www.russianspaceweb.com/luna_glob.html, Retrieved: 20/05/2014.

[141] NASA, "NASA Partners With Commercial Companies For Lunar Lander Capabilities," Internet: http://www.nasa.gov/lunarcatalyst/#.U2H0EfmSy2q, Retrieved: 20/05/2014.

[142] Curran, P. D. R. and Verhagen, D. W., "Risk Management and Reliability," TU Delft, 3 2014, AE3221-I Lecture slides.

[143] Young, K., "US achieves autonomous docking in space," Tech. rep., NewScientist, May 2007.

[144] Space.com staff, "Unmanned Russian supply ship fails to dock at space station," Internet: http://www.space.com/16723-unmanned-russian-supply-ship-fails-to-dock-at-space-station.html, Retrieved: 24/06/2014.

[145] Zandbergen, B., Senior lecturer at AE, Delft University of Technology, Private Correspondence.

[146] Sigma-Aldrich, "Methylhydrazine Material Safety Data Sheet," Tech. rep., Sigma-Aldrich, August 2004.

[147] Terra Industries Inc., "Material Safety Data Sheet," Tech. rep., Terra Industries, January 2011.

[148] Hitachi Maxell, Ltd., Energy Division, "Product Safety Data Sheet," Tech. rep., Maxell, January 2014.

[149] GmbH, V. M., "Material Safety Data Sheet," June 2008.

[150] ESA, "XMM-Newton Operations," Internet: http://www.esa.int/Our_Activities/Operations/XMM-Newton_operations, Retrieved: 13/06/2014.

[151] ESA, "New Norcia - DSA 1," Internet: http://www.esa.int/Our_Activities/Operations/New_Norcia_-_DSA_1, Retrieved: 13/06/2014.

[152] ESA, "Cebreros - DSA 2," Internet: http://www.esa.int/Our_Activities/Operations/Cebreros_-_DSA_2, Retrieved: 13/06/2014.

[153] ESA, "Malargüe - DSA 3," Internet: http://www.esa.int/Our_Activities/Operations/Malarguee_-_DSA_3, Retrieved: 13/06/2014.

[154] United Nations, office for outer space affairs, "United Nations Treaties and Principles On Outer Space, related general assembly resolutions and other documents," .

A FUNCTIONAL FLOW DIAGRAM

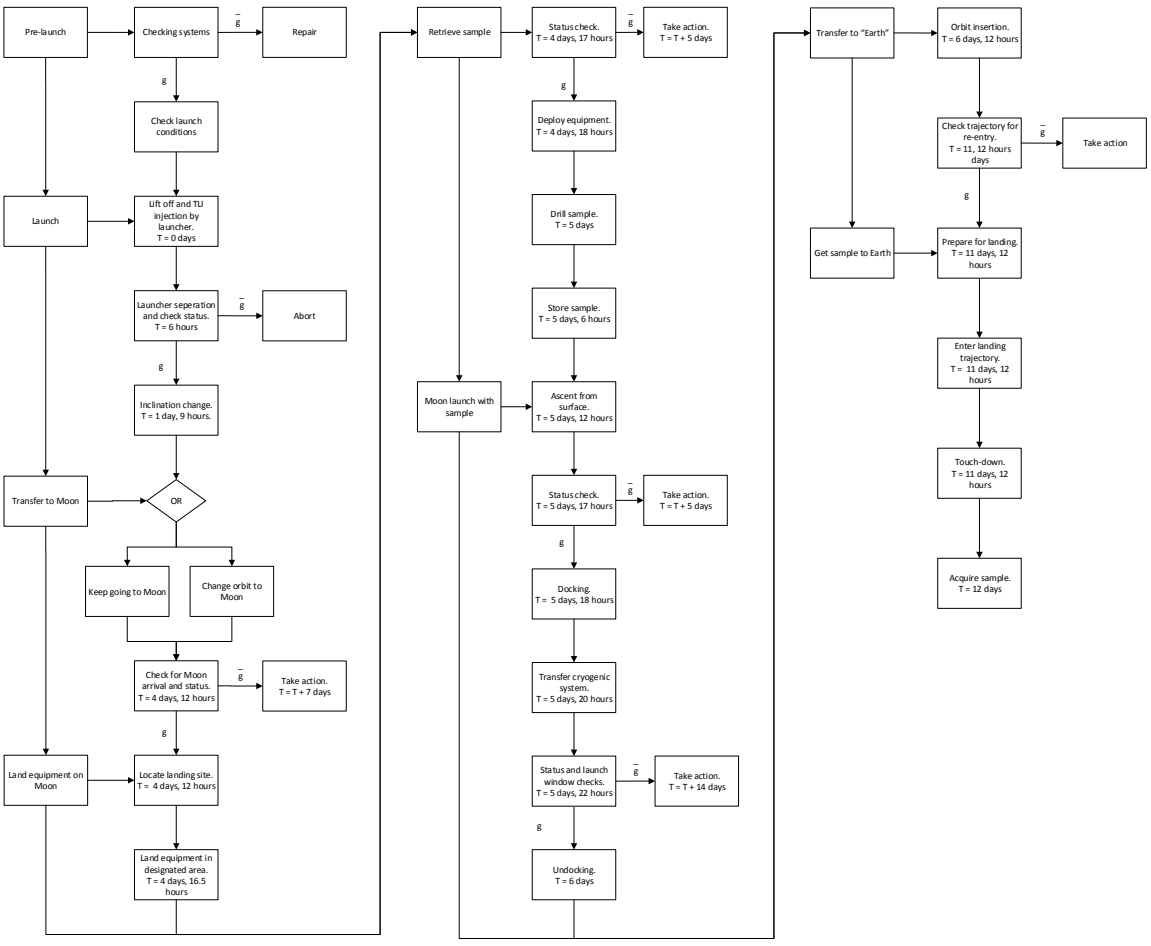

Figure A.1: The FFD.

B FUNCTIONAL BREAKDOWN

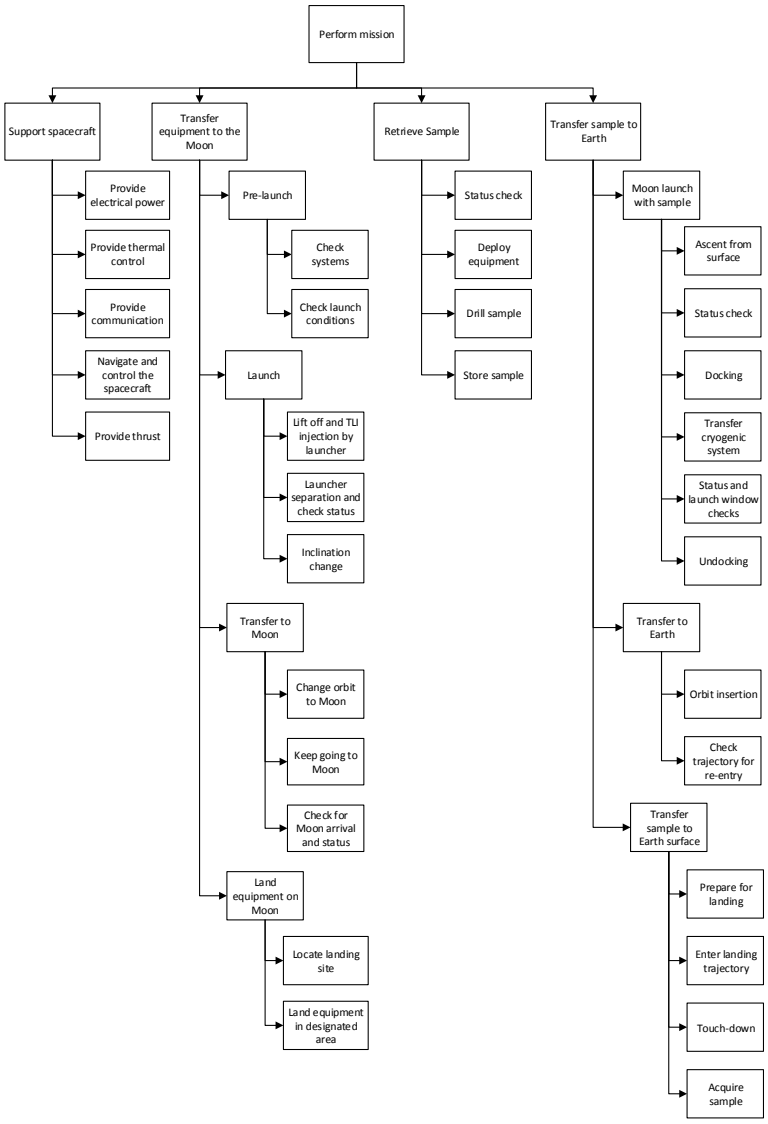

Figure B.1: The FBD.

C SPACE LAW

Mankind venturing into space made it necessary to define laws for space exploration. This automatically means that there are constraints for the mission designed in this report. Preliminary research resulted in a selection of relevant articles. These articles are stated below, and all come from [154], which is a collection of treaties. It should be noted that not all treaties are signed by all State Parties, for example, the Moon Treaty is signed by very few only.

Outer Space Treaty of 1967, Article VIII

> A State Party to the Treaty on whose registry an object launched into outer space is carried shall retain jurisdiction and control over such object, and over any personnel thereof, while in outer space or on a celestial body. Ownership of objects launched into outer space, including objects landed or constructed on a celestial body, and of their component parts, is not affected by their presence in outer space or on a celestial body or by their return to the Earth. Such objects or component parts found beyond the limits of the State Party of the Treaty on whose registry they are carried shall be returned to that State Party, which shall, upon request, furnish identifying data prior to their return.

Part one, A, Article V

> [..] States Parties to the Treaty shall immediately inform the other States Parties to the Treaty or the Secretary-General of the United Nations of any phenomena they discover in outer space, including the Moon and other celestial bodies, which could constitute a danger to the life or health of astronauts.

Part one, E, Article 5, item 2

> If a State Party becomes aware that another State Party plans to operate simultaneously in the same area of or in the same orbit around or trajectory to or around the Moon, it shall promptly inform the other State of the timing of and plans for its own operations.

United Nations Treaties and Principles On Outer Space, Part 1, E, Article 9

> 1. States Parties may establish manned and unmanned stations on the Moon. A State Party establishing a station shall use only that area which is required for the needs of the station and shall immediately inform the Secretary-General of the United Nations of the location and purposes of that station. Subsequently, at annual intervals that State shall likewise inform the Secretary-General whether the station continues in use and whether its purposes have changed.
>
> 2. Stations shall be installed in such a manner that they do not impede the free access to all areas of the Moon of personnel, vehicles and equipment of other States Parties conducting activities on the Moon in accordance with the provisions of this Agreement or of article I of the Treaty on Principles Governing the Activities of States in the Exploration and Use of Outer Space, including the Moon and Other Celestial Bodies.

Since the Lunar SECRet mission is an unmanned mission which does not involve nuclear material, only a few space laws have to be met. As the design is right now, the requirement stated as LCSR-Mission-ConsDesign-01 is met.